# Roles of Microbial Syntrophy, Extracellular Polymeric Substances, and Power Supply Schemes on Electro-methanogenesis

by

Basem Zakaria Reda

A thesis submitted in partial fulfilment of the requirements for the degree of

Doctor of Philosophy

in

ENVIRONMENTAL SCIENCE

Department of Civil and Environmental Engineering

University of Alberta

# Abstract

The concept of electro-methanogenesis by combining the microbial electrolysis cell and anaerobic digestion (MEC-AD) has become a promising method for improving methane generation and improving the stability of digesters. Although the electro-methanogenesis process is often featured as a simple process of coupling MEC with an anaerobic digester, several fundamental and engineering bottlenecks are associated with their practical application. Most importantly, a streamlined roadmap for establishing an active microbiome, process design, optimization, and scale-up has not yet been achieved. Particularly, this doctoral thesis focuses on understanding the roles of microbial syntrophy, extracellular polymeric substances, and power supply schemes on electro-methanogenesis.

First, we reported an experimental investigation of extracellular polymeric substances (EPS), reactive oxygen species (ROS), and the expression of genes associated with extracellular electron transfer (EET) in methanogenic biocathodes electrodes. The MEC-AD systems were examined using two cathode materials: carbon fibers and stainless-steel mesh. A higher methane generation was attained in MEC-AD with stainless-steel mesh as a cathode electrode. A higher abundance of hydrogenotrophic *Methanobacterium* sp. and homoacetogenic *Acetobacterium* sp. appeared to play a major role in superior methanogenesis from stainless steel biocathode than carbon fibers. Moreover, the higher secretion of EPS accompanied by the lower ROS level in stainless steel biocathode indicated that higher EPS perhaps protected cells from harsh metabolic conditions (possibly unfavorable local pH) induced by faster catalysis of hydrogen evolution reaction. In contrast, EET-associated gene expression patterns were comparable in both biocathodes. Thus, these results indicated hydrogenotrophic methanogenesis is the key mechanism, while cathodic

EET has a trivial role in distinguishing performances between two cathode electrodes. These results provide new insights into the efficient methanogenic biocathode development.

Second, previous studies for conventional anaerobic digestion systems have emphasized maintaining an optimum propionate/acetate (HPr/HAc) ratio. To date, the detrimental ratio of HPr/HAc concentrations towards the electro-methanogenesis process has not been examined yet. Thus, this study focused on understanding the impact of different VFAs concentrations with varied HPr/HAc ratios on the microbial community and methanogenesis process. The total cumulative methane production remained almost the same after increasing HPr/HAc ratio from 0.5 to 1.5. When HPr/HAc ratios further increased to 2.5 and 5, the total cumulative methane production markedly decreased. EET-associated gene expression reduced under high HPr/HAc ratios (2.5 and 5) indicates the partial inhibition of biofilm electroactivity. *Geobacter* and *Methanobacterium* species were abundant under lower HPr/HAc ratios, while their abundance decreased under higher HPr/HAc ratios. Therefore, this study demonstrated that higher HPr/HAc ratios would adversely impact methanogenesis rates in MEC-AD systems.

Third, from the perspective of energy saving in the operation of MEC-AD, we focused on developing an intermittent power supply scheme. The applied potential was switched off for 12 and 6 hours/day during the operation of a laboratory-scale MEC-AD system fed with glucose. The results from the operation under continuous applied potential served as the control. The overall biomethane generation and net energy income from the process were unaffected when the applied potential turned off for 6 hours/day. Both quantitative and qualitative analyses of microbial communities suggested that a balanced microbiome could be maintained under short-term switching-off the applied potential. However, performance substantially deteriorated when the applied potential turned off for 12 hours/day. Overall, the results of this study suggest that MEC-

AD operation does not need a continuous power supply, and higher energy efficiency can be effectively achieved by intermittently powering the reactor. However, previous efforts to optimize power supply schemes for MEC-AD systems were limited to the synthetic substrate only. However, conventional digesters are typically operated with more complex substrates. Hence, we investigated the impact of intermittent power supply in MEC-AD fed with mixed primary and sewage sludge. Overall, the electrocatalytic activity of the anode biofilm demonstrated a higher current density at 12 hrs ON mode. Also, the maximum methane generation attained when the applied potential switched ON for 12 hrs/day. The extracellular electron transfer-associated genes showed the highest expression at 12 hrs ON mode. Accordingly, the intermittent applied potential for 12 hrs/day could provide an attractive opportunity to saving electrical energy input in MEC-AD systems, thereby its economic benefits.

# Preface

Chapter 2 of this thesis has been published as B.S. Zakaria and B.R. Dhar, (2019) "Progress towards catalyzing electro-methanogenesis in anaerobic digestion process: Fundamentals, process optimization, design and scale-up considerations" in *Bioresource Technology*, vol. 289, 121738. B.S. Zakaria was responsible for the data collection from the literature, writing original draft, review and editing. B.R. Dhar was responsible for the review, editing, and supervising this work.

Chapter 3 of this thesis has been published as B.S. Zakaria and B.R. Dhar, (2021) "Characterization and significance of extracellular polymeric substances, reactive oxygen species, and extracellular electron transfer in methanogenic biocathode" in *Scientific Reports*, vol. 11, 7933. B.S. Zakaria was responsible for conceptualization and experiment design, experiment and data collection, writing original draft, review, and editing. B.R. Dhar was responsible for the review, editing, and supervising this work.

Chapter 4 of this thesis will be submitted as B.S. Zakaria and B.R. Dhar, (2021) "Investigation of the detrimental ratio of propionate to acetate in a microbial electrolysis cell assisted anaerobic digester" in a peer-reviewed journal. B.S. Zakaria was responsible for conceptualization and experiment design, experiment and data collection, writing original draft, review, and editing. B.R. Dhar was responsible for the review, editing, and supervising this work.

Chapter 5 of this thesis has been published as B.S. Zakaria and B.R. Dhar, (2021) "An intermittent power supply scheme to minimize electrical energy input in a microbial electrolysis cell assisted anaerobic digester" in *Bioresource Technology*, vol. 319, 124109. B.S. Zakaria was responsible for conceptualization and experiment design, experiment and data collection, writing original draft, review, and editing. B.R. Dhar was responsible for the review, editing, and supervising this work.

Chapter 6 of this thesis will be submitted as B.S. Zakaria and B.R. Dhar, (2021) "Insights into intermittent over continuous energization during biomethane recovery from sewage sludge with microbial electrolysis cell assisted anaerobic digester" in a peer-reviewed journal. B.S. Zakaria was responsible for conceptualization and experiment design, experiment and data

collection, writing original draft, review, and editing. B.R. Dhar was responsible for the review, editing, and supervising this work.

# Dedication

To my parents, brother and my beautiful wife.

## Acknowledgements

I would like to express my deep appreciation to my supervisor Dr. Bipro Ranjan Dhar, for the patient guidance, constructive criticism, invaluable support and valuable suggestions. I have been extremely lucky to have a supervisor who improved my research and writing skills, always keen to advise and provide me with the guidance to be an independent researcher.

My sincere thanks also go to my Ph.D. supervisory committee (Dr. Yang Liu and Dr. Zhehui Jin), Ph.D. candidacy exam committee (Dr. Yang Liu, Dr. Zhehui Jin, Dr. Dominic Sauvageau, Dr. Ian D Buchanan and Dr. Hassan Dehghanpour), and PhD defense committee (Dr. Pascal Saikaly, Dr. Lisa Stein, Dr. Yang Liu, Dr. Zhehui Jin, Dr. Maricor Arlos and Dr. Yuntong She) for their time and valuable critical feedback on my thesis work.

I express my warm thanks to all my past and present colleagues for their valuable support. Thanks to Sajib Barua for providing me with training on the equipment and Lab techniques. I also thank Mrs. Chen Liang and Mr. Yupeng (David) Zhao for their laboratory-related training. I sincerely appreciate the help from Arlene Oatway, Nathan Gerein, Dr. Stephen Ogg, and Greg Plummer for providing me with training on different microscopic imaging techniques.

I express my gratitude to the donors of the scholarships (Izaak Walton Killam Memorial Scholarship and Doctoral Recruitment Scholarship) and awards (Graduate Student Teaching Assistant Award, Andrew Stewart Memorial Graduate Prize, Dr Donald R Stanley Graduate Scholarship in Environmental Engineering) that I received during my PhD journey.

I am also thankful to the Natural Sciences and Engineering Research Council (NSERC) of Canada and Future Energy Systems at the University of Alberta for supporting this research project.

# Table of Content

# List of Tables

# List of Figures

# Chapter 1

# Introduction

## 1.1. Background

Developing advanced waste-to-bioenergy technologies can simultaneously expand waste diversion from landfills in an environmentally friendly and cost-effective method. Anaerobic digestion (AD), which represents an attractive option for treating organic waste, produces renewable methane-rich biogas (Barua et al., 2018; Barua and Dhar, 2017; Dhar et al., 2012, 2011; Ryue et al., 2019). However, this existing technology faces several limitations and challenges; most notably, low organic compound removals, instability, and inferior methane recovery (Cai et al., 2018; Jiang et al., 2018; Song et al., 2010). For instance, studies have suggested that a significant portion of methane in traditional digesters would be produced via the acetoclastic route (J. Guo et al., 2015; Shin et al., 2010). Acetoclastic methanogens are identified to grow slowly in comparison with hydrogenotrophic methanogens (doubling time 5-7 days vs. 4-8 hours), which results in the requirement of longer digestion time (Anderson et al., 2003). Particularly, due to inferior acetoclastic methanogenesis kinetics, intermediates (mainly organic acids like acetate) from biodegradation of complex organics can accumulate within the digester and lead to process instability (He et al., 2018). Also, in comparison with hydrogenotrophic methanogens, acetoclastic methanogens are more sensitive to various environmental parameters, including pH, ammonium, and temperature (Cai et al., 2018; Jiang et al., 2018; Song et al., 2010).

In addition to traditional anaerobic digesters, bio-methane can be produced in microbial electrolysis cells (MECs) (Hirano and Matsumoto, 2018; J. Park et al., 2018c; Ren et al., 2018; Wang et al., 2015; Yu et al., 2018; Zhen et al., 2015). Compared to conventional anaerobic digestion, MECs are a relatively emerging process that uses a special type of electroactive bacteria (Logan et al., 2019; Lu and Ren, 2016). The electrons released from bacterial oxidation of simple organic matters like acetate are transferred to the anode electrode and can be transformed into target value-added products such as hydrogen gas, hydrogen peroxide, methane, etc. However, a small amount of external energy may be required to surmount the thermodynamic barrier of a

cathodic reaction needed for the synthesis of a target value-added product (Cheng et al., 2015; Cheng and Logan, 2007; Ditzig et al., 2007). For instance, depending on other energy losses (e.g., mass transfer limitations), an externally applied voltage of 0.5-1.0 V is required for $H_2$ production on the cathode from a MEC fed with acetate (Cheng and Logan, 2007; Ditzig et al., 2007; Logan et al., 2008). The deployment of methanogens on the cathode can enable methane production through $CO_2$ reduction at a relatively lower energy input (Cheng et al., 2009; Siegert et al., 2015). This emerging concept of methanogenesis is called 'electro-methanogenesis' (Cheng et al., 2009). The electro-methanogenesis process can be retrofitted in traditional anaerobic digesters by introducing a pair of electrodes with exogenous energy in the form of applied voltage (Cai et al., 2016; Y. Chen et al., 2016; Cheng et al., 2009; Choi et al., 2017). In the literature, such systems are also referred to as integrated microbial electrolysis cell-anaerobic digestion (MEC-AD) process (Cai et al., 2016; Cerrillo et al., 2018).

In recent years, there has been a growing number of studies on incorporating electro-methanogenesis in the anaerobic digestion process (Cai et al., 2016; Cerrillo et al., 2018; H. Chen et al., 2016; Choi et al., 2017; Liu et al., 2019; Park et al., 2019; Yin et al., 2019). These studies have demonstrated several benefits of catalyzing electro-methanogenesis, including better methane productivity, kinetics, and process stability over traditional digesters (Y. Chen et al., 2016; Choi et al., 2017; Park et al., 2019). A few studies also suggested that electro-methanogenesis could alleviate the inhibitory effect of high levels of toxicants and recalcitrant organics (e.g., ammonia, phenol, etc.) in feedstocks or a decline in performance during operation of digesters at a relatively lower temperature than a typical mesophilic operating temperature (37 ˚C) (Luo et al., 2016; Yu et al., 2019). The most important benefit of electro-methanogenesis is that it can alleviate the dependence on the acetoclastic methanogenesis route. In comparison with acetoclastic methanogens, relatively fast-growing electroactive bacteria enriched on the anode can more efficiently oxidize acetate and directly transfer electrons to the anode surface through extracellular electron transport (Cheng et al., 2009; D. Liu et al., 2016). Ultimately, the transferred electrons can be directly ($CO_2$ reduction to $CH_4$) or indirectly (abiotic $H_2$ production and its subsequent methanogenesis) transformed into methane gas by methanogens grown on the cathode (Cheng et al., 2009; Choi and Sang, 2016; Fu et al., 2015). Thus, electro-methanogenesis has an enormous potential to be used as an effective strategy for developing robust and high-rate

anaerobic digestion processes. Furthermore, in digesters catalyzed with electro-methanogenesis, $CH_4$ content of biogas can be as high as 80-95% due to the consumption of $CO_2$, which can significantly reduce the biogas upgrading costs (Asztalos and Kim, 2015; Baek et al., 2017; Feng et al., 2016; Kokkoli et al., 2018; Xu et al., 2014).

Although the electro-methanogenesis process is often featured as a simple process of coupling MEC with an anaerobic digester, several fundamental and engineering bottlenecks are associated with their practical application. Most importantly, a streamlined roadmap for establishing an active microbiome, process design, optimization, and scale-up has not yet been achieved (Escapa et al., 2015). Thus, the doctoral research attention is given to the electro-methanogenesis pathways, functional microbiome, essential process parameters, and strategies for developing ideal microbiome, developments of electrodes towards scale-up.

## 1.2. Scope and objectives

My doctoral thesis focuses on exploring fundamental insights into the developments of microbial electrolysis assisted anaerobic digestion (MEC-AD) for effective treatment and maximized methane recovery from organic waste. Also, it added new fundamental insights into the electro-methanogenesis, functional microbiome, essential process parameters, and strategies for developing ideal microbiome, developments of electrodes towards scale-up. The specific objectives of this dissertation were:

1. Characterization and significance of extracellular polymeric substances, reactive oxygen species, and extracellular electron transfer in methanogenic biocathode.
2. Investigation of the detrimental ratio of propionate to acetate in a microbial electrolysis cell assisted anaerobic digester.
3. Assessment of an intermittent power supply scheme to minimize electrical energy input in a microbial electrolysis cell assisted anaerobic digester.
4. Insights into intermittent over continuous energization during biomethane recovery from sewage sludge with microbial electrolysis cell assisted anaerobic digester.

## 1.3. Thesis outline

This thesis consists of seven chapters. Chapter 1 demonstrate the background of the doctoral thesis and discussing the scope and objectives of the doctoral research. Chapter 2 provides particular attention to the electro-methanogenesis pathways, functional microbiome, essential process parameters, and strategies for developing ideal microbiome, developments of electrodes towards scale-up. Chapter 3 investigated the significance of extracellular polymeric substances, reactive oxygen species, and extracellular electron transfer in methanogenic biocathode. Chapter 4 investigated the detrimental ratio of propionate to acetate in a microbial electrolysis cell assisted anaerobic digester. Chapter 5 focused on developing an intermittent power supply scheme to minimize electrical energy input in a microbial electrolysis cell assisted anaerobic digester. Chapter 6 provided insights into intermittent over continuous energization during biomethane recovery from sewage sludge with microbial electrolysis cell assisted anaerobic digester. Chapter 7 summarizes the conclusion and the recommendation of future research.

# Chapter 2

# Literature Review

*A version of this chapter was published in Bioresource technology, 289, 121738.*

## 2.1. Introduction

Anaerobic digestion (AD), which represents an attractive option for treating organic waste, produces renewable methane-rich biogas (Barua et al., 2018; Barua and Dhar, 2017; Dhar et al., 2012, 2011; Ryue et al., 2019). Fundamentally, anaerobic digestion is a multi-step complex bioprocess that consists of hydrolysis, fermentation, and methanogenesis stages (Barua and Dhar, 2017; Ma et al., 2013). In such a complex bioprocess, the kinetics of the slowest step usually determines the overall process kinetics. If the kinetics of these steps are unbalanced, intermediates (mainly short-chain fatty acids) from the fermentation of complex organics can accumulate within the digester and lead to process instability as well as lower methane yields (Ma et al., 2013; Tomei et al., 2009). Depending on the characteristics of feedstocks, either hydrolysis or methanogenesis could be rate-limiting (Ma et al., 2013; Tomei et al., 2009). In general, the AD process is limited by hydrolysis rate when digesters are fed with complex feedstocks primarily comprised of particulate organics (Tomei et al., 2009). In contrast, the methanogenesis step could also be rate-limited during digestion of readily biodegradable feedstocks or soluble organics (Tomei et al., 2009). Hence, the development of a balanced microbiome is critical in attaining stable operation and higher methane yields.

The conventional anaerobic digestion process relies on two major pathways of acetoclastic and hydrogenotrophic methanogenesis. Studies have suggested that a significant portion of methane in traditional digesters would be produced via the acetoclastic route (J. Guo et al., 2015; Shin et al., 2010). Acetoclastic methanogens are identified to grow slowly in comparison with hydrogenotrophic methanogens (doubling time 5-7 days vs. 4-8 hours), which results in the requirement of longer digestion time (Anderson et al., 2003). Particularly, due to inferior acetoclastic methanogenesis kinetics, intermediates (mainly organic acids like acetate) from biodegradation of complex organics can accumulate within the digester and lead to process

instability (He et al., 2018). Also, in comparison with hydrogenotrophic methanogens, acetoclastic methanogens are more sensitive to various environmental parameters, including pH, ammonium, and temperature (Cai et al., 2018; Jiang et al., 2018; Song et al., 2010).

In addition to traditional anaerobic digesters, bio-methane can be produced in microbial electrolysis cells (MECs) (Hirano and Matsumoto, 2018; J. Park et al., 2018c; Ren et al., 2018; Wang et al., 2015; Yu et al., 2018; Zhen et al., 2015). Compared to conventional anaerobic digestion, MECs are a relatively emerging process that uses a special type of electroactive bacteria (Logan et al., 2019; Lu and Ren, 2016). The electrons released from bacterial oxidation of simple organic matters like acetate are transferred to the anode electrode and can be transformed into target value-added products such as hydrogen gas, hydrogen peroxide, methane, etc. However, a small amount of external energy may be required to surmount the thermodynamic barrier of a cathodic reaction needed for the synthesis of a target value-added product (Cheng et al., 2015; Cheng and Logan, 2007; Ditzig et al., 2007). For instance, depending on other energy losses (e.g., mass transfer limitations), an externally applied voltage of 0.5-1.0 V is required for $H_2$ production on the cathode from a MEC fed with acetate (Cheng and Logan, 2007; Ditzig et al., 2007; Logan et al., 2008). The deployment of methanogens on the cathode can enable methane production through $CO_2$ reduction at a relatively lower energy input (Cheng et al., 2009; Siegert et al., 2015). This emerging concept of methanogenesis is called ‘electro-methanogenesis’ (Cheng et al., 2009). The electro-methanogenesis process can be retrofitted in traditional anaerobic digesters by introducing a pair of electrodes with exogenous energy in the form of applied voltage (Cai et al., 2016; Y. Chen et al., 2016; Cheng et al., 2009; Choi et al., 2017). In the literature, such systems also referred to as integrated microbial electrolysis cell-anaerobic digestion (MEC-AD) process (Cai et al., 2016; Cerrillo et al., 2018).

In recent years, there has been a growing number of studies on incorporating electro-methanogenesis in the anaerobic digestion process (Cai et al., 2016; Cerrillo et al., 2018; H. Chen et al., 2016; Choi et al., 2017; Liu et al., 2019; Park et al., 2019; Yin et al., 2019). These studies have demonstrated several benefits of catalyzing electro-methanogenesis, including better methane productivity, kinetics, and process stability over traditional digesters (Y. Chen et al., 2016; Choi et al., 2017; Park et al., 2019). A few studies also suggested that electro-methanogenesis could alleviate the inhibitory effect of high levels of toxicants and recalcitrant

organics (e.g., ammonia, phenol, etc.) in feedstocks or a decline in performance during operation of digesters at a relatively lower temperature than a typical mesophilic operating temperature (37 ˚C) (Luo et al., 2016; Yu et al., 2019). The most important benefit of electro-methanogenesis is that it can alleviate the dependence on the acetoclastic methanogenesis route. In comparison with acetoclastic methanogens, relatively fast-growing electroactive bacteria enriched on the anode can more efficiently oxidize acetate and directly transfer electrons to the anode surface through extracellular electron transport (Cheng et al., 2009; D. Liu et al., 2016). Ultimately, the transferred electrons can be directly ($CO_2$ reduction to $CH_4$) or indirectly (abiotic $H_2$ production and its subsequent methanogenesis) transformed into methane gas by methanogens grown on the cathode (Cheng et al., 2009; Choi and Sang, 2016; Fu et al., 2015). Thus, electro-methanogenesis has an enormous potential to be used as an effective strategy for developing robust and high-rate anaerobic digestion processes. Furthermore, in digesters catalyzed with electro-methanogenesis, $CH_4$ content of biogas can be as high as 80-95% due to the consumption of $CO_2$, which can significantly reduce the biogas upgrading costs (Asztalos and Kim, 2015; Baek et al., 2017; Feng et al., 2016; Kokkoli et al., 2018; Xu et al., 2014).

Although the electro-methanogenesis process is often featured as a simple process of coupling MEC with an anaerobic digester, there are still several fundamental and engineering bottlenecks associated with their practical application. Most importantly, a streamlined roadmap for establishing an active microbiome, process design, optimization, and scale-up has not yet been achieved (Escapa et al., 2015). In recent years, a significant research effort has been made to address these objectives. This article is intended to review current research advances towards developing the electro-methanogenesis process. Particular attention is given to the electro-methanogenesis pathways, functional microbiome, essential process parameters, and strategies for developing ideal microbiome, developments of electrodes towards scale-up.

### 2.2. Mechanisms of electro-methanogenesis

Figure 2.1 summarizes all possible pathways for the conversion of organic feedstocks to bio-methane in an anaerobic digester catalyzed by the electro-methanogenesis process. Compared to a conventional anaerobic digester, electro-methanogenesis can induce additional routes for methanogenesis. Like traditional anaerobic digestion, methanogenesis would still occur through

the utilization of acetate/$H_2$ produced from hydrolysis and subsequent fermentation of complex organics. In the most general sense, electroactive bacteria can be emphasized as the key player in promoting electro-methanogenesis (Feng et al., 2016; Zhao et al., 2015; Zhu et al., 2014). The anodic electroactive bacteria oxidize simple organic acids (e.g., acetate) and transfer electrons to the electrode via extracellular electron transport (EET) (Torres et al., 2010). The cathodic electro-methanogenesis occurs via two major pathways: (1) directly via electron transport to electrotrophic methanogens that are coupled with $CO_2$ reduction to $CH_4$, and (2) indirectly from $H_2$ (i.e., abiotic $H_2$ production and subsequent consumption by hydrogenotrophic methanogens) (Choi and Sang, 2016). In addition to hydrogenotrophic methanogenesis, $H_2$ can also be converted to acetate by homoacetogens, and then can be utilized by acetoclastic methanogens or by electroactive bacteria for anodic oxidation (Cheng et al., 2009; Fu et al., 2015).

As compared to the cathode potential of -0.41 V vs. standard hydrogen electrode (SHE) required for abiotic $H_2$ production, electro-methanogenesis via direct electron transport can occur at a less negative cathode potential of -0.24 V vs. SHE (Figure 2.1) (Siegert et al., 2014a). Thus, theoretically, electro-methanogenesis can occur with lower energy input than that required for abiotic $H_2$ production. Maintaining cathode potential more positive than -0.41 V vs. SHE can promote methanogenesis via direct electron transport by eliminating $H_2$ production. However, practically, more negative cathode potential is required to compensate for high electrode overpotential and internal resistance in the system, which ultimately increases the energy input for methane production (Geppert et al., 2016). Therefore, the selection of cathode materials with lower overpotential and minimizing internal resistance in the system would be required for reducing energy input for the electro-methanogenesis process. The enrichment of a balanced microbiome is also essential to realize the benefits of incorporating electro-methanogenesis in conventional digesters (Kokko et al., 2018; S. Xu et al., 2019).

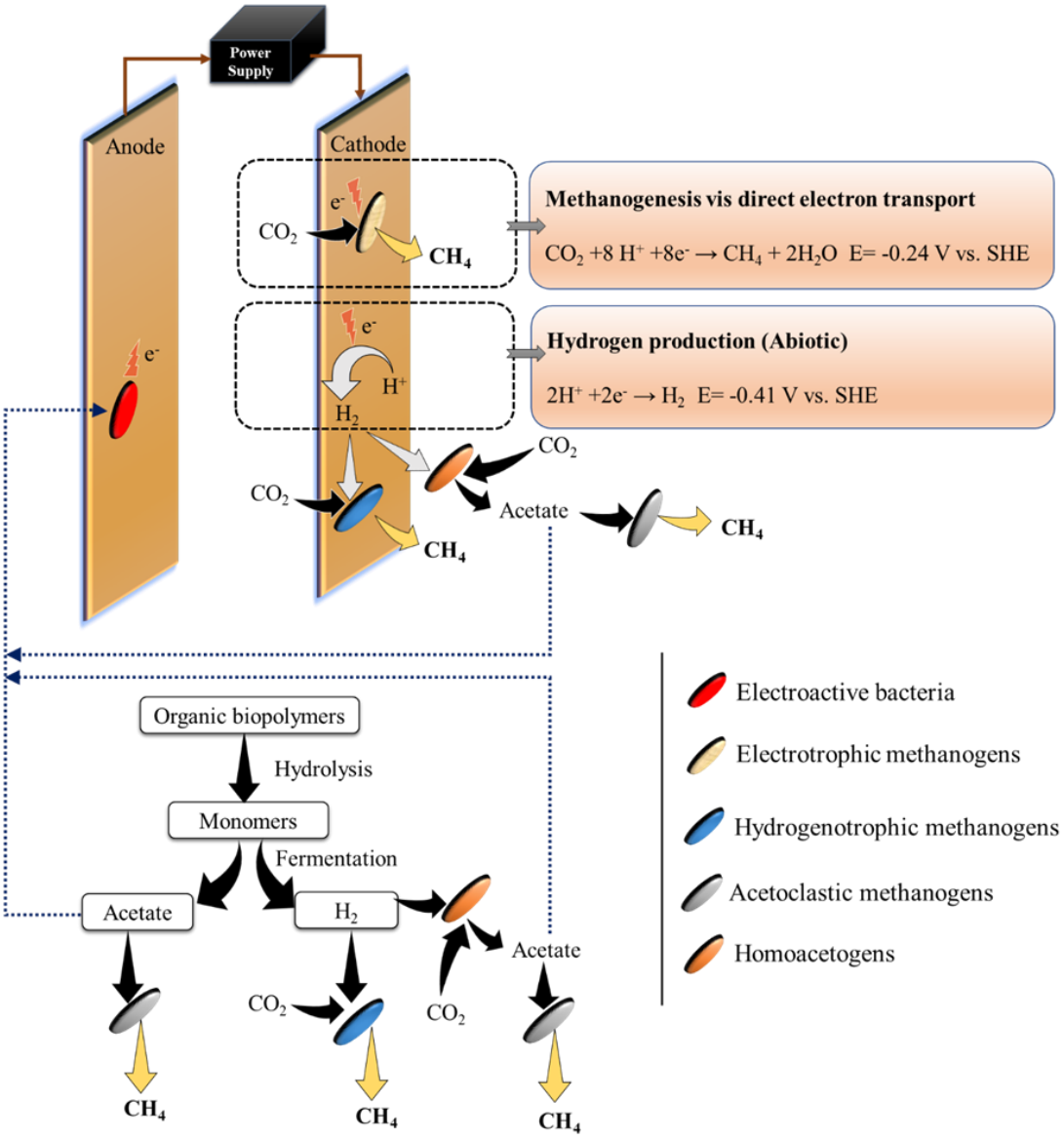


**Figure 2.1** Schematic showing various pathways for electro-methanogenesis in anaerobic digesters

## 2.3. Insights into the functional microbiome

Studies have revealed that the electro-methanogenesis process is functioned through a complex microbiome involving both suspended and attached biomass, which consists of electroactive bacteria, hydrolyzing/fermentative bacteria and methanogens (Y. Chen et al., 2016; Lee et al., 2017; Saratale et al., 2017). Thus, it is essential to characterize both suspended and the electrode attached biomass to clearly elucidate the functional roles of different microbial members and their association in facilitating electro-methanogenesis. Table 2.1 summarizes the microbial communities found in the MEC-AD process.

### *2.3.1. Bacterial community*

As shown in Table 1, only a few studies provided a comprehensive characterization of suspended and attached bacterial communities. However, these studies imply a clear pattern that electroactive and hydrolyzing/fermentative bacteria would dominate the bacterial communities. Although some electroactive bacteria can play dual roles of fermentation and EET to electrodes (Kracke et al., 2015; Lusk et al., 2015; Summers et al., 2010), it has been widely accepted that most of the electroactive bacteria are obligated to build a syntrophic partnership with other bacterial members, such as hydrolyzing/fermentative bacteria, homoacetogens (Summers et al., 2010). Consequently, for simple organic acids, electroactive *Geobacter* species were more dominant in anode biofilms (D. Liu et al., 2016; Luo et al., 2016), while complex substrates (e.g., sludge, glucose, etc.) led to a more diverse community with a higher abundance of various hydrolyzing/fermentative bacterial species, such as *Bifidobacterium* and *Levilinea* (Table 2.1). Regarding suspended bacterial communities, in most cases, different hydrolyzing/fermentative bacteria, such as *Bifidobacterium*, *Cloacamonas* and *Pseudomonas* were predominant (Table 2.1). However, interestingly, a study by Luo et al. (2018) reported dominance of *Geobacter* species in suspended communities, which could be attributed to differences in bioreactor configuration and operating conditions. *Geobacter* species have been shown to be capable of directly transferring electrons to electrotrophic methanogens, in some specific configurations of the conventional anaerobic bioreactor, including up-flow anaerobic sludge blanket (UASB) reactor (Rotaru et al., 2014a). This direct electron transfer process without electrodes is known as direct interspecies

electron transfer (DIET). The readers are referred to the literature for details (Barua et al., 2019c, 2019b; Barua and Dhar, 2017; Rotaru et al., 2014a, 2014b).

The hydrogen scavenging homoacetogens that utilize $CO_2/H_2$ to produce acetate, are often observed to be linked with fermentable substrate utilization in the various configuration of MECs (Dhar et al., 2019; D. Liu et al., 2017). With a few exceptions, there is limited evidence on the significance of homoacetogens in methane-producing MEC-AD systems. Based on an extensive literature search, a study could be found that reported enrichment of *Acetobacterium* on the cathode accompanied by enhanced methanogenesis (D. Liu et al., 2016). The abundance of hydrogenotrophic *Methanobacterium* in their study suggested the possible utilization of acetate by electroactive bacteria, rather than acetoclastic methanogens. However, the insignificance of homoacetogens is not surprising because of their thermodynamic and kinetic features. Homoacetogenesis is thermodynamically less favourable than hydrogenotrophic methanogenesis; standard Gibbs free energy (at pH 7) for hydrogenotrophic methanogenesis and homoacetogenesis are −32.68 kJ/mol of $H_2$ and −24.94 kJ/mol of $H_2$ (Junicke et al., 2016). Additionally, homoacetogens usually have a higher Michaelis–Menten constant ($K_m$) and lower maximum specific growth rate ($\mu_{max}$) than those reported for hydrogenotrophic methanogens (Peters et al., 1998).

### *2.3.2. Archaeal community*

In MEC-AD systems, methanogens can either form biofilms or present as planktonic cells (see Table 2.1). Regardless of differences in feedstocks/inoculum used, in most of the studies, hydrogenotrophic methanogens (e.g., *Methanobacterium*, *Methanospirillum*, etc.) seem to be abundant in archaeal communities (Table 2.1). Their dominance on cathodic biofilms could be attributed to high $H_2$ partial pressure due to cathodic $H_2$ evolution. Also, cathodic $H_2$ synthesis reaction could possibly lead to highly alkaline local pH which can impose free ammonia inhibition effects, as ammonium ion can move towards the cathode to maintain charge neutrality in MECs (Barua et al., 2019d, 2019a; Cerrillo et al., 2016). Previous studies also suggested a higher tolerance of hydrogenotrophic methanogens to pH disturbance and ammonia inhibition over acetoclastic methanogens (Cai et al., 2018; Song et al., 2010). For example, Cai et al. (2018) recently demonstrated that an increase in pH in the microenvironment surrounding the cathode

could significantly influence the methanogenesis rate as well as methanogenic communities in a MEC-AD reactor; *mcr*A gene sequencing revealed that hydrogenotrophic methanogens (mostly *Methanobacterium alcaliphilum*) were predominant on the cathode.

Although several studies suggested that electroactive bacteria could kinetically outcompete acetoclastic methanogens, a few studies also reported the presence of various known acetoclastic methanogens (*Methanosarcina* and *Methanosaeta* species) in cathode biofilms as well as in suspension (see Table 2.1). *Methanosarcina* is the only methanogen that can switch between acetoclastic and hydrogenotrophic methanogenesis routes, while *Methanosaeta* were known to utilize acetoclastic pathway only (Cai et al., 2016; Luo et al., 2018; J. Park et al., 2018c; Siegert et al., 2014b, 2015). Recently, both methanogenic genera have also been identified to be electrotrophic due to their ability to directly accept electrons from their syntrophic partners or conductive materials (i.e., DIET), which can be coupled with $CO_2$ reduction to methane gas (J. H. Park et al., 2018; Rotaru et al., 2014b, 2014a; Zhao et al., 2015). A few studies also revealed the presence of methanogens in anode biofilms accompanied by high methane production (De Vrieze et al., 2014; Yin et al., 2016), which also substantiate the significance of DIET in enhancing methane production from MEC-AD systems. Thus, their versatile metabolic features justify their presence either in cathode biofilms or suspension. It should be noted that most of the studies used 16S rRNA gene sequencing for the characterization of microbial communities, which provides information about the relative composition of the microbial community. However, 16S rRNA gene sequencing provides inadequate information on the metabolic features of different members in the community. Previous studies established a positive correlation between the abundance of *mcr*A genes with $CH_4$ production rate from conventional methanogenic bioassays supplemented with $H_2/CO_2$ (Cai et al., 2018; Morris et al., 2014). Recently, Cai et al. (2018) suggested that instead of 16s sequencing, *mcr*A sequencing could be a more effective tool to clarify the metabolic features of the electro-methanogenic microbiome. Other studies also reported a positive correlation between the $CH_4$ production rate and the abundance of *mcr*A gene copy numbers in the cathodic biofilms (Li et al., 2019; Siegert et al., 2015).

It seems evident that hydrogenotrophic methanogens were mostly dominant in cathode biofilms as well as in suspension. However, to date, literature provides limited information on the relative contributions of suspended and attached methanogenic communities. This fundamental

information can be translated into efficient MEC-AD system design. For instance, optimization of the cathode surface area would be an essential design factor if cathode-attached methanogenic communities primarily generate methane.

**Table 2.1** Microbial communities in single-chamber methane-producing MECs

| Inoculum | Substrate | Anode | | Cathode | | Suspension | | References |
|---|---|---|---|---|---|---|---|---|
| | | Archaeal | Bacterial | Archaeal | Bacterial | Archaeal | Bacterial | |
| **WAS** | Acetate | - | - | Hydrogenotrophic methanogens | - | - | - | (Zhao et al., 2014) |
| **AD sludge** | Molasses | - | *Peptoniphilus* | *Methanosaeta* | - | *Methanosaeta* | *Peptoniphilus* | (De Vrieze et al., 2014) |
| **UASB sludge** | Sewage sludge | - | *Methylovirgulaligni* | *Methanosarcina* | - | - | - | (Feng et al., 2015) |
| **UASB sludge** | Glucose | - | *Bifidobacterium* | *Methanobacterium* | - | *Methanobacterium* | *Bifidobacterium* | (Li et al., 2016) |
| **WAS** | WAS | - | *Levilinea* | - | - | *Methanosaeta* | *Syntrophomonas* | (Zhiqiang Zhao et al., 2016b) |
| **WAS** | Acetate | - | *Geobacter* | *Methanobacterium* | *Acetobacterium* | *Methanospirillum* | - | (W. Liu et al., 2016) |
| **WAS** | Glucose | - | - | - | - | *Methanosaeta* | - | (Zisheng Zhao et al., 2016) |
| **AD sludge** | Acetate and mixed acids | - | - | - | - | *Methanosarcina* | *Geobacter* | (Luo et al., 2018) |
| **AD sludge** | WAS | - | - | - | - | *Methanomicrobiales* | - | (Gajaraj et al., 2017) |
| **AD sludge** | Food waste | - | | - | - | *Methanosarcina* | *Clostridia* | (J. Park et al., 2018c) |
| **AD sludge** | Mixed acids (acetic acid, propionic acid and butyric acid) | - | *Geobacter* | - | - | *Methanobacterium* | - | (Luo et al., 2016) |
| **AD sludge** | Sewage sludge | - | - | - | - | - | *Cloacamonas* | (Feng et al., 2016) |
| **AD sludge** | Raw sludge | - | - | - | - | Hydrogenotrophic methanogens | *Pseudomonas* | (Y. Chen et al., 2016) |

| | | | | | | | | |
|---|---|---|---|---|---|---|---|---|
| **AD sludge** | Acetate | - | *Geobacter* | *Methanobacterium* | *Geobacter* | *Methanobacterium* | *Geobacter* & *Pseudomonas* | (Siegert et al., 2014a) |
| **Sediment from a freshwater bog** | Acetate | - | *Geobacter* | *Methanobacterium* | *Geobacter* | *Methanobacterium* | *Geobacter* | (Siegert et al., 2014a) |

## 2.4. Process optimization

### *2.4.1. Operating parameters*

In general, various extrinsic controllable parameters, including operating temperature, pH, applied voltage/potential, etc. can considerably influence the performance of MEC-AD systems. There have been considerable research emphases on optimization of these parameters. However, most of these studies were carried out with dual-chamber configurations having membranes, while findings from single chamber MEC-AD studies would provide more insights for integrating electro-methanogenesis with conventional digesters. Table 2.2 summarizes the electro-methanogenesis performance in single-chamber MEC-AD studies.

Most of the electro-methanogenesis studies considered applied voltage, in the range of 0.3-1.5 V, as a key process optimization tool (Table 2.2). For instance, Zhiqiang Zhao et al. (2016a) examined the impact of different applied voltages (0.6-1.2 V) on methane production from municipal waste activated sludge. Their results demonstrated enhanced methane productivity with the increase in applied voltage from 0.6 V (760 mL $CH_4$) to 0.8 V (884.7 mL $CH_4$), whereas a further increase in applied voltage resulted in a decrease in methane production (800 mL $CH_4$ at 1.2 V). Likewise, in the range of 0.3–1.5 V, another study found the optimum applied voltage for enhancing methane production from waste activated sludge to be 0.6 V (Y. Chen et al., 2016). Compared to the conventional anaerobic digester, at an optimum voltage of 0.6 V methane production increased by 79.6%. However, current density linearly increased from 0.37 to 2.55 $A/m^2$ with the step-wise increase in applied voltage from 0.3 to 1.5 V. Thus, these findings also revealed a non-linear relationship between applied voltage and methane productivity. Nonetheless, it was evident that an applied voltage of <1 V would be adequate to reasonably enhance methanogenesis over control reactors (H. Chen et al., 2016; Choi et al., 2017; Zhiqiang Zhao et al., 2016b, 2016a; Zisheng Zhao et al., 2016). Moreover, an applied voltage higher than 1 V (particularly 1.2-1.5 V) could adversely affect methanogenesis (H. Chen et al., 2016; Choi et al., 2017; Zhiqiang Zhao et al., 2016a), which could be attributed to the creation of the alkaline environment at higher applied voltages (Zamalloa et al., 2013). Higher voltages can lead to excessive consumption of $H^+$ to produce $H_2$ gas via abiotic cathodic reaction, which can increase pH to highly alkaline values (>8) and inhibit methanogenic activity (Y. Chen et al., 2016; Feng et

al., 2015). Furthermore, higher applied voltages could create micro-aerobic condition through anodic water electrolysis ($2H_2O \rightarrow O_2+4H^+ +4e^-$) (Y. Chen et al., 2016), which can adversely affect anaerobic microbial communities.

The optimization of set cathode potentials was also considered in several studies, while most of them were conducted in dual-chamber MEC-AD systems having abiotic anode. Most of these dual-chamber studies demonstrated an almost similar trend that a cathode potential more negative than -0.5 V vs. SHE would be required for promoting electro-methanogenesis (Van Eerten-Jansen et al., 2013; Zhen et al., 2016b). For instance, Zhen et al. (2016a) reported that methane production linearly increased with applying more negative cathode potentials in a dual-chamber MEC having hybrid graphite fiber biocathode; methane production rate increased from 6.4 to 80.9 mL/L-d when cathode potential switched from -0.9 V to -1.4 V vs. Ag/AgCl, respectively. This trend is quite expected from the fact that more negative cathode potential can provide more driving force compared to the thermodynamic equilibrium (Geppert et al., 2016; Zamalloa et al., 2013). At more negative cathode potential, anode potential may become more positive, which would be problematic in single chamber MEC-AD systems. Several studies previously reported that more positive anode potentials could adversely affect electroactive bacterial communities in anode biofilms by allowing enrichment of non-electroactive competitive bacterial communities (Dhar et al., 2016b, 2016a; Torres et al., 2009). Based on extensive literature search, a study could be found that examined the impact of different cathode potentials (-0.6, -0.8, -1.0, -1.1 V vs. Ag/AgCl) on methane production from a single chamber MEC-AD (D. Liu et al., 2017). Compared to -0.6 V vs. Ag/AgCl, more negative cathode potentials (-0.8 V and -1.0 V vs. Ag/AgCl) only marginally increased methane productivity by ~10%. However, cathode potential of -1.1 V vs. Ag/AgCl was unable to provide methane production for a prolonged period (>72 h). In contrast, a dual-chamber MEC-AD in their study showed sustainable methane production during 30 days of the total experimental period, where an optimum cathode potential was found to be -1.0 V vs. Ag/AgCl. The measurement of oxygen reduction potential (ORP) indicated $O_2$ formation through anodic water electrolysis. Authors postulated that anodic microbial consortia were inhibited due to $O_2$ generation. Also, $O_2$ diffused from anode to the cathode in a single-chamber configuration could inhibit methanogens due to the absence of membrane between two chambers.

Although previous studies mainly focused on the enhancement of methanogenesis, a few studies also shown improved hydrolysis/fermentation from MEC-AD process, indicated by the changes in volatile suspended solids (VSS), soluble chemical oxygen demand (SCOD), and volatile fatty acids (VFA) concentrations (Asztalos and Kim, 2015; Y. Chen et al., 2016; Zamalloa et al., 2013). Y. Chen et al. (2016) reported that the hydrolysis rates in waste activated sludge fed MEC-AD system operated at 0.3–0.6 V were comparable to the conventional anaerobic digester as indicated by the same VFA levels (1600 mg/L), while 1.2–1.4 V greatly enhanced hydrolysis with high VFA levels (2250-2500 mg/L). It has been suggested that micro-aerobic environment created through anodic water electrolysis could assist in the hydrolysis of particulate organics (Y. Chen et al., 2016; Zamalloa et al., 2013). Although some electroactive bacteria can facilitate their metabolic activity under microaerobic environment (Toh et al., 2011), as mentioned above, the higher applied voltage would adversely influence methanogenic activity due to micro-aerobic conditions and pH changes. A study by Feng et al. (2016) showed that increasing applied voltage from 0.3 V to 0.7 V could significantly increase the abundance of various hydrolyzing bacteria species (e.g., *Saprospiraceae*, *Fimbriimonas,* etc.) in suspended microbial communities. Thus, the enhanced hydrolysis from MEC-AD systems could be the results of multiple mechanisms.

As shown in Table 2.2, most of the electro-methanogenesis studies used mesophilic operating temperature (34-37 ˚C) possibly because conventional anaerobic digesters are mostly operated under this condition. However, a few studies suggested that MEC-AD operated at psychrophilic (or ambient) temperature could provide comparable performance with conventional mesophilic anaerobic digesters (Asztalos and Kim, 2015; W. Liu et al., 2016), which could be attributed to the effective metabolic activity of various electroactive bacteria (e.g., *Geobacter* species) under ambient temperature (Ren et al., 2017). Also, hydrogenotrophic methanogens widely identified as key methanogens in MEC-AD systems are relatively less susceptible to low temperature than acetoclastic methanogens. To date, optimization of operating temperature has received little attention. Ahn et al. (2017) examined the impact of various operating temperatures within mesophilic temperature regimes (30, 35, and 40 ˚C). In their study, increasing temperature from 30 ˚C and 40 ˚C linearly increased VSS removal efficiencies, indicating a significance of optimizing operating temperature for electro-methanogenesis. However, maximum methane yield and current density were obtained at 35 ˚C. Authors suggested that some electroactive bacteria

might be inhibited at 40 ˚C, which ultimately affected methane productivity. Thus, optimization of operating temperature would be essential to balance the activity of microbes involved in various biochemical steps, including hydrolysis, fermentation, anodic respiration, and methanogenesis.

### *2.4.2. Development of start-up strategy*

The development of an effective method for a quick and reliable start-up would a key-step for commercialization of MEC-AD process. The time required for the start-up of MECs can be considerably longer depending on various factors, such as operating conditions and inoculum selection. These factors can considerably influence the enrichment and acclimation of a balanced microbiome with maximum activity. However, effective methods to establish electro-methanogenic microbiome have not been well studied for MEC-AD. A few recent studies suggested setting a cathode potential more negative than the potential required for abiotic $H_2$ production (i.e., -0.41 V vs. SHE) for an effective selection of active methanogens (Siegert et al., 2014a). As discussed previously, it was evident that the operation of single-chamber MEC-AD under controlled cathode potential would be technically unfeasible. Perhaps enriching methanogenic microbiome in a dual-chamber reactor under optimum cathode potential and then transferring to a single chamber (i.e., conventional digester) reactor operated under applied voltage would be a viable approach which is yet to be investigated. Nonetheless, the control of working electrode potential is not a practical approach for large-scale reactors due to the heterogeneous distribution of applied potential within a large electrode (Jiang and Zeng, 2018). Also, the inoculation of a large-scale system would require a substantial amount of inoculum. Overall, the enrichment of a significant amount of inoculum for large-scale reactor using a potentiostat would be challenging.

Besides operating condition, inoculum selection is also essential to provide rapid start-up of MEC-AD systems. To date, a few studies attempted to compare various inoculum sources for MEC-AD systems. Siegert et al. (2014b) compared two inoculum sources: (1) anaerobic digester sludge dominated by acetoclastic *Methanosaeta*, and (2) anaerobic bog sediment enriched with $H_2$-utilizing methanogens. The MEC inoculated with bog inoculum showed superior methane production rate. Microbial community analysis targeting 16s rRNA gene identified the hydrogenotrophic genera *Methanobacterium* and *Methanobrevibacter* as the key methanogens in

MECs, and their presence in the inoculum significantly influenced the methanogenesis kinetics. A recent study by Cerrillo et al. (2017) also compared two different inoculum sources: (1) a mixture of biomass from a MEC and granular sludge from a full-scale anaerobic digester, and (2) granular sludge from an UASB reactor fed with methanol. Interestingly, both inoculums showed comparable performance regarding methanogenesis rate, and hydrogenotrophic methanogens mostly dominated archaeal community. Thus, one possibility for developing high-rate electro-methanogenic digester would be the use of inoculum pre-enriched with hydrogenotrophic methanogens. Dykstra and Pavlostathis (2017) suggested that mixed culture digester sludge could be further acclimatized with $H_2/CO_2$ to pre-enrich hydrogenotrophic methanogens and thereby improve methane production from MEC-AD. Another approach suggested in the literature to shorten the start-up time of MEC-AD systems is the deployment of pre-acclimated electrode materials (De Vrieze et al., 2014; R. Xu et al., 2019). For instance, De Vrieze et al. (2014) reported that retrofitting pre-inoculated electrode in a failed digester could lead to immediate recovery of methanogenic activity.

**Table 2.2** Summary of electro-methanogenesis studies conducted with single-chamber MECs

| Volume (L) | Electrodes | | Applied Voltage (V) | Temperature (°C) | Operating Mode | Inoculum | Substrate (gCOD/L) | Max. $CH_4$ production/ yield/rate | Max. Current | References |
|---|---|---|---|---|---|---|---|---|---|---|
| | Anode | Cathode | | | | | | | | |
| 0.8 | Carbon felt | Carbon felt | 0.5 | 34 | Fed batch | Anaerobic sludge of municipal sludge digester (10 g/L) | Molasses (44.7 g/L) | 65.5 mL/L/d | 3.36 $A/m^2$ | (De Vrieze et al., 2014) |
| 0.08 | Carbon felt | Carbon felt | 1 | 34 | Fed batch | Anaerobic sludge of municipal sludge digester (10 g/L) | Molasses (44.7 g/L) | 127.5 mL/L/d | 6.78 $A/m^2$ | (De Vrieze et al., 2014) |
| 0.25 | Plain carbon cloth | Plain carbon cloth | 0.4, 0.7, 0.8 | 55 | Fed batch | Thermophilic anode MFC effluent | Acetate (COD 0.8 g/L) | 1103 $mmol/m^2/d$ at 0.8 V | NA | (Fu et al., 2015) |
| 0.18 | Carbon fiber brushes | Stainless-steel mesh | 1.2 | 22.5 | Continuous fed-batch | Digested sludge + Waste activated sludge | Waste activated sludge (VSS, 5.20 g/L, COD 7.89 g/L) | 25.6 mL/d | 15-25 $A/m^3$ | (Asztalos and Kim, 2015) |
| 0.5 | Graphite brush | Graphite rod | 0.6 | 37 | Fed batch | Anaerobic sludge from waste sludge treatment plant (VSS 43 g/L) | Waste activated sludge (VSS 41 g/L) | 2998.4 ml | 0.35 $A/m^2$ | (Zhao et al., 2015) |

| | | | | | | | | | | |
|---|---|---|---|---|---|---|---|---|---|---|
| 2 | Pair of Fe tube | Graphite pillar | 0.3, 0.6 | 35 | Fed batch | Sludge of UASB reactor (TCOD 50 g/l) | Raw sludge (TCOD 114.2 g/L) | 170.2 L/Kg VSS at 0.3 V | 4.3 $A/m^3$ | (Feng et al., 2015) |
| 1 | Graphite rod | Graphite rod | 1 | 35 | Semi-continuous | Sludge of UASB reactor (VSS 11.52 g/L) | Glucose (COD 7 g/L) | 248 mL/h | 51 $A/m^2$ | (Li et al., 2016) |
| 0.75 | Graphite fiber | Graphite fiber | 0.3 V | 35 | Semi-batch | Anaerobic digester of sewage sludge | Glucose (COD 3 g/L) | 322.9 mL/g COD | 2.65 mA | (Feng and Song, 2016) |
| 12 | Graphite fiber | Graphite fiber | 0.3, 0.5, 0.7 | 25 | Batch | Activated Sludge from mesophilic MEC-AD | Sewage sludge (TCOD 32-47 g/L) | 370 mL/L.d at 0.3 V | 392 $mA/m^3$ at 0.7 V | (Feng et al., 2016) |
| 4 | Carbon felt tube | Graphite pillar | 0.6 | 35 | Fed batch | Waste sludge | Waste activated sludge (VSS, 30 g/L, TSS, 45 g/L) | 1363.4 mL | 0.1 $A/m^2$ | (Zisheng Zhao et al., 2016) |
| 0.5 | Graphite brush | Graphite rod | 0.8 | 37 | Continuous | Waste sludge | Waste activated sludge (VSS, 28 g/L, TSS, 101 g/L) | 884.7 mL | 0.0134 $A/m^2$ | (Zhiqiang Zhao et al., 2016b) |
| 0.5 | Graphite brush | Graphite rod | 0.6, 0.8, 1, 1.2 | 37 | Fed batch | Waste sludge | Waste activated sludge (VSS, 28 | 884.7 mL at 0.8 V | 0.088 $A/m^2$ at 1.2 V | (Zhiqiang Zhao et al., 2016b) |

| | | | | | | | | | | |
|---|---|---|---|---|---|---|---|---|---|---|
| | | | | | | | g/L, TSS, 101 g/L) | | | |
| 0.225 | Graphite felt | Carbon paper | 0.5 | 35 | Fed batch | Anaerobic sludge of sewage sludge digester | Mixed acids (Acetic, propionic & butyric acid, each 0.5 g/L) | 84 mL | N/A | (Luo et al., 2016) |
| 0.23 | Carbon felt | Stainless-steel | 1 | 25 | Fed batch | Waste activated sludge | Acetate (COD 10 g/L) | 225.5 mL/g COD | 166.7 $A/m^3$ | (Yin et al., 2016) |
| 0.23 | Carbon felt | Stainless-steel | 1 | 25 | Fed batch | WAS + Anode MEC effluent | Acetate (COD 10 g/L) | 272 mL/g COD | 304 $A/m^3$ | (Yin et al., 2016) |
| 0.23 | Carbon felt | Stainless-steel | 1 | 25 | Fed batch | WAS + Anode MEC effluent + *Methanosarcina* | Acetate (10 COD g/L) | 360 mL/g COD | 304 $A/m^3$ | (Yin et al., 2016) |
| 0.7 | Graphite fiber brush | Stacked of 2 layers stainless-steel mesh | 0.5, 0.7, 0.9 | 35 | Fed batch | Activated sludge | Artificial beer brewery wastewater (COD 1 g/L) | 100 mL/g COD at 0.9 V | 8.4 mA at 0.9 V | (Guo et al., 2017a) |
| 0.7 | Graphite fiber brush | Stacked of 5 layers stainless-steel mesh | 0.5, 0.7, 0.9 | 35 | Fed batch | Activated sludge | Artificial beer brewery wastewater (COD 1 g/L) | 145 mL/g COD at 0.9 V | 12.9 mA at 0.9 V | (Guo et al., 2017a) |

| | | | | | | | | | | |
|---|---|---|---|---|---|---|---|---|---|---|
| 0.7 | Graphite fiber brush | Stacked of 8 layers stainless-steel mesh | 0.5, 0.7, 0.9 | 35 | Fed batch | Activated sludge | Artificial beer brewery wastewater (COD 1 g/L) | 260 mL/g COD at 0.9 V | 12.6 mA at 0.9 V | (Guo et al., 2017a) |
| 1 | Activated carbon fiber textile | Activated carbon fiber textile | 0.3-1.5 | 35 | Fed batch | Activated sludge | Raw sludge (VS 29.7 g/L, COD 685 g/L) | 140.9 L/kg VS at 0.6 V | 2.55 $A/m^2$ at 1.2 V | (Y. Chen et al., 2016) |
| 0.8 | Pair of $Ti/RuO_2$ mesh plates | Pair of $Ti/RuO_2$ mesh plates | 0.4, 0.6, 0.8, 1 | 35 | Semi-continuous | Mesophilic kitchen waste (VS 6.3 g/L, TS 11 g/L) | *E. densa* harvested from domestic wastewater & lake water (TS 50 g/L) | 248 mL/L.d at 1 V | 8.9 mA at 0.8 V | (Zhen et al., 2016a) |
| 0.5 | Graphite brush | Carbon cloth | 0.8 | 23 | Fed batch | Waste activated sludge | Waste activated sludge (VSS 14 g/L, TSS 20 g/L) | 138 mL/L reactor.d | 11.8 mA | (W. Liu et al., 2016) |
| 0.5 | Graphite brush | Graphite rod | 0.6 | 37 | Fed batch | Anaerobic inoculum sludge (VSS 28 g/L, TSS 77 g/L) | Waste activated sludge (VSS 43 g/L, TSS 101 g/L) | 230 mL/d | NA | (Zhiqiang Zhao et al., 2016a) |

| | | | | | | | | | | |
|---|---|---|---|---|---|---|---|---|---|---|
| 0.8 | Reticulated vitreous carbon | Reticulated vitreous carbon | 0.3, 0.6 | 35 | Fed batch | Mesophilic digested sludge of (COD 3 g/L) | Glucose (COD 1 g/L) | 0.011 L/L.d at 0.3 V | 0.122 $A/m^2$ at 0.6 V | (Gajaraj et al., 2017) |
| 0.8 | Reticulated vitreous carbon | Reticulated vitreous carbon | 0.3, 0.6 | 35 | Fed batch | Mesophilic digested sludge of (COD 3 g/L) | Waste activated sludge (COD 10 g/L) | 0.020 L/L.d at 0.3 & 0.6 V | 0.067 $A/m^2$ at 0.3 V | (Gajaraj et al., 2017) |
| 0.27 | Carbon fiber brush | Carbon fiber brush | 0.5, 0.7, 1, 1.5 | 35 | Batch | Anaerobic digestion effluent (VSS 13 g/L, TSS 18 g/L) | Glucose (COD 2 g/L) | 408 mL/g COD at 1 V | 19.04 $A/m^3$ at 1 V | (Choi et al., 2017) |
| 2.5 | graphite felt | graphite felt | 0.3 | 30-40 | Fed batch | Sewage sludge of MEC effluent | Raw sludge (VSS 17.1 g/L, TCOD 29.2 g/L) | 1.11 $m^3/m^3$ at 35 ˚C | 1.63 $A/m^3$ at 35 ˚C | (Ahn et al., 2017) |
| 20 | Graphite carbon mesh | Graphite carbon mesh | 0.3 | 35 | SBR | Anaerobic digestion effluent of food waste | Food waste (TCOD 60.3 g/L) | 17 L/d | N/A | (J. Park et al., 2018c) |
| 1 | Graphite rod | Graphite rod | $E_{anode}$ - 0.25, - 0.3, - 0.35, - 0.4 V vs Ag/AgCl | 25 | Continuous | Aerobic activated sludge of municipal sewage plant (VSS 12 g/L, TSS 17 g/L) | Acetate (COD 3 g/L) | 77.7 mL/h at -0.25 V vs Ag/AgCl | 0.47 A at -0.25 V vs Ag/AgCl | (Zhao et al., 2014) |

| | | | | | | | | | | |
|---|---|---|---|---|---|---|---|---|---|---|
| 0.35 | Graphite rod | Graphite rod | $E_{cathode}$ - 0.8, -1, -1.2 V vs Ag/AgCl | 55 | Fed batch | Thermophilic anaerobic sludge | Glucose (1560 mmol $e^-$) | 0.6 L/L/d at -1 V vs Ag/AgCl | -20 mA at -1.2 V vs Ag/AgCl | (S. Y. Liu et al., 2017) |

## 2.5. System design and scale-up considerations

### *2.5.1. Electrode materials*

As shown in Table 2.2, carbon-based electrodes have been a popular choice as cathode material for electro-methanogenesis studies, while only a few studies used metal-based cathode. It is not possible to systematically compare and comment on a superior cathode material for electro-methanogenesis, as most of these studies used different system configuration, feedstock, inoculum, and operating conditions. However, a few systematic studies on the comparison of various electrode materials under identical operating condition suggested that careful selection of cathode materials would be essential to reduce cathodic overpotential and attain a reasonable methane production rate (D. Liu et al., 2018; Siegert et al., 2014a; Zhen et al., 2016b). Electrode materials having high overpotentials may lead to inferior electron transfer activity and thereby increase energy input (Guo et al., 2017a; Pinto et al., 2011). As mentioned previously, electro-methanogenesis via $CO_2$ reduction under standard condition can occur via direct electron transfer at a potential of -0.240 V vs. SHE, or via $H_2$ consumption via hydrogenotrophic methanogenesis at a potential of -0.410 V vs. SHE. However, more negative cathode potential (e.g., -0.5 V vs. SHE) is usually required to compensate for large electrode overpotential (Siegert et al., 2014a; Zhen et al., 2016b), which ultimately increase the overall energy input for methane production. Zhen et al. (2016b) found that modification of plain carbon stick with a layer of graphite felt could potentially reduce the overpotential of carbon stick via serving as 'artificial pili' for electron transport between methanogen and cathode electrode. Another study by D. Liu et al. (2018) exhibited that deployment of granular activated carbon (GAC) as methanogenic biocathode could lead to methane production at cathode potential of -0.52 V vs. Ag/AgCl (-0.32 Vs. SHE) accompanied by undetectable $H_2$ production, suggesting that GAC can be an attractive cathode material for designing MEC-AD systems.

### *2.5.2. Surface chemistry of electrodes*

Surface chemistry of electrode materials can significantly influence the bio-electroactivity of microorganisms. Most importantly, surface chemistry can play a crucial role in both direct or indirect electron transfer mechanisms by impacting electrode-microbe interactions (K. Guo et al.,

2015; S. Y. Liu et al., 2017; Siegert et al., 2015; Zhang et al., 2013; Zhen et al., 2018). Recently, there has been rising interest on surface modification of electrode materials with nanomaterials and metal catalysts (e.g., carbon nanotube, graphene, iron nanoparticles, etc.) and thereby tailoring various physical and electrochemical properties, including surface area, surface charge, electrical conductivity, biocompatibility (Feng and Song, 2016; Siegert et al., 2015; Tang et al., 2015; Zhang et al., 2013; Zhen et al., 2018). For instance, heat treatment could lead to the formation of 3D iron oxide nanoparticles on the surface of stainless-steel electrode, which provided elevated surface area and biocompatibility for robust biofilm formation on the cathode (K. Guo et al., 2015; S. Y. Liu et al., 2017). Also, the modification of cathode electrode with chitosan and cyanuric chloride to provide positively charged surface has been suggested to improve microbe-electrode interaction (Zhang et al., 2013), as positively charged surface can enhance adhesion of negatively charged microbial cells (K. Guo et al., 2015). However, limited efforts have been devoted to the optimization of these electrode materials for electro-methanogenesis (Guo et al., 2017a; D. Liu et al., 2018; Saheb-Alam et al., 2018). S. Y. Liu et al. (2017) demonstrated that heat treatment of stainless steel felt cathode could increase methane production rate by 1.4 times compared with the untreated stainless steel felt at cathode potential of -1.3 V, while minor enhancement in methane production rates was observed when the cathode potential was fixed at -1.1 V. Thus, more research is needed to better optimize cathode materials, particularly with regards to applied voltage/potential.

### *2.5.3. Electrode surface area*

The electrode surface area is directly related to the required reactor volume, which is one of the essential considerations in scale-up or commercialization of any microbial electrochemical systems. Theoretically, increasing electrode surface area can reduce the overpotential and thereby should increase the electrochemical efficiency of the corresponding electrode (Call et al., 2009; Selembo et al., 2010; Siegert et al., 2014b). Although optimization of the specific surface area of the anode has been extensively investigated for improving the current density of microbial electrochemical systems, very few studies attempted to optimize electrode surface area for MEC-AD. Guo et al. (2017a) examined the effect of different ratios of cathode surface areas to the spatial volume of the anode (1, 2.5 and 4 $cm^2/cm^3$) on electro-methanogenesis performance, where the

spacing between anode and cathode module was fixed at 3 cm. Interestingly, increasing cathode/anode ratio did not affect methane generation rate at a lower applied voltage of 0.5 V, while methane production rate gradually increased with increasing cathode/anode ratio at a higher applied voltage (0.7-0.9 V). However, COD removal efficiencies remained almost constant at different conditions, emphasizing that the inferior cathodic reaction mainly limited methane yield when the cathode surface area was inadequate to enable retention of methanogenic biomass. A study by De Vrieze et al. (2014) also revealed that the primary mechanism behind the enhancement of electro-methanogenesis was the retention of methanogenic biomass on the electrode; however, their study suggested that the role of applied potential would have little effect in enhancing the methane production rate. Nonetheless, these studies emphasized that high cathode surface area would be required to drive methane production rates from electro-assisted digesters reasonably.

### *2.5.4. Electrode spacing*

Another critical design parameter that can influence the performance of a microbial electrochemical system is the spacing between the anode and cathode electrodes (Call et al., 2009; Park et al., 2017). Several studies revealed that reducing the distance between anode and cathode electrodes can significantly reduce the internal resistance by improving ionic diffusion rates in microbial electrochemical systems (Liang et al., 2011; Yao et al., 2014; X. Zhang et al., 2009). Like electrode materials and specific surface areas, only a few studies investigated the effect of electrode spacing on electro-methanogenesis kinetics (Im et al., 2015; Park et al., 2017; Rader and Logan, 2010). Park et al. (2017) reported a 51% decrease in methane production with increasing the spacing between the anode and cathode electrodes from 1 cm to 5 cm at a fixed applied voltage of 0.3 V, likely attributed to the elevated internal resistance in the system which accompanied by inferior protons transport from anode to the cathode chamber. Additionally, computational fluid dynamics (CFD) modelling in their study suggested that mixing velocity can alleviate the internal resistance at higher electrode distance, and considerably increase the methane production rate. Thus, it was evident that the development of electrode materials must coincide with the optimization of electrode spacing.

Furthermore, the shape and orientation of electrode materials would be an essential consideration in the selection of electrode spacing. Recently, a comprehensive review

by Kariyama et al. (2018) suggested that a mixing strategy can significantly influence performance (i.e., energy recovery efficiency) of conventional anaerobic digesters; intermittent mixing has been identified to be enough for optimum digester performance. Therefore, further understanding of the role of various mixing strategies (i.e., mode and intensity) would be essential to provide an optimum hydrodynamic condition for biofilms as well as improving net energy efficiency in MEC-AD systems.

## 2.6. Research gaps and outlook

Small- and medium-sized AD projects are usually perceived as economically unattractive due to high capital costs and longer payback periods. In recent years, many countries have implemented financial incentives for biogas-based electricity production. Therefore, the overall acceptance of the anaerobic digestion process considerably increased. In this regard, if AD process performance can be enhanced through electro-methanogenesis, the economic and environmental benefit of AD projects will be very attractive. The adoption of MEC-AD has the potential to offer high-quality biogas due to the reduction of $CO_2$ to $CH_4$ gas, which can reduce the biogas upgrading cost. Moreover, retrofitting MEC would be a pragmatic solution to increase the capacity of existing AD facility, which will ultimately help to balance population growth and sustainable waste management. The MEC-AD systems have been studied for about 10 years. Like other microbial electrochemical technologies, technology readiness level of MEC-AD is still low. While significant research progresses have been made in terms of fundamental understanding and process development at bench-scale, numerous challenges still need to be addressed. Although most of the MEC-AD studies reported improved methane yields and organics (COD and VSS) removal efficiencies over conventional, it is not possible to systematically compare their performance due to differences in system configuration, feedstock, inoculum, and other operating parameters. Figure 2.2 summarizes the major research gaps identified by this review. The complex interactions between process configuration/parameters (e.g., electrode, applied voltage, temperature, etc.) and functional microbiome has still not been completely understood. Several strategies have been suggested for acclimation of the inoculum to promote faster start-up, while inoculation efficiencies of these methods should be methodically compared. Furthermore, for commercialization, a significant effort will be needed to develop a scalable process design/configuration which include

multiple aspects, such as electrode materials, surface area, surface chemistry, and spacing. Also, it is evident that process conditions (i.e., applied voltage) has a complex influence on the optimum electrode configuration. To date, majority of studies explored these aspects individually. Thus, further studies would be needed to systematically combine these aspects.

To date, there have been limited studies on techno-economic assessment on MEC-AD systems. Recently, Beegle and Borole (2017) compared the economic efficiency of waste valorization through integrated MEC-AD process. They found that integrated process has more potential to of higher energy efficiency and economic benefits than AD or MEC alone. Among various key variables, energy efficiency, biodegradability and sales price of biogas have shown to have more impact on 20-year net present value (NPV), while other variables like capital cost, O&M costs, and organic loading rate had minor effects. The improvement of energy efficiency would require more understanding of fundamentals and effective system design, while biodegradability of complex feedstocks can be enhanced through pre-treatment. Nonetheless, most of the economic feasibility studies on various microbial electrochemical technologies are primarily based on lab-scale results. Therefore, comprehensive techno-economic analysis and life-cycle assessments based on pilot-scale MEC-AD systems are warranted.

## 2.7. Conclusions

A state-of-art review of electro-methanogenesis with a focus on fundamentals, process optimization, and scale-up considerations was conducted. Electro-methanogenesis is still in the embryonic stage in terms of commercial readiness but is expected to be an attractive option to enhance the efficiency of conventional anaerobic digestion. The major challenges in applying electro-methanogenesis include inadequate understanding of interrelationships between system components and process parameters as well as their complex interactions with the functional microbiome and process performance. Future research should consider bridging these aspects along with comprehensive economic assessment to pave a roadmap for engineering MEC-AD process as a next-generation biogas technology.

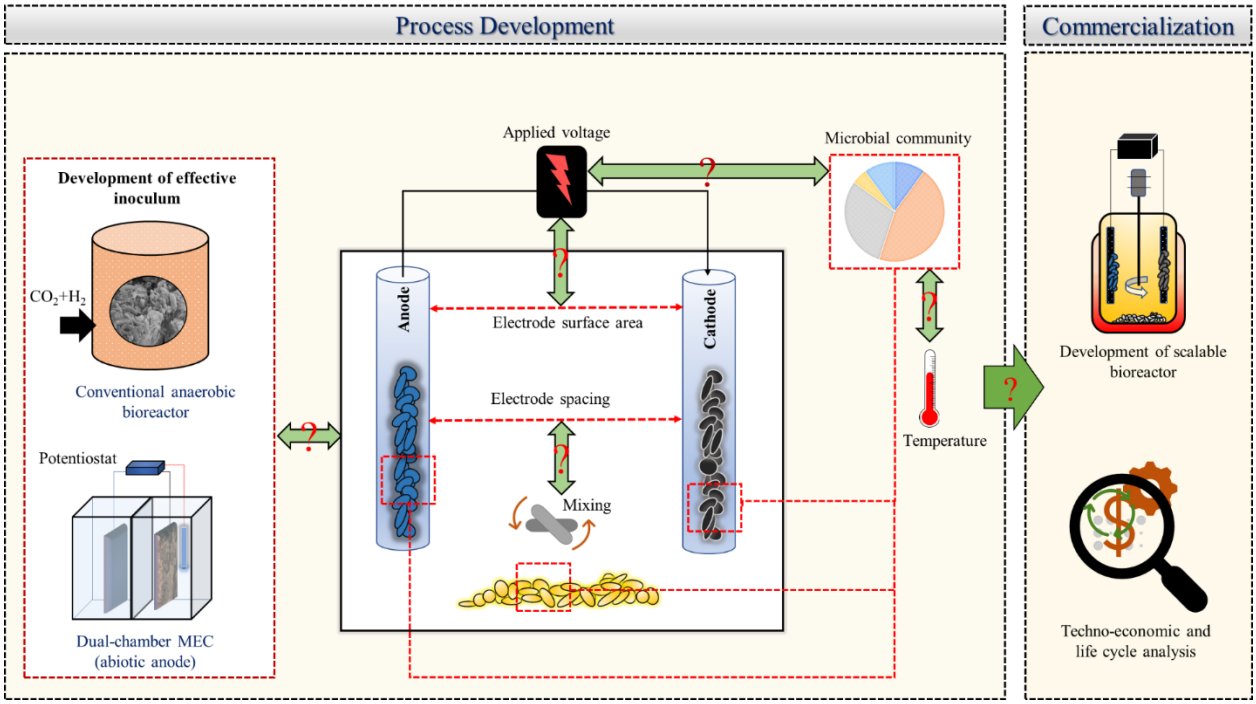


**Figure 2.2** A roadmap for developing MEC-AD process. Question marks denote the research gaps

# Chapter 3

# Characterization and significance of extracellular polymeric substances, reactive oxygen species, and extracellular electron transfer in methanogenic biocathode

*A version of this chapter was published in Scientific Reports, vol. 11, 7933.*

## 3.1. Introduction

The concept of electro-methanogenesis by combining the microbial electrolysis cell (MEC) and anaerobic digestion (AD) has become a promising method for process intensification and improving the stability of digesters (Choi et al., 2017; Huang et al., 2020; J. Park et al., 2018c; Zakaria et al., 2020; Zakaria and Dhar, 2021a). The integrated process is called microbial electrolysis cell assisted anaerobic digester (MEC-AD). In MEC-AD systems, methane can be produced via multiple pathways, such as (1) direct electron transfer from the cathode to electrotrophic methanogens coupled with $CO_2$ reduction to methane, and (2) hydrogenotrophic methanogenesis of $H_2$ produced via cathodic hydrogen evolution reaction (HER) (Huang et al., 2020; Villano et al., 2010; Zakaria et al., 2020; Zakaria and Dhar, 2019). Moreover, methane can also be produced via direct interspecies electron transfer (DIET) between electroactive bacteria (EAB) and electrotrophic methanogens in cathode and anode electrodes (Siegert et al., 2015, 2014a; Zakaria and Dhar, 2019). Nonetheless, a considerable portion of methane would still be generated via conventional acetoclastic and hydrogenotrophic methanogenesis pathways.

The activity of anodic EAB was identified as one of the key factors for boosting the methanogenesis process in MEC-AD systems. EAB can outcompete acetoclastic methanogens due to faster growth kinetics (Cheng et al., 2009), and divert electrons from acetate to anode via extracellular electron transport (EET). The transferred electrons can be utilized for hydrogen production via a cathodic HER. Thus, fast-growing hydrogenotrophic archaea can be augmented on the biocathode. Several studies reported enrichment of known hydrogenotrophic methanogens, such as *Methanobacterium* and *Methanobrevibacter* in the biocathode (Cheng et al., 2009; Dykstra and Pavlostathis, 2017; Siegert et al., 2015, 2014a). Thus, MEC-AD can provide faster

methanogenesis rates compared to conventional anaerobic digesters. Furthermore, MEC-AD systems could provide better process stability due to the faster utilization of volatile fatty acids (VFAs) by EAB (Cheng et al., 2009; D. Liu et al., 2016). The accumulation of VFAs has been widely reported as a critical factor influencing failure or process instability of digesters operated at high organic loading rates (He et al., 2018; Ma et al., 2013; Tomei et al., 2009). A few studies also suggested that MEC-AD systems could provide better resilience to inhibitory compounds (e.g., phenol, ammonia, etc.) and decline of digester performance at lower temperatures (Luo et al., 2016; Yu et al., 2019). Thus, MEC-AD systems can provide numerous benefits over conventional AD.

Despite significant research efforts towards developing MEC-AD systems, studies exploring the significance of extracellular polymeric substance (EPS) in biocathode are limited. Biofilm EPS can have many functions, including attachment of cells to solid surfaces, maturation of biofilm structures, and protection of cells from harsh environmental conditions (Xiao et al., 2017; Zakaria and Dhar, 2020; Zhang et al., 2011). A few recent studies validated the significance of EPS in EET within electroactive anode biofilms (Rollefson et al., 2011; Tan et al., 2019; Tian et al., 2019; Xiao et al., 2017). In general, EPSs are composed of proteins, extracellular DNA (eDNA), humic acids, polysaccharides, etc., that are secreted by microbes in pure and mixed cultures (Xiao et al., 2017; Zakaria and Dhar, 2020). Notably, humic acids, eDNA, and heme-binding proteins showed redox properties, serving as immobilized electron carriers in electroactive biofilms (Rollefson et al., 2011; Tan et al., 2019; Xiao et al., 2017). Interestingly, EPS extracted from anaerobic digesters also exhibited redox properties and identified as an essential route for DIET between syntrophic bacteria and methanogens (Ye et al., 2018; Yu, 2020). As direct electron transport from the cathode-to-methanogen and bacteria-to-methanogens can promote electro-methanogenesis in the biocathode, it can be assumed that biocathode EPS can potentially be linked with MEC-AD performance. However, to the best of the authors' knowledge, reports on biocathode EPS characteristics and expressions of EET genes in MEC-AD systems are still scarce.

The optimization of applied voltage/potential and inoculation method has been broadly investigated to enrich a syntrophically balanced microbiome for MEC-AD systems (Villano et al., 2016; Zakaria and Dhar, 2021a). Previous studies also substantiated the importance of persuasive system design (Guo et al., 2017b; Ma et al., 2017; Noori et al., 2020). Particularly, cathode

materials with low overpotential, large surface area, and good conductive properties were found to play a deterministic role in MEC-AD performance (Choi et al., 2017; De Vrieze et al., 2014; D. Liu et al., 2017; W. Liu et al., 2016). Carbon-based electrodes, such as carbon fiber, carbon cloth, and carbon brush, have been mostly employed in previous studies due to their high surface area and biocompatibility properties (Choi et al., 2017; De Vrieze et al., 2014; W. Liu et al., 2016). Furthermore, low-cost 3D porous carbon-based composite materials have been developed for the efficient growth of biofilms (Bian et al., 2018; Singh et al., 2021, 2018). However, carbon-based electrodes provide slow catalysis for cathodic HER, which seems to be critical for enriching hydrogenotrophic methanogens (Kim et al., 2017; W. Liu et al., 2016; J. Park et al., 2018c). Some previous studies employed metal catalysts (e.g., nickel, platinum, etc.) on carbon electrodes to accelerate HER (Kim et al., 2017; W. Liu et al., 2016; J. Park et al., 2018c), while these catalysts are still expensive. In contrast, non-precious metal electrodes, such as stainless steel, have shown an excellent low-cost alternative (Call et al., 2009; Dykstra and Pavlostathis, 2017; D. Liu et al., 2017; J. Park et al., 2018b; Wang et al., 2016). However, to date, limited information is available on how carbon and metal-based electrodes shape biocathode structures in terms of EPS, expression of EET genes, and microbial communities.

Considering the research gaps mentioned above, the main goal of this study was to provide fundamental insights into the EPS characteristics and EET genes in methanogenic biocathode. The novelty of this study is two folds. First, this study presents, for the first time, a comprehensive characterization and significance of EPS and expression of EET genes for methanogenic biocathode. Second, underlying mechanisms of methanogenesis performance with carbon and metal cathodes were evaluated with a multifaceted approach combining molecular biology, microscopic and electrochemical tools.

## 3.2. Materials and methods

### *3.2.1. Experiment*

Two single chamber MEC-AD systems (working volume of 360 mL), constructed with plexiglass, were used in this experiment. Carbon fibers (2293-A, 24A, Fibre Glast Development Corp., Ohio, USA) fixed onto a stainless-steel frame (which was not exposed to the liquid medium)

was used as an anode electrode in both reactors. A similar carbon fiber module was used as a cathode electrode in one reactor (referred to as 'CF-CF'), and a stainless-steel mesh (304 stainless steel, McMASTER-CARR, USA) was used as a cathode in the other reactor (referred to as 'CF-SS'). The specific surface area provided by the stainless-steel electrode was 4.2 $m^2/m^3$. Considering every single filament in the carbon fiber bundle (**Error! Not a valid bookmark self-reference.**), the specific surface area of the carbon fibers module was estimated at 3609 $m^2/m^3$. Moreover, considering all filaments in a bundle as a single fiber, the surface area was estimated at 41 $m^2/m^3$. The detailed calculation of the specific surface areas is provided in the Supplementary Information. The Ag/AgCl reference electrode (MF-2052, Bioanalytical System Inc., USA) was positioned close (<1 cm) to the anode electrode.

Both reactors were inoculated with mesophilic anaerobic digester sludge and effluent from a dual-chamber mother MEC operated with sodium acetate as an electron donor for >12 months. Initially, sodium acetate (1600±55 mg COD/L) supplemented phosphate buffer (50 mM) and trace minerals were used as a substrate. The details of the trace minerals can be found elsewhere (Zakaria and Dhar, 2021a). Both reactors were operated with acetate in fed-batch mode until peak current densities reached ~77 $A/m^3$. Then, the substrate was switched to glucose (2150±31 mg COD/L), while buffer and trace minerals composition remained the same. With glucose, reactors were operated for about six months under batch mode in repetitive cycles. The biogas produced from the reactors were collected in gasbags. A decrease in daily methane production to <3 mL was considered an indicator for replacing the substrate medium. During experiments, the anode potential was fixed at -0.4 vs. Ag/AgCl with a potentiostat (Squidstat Prime, Admiral Instruments, Arizona, USA). This anode potential was selected to enrich and maintain kinetically efficient EAB as suggested in the literature (Dhar et al., 2016a; Torres et al., 2009; Zakaria et al., 2019). The reactors were operated at room temperature (21±1°C) with continuous mixing (130±5 rpm) of the liquid medium with magnetic stirrers.

### *3.2.2. EPS and ROS analyses*

For EPS analysis, biomass samples were washed three times with 0.1 M PBS (pH 7.4), and then the supernatant was removed after centrifugation at 3000 × g for 15 min at 21°C. EPS extraction was performed using two methods: cation-exchange resin (CER) and heating method.

Applying cation-exchange resins and heating methods was highly efficient in several previous studies for the EPS extraction from biofilms, particularly carbohydrates, proteins, and eDNA (Cho et al., 2012; Dai et al., 2016; Jachlewski et al., 2015; Tan et al., 2019; Xiao et al., 2017). In addition, the pellets were collected to examine the cell lysis interference using a Glucose-6-Phosphate Dehydrogenase kit (Sigma-Aldrich, USA). The details of EPS extraction and analytical methods for various EPS components (proteins, carbohydrates, eDNA, heme-binding proteins, and uronic acid) are provided in the Supplementary Information. These five major EPS components were selected based on the EPS components previously found in electroactive anode biofilms (Stöckl et al., 2019; Xiao et al., 2017; Yang et al., 2019b, 2019a). Furthermore, these EPS components were also found in archaeal biofilms in conventional anaerobic biofilm reactors (van Wolferen et al., 2018; Zhang et al., 2019). Both EPS extraction methods (CER and heating method) provided similar results (Table A.1). Hence, we reported the results from the CER method. Confocal laser scanning microscopy (CLSM) was used to visualize and examine the EPS structure (for method, see Supplementary Information). The quantitative analysis of EPS biovolumes and intensities was carried out using biofilm image processing COMSTAT software (COMSTAT2, Version 2.1, Dk, http://www.comstat.dk/) (Heydorn et al., 2000; Vorregaard, 2008). For electrochemical characteristics, cyclic voltammetry (CV) of extracted EPS from biocathodes was performed. 2 mL of extracted EPS was transferred to an electrochemical cell having screen printed electrodes (A-AD-GG-103-N, Zimmer and Peacock Ltd., Royston, UK). The working electrode potential was ramped between −0.8 and 0.8 V vs. Ag/AgCl at a scan rate of 1 mV/s using a potentiostat (Squidstat Prime, Admiral Instruments, USA); the current was recorded every 1 second.

The ROS levels in biofilms were visualized using CLSM. We collected different parts of electrodes, then washed them three times using 0.1 M PBS to remove any debris. Samples were stained with 2',7'-Dichlorofluorescein diacetate (10 μM) (Thermo Fisher, USA) for one hour. The visualization (Figure 3.8) was then performed with excitation and emission wavelength of 495 nm and 520 nm, respectively. The quantification of ROS levels was then performed using image processing COMSTAT software (COMSTAT2, Version 2.1, Dk, http://www.comstat.dk/) (Heydorn et al., 2000; Vorregaard, 2008). Microscopic visualization of biofilms was performed using a scanning electron microscope (SEM, Carl Zeiss, Cambridge, UK). Several images from

different locations of electrodes were captured. The detailed protocol could be found elsewhere (Zakaria and Dhar, 2020).

### *3.2.3. Microbial communities and gene expression analyses*

For microbial analyses, genomic DNA was extracted from the anode and cathode biofilms using PowerSoil DNA Isolation Kit (MoBio Laboratories, Carlsbad, USA) according to the manufacturer's instructions. The purity and concentration of DNA were measured with Nanodrop spectrophotometer (Model 2000C, Thermo Scientific, USA). The extracted DNA was stored immediately at -70 ˚C prior to the sequencing. Illumina Miseq Sequencing was performed by the Research and Testing Laboratory (Lubbock, TX, USA) targeting 16S rRNA gene using bacterial primers 341F: 5' CCTACGGGNGGCWGCAG 3' and 805R: 5' GACTACHVGGGTATCTAATCC 3' (Klindworth et al., 2013; Logares et al., 2013), archaeal primers 517F: 5' GCYTAAAGSRNCCGTAGC 3' and 909R: 5' TTTCAGYCTTGCGRCCGTAC 3' and specific *mcr*A archaeal primers *mcr*Af: 5' GGTGGTGTMGGATTCACACARTAYGCWACAGC 3' and *mcr*Ar: 5' TTCATTGCRTAGTTWGGRTAGTT 3' (Morris et al., 2014).

For evaluating microbial diversity, the nucleotide sequence reads were sorted out using a data analysis pipeline. Short sequences, noisy reads and chimeric sequences were removed through a denoising step and chimera detection, respectively. Then, each sample was run through the analysis pipeline to establish the taxonomic information for each constituent read. Microbial taxonomy was assigned using the Quantitative Insights Into Microbial Ecology (QIIME) pipeline (QIIME2, Version 2021.2, http://qiime.org, Bolyen et al., 2019). Principal component analysis (PCA) of cathodic microbial communities was conducted using weighted Unifrac metrics to show the relation between genera and PCs. The expressions of EET genes (i.e., *pil*A, *omc*B, *omc*C, *omc*E, *omc*Z, and *omc*S) were also quantified (for details and method, see Supplementary Information). The primers and design methods are listed in Table A.2.

### *3.2.4. Analytical methods and statistical analysis*

Current and applied voltage/potential were recorded every 4.8 min using a computer connected with the potentiostat. The chemical oxygen demand (COD) was measured with HACH

method using UV-spectrophotometer (Model DR 3900, HACH, Germany). The volatile fatty acids, VFAs (acetate, propionate, and butyrate), concentrations were measured with an ion chromatography (Dionex ICS-2100, Thermo Scientific, USA) (Zakaria et al., 2019). Electrochemical impedance spectroscopy (EIS) was performed for both reactors using a multi-channel VSP potentiostat (VSP, Bio-Logic Science Instruments, France). The detailed methodology is provided in the Supplementary Information. The biogas produced from reactors was collected with 500 mL gas bags. The composition of biogas (i.e., methane content) was analyzed with a gas chromatograph (7890B, Agilent Technologies, Santa Clara, USA) equipped with a thermal conductivity detector and two columns (Molsieve 5A and Hayesep). To reveal the statistical difference between the results collected from two reactors, the student's paired t-test (JMP Software, Version 11.0.0, SAS Institute Inc., Cary, NC, US, https://www.jmp.com/) was used.

## 3.3. Results and discussion

### *3.3.1. MEC-AD performance*

The performance of the two configurations was compared based on volumetric current density and methane productivity. As shown in Figure 3.1, the maximum current density from the CF-SS reactor reached 34.1±0.3 $A/m^3$, which was significantly higher ($p=0.01$) than CF-CF (27.6±0.2 $A/m^3$). Although the methane generation patterns were comparable in both reactors (Figure 3.2), CF-SS showed higher ($p=0.03$) daily methane production than CF-CF throughout the batch cycle. The total cumulative methane production was substantially higher in CF-SS (179.5±6.7 vs. 100.3±7.9 mL $CH_4$; $p=0.01$). Both reactors used carbon fiber as the anode electrode and were operated under identical operating conditions (e.g., mixing speed, substrate, inoculation, etc.). Hence, the differences in system performance could be closely tied to the difference in the cathode electrode. As discussed later, stainless steel mesh cathode in CF-SS facilitated denser biofilms formation with more methanogenic biomass.

Anode electrodes providing high specific surface areas have been efficient for enhancing the performance of various bio-electrochemical systems (Choi et al., 2017; De Vrieze et al., 2014; Guo et al., 2017b; D. Liu et al., 2017; W. Liu et al., 2016). Therefore, carbon-based electrodes,

such as carbon brush, activated carbon, have also been widely used for various biocathode applications, including electro-methanogenesis (Choi et al., 2017; De Vrieze et al., 2014; W. Liu et al., 2016). Notably, the rough surface of carbon fiber was found to be efficient for developing EAB biofilms (Li et al., 2017). Although we cannot rule out that different textures (diameter of carbon fiber and stainless steel wire) could also lead to distinct colonization of biomass (Champigneux et al., 2018; He et al., 2011), the specific surface area provided by electrodes is often considered a critical factor. This study shows that stainless steel cathode having a relatively lower specific surface area than carbon fibers (4.23 vs. 3609 $m^2/m^3$) resulted in a superior methanogenic activity. It has been previously suggested that the agglomeration of fibers in the liquid phase could reduce the available specific surface area for biofilms formation (Babapoor et al., 2015). Nonetheless, considering all carbon fiber filaments in a bundle as a single fiber, the specific surface area provided by the carbon fiber was still higher than stainless-steel (4.23 vs. 41 $m^2/m^3$). In general, carbon-based electrodes are considered inferior catalysts for HER than metal and carbon-metal composite electrodes (Call et al., 2009; Dykstra and Pavlostathis, 2017; D. Liu et al., 2017; J. Park et al., 2018b; Wang et al., 2016). Previous MEC-AD studies substantiated the role of hydrogenotrophic methanogenesis. It is also reasonable that acetoclastic methanogens would likely be washed out at low residence time (<7 days) used in this study (Gaby et al., 2017; Zakaria and Dhar, 2019). EIS analysis also indicated that stainless-steel biocathode could reduce various intrinsic internal resistances in CF-SS compared to CF-CF (see Supplementary Information). As shown in the Nyquist plot (Figure A.2), the overall internal impedance of CF-SS (52.62 Ω) was lower than that of CF-CF (77.28 Ω). Thus, stainless-steel cathode largely influenced the internal resistances, which influenced the HER kinetics and, ultimately, growth and activities of hydrogenotrophic methanogens. Previous studies also suggested that lower ohmic resistance in MECs could provide faster HER kinetics (Hou et al., 2014; Yuan and He, 2017). Thus, the inferior methane recovery from the CF-CF reactor than the CF-SS reactor was likely due to the inferior HER on carbon fibers and subsequent hydrogenotrophic methanogenesis.

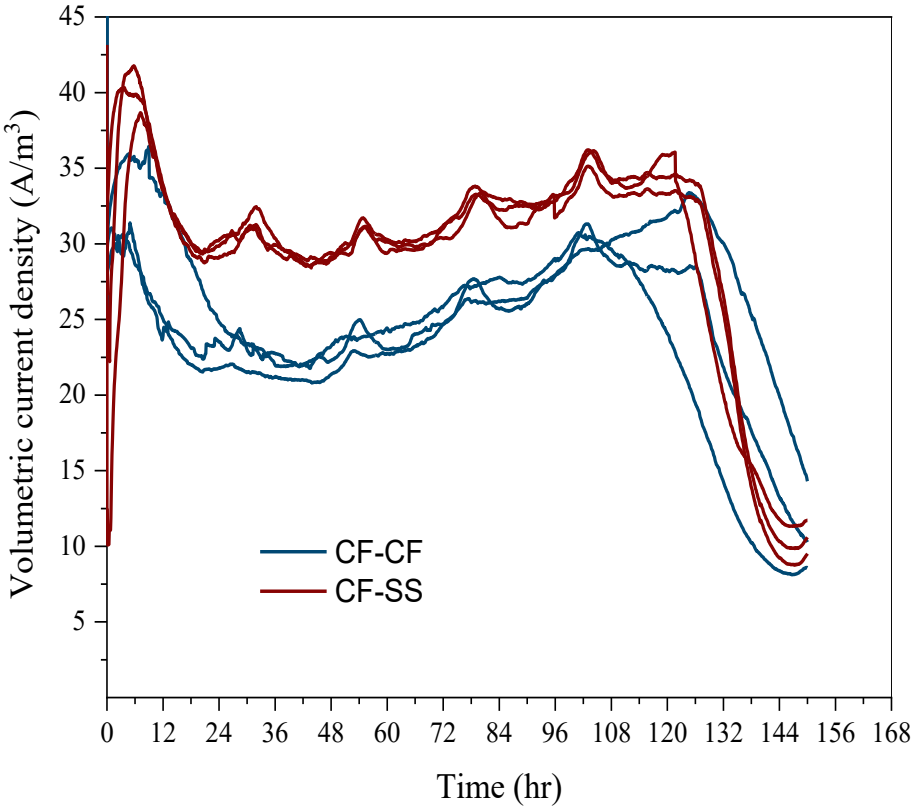


**Figure 3.1** Volumetric current densities from CF-CF and CF-SS reactors. Note. Volumetric current densities indicate the current normalized by the total working volume of the reactor. The results from 3 representative batch cycles during steady-state are shown here. The error bars indicate the standard deviation of three replicates (n = 3)

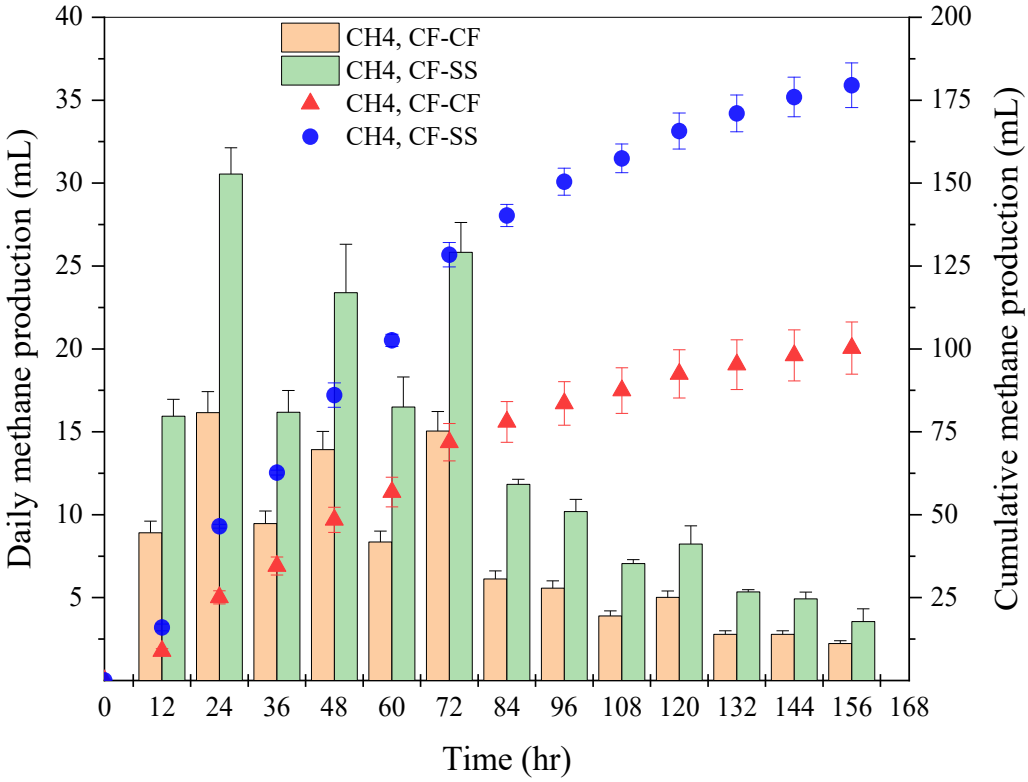


**Figure 3.2** Methane production from CF-CF and CF-SS reactors. The error bars indicate the standard deviation of three replicates (n = 3)

### *3.3.2. Organics removal and VFAs profiles*

The effluent COD concentration from CF-SS (215±2.8 mg/L) was considerably lower (p=0.001) than that of CF-CF (382±3.0 mg/L) (Figure 3.3). Correspondingly, COD removal efficiency in CF-SS (89.9±0.5%) was significantly higher (p=0.012) than that of CF-CF (83±1.7%). Figure 3.3 show the VFAs profiles during batch operation. For both reactors, the acetate concentrations were relatively higher than propionate and butyrate throughout the operational period. The CF-SS reactor showed the highest acetate concentration of 439±2 mg COD/L, while propionate (94±0.1 mg COD/L) and butyrate (61±0.3 mg COD/L) concentrations were relatively lower. In contrast, CF-CF exhibited the highest acetate concentration of 320±0.4 mg COD/L, which was lower than that observed in CF-SS. Propionate concentrations were

relatively higher in CF-CF, with the highest concentration of 118±0.4 mg COD/L. The highest butyrate concentration (64.8±1.3 mg COD/L) in CF-CF was comparable to CF-SS (61±0.3 mg COD/L). CF-SS also showed a lower accumulation of VFAs in the final effluent than CF-CF (52.6±0.5 vs. 133.5±1.0 mg COD/L; p=0.005).

Throughout the batch operation, propionate concentrations in CF-SS remained relatively lower than those observed in CF-CF, indicating faster conversion of propionate in the CF-SS. The fermentation of propionate to acetate is a vital process towards anodic respiration (by EAB) and acetoclastic methanogenesis. However, propionate fermentation to acetate is energetically unfavorable in terms of Gibbs free energy (Krylova and Conrad, 1998). Thus, maintaining lower hydrogen partial pressure would be critical for propionate fermentation to acetate. Even though stainless-steel cathode would be expected to provide superior HER than carbon fibers (Call et al., 2009; Dykstra and Pavlostathis, 2017), no hydrogen was detected in biogas from both reactors. This might be due to the rapid consumption of hydrogen by hydrogenotrophic methanogens, as suggested in previous studies (Asztalos and Kim, 2015; Dykstra and Pavlostathis, 2017). Moreover, enhanced homoacetogenic activity ($H_2 + CO_2 \rightarrow$ acetate) could assist in maintaining lower hydrogen partial pressure in biocathode (Asztalos and Kim, 2015; Dykstra and Pavlostathis, 2017). Microbial community analysis also coincided with these notions (discussed later). Thus, the VFA profiles suggest that the microbiome in CF-SS more rapidly utilized hydrogen produced via fermentation and cathodic HER.

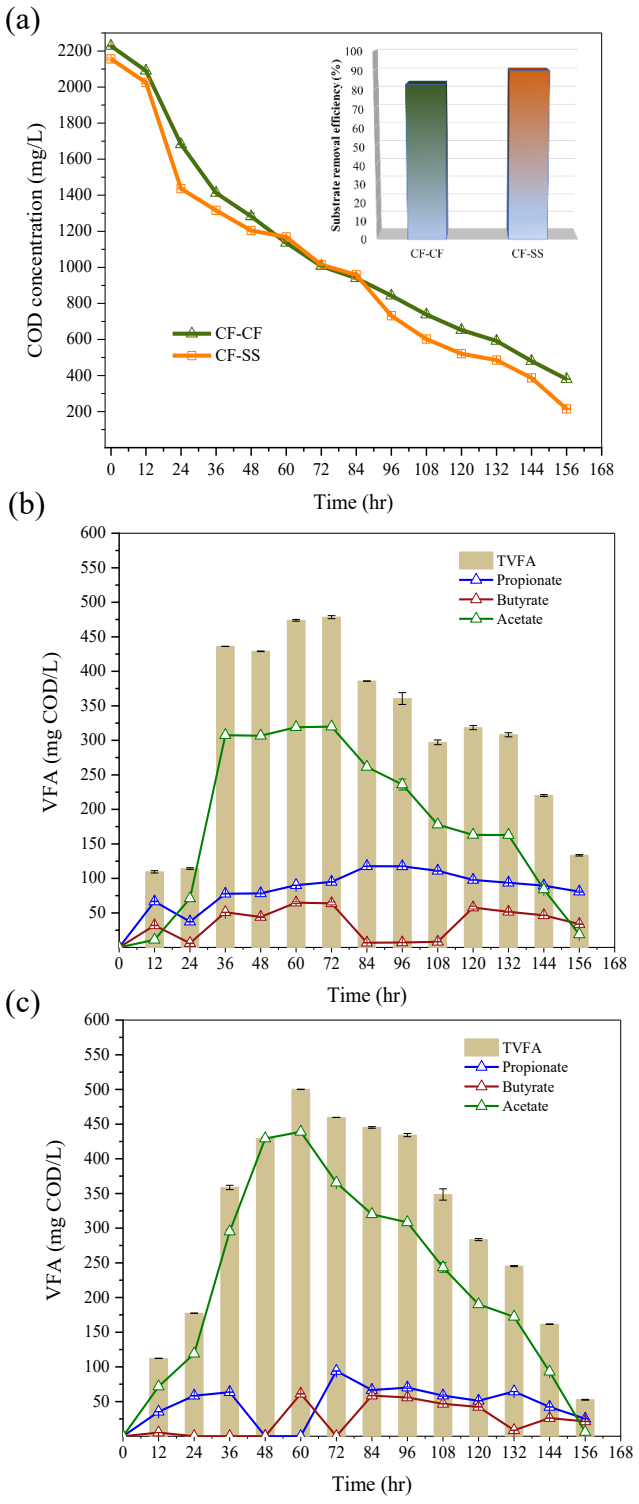


**Figure 3.3** COD concentration (a), and VFA profiles (b, c) in CF-CF and CF-SS reactors. The error bars show the standard deviation of three replicates (n = 3)

### *3.3.3. EPS characteristics*

As shown in Figure 3.6a, the EPS composition of anode biofilms in both reactors was quite similar and was not affected by the different cathode materials used. Protein was found as the major EPS component in anode biofilms, consistent with recent reports on EPS composition in pure culture *Geobacter* biofilms (Stöckl et al., 2019; Tan et al., 2019). *Geobacter* species were also abundant in anode biofilms in both reactors in this study (discussed later). The concentrations of major EPS components (carbohydrates, proteins, and hemes) in the cathode biofilms in CF-SS were higher than those of CF-CF. Notably, carbohydrates and proteins in cathodic EPS were markedly higher in CF-SS than CF-CF (carbohydrates: 52.2±0.2 vs. 25.8±0.5 mg/cm$^2$; proteins: 212.8±3.4 vs. 170±1.3 mg/cm$^2$). The heme-binding proteins, uronic acid, and eDNA also showed the same patterns. Overall, cathodic biofilms developed on the stainless-steel electrode exhibited markedly higher EPS levels ($p=0.03$).

Moreover, electrode surfaces were visualized with CLSM (Figure 3.7). The CLSM images showed that EPS was more uniformly distributed on the stainless-steel biocathode in CF-SS than the carbon fiber electrodes in both reactors. The biovolume of cathode biofilms in CF-SS was estimated at 30.2±4.2 μm$^3$/μm$^2$, which was two times higher than that estimated for cathode biofilms in CF-CF (13.5±2.8 μm$^3$/μm$^2$) (Figure 3.6b). The biovolumes estimated for anode biofilms in both reactors were comparable ($p=0.007$). The intensities of EPS and eDNA were also quantified (Figure 3.6c). Like estimated biovolume, EPS and eDNA intensities in stainless steel biocathode were higher than those estimated for carbon fiber biocathode ($p=0.008$). Simultaneously, EPS and eDNA intensities were comparable for anode biofilms in both reactors ($p=0.20$). Thus, CLSM imaging and COMSTAT (COMSTAT2, Version 2.1, Dk, http://www.comstat.dk/) ("Comstat 2," n.d.; Heydorn et al., 2000; Vorregaard, 2008) analysis further confirmed that the stainless-steel biocathode resulted in the highest EPS production. The SEM imaging of biofilms also corroborated these results (Figure 3.5). The biofilms did not fully cover the surfaces of carbon fibers, while biofilms grown on stainless steel cathode in CF-SS were evenly denser than anode/cathode biofilms grown on carbon fiber electrodes. The anode/cathode biofilms grown on carbon fibers exhibited substantial heterogeneity. In contrast, a large secretion of EPS could accelerate the surface attachment of cells on the stainless-steel.

Studies on the EPS in electroactive biofilms received less attention and primarily focused on understanding their role in anodic EET. A few reports revealed redox-active features of anodic EPS in model EAB biofilms (e.g., *Geobacter sulfurreducens*, *Shewanella oneidensis,* and *Pseudomonas putida*) (Stöckl et al., 2019; Tan et al., 2019; Xiao et al., 2017). Notably, higher levels of proteins in anode biofilms were correlated with higher EET efficiency. In this study, despite differences in volumetric current densities, both EPS composition and concentrations were quite similar in anode biofilms in both reactors. Instead, the difference in cathodic EPS levels was likely linked to current densities and methane productivity. As mentioned earlier, EPS can serve as immobilized redox cofactors (i.e., electron carriers) for facilitating EET in anodic EAB biofilms (Tan et al., 2019; Xiao et al., 2017). EAB can also regulate EPS generation to balance EET and protect cells (Yang et al., 2019a). The existing literature provides limited information on the roles of EPS in methanogenic biocathode. However, a few reports suggested that EPS could play similar roles (EET and cell protection) in archaeal biofilms in conventional digesters in the presence of conductive additives (Mostafa et al., 2020; Ye et al., 2018). Interestingly, a recent study demonstrated that the addition of iron-based conductive materials in conventional anaerobic bioreactors could enhance redox-active EPS contents in methanogenic biomass (Ye et al., 2018), which was positively correlated with methanogenesis rates. Conductive materials promote the syntrophic DIET from bacteria to archaea and thereby enhance methanogenesis (J. H. Park et al., 2018). Therefore, the CV of biocathode EPS from two reactors was performed to identify their redox activity (Figure 3.4) qualitatively.

As shown in Figure 3.4, the voltammograms of cathodic EPS extracted from both reactors showed distinct redox peaks, indicating their redox capability. However, redox peaks were observed at different potentials, suggesting that redox properties would be different for EPS extracted from two biocathodes. The peak current from stainless steel biocathode EPS was considerably higher than the EPS extracted from carbon fiber biocathode. This difference could be associated with higher levels of redox-active EPS in stainless steel biocathode, as previously suggested in the literature for anodic EAB biofilms (Stöckl et al., 2019; Xiao et al., 2017). Despite higher EPS levels in stainless-steel biocathode and differences observed in CV patterns, the expressions of genes associated with EET were comparable in both biocathodes (discussed later). Thus, it can be inferred that redox activities of EPS did not play a decisive role in differentiating

between the performances observed from the two systems. Instead, EPS variations might be more associated with the protection of cells from harsh metabolic environments. Nonetheless, future investigation is warranted to reach a more thorough understanding and quantitative characterization of redox properties of EPS.

A recent study reported that the current from anode biofilms was positively associated with EPS protein content and negatively correlated to carbohydrates in EPS (Yang et al., 2019a). In this study, both carbohydrates and proteins in EPS were considerably higher in stainless steel biocathode than that of carbon fiber biocathode (Figure 3.6). The secretion of carbohydrates could be associated with harsh environmental conditions (Yu, 2020; Zakaria and Dhar, 2020) to provide a protective layer and maintain the redox activity of proteins involved in EET (Rollefson et al., 2011; Yu, 2020). It is possible that enhanced HER in stainless steel cathode could create highly alkaline conditions near the cathode (Cai et al., 2018; Cerrillo et al., 2016; Zakaria and Dhar, 2019), which might induce more EPS secretion. Based on a recent report, hydrogenotrophic methanogenesis could be the dominant pathway under alkaline pH (Wormald and Humphreys, 2019). As discussed later, stainless steel biocathode also showed a higher abundance of hydrogenotrophic methanogens in this study. Thus, it appeared that higher enrichment of hydrogenotrophic methanogens promoted by faster HER kinetics on stainless steel cathode was possibly associated with higher EPS excretion. While further investigation is needed to get more insights into the function of EPS on electro-methanogenesis, these results suggested that different cathode materials could influence EPS secretion and methanogenic activity due to differences in HER kinetics.

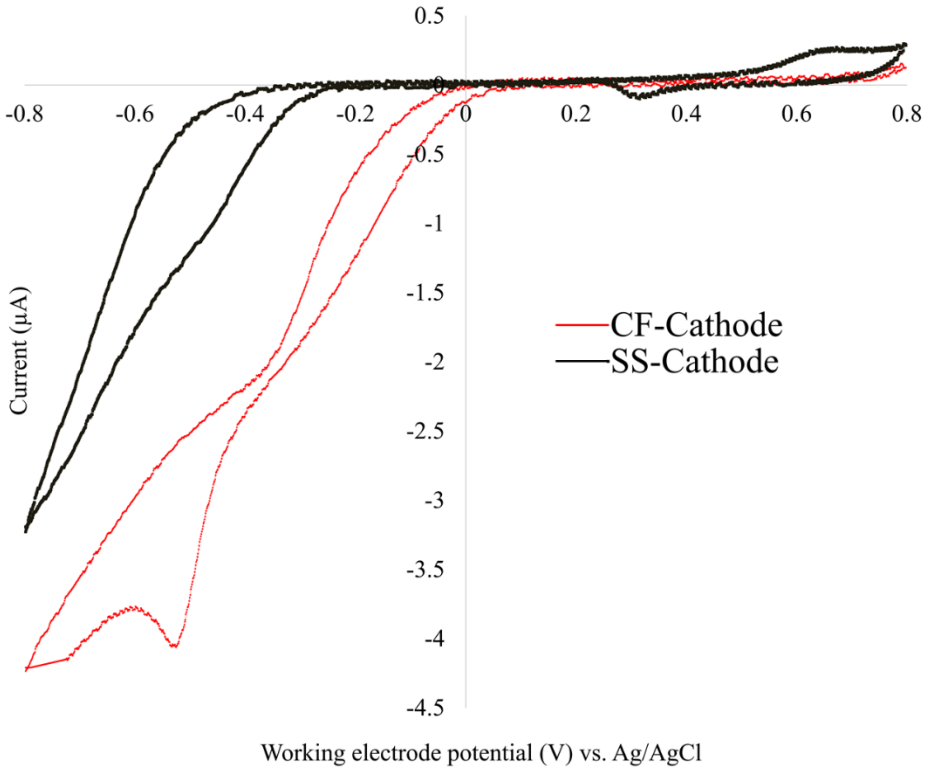


**Figure 3.4** Cyclic voltammetry of EPS extracted from biocathode in CF-CF and CF-SS reactors

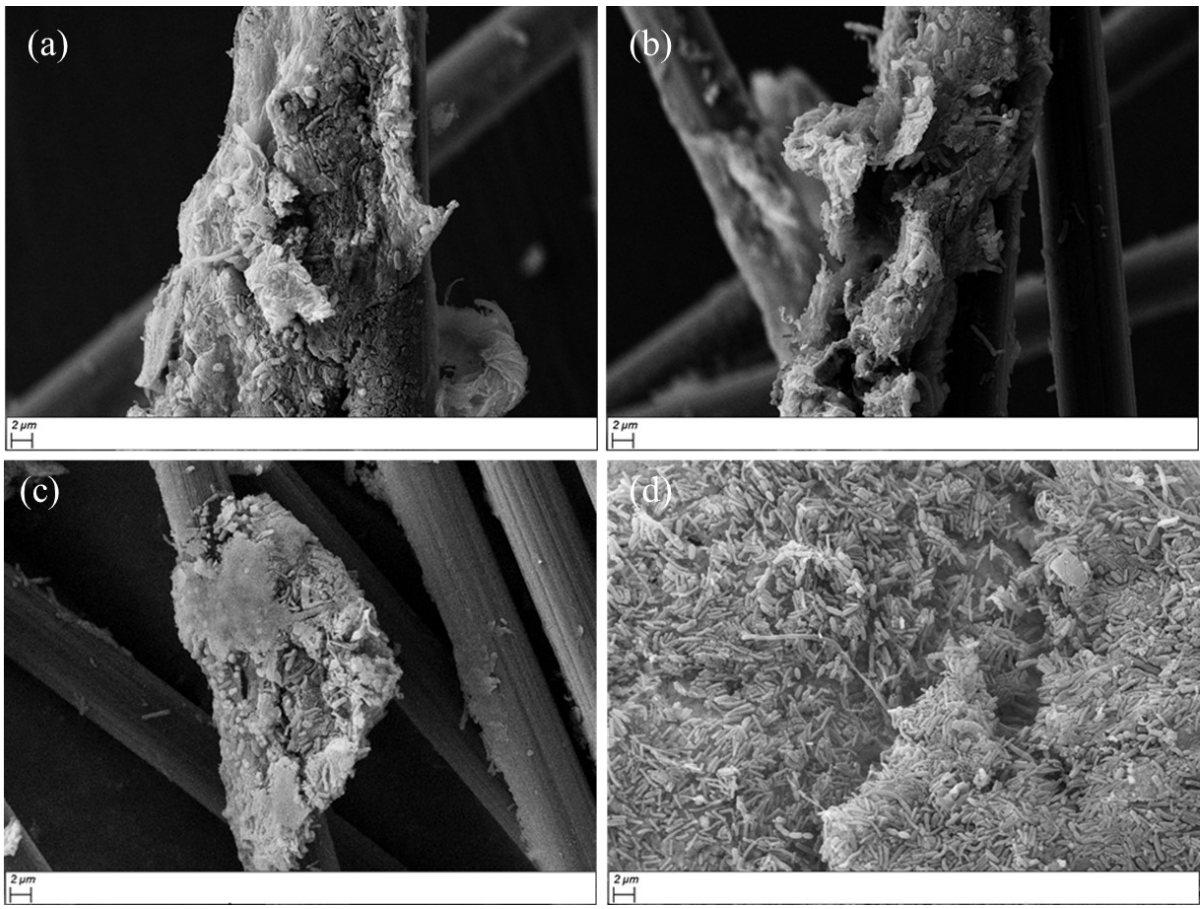


**Figure 3.5** Representative SEM images of biofilms developed on anode (CF-CF) (a), cathode (CF-CF) (b), anode (CF-SS) (c), and cathode (CF-SS) (d)

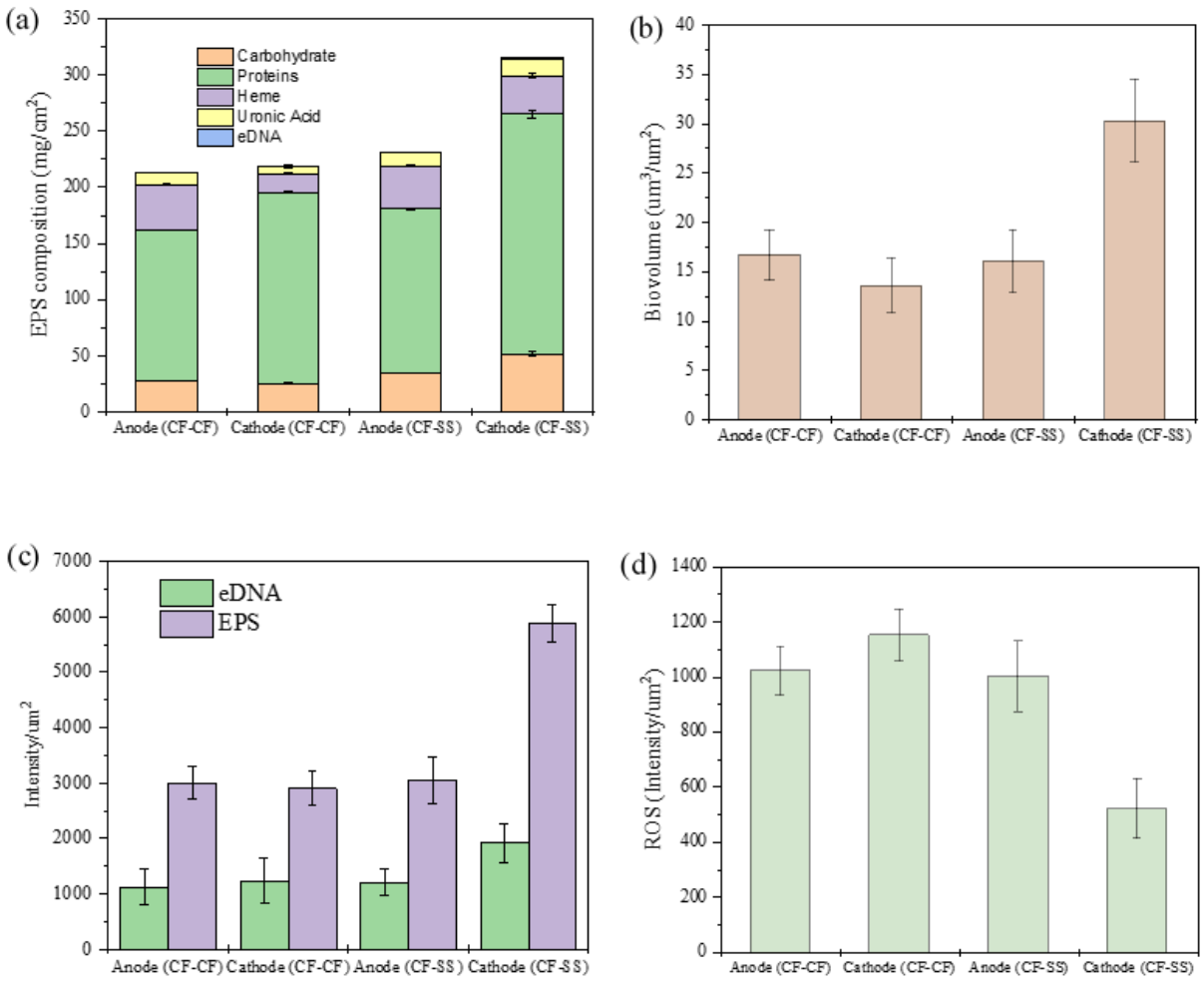


**Figure 3.6** EPS levels in biofilms (a), EPS quantitative analysis using CLSM; biovolume (b), and fluorescence intensity (c), and reactive oxygen species (ROS) intensities (d) of CF-CF and CF-SS reactors. Note. The error bars indicate the standard deviation of three replicates (n = 3)

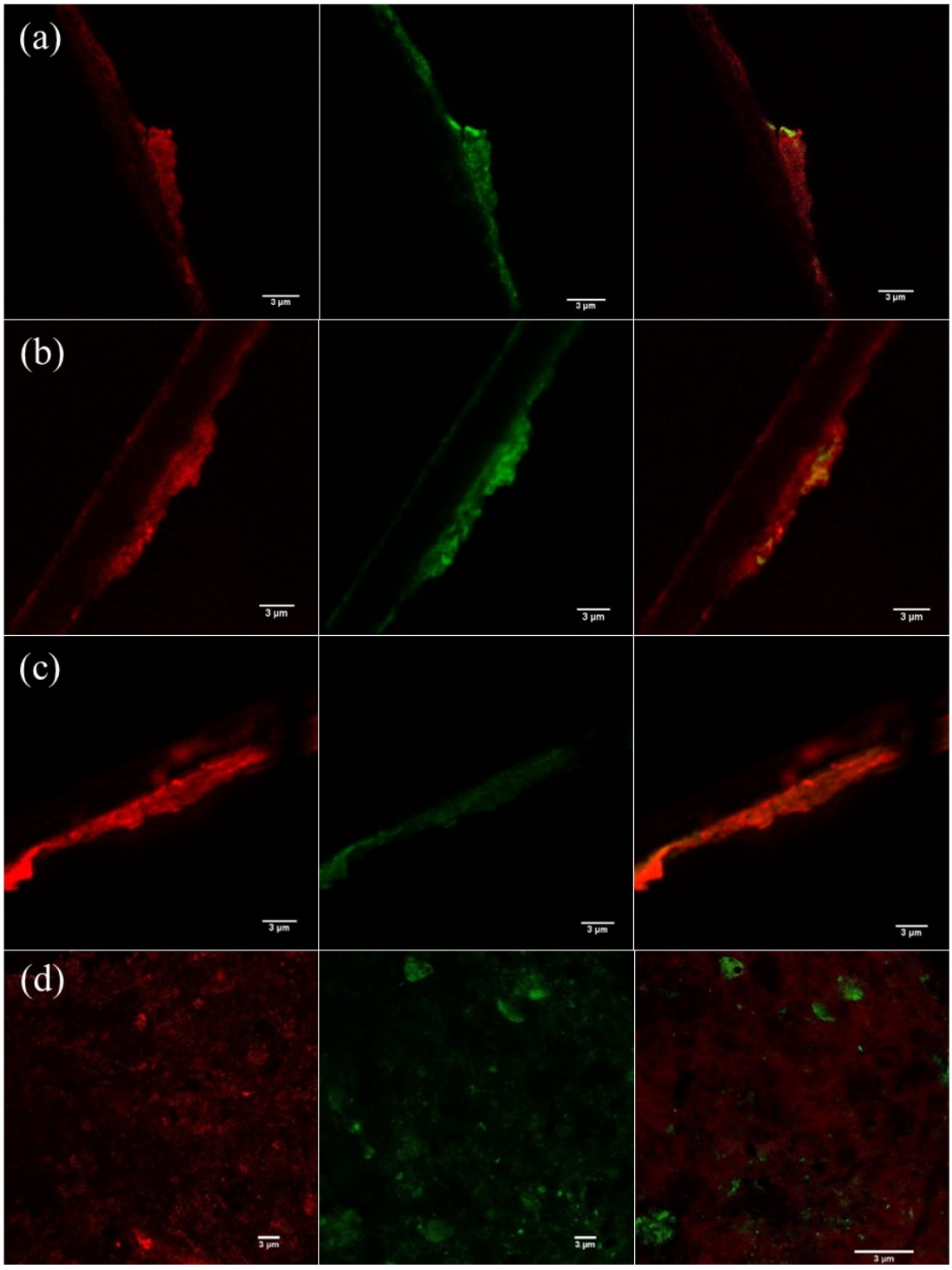


**Figure 3.7** Representative confocal microscopic images of EPS with 3 µm scale; anode (CF-CF) (a), cathode (CF-CF) (b), anode (CF-SS) (c), and cathode (CF-SS) (d). The green color represents eDNA and the red color indicates EPS

### *3.3.4. ROS levels*

The quantitative measurement of ROS demonstrated a significant difference between biofilms grown on stainless steel and carbon fibers (Figure 3.6d and Figure 3.8). The lowest ROS level was observed for cathode biofilms formed on stainless steel, while ROS levels were very similar in anode/cathode biofilms developed on carbon fibers. Recent studies reported ROS accumulation in anaerobic digesters (Tian et al., 2019; Zheng et al., 2019), while ROS is usually thought to be produced during aerobic metabolism. It has been suggested that unfavorable metabolic conditions (e.g., inhibition by toxicants, pH changes) could lead to ROS accumulation in digesters (Tian et al., 2019; Zheng et al., 2019). ROS accumulation may suppress metabolic activities, leading to the deterioration of digester performance. As we used synthetic glucose medium as a substrate, the potential unfavorable metabolic conditions induced by any toxic compounds can be ruled out. Thus, potential local pH changes by HER can be considered as an unfavorable metabolic condition. The HER in both biocathode can lead to alkaline pH due to protons reduction ($2H^+ + 2e^- \rightarrow H_2$), while effects will likely be more intense on stainless steel cathode (Call et al., 2009; Dykstra and Pavlostathis, 2017; D. Liu et al., 2017; J. Park et al., 2018b; Wang et al., 2016). Thus, the lowest ROS level in stainless steel biocathode suggests that higher EPS levels provided some degree of protection to the cathodic microbiome from potential environmental stress (e.g., local alkaline pH due to superior HER). However, potential mechanisms relating to EPS and ROS levels should be further explored.

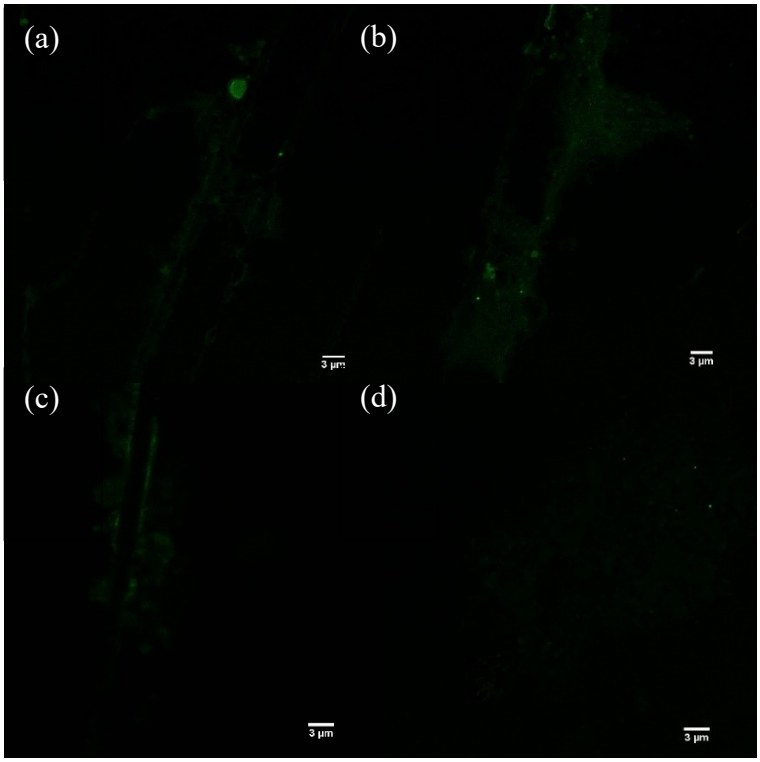


**Figure 3.8** CLSM of reactive oxygen species (ROS). Anode (CF-CF) (a), cathode (CF-CF) (b), anode (CF-SS) (c), and cathode (CF-SS) (d). (This figure has been analyzed using COMSTAT2, Version 2.1, Dk, http://www.comstat.dk/)

### *3.3.5. Microbial quantity and diversity*

Figure 3.9 shows the quantitative assessment of microbial communities performed with qPCR. The total microbial cell counts (16S) in anode biofilms in CF-SS were slightly higher than that of CF-CF ($9\times10^8$ vs. $8\times10^8$ cells/cm$^2$) (Figure 3.9a). An almost similar pattern was observed for cathode biofilms; however, the difference was more prominent ($1\times10^{11}$ vs. $6\times10^8$ cells/cm$^2$). The archaeal cell numbers also showed similar patterns, with the highest archaeal cell numbers for the stainless steel biocathode.

Furthermore, *mcr*A gene copies were quantified (Figure 3.9b), considered a biomarker for hydrogenotrophic methanogenesis (Wilkins et al., 2015). A few recent reports also confirmed the

positive link between *mcr*A gene copies and methanogenesis rates in MEC-AD reactors (Alonso et al., 2020; Morris et al., 2014; Wilkins et al., 2015). The highest number of *mcr*A gene copies was observed for the stainless steel biocathode ($4\times10^6$ cells/cm$^2$; 100 times higher than carbon fiber biocathode). The *mcr*A gene copies in anodic biofilms for both systems were comparable. Thus, the higher abundance of *mcr*A gene copies within the stainless steel biocathode corroborated with higher methane productivity in the CF-SS reactor.

The alpha diversity of microbial communities was also estimated (Table A.3). The higher values of Chao 1, phylogenetic distance, OTUs, Pielou's evenness, and Shannon index clearly showed that the richness and diversity indices were relatively higher in CF-SS than CF-CF ($p$ = 0.02). Notably, cathode biofilms in CF-SS showed more diversity with the Shannon index of 5.10, as compared to CF-CF (3.95) ($p$ = 0.03). These results indicated that the stainless-steel electrode persuaded the richness and diversity of the microbial communities.

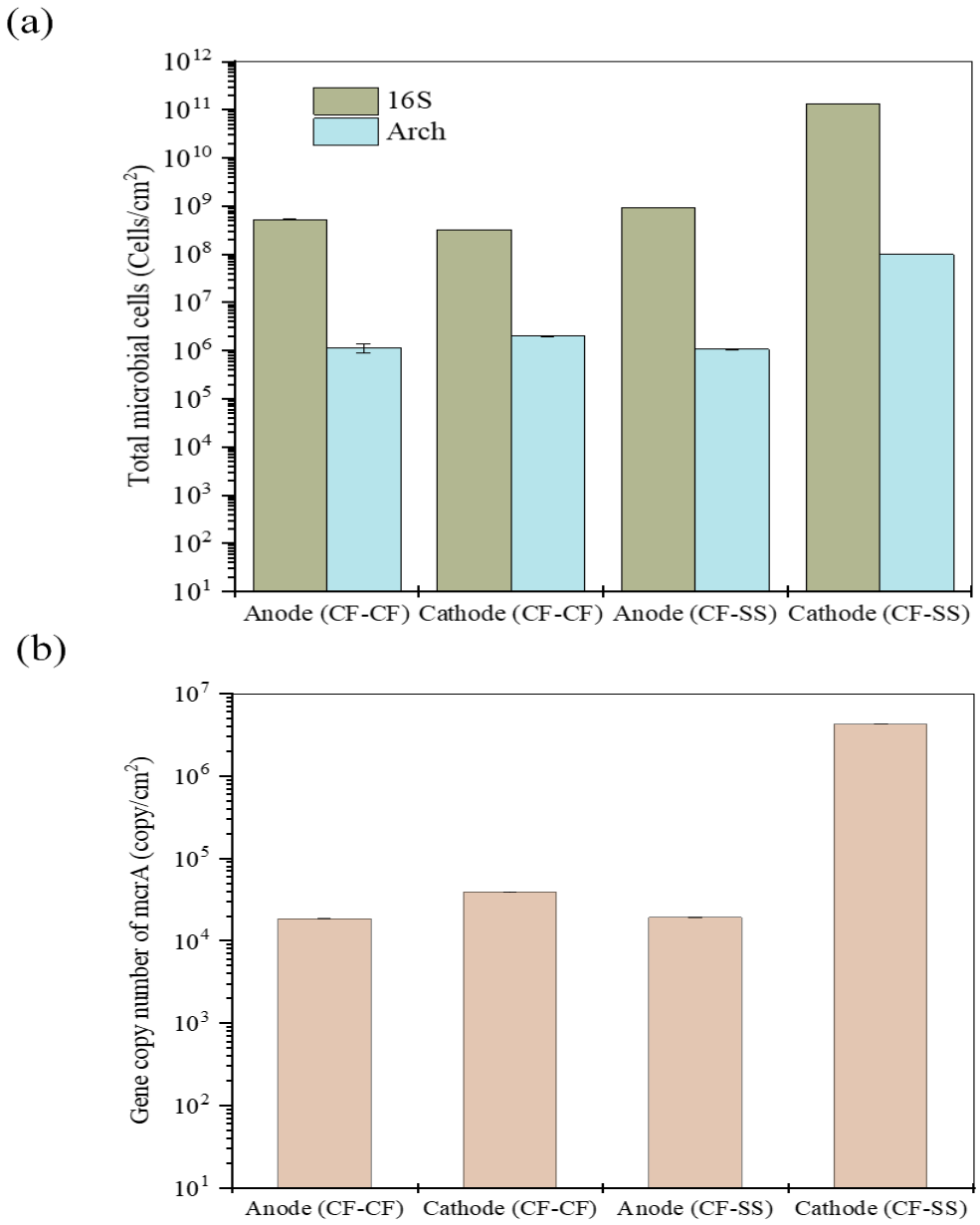


**Figure 3.9** Total cell number using 16s and archaeal primers (a), and mcrA gene copies (b). The error bars indicate the standard deviation of three replicates (n = 3)

### *3.3.6. Microbial community composition, and gene expression*

#### *3.3.6.1. 16S rRNA sequencing*

Microbial communities in two reactors were analyzed with specific bacterial, archaeal, and *mcr*A primers. Proteobacteria was the most abundant phylum in anode biofilms in both reactors; however, its relative abundance was much higher in CF-SS (85%) than CF-CF (47%) (Figure A.3 Relative abundance of microbial community. Bacterial primer phylum level (a), and archaeal primer phylum level (b)). The relative abundances of Bacteroidetes (26%) and Firmicutes (14%) in CF-CF were considerably higher than CF-SS (6% and 4%, respectively). Also, Synergistetes (6%) and Lentisophaerae (4%) were present at slightly higher abundances in CF-CF, while in CF-SS, they were 1% and 3%, respectively. Proteobacteria was also the most abundant in both cathode biofilms; their relative abundances (64%-68%) were also similar. However, the abundance of Bacteroidetes was higher in CF-CF (17%) than CF-SS (6%). On the contrary, the phylum Firmicutes (20%) was the second most abundant in CF-SS, while its abundance in CF-CF was considerably lower (9%).

At the genus level, *Geobacter,* belong to Proteobacteria, was the most abundant in anode biofilms (CF-CF: 22%; CF-SS: 59%) in both systems (Figure 3.10a). Geobacter is a highly efficient EAB with the capability to facilitate EET from simple organic acids like acetate (Yang et al., 2019a; Zakaria et al., 2019). In CF-CF, *Bacteroides* was the second most dominant genus (12%), followed by *Enterobacteriaceae* (10%) and *Dysgonomonas* (5%). In contrast, the second abundant genus in CF-SS was *Enterobacteriaceae* (23%), followed by *Dysgonomonas* (3%) and *Victivallis* (3%).

The cathode biofilms in both reactors were dominated by the genus *Enterobacteriaceae* (CF-CF: 42%; CF-SS: 60%). In CF-CF, *Bacteroides* (12%), *Pleomorphomonas* (9%), and *Desulfovibrio* (4%) were the other dominant genera. In contrast, *Acetobacterium* was the second abundant genus (16%), followed by *Bacteroides* (5%), *Dysgonomonas* (3%), and *Desulfovibrio* (2%) in CF-SS. *Acetobacterium*, known homoacetogenic bacteria, can utilize $H_2$ and $CO_2$ to produce acetate (Dhar et al., 2019; D. Liu et al., 2017). Then, acetate can be consumed by either acetoclastic archaea or EAB (Cheng et al., 2009; Fu et al., 2015; Zakaria and Dhar, 2019). The

enrichment of *Acetobacterium* on the stainless-steel biocathode indicates the occurrence of higher catalysis of HER. As mentioned earlier, $H_2$ gas has not been observed in the biogas samples. This might be due to the rapid utilization of the generated $H_2$ via hydrogenotrophic methanogens and homoacetogenic *Acetobacterium*, as suggested in the literature (Asztalos and Kim, 2015; Dykstra and Pavlostathis, 2017). The presence of the highest acetate concentration (439±2 mg COD/L) in CF-SS corroborated with a higher abundance of *Acetobacterium*. Moreover, *Acetobacterium* can maintain a lower hydrogen partial pressure to provide thermodynamically favorable conditions for propionate and butyrate fermentation to acetate. This notion is also supported in part by the lower propionate concentrations in CF-SS compared to the CF-CF.

### *3.6.2. Archaeal and mcrA primer sequencing*

For the archaeal phylum, relative abundances of Euryarchaeota were 32% and 51% in CF-CF and CF-SS, respectively (Figure A.3 Relative abundance of microbial community. Bacterial primer phylum level (a), and archaeal primer phylum level (b)). At the genus level, the abundance of *Methanobacterium* was almost similar (13-14%) in the anode biofilms in both systems (Figure 3.10b). However, the abundance of *Methanobacterium* in cathode biofilms of CF-SS was higher than CF-CF (51% vs. 32%). Previous studies also reported the enrichment of known hydrogenotrophic methanogens in methanogenic biocathode (Cheng et al., 2009; Dykstra and Pavlostathis, 2017; Siegert et al., 2015, 2014a). Moreover, *mcr*A gene sequencing was performed (Figure 3.10c) to understand the taxonomy of methanogens (Alonso et al., 2020; Morris et al., 2014; Wilkins et al., 2015). In the anodic biofilms, the abundances of *Methanobacterium* species were almost similar, including *formicicum* (CF-CF: 67%; CF-SS: 71%) and *subterraneum* (CF-CF: 34%; CF-SS: 29%). In the cathodic biofilms, CF-SS showed more diverse species of *Methanobacterium*; *formicicum* (54%), *subterraneum* (24.4%), and *palustre* (22%), as compared to CF-CF; *formicicum* (81%), and *subterraneum* (19%). Thus, the higher abundance and diverse species of hydrogenotrophic *Methanobacterium* on stainless steel cathode might have contributed to the faster methanogenesis via hydrogen utilization.

### *3.6.3. Principal component analysis*

The PCA analysis of biocathode bacterial and archaeal communities was performed to evaluate the relation between genera and PCs (Figure 3.11). Based on 16S rRNA bacterial sequencing of biocathode, the superior performance of CF-SS was related to the enrichment of homoacetogenic Acetobacterium (Figure 3.11a). However, the other genera might have an indirect relation to the superior performance of CF-SS. Based on archaeal sequencing of biocathode, hydrogen-consuming Methanobacterium and Acetobacterium primarily contributed to the superior performance of stainless steel biocathode (Figure 3.11b).

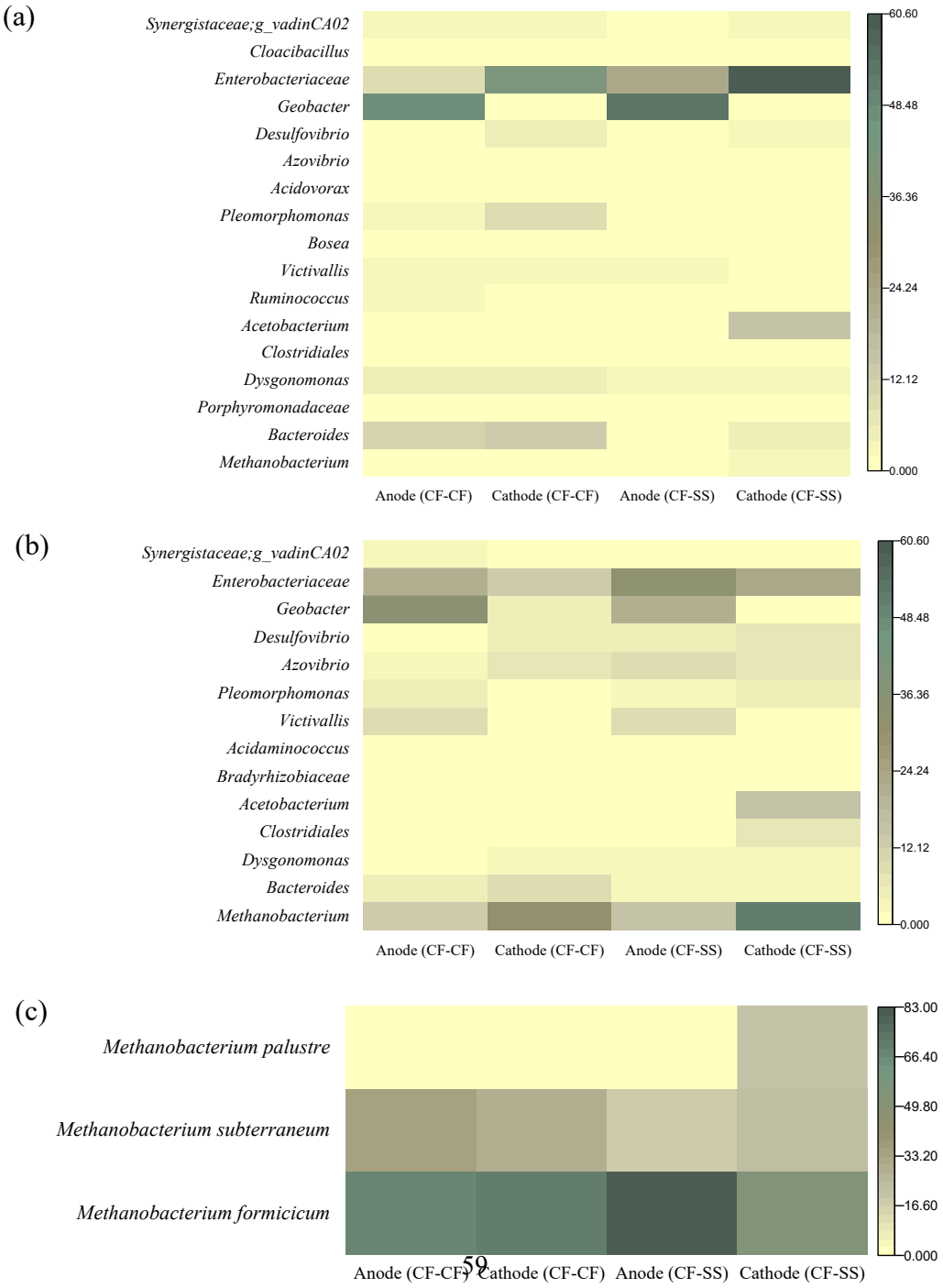


**Figure 3.10** Relative abundance of microbial communities analyzed with bacterial primer (a), archaeal primer (b), and *mcr*A primer (c) at the genus level

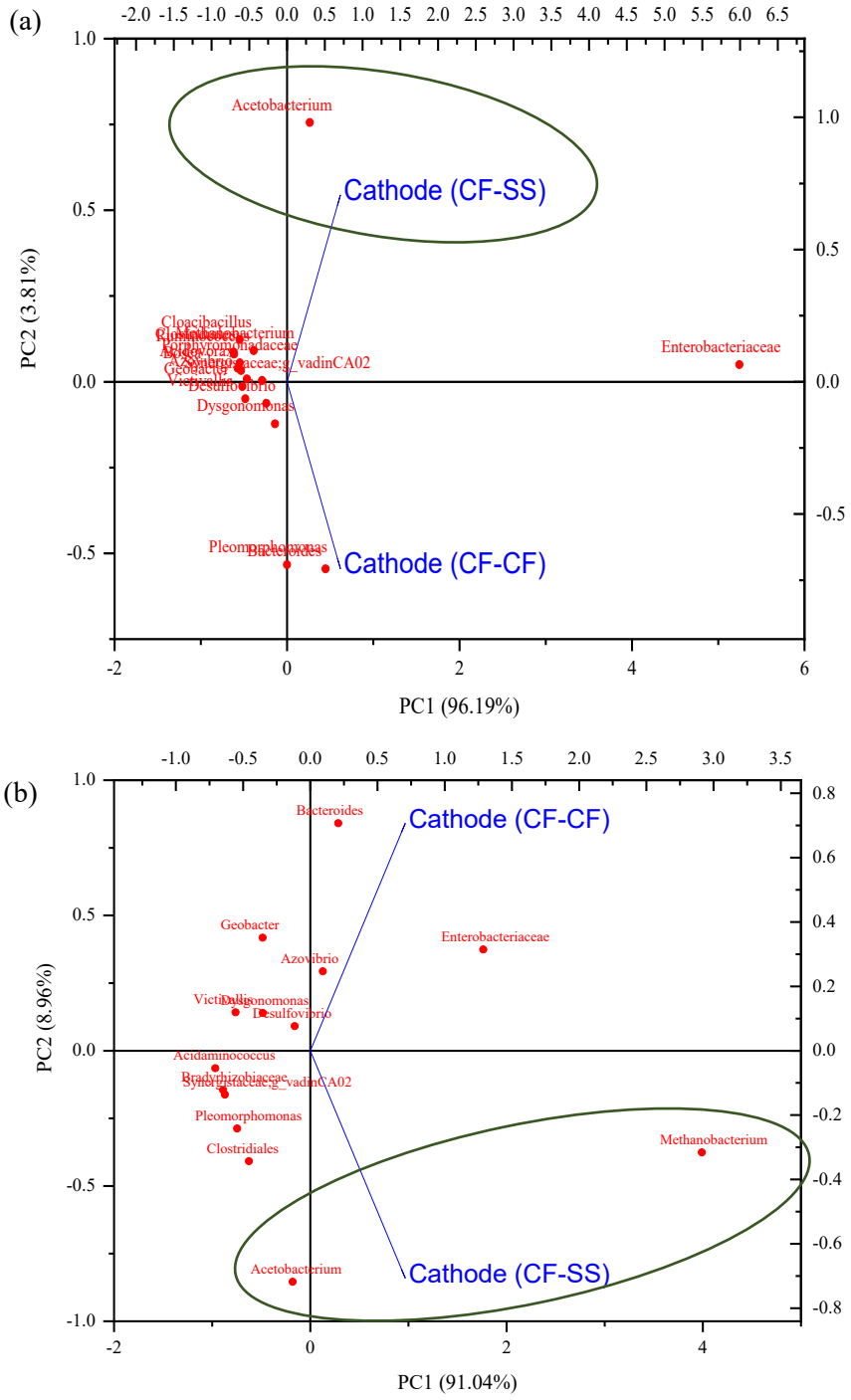


**Figure 3.11** Principal Component Analysis of the bacterial (a) and archaeal (b) communities in biocathode of CF-CF and CF-SS reactors

### *3.3.7. Expression of EET genes*

The gene expression for *pil*A and c-type cytochromes (Figure 3.12) shows trivial differences in their expression levels in anode/cathode biofilms between both reactors. Moreover, compared to anode biofilms, the EET-associated genes were less expressed in cathode biofilms in both reactors. Based on the authors' knowledge, this study first reports the expression of EET genes for methanogenic biocathode. The EET from EAB to the anode has been demonstrated to be facilitated via c-type cytochromes and conductive nanowire or pili (Hernández-Eligio et al., 2020), while the significance of EET in methanogenic biocathode is still ambiguous. However, previous reports postulated that conductive pili and c-type cytochromes could play an important role in DIET from EAB to methanogens (J.-H. Park et al., 2018; Rotaru et al., 2014b). Notably, some bacteria (e.g., *Enterobacteriaceae*, *Desulfovibrio*, etc.) found in biocathode in this study could express different cytochromes and/or conductive pili (Gardy et al., 2003; Hernández-Eligio et al., 2020). Furthermore, a recent study suggested that *Methanobacterium* species could produce methane via DIET (Zheng et al., 2020). Nonetheless, the expressions of these EET genes were quite comparable in both systems, indicating higher current density and methane productivity from the CF-SS reactor was not attributed to the overexpression of EET genes.

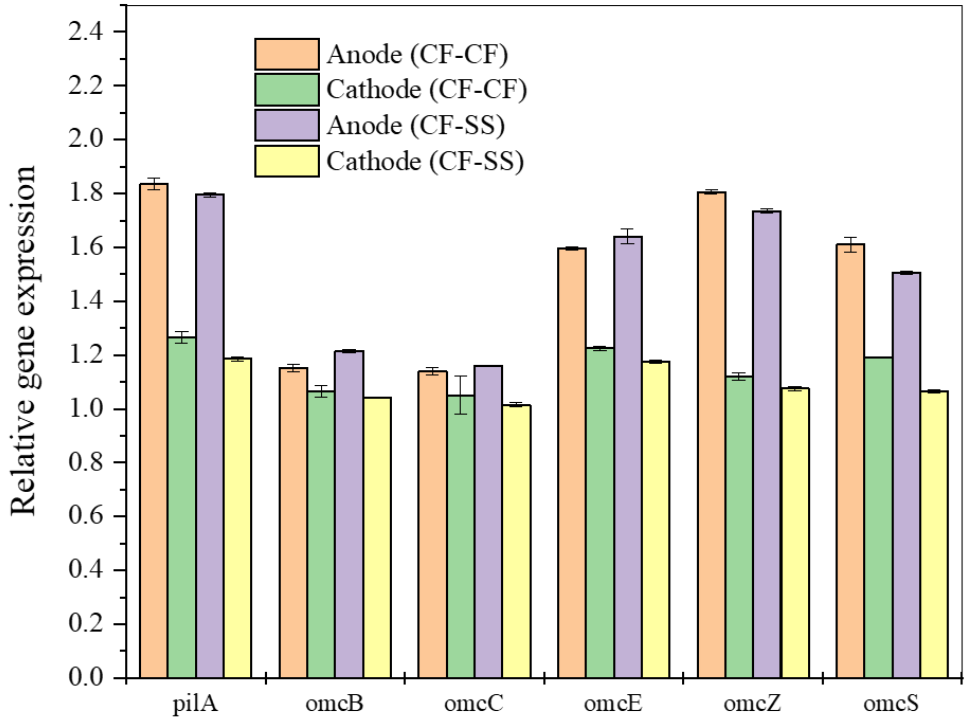


**Figure 3.12** Expression of genes known to regulate extracellular electron transfer in biofilms. The error bars indicate the standard deviation of three replicates (n = 3)

### *3.3.8. Conclusions*

This study provides new insights into the characteristics and significance of EPS and expressions of EET genes in methanogenic biocathode. As compared to the carbon fiber, significantly higher EPS levels were observed in the stainless steel biocathode. Protons reduction to $H_2$ during HER can create local alkaline pH on the cathode. Thus, it could be posited that the highest EPS secretion in stainless steel biocathode could be linked with faster HER. One important finding of this current study is that EET may not play a decisive role in differentiating performances in MEC-AD systems using different electrode materials. Instead, the effective catalysis of HER, lower internal resistance, and higher abundances of $H_2$-utilizing methanogens and homoacetogens on stainless steel cathode appeared to be the primary reason behind the higher methanogenic activity. Nonetheless, based on EET gene expression patterns and redox activity of biocathode-derived EPS, EET would still be involved in cathodic electro-methanogenesis.

Regarding the engineering significance of the results, carbon-based cathode electrodes have been mostly used in MEC-AD systems due to their excellent biocompatibility and higher surface area over metal-based electrodes. While carbon fibers provided a higher specific surface area, stainless steel mesh outperformed carbon fibers under similar operating conditions (e.g., anode electrode, inoculum, mixing, etc.). Given that most of the single-chamber MEC-AD studies used carbon-based biocathode, the results of this study are significant for selecting efficient cathode materials to realize improved performance. However, it should be noted that the results presented here are from specific operating conditions with two selected electrode materials. Hence, further research is warranted with more carbon and metal electrodes with similar textures and surface areas.

# Chapter 4

# Investigation of the detrimental ratio of propionate to acetate in a microbial electrolysis cell assisted anaerobic digester

*A version of this chapter will be submitted in a journal for peer-review and publication*

## 4.1. Introduction

Integrating microbial electrolysis cells with anaerobic digestion is a promising approach for a more robust and stable microbiome in attaining enhanced biomethane recovery from various organic wastes (Huang et al., 2020; J. Park et al., 2018c; Zakaria and Dhar, 2019, 2021b). Such an integrated process is called microbial electrolysis cell-assisted anaerobic digestion (MEC-AD). In MEC-AD systems, simple organic substrates like acetate can be efficiently utilized by anodic electroactive bacteria, such as *Geobacter, Shewanella, Pseudomonas,* etc. (Hari et al., 2017; Shao et al., 2019; Yang et al., 2015). On the cathode electrode, methanogens can utilize electrons and electrochemically produced $H_2$ for methane production.

Fermentation is essential for converting complex organic substrates to simple organic acids before being utilized via anodic electroactive bacteria (L. Lin et al., 2019b; Ruslan and Vadivelu, 2019). Notably, volatile fatty acids (VFAs) are essential intermediates resulted from the fermentation process, which affects the process efficiency and stability (Hari et al., 2017; J. Park et al., 2018a; Sun et al., 2012). The VFAs are primarily composed of acetic acid, butyric acid, and propionic acid. Previous studies reported the following utilization sequence of VFAs in MECs: acetate>butyrate>propionate (Lee et al., 2015; Lin et al., 2019; Yang et al., 2015; Shao et al., 2019). However, several studies reported that electroactive bacteria could not directly oxidize propionate or butyrate (Hari et al., 2017; Park et al., 2018a; Sun et al., 2012; Dhar et al., 2015, 2013; Hari et al., 2016a; Lin et al., 2019; Speers and Reguera, 2012; Yang et al., 2015).

Propionate is one of the critical metabolites produced during anaerobic digestion of complex organics and can represent up to 35% of the total carbon flow to methane in conventional digesters (Dyksma and Gallert, 2019). Furthermore, propionate accumulation has been frequently identified

when conventional anaerobic digesters became unstable (Franke-Whittle et al., 2014; Gallert and Winter, 2008; Pullammanappallil et al., 2001; Wang et al., 2009). However, several studies reported low current density from MECs fed with propionate (Torres et al., 2007; Yang et al., 2015). Propionate oxidation in MECs requires syntrophic interactions between fermenters and electroactive bacteria (Hari et al., 2016b; Yang et al., 2015). Fermenters oxidize propionate firstly to acetate and $H_2$, and then acetate could be utilized directly by electroactive bacteria (Hari et al., 2016b; L. Lin et al., 2019b; Yang et al., 2015). Theoretically, the Gibbs free energy of the syntrophic conversion of propionate to acetate is endergonic, close to $\Delta G$ +76.1 kJ/ mol propionate (Krylova and Conrad, 1998). Therefore, the accumulation of acetate and other fermentable products, i.e., $H_2$, produced from propionate degradation would increase $\Delta G$, which shift the reaction into more endergonic and thermodynamically unfavorable. Thus, syntrophic interactions between fermentative and electroactive bacteria along with $H_2$-utilizing methanogens are required to maintain the $H_2$ partial pressure and acetate levels as low as possible to allow exergonic propionate conversion (Yasri et al., 2019).

Inhibition of conventional anaerobic digesters at higher propionate concentrations has been widely reported (Franke-Whittle et al., 2014; Wang et al., 2009). For instance, propionate concentrations >20 mM were detrimental to the methanogenesis process (Gallert and Winter, 2008; Pullammanappallil et al., 2001). Wang et al. (2009) found that acetate of 2400 mg/L and butyrate 1800 mg/L resulted in no inhibition of methanogenesis. However, a propionate concentration of 900 mg/L resulted in the deterioration of the methanogenesis. Previous studies also reported that the high acetate concentrations could inhibit the degradation of propionate (Lee et al., 2015; L. Lin et al., 2019b). Therefore, maintaining an optimum propionate to acetate (HPr/HAc) has been emphasized by previous studies (Franke-Whittle et al., 2014; Hill et al., 1987; Kor-Bicakci et al., 2020). For instance, Kor-Bicakci et al. (2020) found a mild inhibition of the AD system when HPr/HAc ratio exceeded 1.4. Thus, the removal of propionate is required for a stable process. To date, the detrimental ratio of propionate/acetate concentrations towards the electromethanogenesis process has not been examined yet. Thus, understanding the impact of different VFAs concentrations with varied propionate and acetate ratios on the microbial community and methanogenesis process would be essential for developing high-rate MEC-AD systems.

## 4.2. Methodology

### *4.2.1 MEC-AD configuration*

The experiment was conducted in a single-chamber MEC-AD reactor manufactured with plexiglass with a total volume of 400 mL and a working volume of 360 mL. Carbon fibers (2293-A, 24A, Fibre Glast Development Corp., Ohio, USA) integrated with a stainless-steel frame (as a current collector) were used as anode and cathode electrodes. As previously described by Zakaria and Dhar (2021a) before use, carbon fibers were pre-treated. Ag/AgCl (+0.19 V vs. SHE, MF-2052, Bioanalytical System Inc., West Lafayette, IN, USA) was inserted as the reference electrode within <1 cm of the anode electrode. The reactor was operated with a fixed anode potential of -0.4 V vs. Ag/AgCl using a potentiostat (Squidstat Prime, Admiral Instruments, Arizona, USA). Current and voltage were recorded every 4.8 min using a Squidstat Prime software connected with a potentiostat (Squidstat Prime, Admiral Instruments, USA). The reactor operated with continuous stirring at 130±5 rpm at room temperature (21±1 °C).

### *4.2.2 Start-up and operation*

The reactor was inoculated with anaerobic digester sludge and effluent from a mother MEC reactor that has been in operation for > 12 months with a 25 mM sodium acetate medium. The anaerobic digester sludge was collected from the Gold Bar Wastewater Treatment Plant (Edmonton, AB, Canada). In the enrichment phase, the reactor was operated in a semi-continuous mode with an anaerobic glucose medium (2235±31 mg COD/L) supplemented with 50 mM phosphate-buffered saline (PBS, pH=7.05) and trace minerals. The trace minerals mixture was added, according to c). After reaching the steady-state current (indicated by maximum peak current of ~14 mA in multiple operating cycles), the reactor switched to the fed-batch operating mode for experiments to evaluate the effects of various propionate to acetate ratios.

At the beginning of each fed-batch cycle, the reactor was evacuated and fed with an anaerobic medium having a mix of acetate (HAc), propionate (HPr), and butyrate (HBu) as a carbon source. The buffer and trace minerals remained the same as the glucose medium. The total VFAs concentration was fixed at 2000±37 mg COD/L during the entire experiment. Depending on the experimental conditions, HPr/HAc ratios were varied, while butyrate concentration was fixed

throughout the experiment (Table 4.1). The fed-batch cycle was considered as completed when the current declined < 2 mA. Then, the substrate medium was replaced with a fresh medium. Each HPr/HAc ratio was operated for several consecutive cycles. All the medium was flushed with nitrogen gas (99.99%) for 5 minutes prior to feeding to maintain anaerobic condition.

**Table 4.1** Summary of experimental conditions under different propionate to acetate (HPr/HAc) ratios

| | **HPr/HAc ratios** | | | |
|---|---|---|---|---|
| | 0.5 | 1.5 | 2.5 | 5 |
| **Acetate, mg COD/L** | 1200±3 | 735±4 | 528±2 | 315±4 |
| **Propionate, mg COD/L** | 617±4 | 1075±3 | 1324±3 | 1560±3 |
| **Butyrate, mg COD/L** | 185±3 | 176±2 | 182±2 | 183±2 |
| **TCOD, mg/L** | 2002±4 | 1986±5 | 2034±3 | 2058±4 |

### *4.2.3. Characterization of EPS composition*

The anode and cathode biofilms were analyzed for various EPS components: carbohydrates, proteins, heme-binding proteins, uronic acid, and eDNA. Several portions of anode and cathode biofilms were collected at the end of the fed-batch cycles of each condition using aseptic scissors. The detailed protocol of sample preparation, EPS extraction, and characterization can be found in the literature (Zakaria and Dhar, 2021). Briefly, two methods were used for EPS extraction: cation-exchange resin (CER) and heating method. It should be noted that these two methods were reported to be highly efficient for EPS extraction in several previous studies (Dai et al., 2016; Tan et al., 2019; Xiao et al., 2017). Moreover, both methods provided consistent EPS extraction efficiency in our previous study (Zakaria and Dhar, 2021b). EPS levels were presented as the mass of EPS per unit surface area of the electrode (mg/cm$^2$) for comparing EPS levels under different conditions.

### *4.2.4 Characterization of Microbial Community*

#### *4.2.4.1. DNA extraction and sequencing*

Several portions of the anode and cathode biofilms were collected using an aseptic scissor for each condition. According to the manufacturer's instructions, the genomic DNA was extracted using PowerSoil DNA Isolation Kit (MoBio Laboratories Inc., Carlsbad, USA). DNA yield and purity were measured spectrophotometrically using a Nanodrop spectrophotometer (2000C, Thermo Scientific, USA) and then normalized based on the surface area of the electrode portion. The extracted DNA samples were stored at -70 ˚C prior to the PCR analysis and sequencing. The DNA samples were sent to Research and Testing Laboratory (Lubbock, TX, USA) to perform Illumina Miseq Sequencing. For the sequencing primers, universal bacterial primer; 341F: 5' CCTACGGGNGGCWGCAG 3' and 805R: 5' GACTACHVGGGTATCTAATCC 3' (Klindworth et al., 2013; Logares et al., 2013), and archaeal primer; 517F: 5' GCYTAAAGSRNCCGTAGC 3' and 909R: 5' TTTCAGYCTTGCGRCCGTAC 3' (Morris et al., 2014) were used to target the 16S rRNA gene. The quantification of 16S rRNA of bacteria and archaea and Methyl Coenzyme-M reductase gene (*mcr*A) gene copies was performed using qPCR (Zakaria and Dhar, 2021b). The detailed protocol for qPCR and primers are listed in our previous study (Zakaria and Dhar, 2021b).

### *2.4.2. Bioinformatics analysis*

Bioinformatics analysis was performed, as previously described in the literature (Zakaria and Dhar, 2021). The nucleotide sequence reads were analyzed using QIIME 2 pipeline (Quantitative Insights Into Microbial Ecology pipeline, v. 2021.4, http://qiime.org; Caporaso et al. (2010). DADA2 was used to filter the sequenced amplicon errors by removing chimeric sequences, reads, and short sequences (Bolyen et al., 2019). Then, the sequences were assigned to Operational Taxonomic Units (OTUs) using UCLUST at 97% identity and aligned with the Greengenes reference database (v. 13.8) (Edgar, 2010). Microbial diversity was represented by analyzing several alpha and beta diversity metrics using QIIME 2. Alpha diversity was calculated by different indices of richness and evenness, including Chao1, Shannon, OTUs, and Pielou’s evenness. Beta diversity was analyzed using a weighted UniFrac distance matrix to show the community dissimilarities in the phylogenetic relationships and then visualized as principal coordinates

analysis (PCoA) plots. Also, the phylogenetic diversity was constructed as a rooted phylogenetic tree using mafft program. The Qiime 2 artifact has been used to filter the alignment to remove the highly variable positions. Then, the pipeline used FastTree to generate the phylogenetic tree, and it is constructed using the online tool Interactive Tree of Life (iTOL, v. 6.1.1, Letunic and Bork, 2007, https://itol.embl.de). Chord diagram was created using OTU taxonomic units analyzed from QIIME 2.

### *2.4.3. Correlation Coefficients*

Bacterial and archaeal taxa with an abundance of ≥1% were correlated with each condition using Spearman's rank correlation (Khafipour et al., 2020). The correlation coefficient (Spearman's Rho) and *p*-values were calculated for each condition. The correlation coefficient values ranged from -1 to +1, the higher positive values indicating stronger correlation and lower negative values indicating weak correlation. Alpha value for the correlation confidence intervals was set up as 0.05. Correlation analysis of bacteria and archaeal abundances along with different parameters at each condition were visualized in scatterplot matrix and principal component analysis (PCA) generated by JMP software (v. 11.0.0, SAS Institute Inc., Cary, NC, US, https://www.jmp.com).

### *2.4.4. EET genes expression*

The changes in expressions of genes associated with EET (*pil*A*, omc*B*, omc*C*, omc*E*, omc*Z, and *omc*S) were assessed for different experimental conditions. The primer design approach was previously described in the literature (L. Lin et al., 2019a; Zakaria and Dhar, 2021b). *rec*A housekeeping gene has been used as a reference gene (Rivas et al., 2005). The total RNAs of anode and cathode biofilms were extracted for each test condition. The detailed method and the primers used in this study are listed in our previous study (Zakaria and Dhar, 2021b).

### *4.2.5. Analytical methods*

The influent and effluent samples from the reactor at each condition were filtered with 0.45 µm pore size for COD measurements with the HACH method using UV-spectrophotometer (Model DR 3900, HACH, Germany). The concentrations of VFAs (acetate, propionate, and

butyrate) were measured after filtration with 0.2 μm pore size by an ion chromatograph (Dionex ICS-2100, Thermo Scientific, USA) equipped with an electrochemical detector (ECD) and microbore AS19, 2 mm column. The biogas was collected using a 500 mL gas bag, and biogas composition (i.e., methane content) was examined by a gas chromatograph (7890B, Agilent Technologies, Santa Clara, USA).

## 4.3. Results and discussion

### *4.3.1. Methane generation*

Figure 4.1 shows the total cumulative methane production and yields under various HPr/HAc ratios. The total cumulative methane production (426-434 L $CH_4/m^3$) and yields (71.1-73%) remained almost the same after increasing HPr/HAc ratio from 0.5 to 1.5 ($p=0.8$). In contrast, methane production reached a plateau after different operational times (144 vs. 204 h), indicating higher HPr/HAc ratio slowed down methanogenesis rates. When HPr/HAc ratios further increased to 2.5 and 5, the total cumulative methane production markedly decreased to 348±11.9 L $CH_4/m^3$ (after 192 h) and 332±8.7 L $CH_4/m^3$ (after 228 h) ($p=0.008$), respectively. Moreover, methane yields decreased to 56.3±1.5% and 42.7±1.7%, respectively ($p=0.009$). Based on previous reports, HPr/HAc ratios >1.4 could lead to deterioration of methane generation in traditional anaerobic digesters (Franke-Whittle et al., 2014; Hill et al., 1987; Kor-Bicakci et al., 2020). Nonetheless, limited information is available in the literature on the effects of various HPr/HAc ratios on MEC-AD systems. This study demonstrated that higher HPr/HAc ratios would also adversely impact methane yields as well as methanogenesis rates in MEC-AD systems.

Inferior digester performance at higher propionate concentrations has frequently been reported for conventional AD (Franke-Whittle et al., 2014; Wang et al., 2009). Although anode biofilms can efficiently utilize propionate in MECs, several studies reported that propionate could not be directly utilized by anodic electroactive bacteria (Dhar et al., 2015, 2013; Hari et al., 2016a). Instead, electroactive bacteria would require syntrophic partners (e.g., propionate fermenters) for propionate utilization. In this study, higher HPr/HAc ratios also impacted current densities from MEC-AD. Notably, higher HPr/HAc ratios 2.5 and 5 considerably decreased current densities, suggesting corroboration between current density and methane recovery (Figure 4.2).

Moreover, known acetogens were selectively enriched on the cathode biofilms at higher HPr/HAc ratios of 2.5 and 5 (discussed later). The enrichment of some specific acetogens, particularly *Sporomusa*, on the cathode biofilms resulted in significant losses of COD from being utilized for the methanogenesis process. In addition to $H_2$ utilization (usually $H_2/CO_2$ conversion to acetate) (May et al., 2016; Tremblay et al., 2017), electrotrophic activity of acetogenic *Sporomusa* species in cathode biofilms have been reported in the literature (Aryal et al., 2017; Nevin et al., 2011, 2009; Zaybak et al., 2013). For instance, Aryal et al. (2017) found several species of *Sporomusa,* such as *ovata, acidovorans*, and *malonica,* could utilize electrons on the cathode electrode and reduce $CO_2$ to organic compounds (e.g., acetate). Notably, acetogenic species accounted for the consumption of >80% of the available electrons on the cathode (Nevin et al., 2011). In biofilms environment, acetogens can even outcompete hydrogenotrophic methanogens for $H_2$ (Parameswaran et al., 2012). Although the co-existence of acetogens and methanogens has also been reported for biocathode in MEC-AD, our results suggest that high HPr/HAc ratios can proliferate the growth of acetogens in biocathode and consequently hinder the availability of $H_2$ or electrons to methanogens.

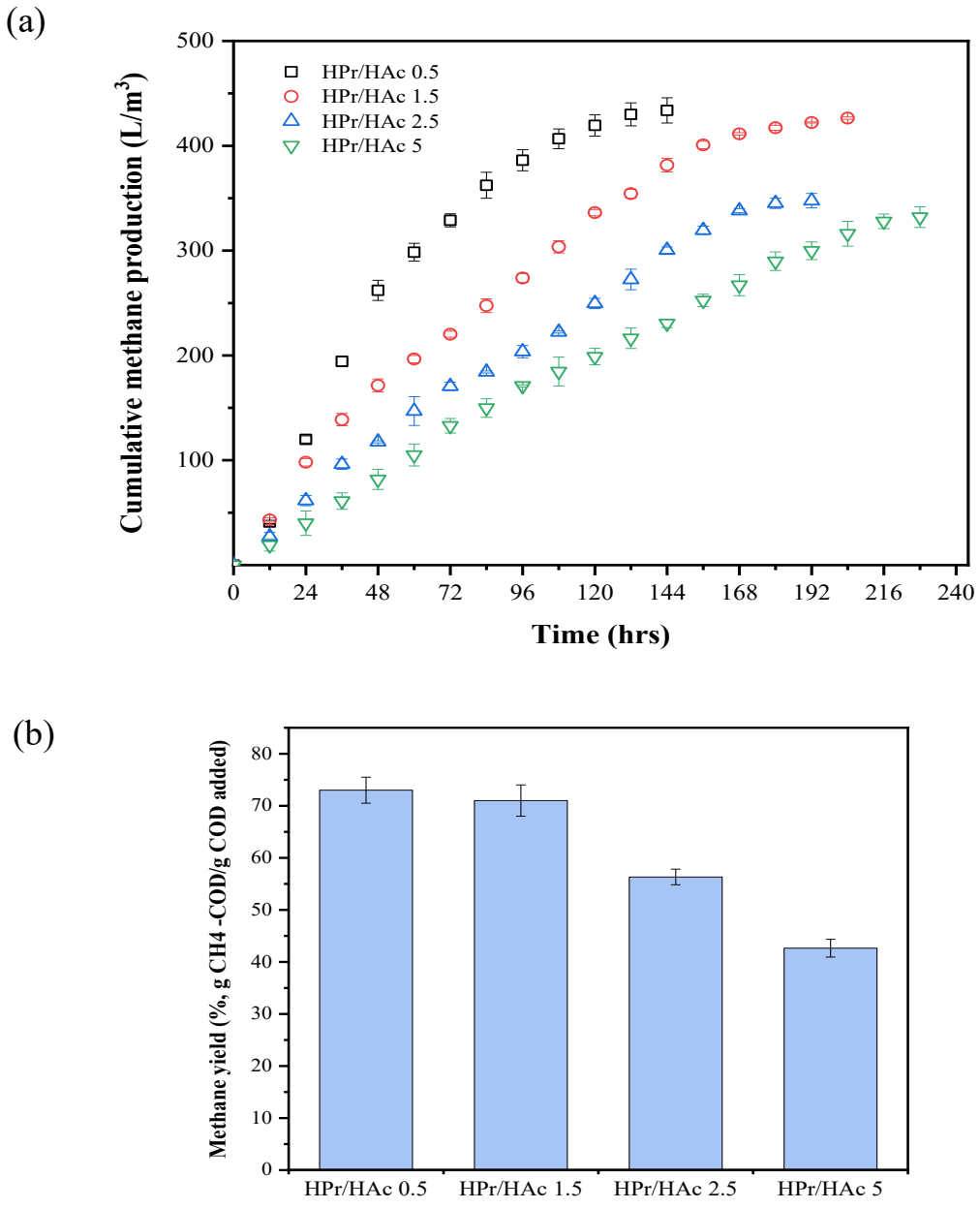


**Figure 4.1** Cumulative methane production (a) and methane yield (b) at different HPr/HAc. Note. The error bars indicate the standard deviation of three replicates (n = 3)

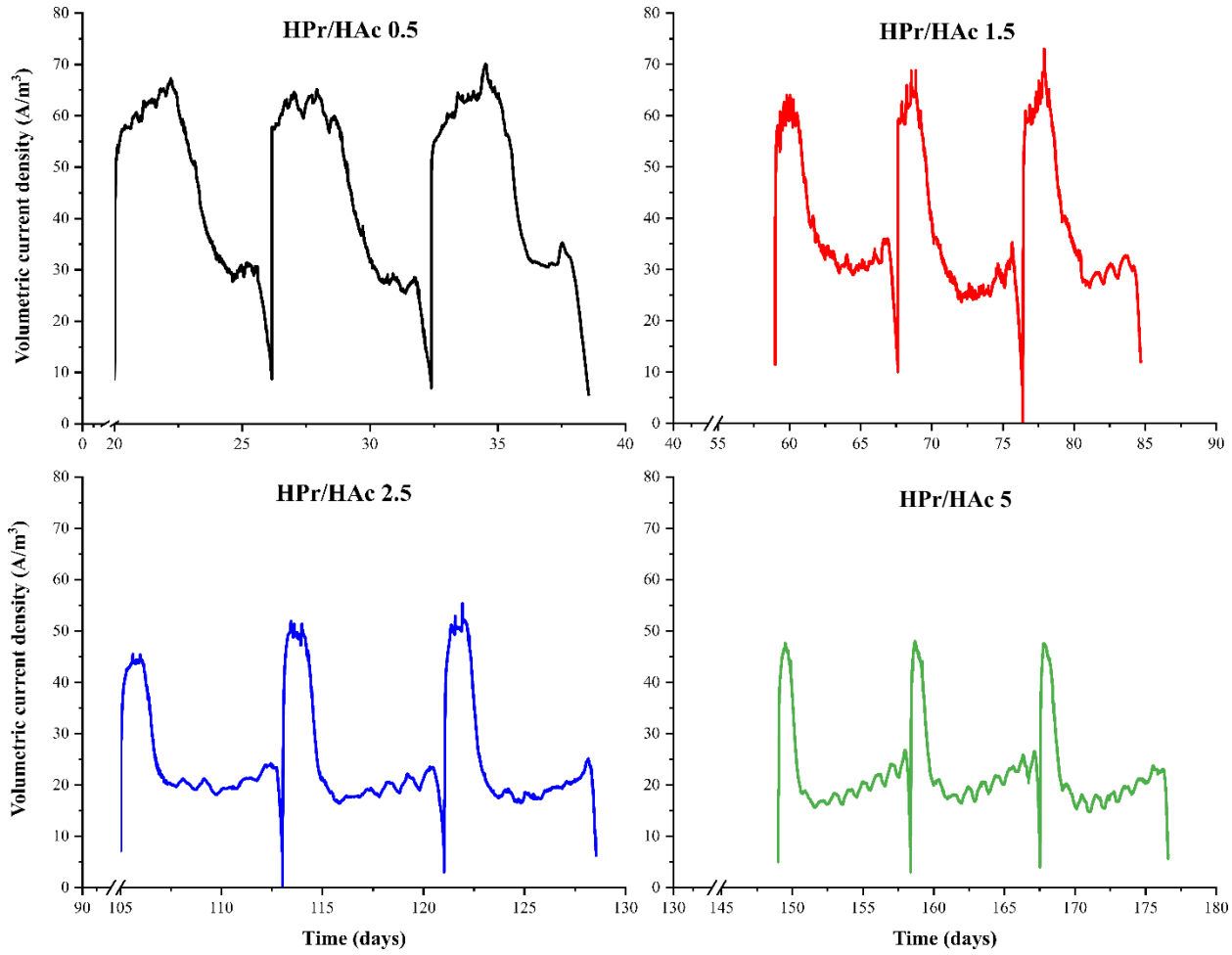


**Figure 4.2** Volumetric current densities at different HPr/HAc ratios. Note. Volumetric current densities indicate the current normalized by the total working volume of the reactor. The results from 3 representative batch cycles during steady-state are shown here

### *4.3.2. COD removal and VFAs profile*

Figure 4.3a shows changes in COD and VFAs during operation under various HPr/HAc ratios. As shown in Figure 4.3a, the final COD and VFAs concentrations were comparable under different HPr/HAc ratios ($p=0.5$), while their degradation profiles differed. Notably, propionate and acetate degradation profiles were distinct under different HPr/HAc ratios, which primarily affected the COD degradation profiles. In contrast, butyrate degradation profiles were comparable for different conditions. Even though overall COD removal efficiencies were comparable for all conditions (Figure 4.3a), methane yields varied considerably (Figure 4.1b). As mentioned earlier, methane yields gradually decreased with increasing HPr/HAc ratios, indicating that a significant portion of removed COD was presumably utilized through various processes other than methane production. As discussed later, various fermentative bacteria belong to class *Clostridia* and *Synergistia* were enriched at higher HPr/HAc ratios. Thus, such low methane yields (i.e., COD loss) might be attributed to a higher yield of fermentative bacterial biomass.

Figure 4.3b shows the temporal changes in HPr/Hac ratios during the reactor's operation under different conditions. For the initial HPr/HAc of 0.5, HPr/HAc ratio started to increase slowly from 0.5 to 1.0. For initial HPr/HAc of ratio 1.5, HPr/HAc ratio reached 5.1 after 108 h and then decreased sharply to 1.3 at the end of the batch cycle. However, for an initial HPr/HAc ratio of 2.5 and 5, HPr/HAc ratios fluctuated during the batch cycles. For the initial HPr/Hac ratio of 2.5, HPr/HAc ratio reached a maximum of 8.1 and then gradually decreased to 1.7 at the end of the batch cycle. For HPr/Hac of 5, HPr/HAc ratio sharply reached as high as 23.7 and then fluctuated until reaching 2.2 at the end of the cycle. The sharp increase of the HPr/HAc ratios at the initial HPr/HAc 2.5 and 5 conditions indicated that the acetate consumed rapidly initially. Then propionate started to ferment slowly (Figure 4.3a). Thus, high propionate oxidation was noticed at low concentrations of acetic acid (less than 200 mg COD/L). In other words, high acetate concentrations affected the oxidation of the propionate. Theoretically, the Gibbs free energy of the syntrophic conversion of propionate to acetate is endergonic, which close to $\Delta G$ +76.1 kJ/mol propionate (Krylova and Conrad, 1998). Moreover, the accumulation of acetate and other fermentable products produced from propionate degradation would increase $\Delta G$, which shift the reaction into more endergonic and thermodynamically unfavorable. Thus, the inferior propionate

degradation at higher acetate concentration observed in this study was consistent with these fundamental notions.

(a)

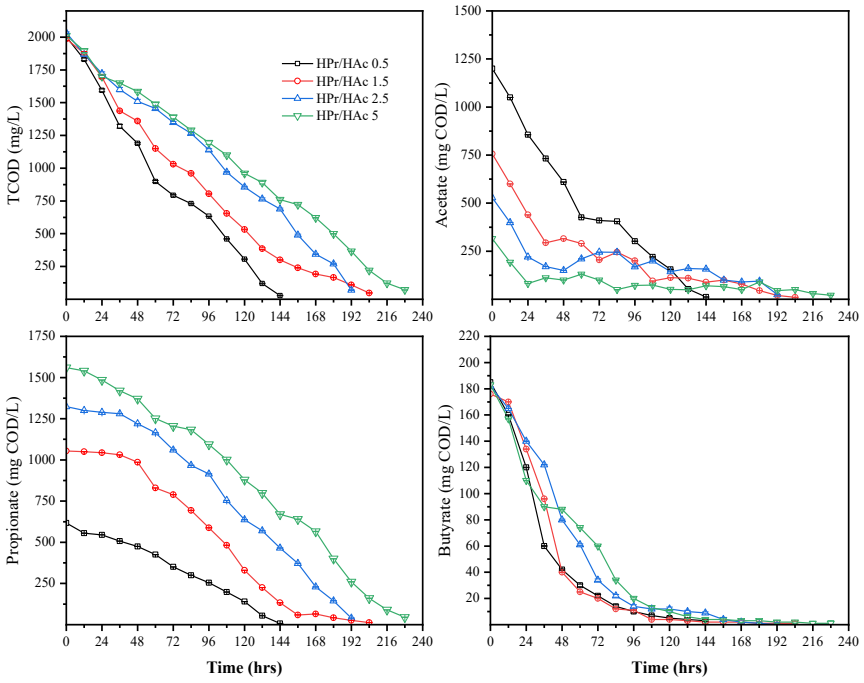


(b)

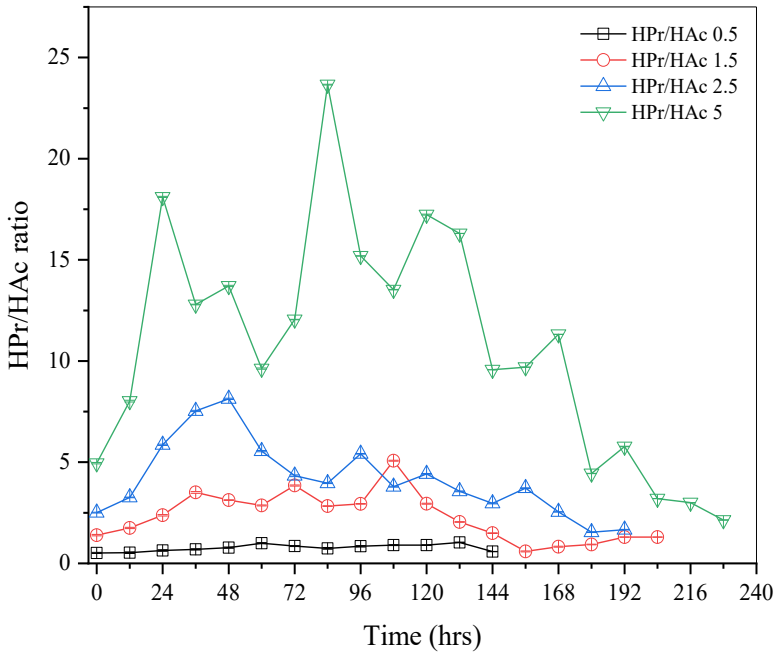


**Figure 4.3** Changes in COD concentrations (a) and ratios (b) at different HPr/HAc ratios. Note. The error bars indicate the standard deviation of three replicates (n = 3)

### *4.3.3. EPS composition*

Figure 4.4 showed the EPS composition of anode and cathode biofilms at different HPr/HAc ratios. The EPS composition under lower HPr/HAc ratios of 0.5 and 1.5 was similar in anode and cathode biofilms (p=0.7). The changes in EPS composition were comparable, with a decreasing trend in overall EPS levels under higher HPr/HAc ratios (2.5 and 5) (p=0.02). The carbohydrate fraction of EPS increased in anode biofilms at higher HPr/HAc ratios of 2.5 (50.4±0.7 mg/cm$^2$) and 5 (57.8±0.4 mg/cm$^2$) in comparison to ratios of 0.5 (26.6±1.3 mg/cm$^2$) and 1.5 (34.7±0.3 mg/cm$^2$). In contrast, protein fraction of EPS considerably decreased at higher HPr/HAc ratios of 2.5 (100.4±1.1 mg/cm$^2$) and 5 (75.4±0.5 mg/cm$^2$) than ratios of 0.5 (136.5±2.0 mg/cm$^2$) and 1.5 (133.3±0.6 mg/cm$^2$). Similar trends were observed for heme, uronic acids, and eDNA. eDNA levels were much lower than other EPS fractions < 1 mg/cm$^2$. EPS composition on the cathode biofilms showed similar patterns to the anode biofilms. The ratios of the carbohydrates to proteins increased from 0.2-0.3 at lower HPr/HAc ratios (0.5 and 1.5) to 0.5-0.8 at higher HPr/HAc ratios (2.5 and 5).

Despite biofilm EPS has multiple functions (e.g., biofilms maturation, cells attachments, and protection), recent studies reported the potential role of EPS in extracellular electron transfer (EET) in conductive biofilms (Stöckl et al., 2019; Tan et al., 2019; Xiao et al., 2017; Angelaalincy et al., 2018). Notably, several reports suggested lower EET efficiency at low EPS protein levels in the anode biofilms (Stöckl et al., 2019; Tan et al., 2019; Xiao et al., 2017). A recent study reported hindered EET in *Geobacter* anode biofilms at higher carbohydrate levels (Yang et al., 2019b). Another study reported deterioration in the current generation at high carbohydrate to protein ratios in anode biofilms (Yang et al., 2019a). As mentioned earlier, current density also decreased at higher HPr/HAc ratios in this study (see Figure 4.2). In addition to direct facilitation of EET, EPS components could immobilize redox cofactors that facilitate EET in anode biofilms (Tan et al., 2019; Xiao et al., 2017). However, the roles of EPS in cathodic methanogenic biofilms have rarely been investigated. A few recent reports suggested that EPS components might provide cell protection in methanogenic biocathode under harsh metabolic conditions (e.g., recalcitrant compounds like phenol, high pH) (Mostafa et al., 2020; Zakaria and Dhar, 2021b). Consequently, EPS could ease cathodic electron transport, which subsequently enhances the electro-

methanogenesis process. In this study, higher HPr/HAc ratios clearly altered EPS compositions, closely related to the current density and methanogenesis performance. It can be hypothesized that a decrease in protein levels might hinder potential electron exchange between cell-to-electrode and cell-to-cell and thereby affected MEC-AD performance.

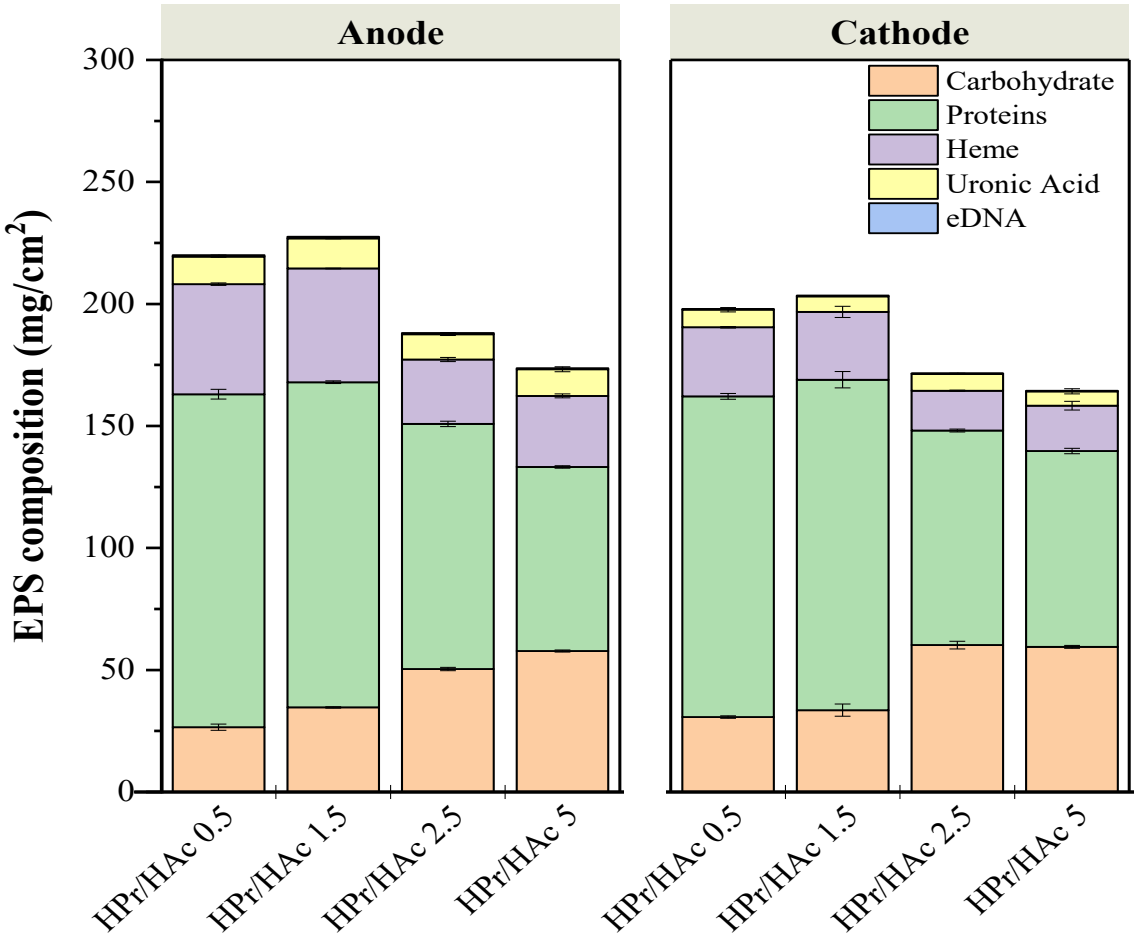


**Figure 4.4** EPS composition at different HPr/HAc ratios. Note. The error bars indicate the standard deviation of three replicates (n = 3).

### *4.3.4. EET expression*

Figure 4.5 shows expressions of EET-associated genes (c-type cytochromes and *pil*A) under different HPr/HAc ratios. The EET-associated gene expression remained unchanged when HPr/HAc ratios changed from 0.5 and 1.5 (p=0.8). However, with increasing HPr/HAc ratios to 2.5 and 5, their relative expression dramatically decreased (p=0.01). Multi-heme c-type cytochromes and electrically conductive e-pili are known to facilitate EET (Gorby and Lovley, 1991; Hernández-Eligio et al., 2020; Lovley and Walker, 2019; Reguera et al., 2005). In addition to EET by electroactive bacteria (e.g., *Geobacter* sp.), some specific methanogens can also directly accept electrons from their syntrophic partners, electrode, or conductive materials, known as direct interspecies electron transfer (DIET) (Gao and Lu, 2021; Lovley, 2017; Rotaru et al., 2014a). Notably, DIET activity of known hydrogenotrophic methanogen, typically enriched in methanogenic biocathode (e.g., *Methanospirillum, Methanobacterium* species), have also been reported in the literature (Walker et al., 2019; Zheng et al., 2020). As discussed later, *Geobacter* and *Methanobacterium* species were abundant under lower HPr/HAc ratios, while their abundance decreased under higher HPr/HAc ratios. Thus, reducing EET-associated gene expression under high HPr/HAc ratios (2.5 and 5) indicates the partial inhibition of biofilm electroactivity. These results were consistent with reduced EPS protein levels at higher HPr/HAc ratios and corroborated with the low current generation and lower methanogenesis process.

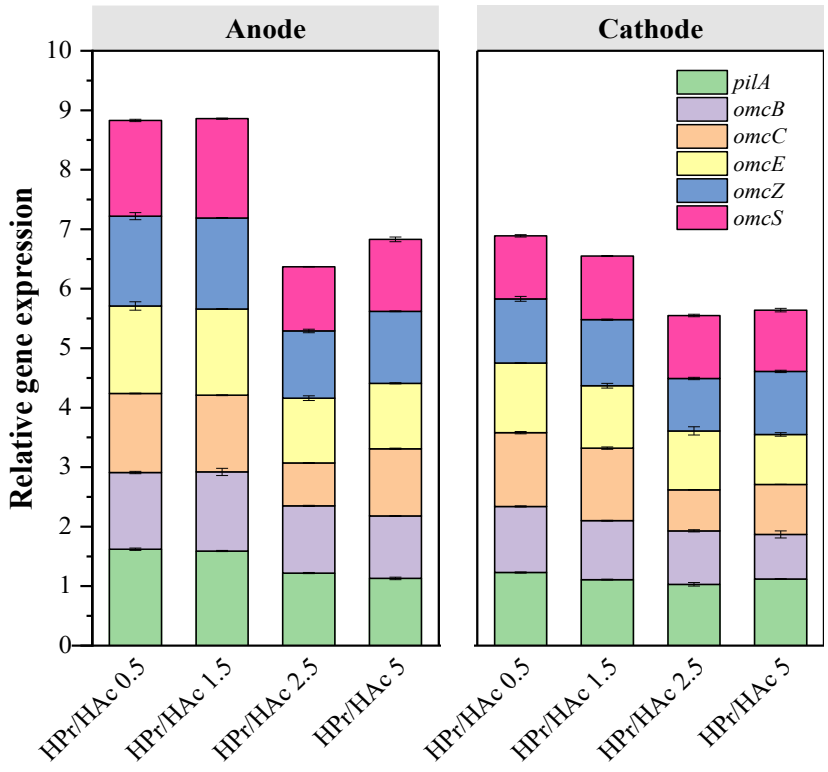


**Figure 4.5** Extracellular electron transfer genes expression at different HPr/HAc ratios. Note. The error bars indicate the standard deviation of three replicates (n = 3)

### *4.3.5. Microbial community analysis*

### *3.5.1. Microbial diversity*

The bacterial and archaeal diversities were assessed with QIIME2 (Figure 4.6) via analyzing the alpha and beta diversity metrics. Significant differences were observed in the microbial diversity and richness under various HPr/HAc ratios. The alpha diversity metrics of the anodic bacterial community increased with increasing HPr/HAc ratios (Figure 4.6a) ($p$ = 0.01). The microbial richness of Chao1 index and observed species (OTUs) were significantly increased from 100 to 176 and 120 to 211, respectively ($p$ = 0.03). Similar patterns were observed for the microbial diversity of the Shannon index and community evenness (Pielou's). The alpha diversity matrics of the biocathode bacterial community also increased; however, at a smaller degree than

the anode biofilms (Figure 4.6a). For the archaeal community, the alpha diversity matrics showed a decrease in the richness and evenness in terms of Chao1 index, OTUs, and Pielou's evenness (Figure 4.6b). However, biocathode archaeal diversity was significantly increased under higher HPr/HAc ratios (2.5 and 5) with no significant change in the Shannon diversity index in the anode biofilms (Figure 4.6b).

Beta diversity was also calculated to evaluate the dissimilarities in the bacterial and archaeal communities on the anode and cathode biofilm by assessing the weighted UniFrac distance (Figure 4.7). The bacterial and archaeal communities showed similarity at lower HPr/HAc ratios of 0.5 and 1.5 on the anode biofilms, which are significantly distinct from the higher HPr/HAc ratios of 2.5 and 5 (Figure 4.7a). On the cathode electrode, the microbial community at the HPr/HAc 0.5 was significantly distinct from the higher HPr/HAc ratios of 1.5 to 5 (Figure 4.7b).

These results imply that higher HPr/HAc ratios induced a higher microbial richness, evenness, and diversity for the anodic bacterial communities with less observed differences in the cathode biofilms. On the contrary, for the archaeal community, the higher HPr/HAc ratios decreased the alpha diversity metrics on the anode and cathode biofilms, except for an increase in the Shannon index diversity on the cathode biofilms.

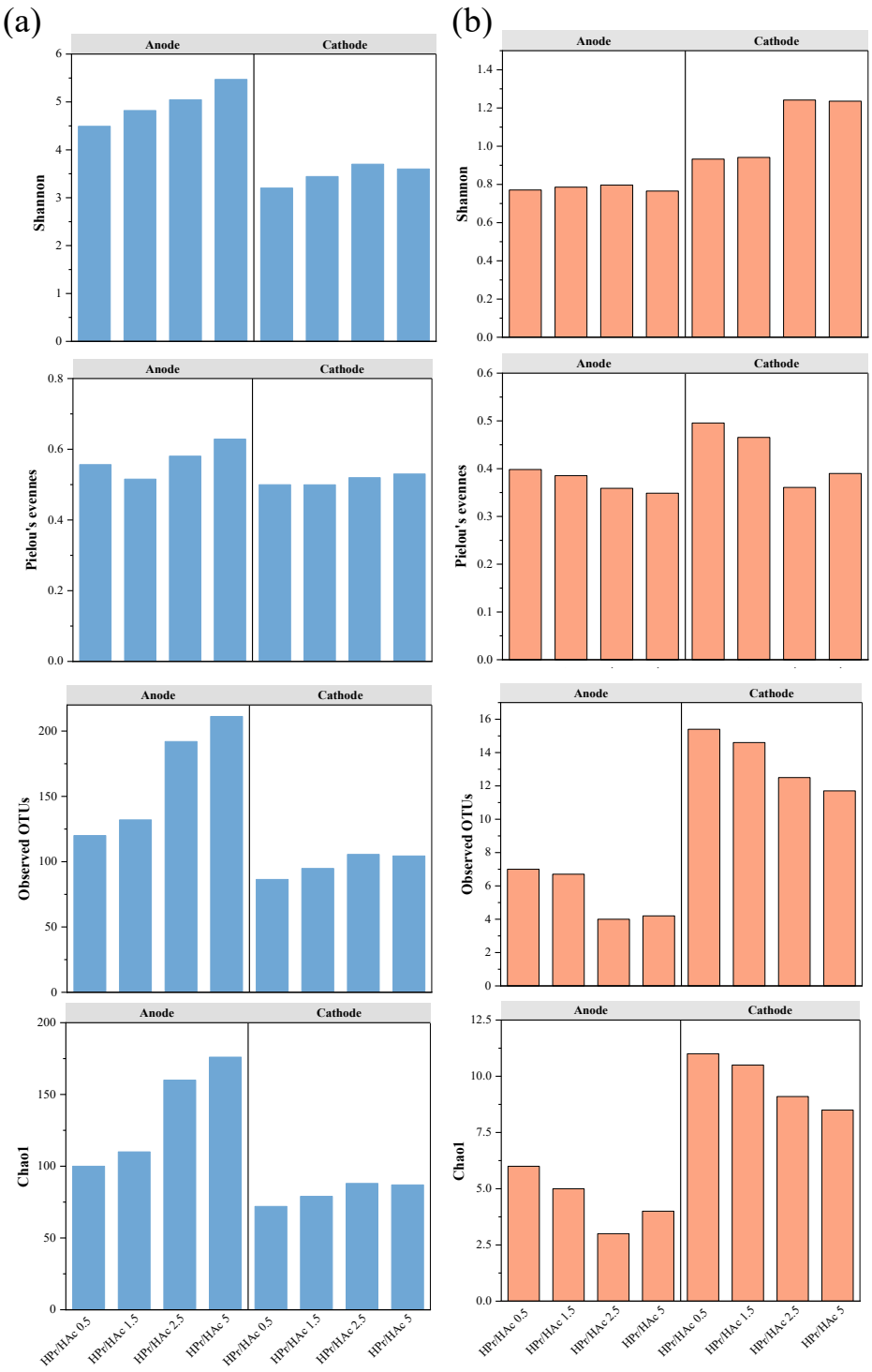


**Figure 4.6** Alpha diversity indices using bacterial primer (a), and archaeal primer (b) at different HPr/HAc ratios

(a)

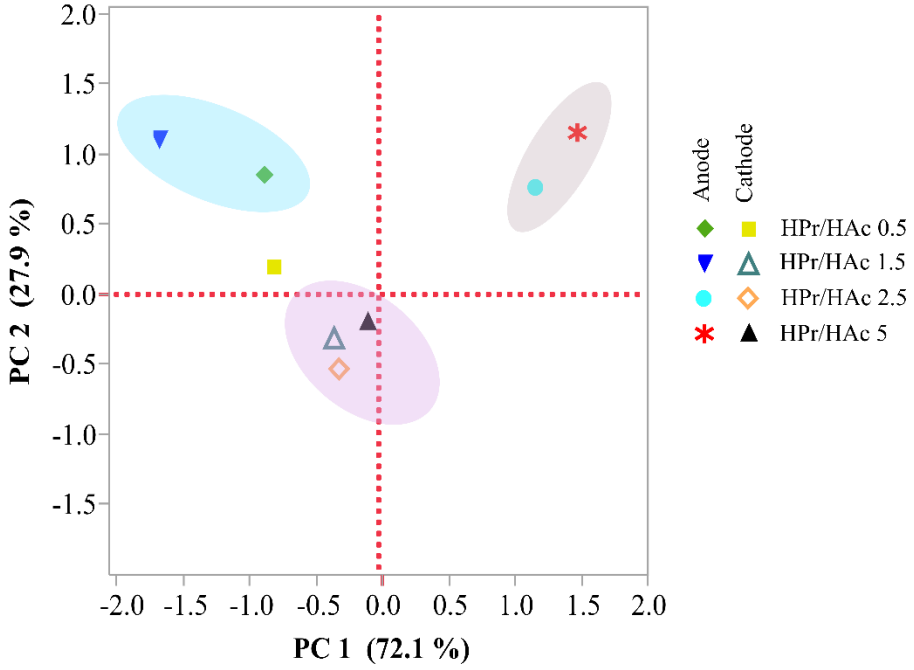


(b)

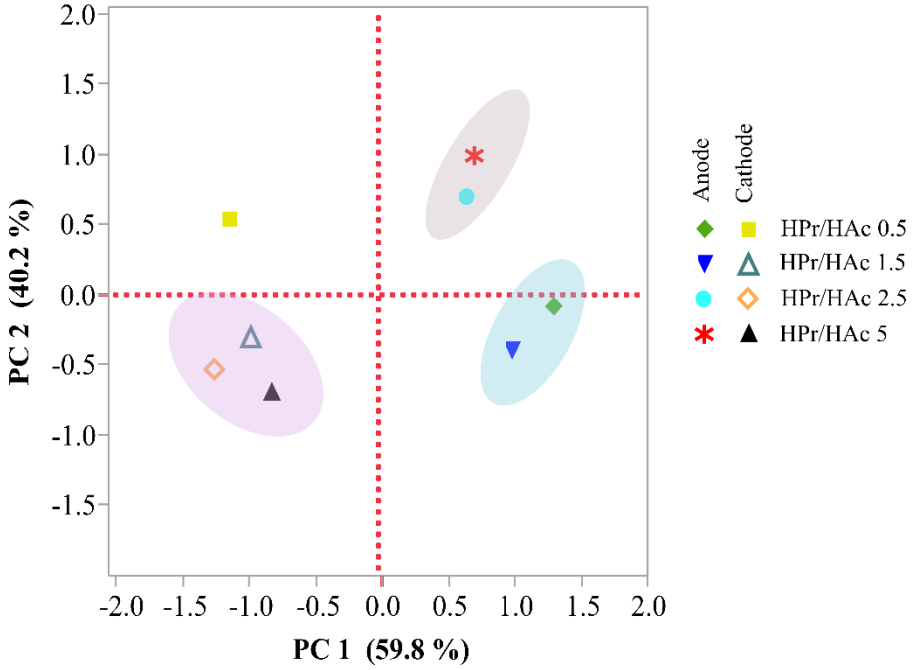


**Figure 4.7** Beta diversity indices using bacterial primer (a), and archaeal primer (b) at different HPr/HAc ratios

### *3.5.2. Quantitative analysis with qPCR*

Figure 4.8 shows the quantitative assessment of bacterial and archaeal communities performed with specific primers using qPCR. For the universal primers, the total microbial cell counts in anode biofilms were significantly increased at higher HPr/HAc ratios 2.5 (6 x $10^{12}$ copies/$cm^2$) and 5 (4 x $10^{12}$ copies/$cm^2$) than lower HPr/HAc ratios of 0.5 (9 x $10^{10}$ copies/$cm^2$) and 1.5 (3 x $10^{11}$ copies/$cm^2$) (p=0.005). On the contrary, the microbial cell counts on the cathode biofilms were higher at lower HPr/HAc 0.5 (4 x $10^9$ copies/$cm^2$) and 1.5 (2 x $10^9$ copies/$cm^2$) in comparison to the higher HPr/HAc ratios of 2.5 (4 x $10^8$ copies/$cm^2$) and 5 (4 x $10^8$ copies/$cm^2$). For the archaeal primers, the total archaeal counts at lower HPr/HAc ratios (0.5 and 1.5) were quite similar in both anode and cathode biofilms, while showed a significant decrease at higher HPr/HAc ratios of 2.5 and 5 (3-7 × $10^6$ copies/$cm^2$ vs. 7-8 × $10^5$ copies/$cm^2$), respectively. These results showed that higher concentrations of propionate (HPr/HAc 2.5 and 5) led to the colonization of higher bacterial biomass, possibly for the requirement of syntrophic interactions between fermenters and electroactive bacteria on the anode biofilms.

Furthermore, *mcr*A gene copies were quantified (Figure 4.8). The functional mcrA gene has been considered a gene biomarker for the phylogenetic characterization of methanogens (Wilkins et al., 2015; Zakaria and Dhar, 2021b). It has been reported in the literature there is a positive correlation between methanogenesis rate and *mcr*A gene copies (Morris et al., 2014; Wilkins et al., 2015; Zakaria and Dhar, 2021b). In both anode and cathode biofilms, increasing HPr/HAc ratios decreased *mcr*A gene copies considerably. However, a greater reduction was observed in the cathode biofilms. Thus, these results are consistent with the inferior methane production observed under higher HPr/HAc ratios of 2.5 and 5.

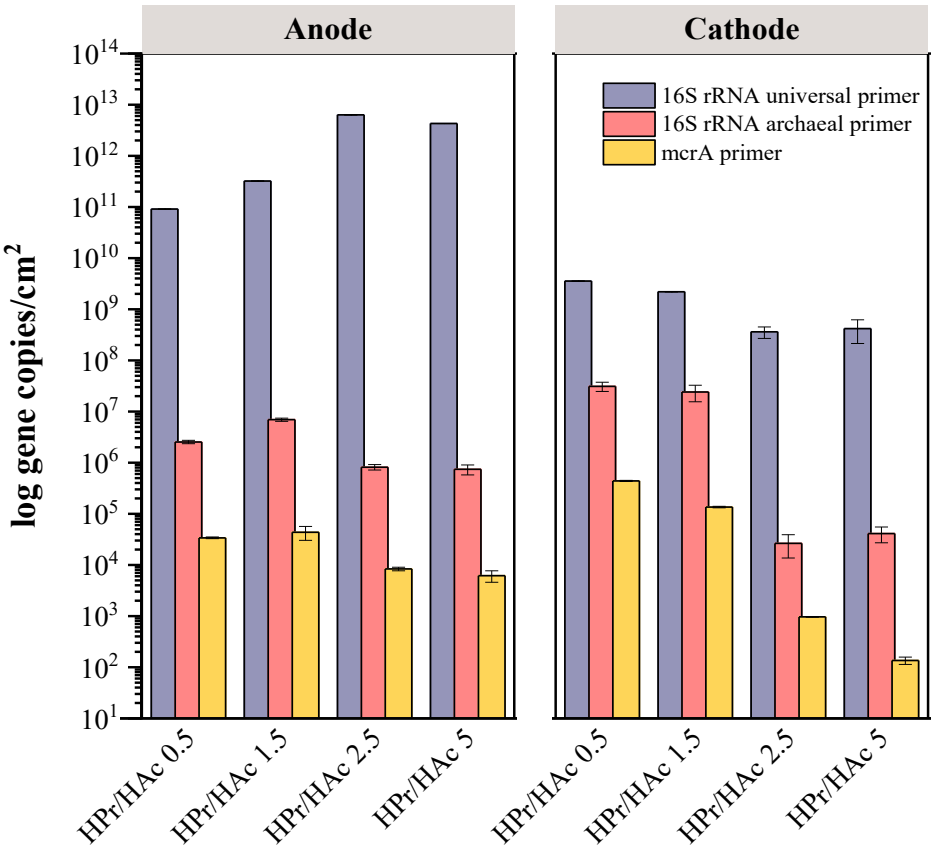


**Figure 4.8** Gene copy numbers under different HPr/HAc ratios

### *3.5.3. Microbial abundance*

Figure 4.9 shows the effect of different HPr/HAc ratios on the microbial community composition. At the phylum level, Proteobacteria was the most abundant phylum at HPr/HAc ratios of 0.5 (61%) and 1.5 (67%); the abundances significantly decreased with increasing HPr/HAc ratios to 2.5 (16%) and 5 (18%) **(**Figure 4.9a). Alternatively, Synergistetes phylum significantly increased and became the most abundant at higher HPr/HAc ratio of 2.5 (46%) and 5 (50%) with low abundances at HPr/HAc ratios of 0.5 (14%) and 1.5 (11%). Also, abundance of Firmicutes increased with increasing HPr/HAc ratios: 0.5 (1%), 1.5 (3%), 2.5 (18%) and 5 (19%). The abundance of Bacteroidetes remained almost unchanged (12-16%) for increasing HPr/HAc ratios from 0.5 to 2.5; however, it dramatically decreased to 6% at a higher HPr/HAc ratio of 5.

At the genus level, *Geobacter* belongs to Proteobacteria was the most abundant at HPr/HAc ratios of 0.5 (54%) and 1.5 (53%) **(**Figure 4.9b). However, after increasing HPr/HAc ratios to 2.5 and 5, the abundance of *Geobacter* genus showed a significant decrease (10-11%). Alternatively, *vadin*CA02, a member of *Synergistia*, became the most abundant genus at HPr/HAc ratios of 2.5 (47%) and 5 (51%) than lower ratios of 0.5 (14%) and 1.5 (11%). Also, the relative abundance of *Acetobacterium* belongs to *Clostridia* increased at HPr/HAc ratios of 2.5 (13%) and 5 (14%) compared to~1% abundance at lower HPr/HAc ratios of 0.5 and 1.5. Bacteroides had the second highest abundance at HPr/HAc ratios of 0.5 (15%), 1.5 (11%), and 2.5 (11%); however, it showed a significant decrease to 3% at HPr/HAc ratio of 5. In addition, higher enrichment of *Christensenellaceae* and *Sporomusa*, members of *Clostridia*, was observed at higher HPr/HAc ratios of 2.5 (2% and 3%) and 5 (2% and 4%, respectively). In comparison, their abundances were < 1% at low HPr/HAc ratios of 0.5 and 1.5. Other genera (*Petrimonas, Xanthobacter*) belong to Proteobacteria, and Bacteroidetes were enriched at higher HPr/HAc ratios of 2.5 (1-3%) and 5 (2-4%). On the other hand, their abundances were <1% at low HPr/HAc ratios of 0.5 and 1.5.

Overall, higher HPr/HAc ratios (2.5 and 5) considerably shifted the microbial communities at phylum and genus levels. *Geobacter*, the most kinetically efficient electroactive bacteria (Dhar et al., 2017; Malvankar et al., 2012; Torres et al., 2010), was markedly decreased at higher HPr/HAc ratios corroborated with decreased current densities (Figure 4.2). The high abundance of *Geobacter* in anode biofilms at lower HPr/HAc ratios (i.e., higher acetate levels) is consistent with several previous studies fed MEC with acetate (D. Liu et al., 2016; Luo et al., 2016). However, degradation of a complex fermentable substrate (e.g., propionate) would require more diverse fermentative species to establish a syntrophic interaction with electroactive bacteria. In this study, higher HPr/HAc ratios of 2.5 and 5, members of *Clostridia* and *Synergistia* were significantly increased. Notably, these members were reported to be propionate oxidizers in MECs (Hari et al., 2017, 2016b; Ruiz et al., 2014). For instance, diverse phylotypes of *Clostridia* and *Synergistia* were enriched in MEC fed with higher propionate concentrations (Hari et al., 2017).

The cathode biofilms also showed a shift in the microbial communities similar to the anode biofilm. Bacteroides (12% vs. 20% vs. 27% vs. 23%) was the most abundant bacterial genus in the cathode biofilms and showed a substantial enrichment with increasing HPr/HAc ratios of 0.5 to 5. On the contrary, *Acetobacterium* was the second most dominant genus at HPr/HAc ratio of 0.5

(8%), with < 1% abundance at higher HPr/HAc ratios of 1.5, 2.5, and 5. Notably, the enrichment of *Acetobacterium* was accompanied by enhanced methanogenesis. *Acetobacterium*, a hydrogen scavenging homoacetogens, could utilize $H_2/CO_2$ to produce acetate and then can be utilized by members of electroactive bacteria on the anode biofilm (Cheng et al., 2009; Fu et al., 2015). A recent study showed the enhancement of methanogenesis in MEC-AD systems accompanied by the enrichment of homoacetogens (D. Liu et al., 2016; Zakaria and Dhar, 2021b). Alternatively, the abundance of *Sporomusa* (3% vs. 4% vs. 16% vs. 19%) and vadinCA02 (3% vs. 2% vs. 7% vs. 8%) increased at higher HPr/HAc ratios. Other genera, *Bosea, Desulfovibrio, Geobacter* represented between 1% and 3% with the exception of *Desulfovibrio* at HPr/HAc ratio of 5 represented 4%.

As previously discussed, members of *Clostridia* and *Synergistia* were reported to be propionate oxidizers in MECs fed with propionate (Hari et al., 2017, 2016b; Ruiz et al., 2014). Also, the enrichment of acetogens, particularly *Sporomusa*, in the cathode biofilms at higher HPr/HAc ratio 2.5 and 5 resulted in significant losses of electrons or $H_2$ from being utilized by methanogenic archaea. Notably, acetogenic *Sporomusa* species can utilize electrons/$H_2$ and $CO_2$ to acetate and other multicarbon compounds (Aryal et al., 2017; Izadi et al., 2020; Nevin et al., 2011, 2009; Zaybak et al., 2013). Thus, the availability of $H_2$ and/or electrons for methanogens in biocathode would be hindered (Georg et al., 2020; Zakaria and Dhar, 2021a).

For both anode and cathode biofilms, *Methanobacterium* was the most abundant archaeal genera under all conditions. Previous studies also reported known hydrogenotrophic methanogens, particularly *Methanobacterium*, as key methanogen enriched in MEC-AD reactors regardless of the substrate (Cerrillo et al., 2017; Dykstra and Pavlostathis, 2017; Siegert et al., 2014a). The high abundance of known hydrogenotrophic *Methanobacterium* suggested that acetate was primarily utilized by electroactive bacteria rather than acetoclastic methanogens (D. Liu et al., 2016; Zakaria and Dhar, 2019). The abundance of *Methanobacterium* was negatively affected with increasing HPr/HAc ratios from 0.5 to 5 (anode: 8% to 5%; cathode: 58% to 26%).

Nonetheless, 16S rRNA gene sequencing could not detect the low-abundant archaeal genera. Based on the phylogenetic tree analysis using sequencing results of a specific archaeal primer, more diverse methanogenic archaea existed at higher HPr/HAc ratios (Supplementary

information). At a low HPr/HAc ratio of 0.5, only three different species (*Methanobacterium, Methanosarcina, and Methanobrevibacter*) were detected. However, at higher HPr/HAc ratios, 4-5 other archaeal genera were observed (Figure B.3 Phylogenetic tree using bacterial and archaeal primer at HPr/HAc ratio of 0.5

and Figure B.5 Phylogenetic tree using bacterial and archaeal primer at HPr/HAc ratio of 2.5

). For instance, at a high HPr/HAc ratio of 5, *Methanobacterium, Methanobrevibacter, Methanosarcina, Methanoculleus,* and *Methanolinea* were existed (Figure B.6 Phylogenetic tree using bacterial and archaeal primer at HPr/HAc ratio of 5

). Nonetheless, the methanogenesis process was negatively affected at higher HPr/HAc ratios. Thus, these results suggested that the abundance of archaeal genera might be the most critical factor for enhancing the methanogenesis process regardless of the diversity of these genera. Thus, the higher abundance of the archaeal population might have contributed to the superior MEC-AD performance under low HPr/HAc ratios.

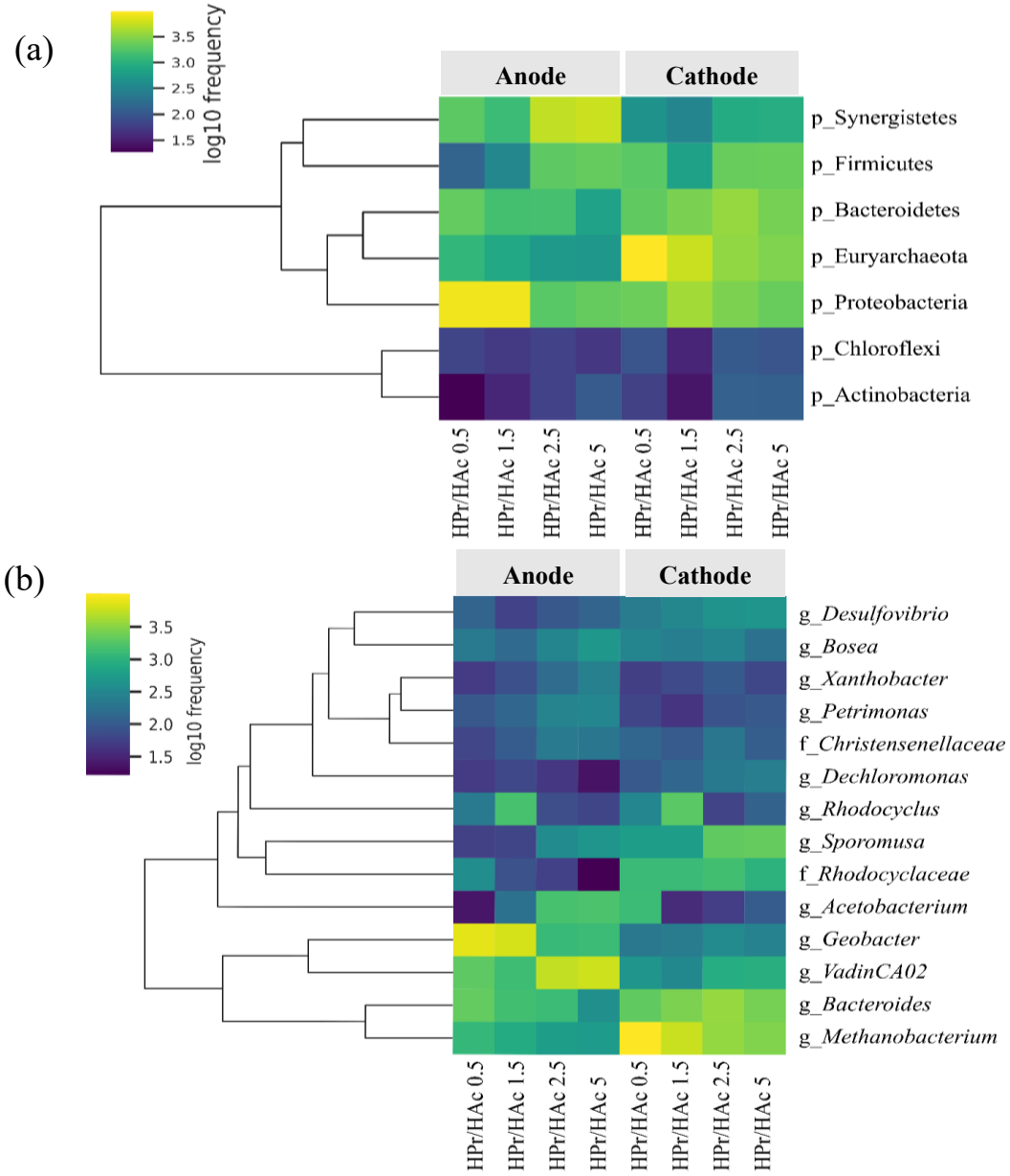


**Figure 4.9** Relative abundance of microbial communities at phylum level (a), and genus level (b)

### *3.5.4. Correlation analysis*

Figure B.1 Principal Component Analysis of the microbial communities at different HPr/HAc ratios shows a principal components analysis (PCA) loading plot for the abundances of the microbial communities at different HPr/HAc ratios. PCA analysis shows the clustering of *Methanobacterium, Geobacter,* and *Rhodocyclaceae* with HPr/HAc ratios of 0.5 and 1.5. However, these genera have been negatively affected at higher propionate concentrations (HPr/HAc ratios of 2.5 and 5). However, several other fermenters (*vadin*CA02, *Sporomusa*, etc.) are dominated and closely located at the same quadrants of HPr/HAc ratios of 2.5 and 5. Furthermore, the scatterplot matrix and correlation coefficients indicated a relatively positive correlation of *Methanobacterium* (r=1.0)*, Geobacter* (r=0.9) and *Rhodocyclaceae* (r=0.8) at higher acetate concentrations (i.e., HPr/HAc ratios 0.5 and 1.5) (Figure B.2 Scatterplot matrix of the microbial communities at different HPr/HAc ratios and (Table B.2 Correlation analysis of the microbial communities at different HPr/HAc ratios

**Figure B.3** Phylogenetic tree using bacterial and archaeal primer at HPr/HAc ratio of 0.5**Table B.2** Correlation analysis of the microbial communities at different HPr/HAc ratios. These genera showed a negative correlation (-1.0, -0.9, and -0.8, respectively) at higher propionate concentrations (i.e., HPr/HAc ratios 2.5 and 5). These results further indicate that higher HPr/HAc ratios significantly shifted the microbial community abundances, particularly *Methanobacterium* and *Geobacter.*

### *3.5.5. Chord diagram*

The chord diagram shows the relationship between microbial genera abundances on the anode and cathode biofilms (Figure 4.10). In anode biofilms, Geobacter was closely associated with the enrichment of hydrogenotrophic methanogen (*Methanobacterium*) (see Figure 4.12a). A recent study confirmed DIET-based syntrophy between *Geobacter* and *Methanobacterium* (Zheng et al., 2020). Acetogenic genera *Vadin*CA02, *Sporomusa, Bosea*, and *Petrimonas,* were closely associated together. For cathode biofilms, *Methanobacterium* showed a close association with *Acetobacterium*. As previously discussed, the enrichment of *Acetobacterium* accompanied by enhanced methanogenesis. Acetobacterium, known as hydrogen scavenging homoacetogens, can utilize $H_2/CO_2$ to produce acetate, which anodic electroactive bacteria can utilize (Cheng et al., 2009; Fu et al., 2015). A previous study also reported enhanced methanogenesis accompanied by the enrichment of homoacetogens in biocathode (D. Liu et al., 2016). However, Geobacter and other acetogenic genera, i.e., *Sporomusa* and *Vadin*CA02 in cathode biofilms, were not linked to the enrichment of Methanobacterium. These results further revealed that enrichment of acetogens in cathode biofilms affected the growth of methanogens at higher HPr/HAc ratios.

(a)

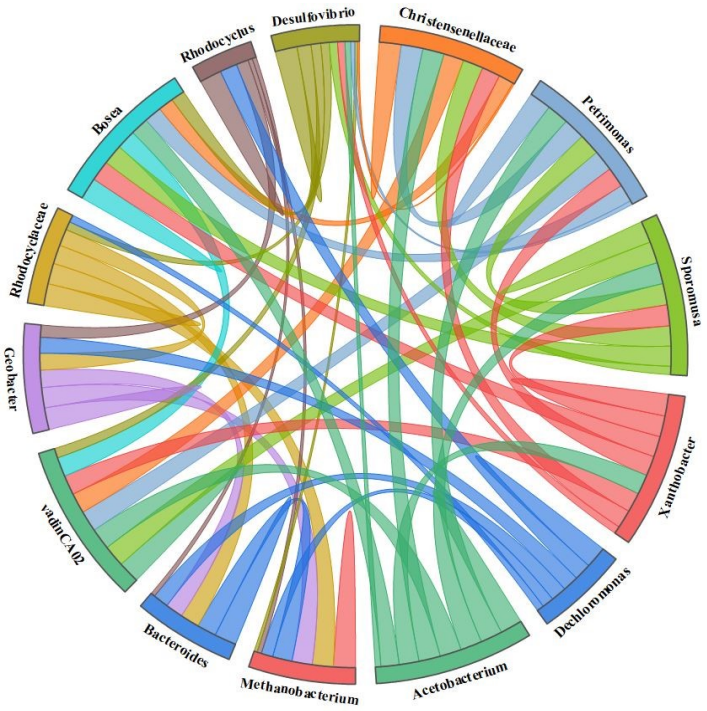


(b)

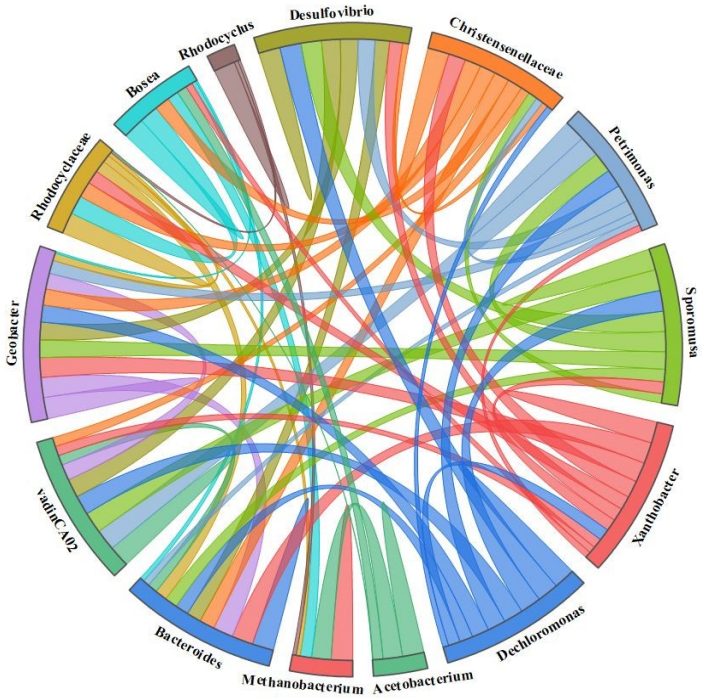


**Figure 4.10** Chord diagram of the microbial communities at anode biofilms (a), and cathode biofilms (b)

### *4.3.6. Multivariate analysis*

The multivariate principal components analysis was performed to evaluate the correlation between various process variables and different HPr/HAc ratios. As shown in Figure 4.11, for anode biofilms, most of the process variables (COD removal efficiency, EET gene expression, EPS, archaeal cells, mcrA copies, methane, etc.) are located close to the lower HPr/HAc ratios of 0.5 and 1.5. On the other hand, bacterial cell numbers (represented by 16S rRNA gene copies) are located in a different quadrant, closely linked to the higher HPr/HAc ratios of 2.5 and 5. For cathode biofilms, all the process variables are located in the same quadrants of HPr/HAc ratios of 0.5 and 1.5.

Moreover, correlation coefficients and scatterplot matrix were tested to examine the correlation of process variables to different HPr/HAc ratios (Figure 4.12 and Table 4.3). The process variables showed a relatively high positive correlation to higher acetate concentrations (HPr/HAc ratios 0.5 and 1.5). In comparison, a relatively negative correlation was observed at higher propionate concentrations (HPr/HAc ratios 2.5 and 5). For instance, EET gene expression showed a relatively positive correlation on the anode and cathode biofilms ($r = 0.8$ and 0.9, respectively) at higher acetate concentrations (HPr/HAc ratios 0.5 and 1.5). However, a noticeable negative correlation was observed at anode and cathode biofilms ($r = -0.8$ and -0.9, respectively) at higher propionate concentrations (HPr/HAc ratios 2.5 and 5). Also, other process variables such as EPS, methane, archaeal cells, etc., showed similar trends. The only exception is the high positive correlation of bacteria cells ($r = 0.8$) enriched on the anode biofilms at higher HPr/HAc ratios of 2.5 and 5.

Thus, these analyses further indicate that a higher MEC-AD efficiency based on most of the process variables was obtained at low HPr/HAc ratios of 0.5 and 1.5. However, at higher HPr/HAc ratios of 2.5 and 5, most of the variables considered in the analysis were negatively correlated, which consequently corroborated with inferior MEC-AD performance.

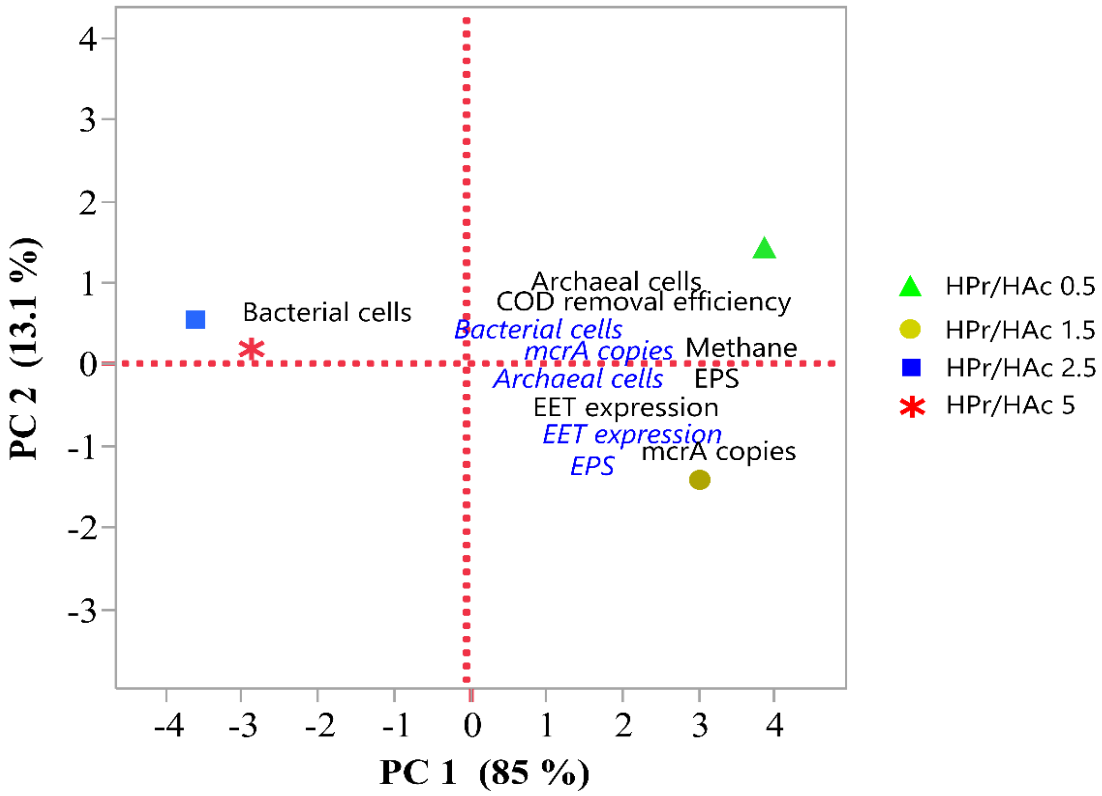


**Figure 4.11** Principal Component Analysis of the process variables components at different HPr/HAc ratios. Note. The anode biofilm variables are in black color and the cathode biofilm variables are in blue color

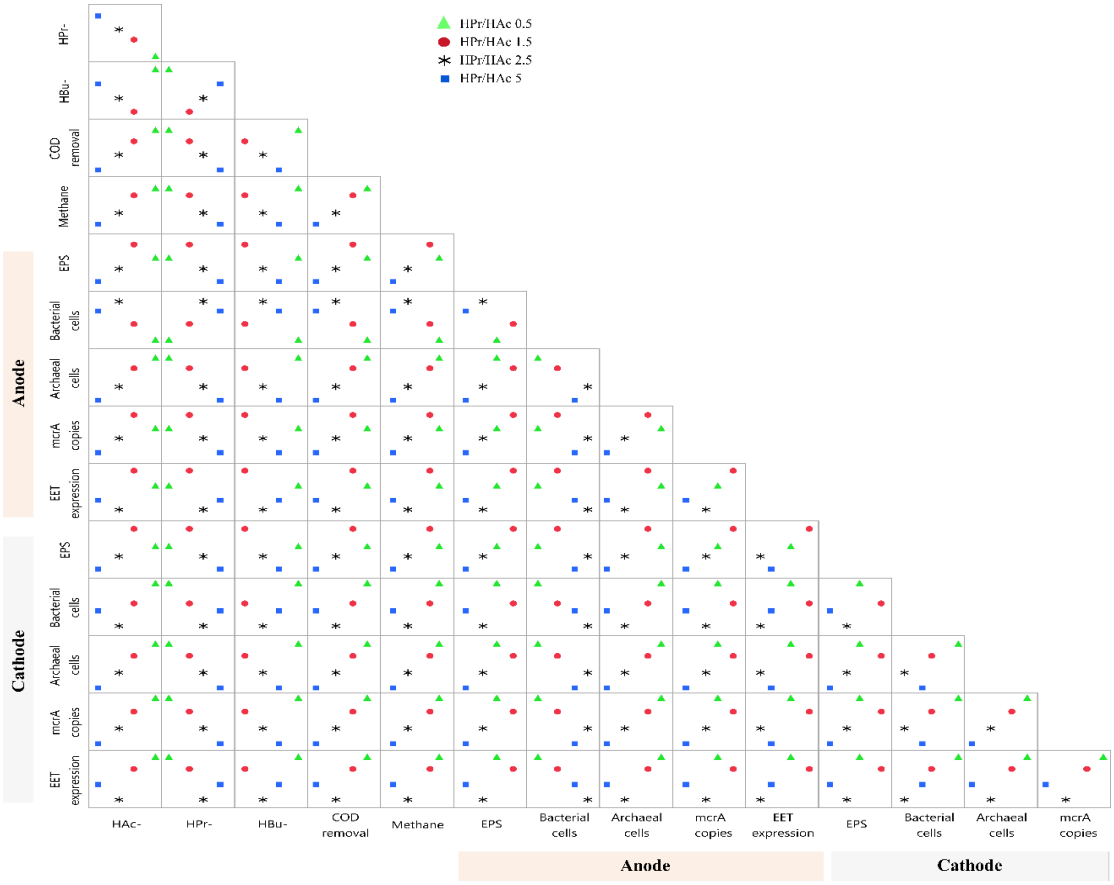


**Figure 4.12** Scatterplot matrix of the process variables components at different HPr/HAc ratios

**Table 4.2** Correlation analysis of the process variables components at different HPr/HAc ratios

| | | HAc- | HPr- | HBu- | COD removal (%) | Methane | EPS | Bacterial cells | Archeal cells | mcrA copies | EET expression | EPS | Bacterial cells | Archeal cells | mcrA copies | EET expression |
|---|---|---|---|---|---|---|---|---|---|---|---|---|---|---|---|---|
| | | | | | | | Anode | | | | | Cathode | | | | |
| Anode | HAc- | 1.0 | | | | | | | | | | | | | | |
| | HPr- | -1.0 | 1.0 | | | | | | | | | | | | | |
| | HBu- | 0.2 | -0.1 | 1.0 | | | | | | | | | | | | |
| | COD removal efficiency (%) | 1.0 | -1.0 | 0.1 | 1.0 | | | | | | | | | | | |
| | Methane | 0.9 | -0.9 | -0.3 | 0.9 | 1.0 | | | | | | | | | | |
| | EPS | 0.8 | -0.8 | -0.4 | 0.8 | 1.0 | 1.0 | | | | | | | | | |
| | Bacterial cells | -0.8 | 0.8 | 0.2 | -0.9 | -0.9 | -0.9 | 1.0 | | | | | | | | |
| | Archeal cells | 0.4 | -0.4 | -0.8 | 0.5 | 0.7 | 0.8 | -0.7 | 1.0 | | | | | | | |
| | mcrA copies | 0.7 | -0.8 | -0.5 | 0.8 | 1.0 | 1.0 | -0.9 | 0.9 | 1.0 | | | | | | |
| | EET expression | 0.8 | -0.8 | -0.3 | 0.9 | 1.0 | 0.9 | -1.0 | 0.8 | 1.0 | 1.0 | | | | | |
| Cathode | EPS | 0.8 | -0.8 | -0.4 | 0.9 | 1.0 | 1.0 | -0.9 | 0.8 | 1.0 | 1.0 | 1.0 | | | | |
| | Bacterial cells | 1.0 | -1.0 | 0.1 | 1.0 | 0.9 | 0.9 | -0.9 | 0.5 | 0.8 | 0.9 | 0.9 | 1.0 | | | |
| | Archeal cells | 0.9 | -0.9 | -0.1 | 1.0 | 1.0 | 0.9 | -1.0 | 0.7 | 0.9 | 1.0 | 0.9 | 1.0 | 1.0 | | |
| | mcrA copies | 1.0 | -1.0 | 0.3 | 1.0 | 0.8 | 0.7 | -0.8 | 0.3 | 0.7 | 0.8 | 0.7 | 1.0 | 0.9 | 1.0 | |
| | EET expression | 0.9 | -0.9 | -0.1 | 1.0 | 1.0 | 0.9 | -1.0 | 0.6 | 0.9 | 1.0 | 0.9 | 1.0 | 1.0 | 0.9 | 1.0 |

## 4.4. Conclusion

This study focused on maintaining an optimum propionate/acetate (HPr/HAc) ratio towards the electro-methanogenesis process and the microbial community. The total cumulative methane production remained almost the same after increasing HPr/HAc ratio from 0.5 to 1.5. When HPr/HAc ratios further increased to 2.5 and 5, the total cumulative methane production markedly decreased. EET-associated gene expression reduced under high HPr/HAc ratios (2.5 and 5) indicates the partial inhibition of biofilm electroactivity. *Geobacter* and *Methanobacterium* species were abundant under lower HPr/HAc ratios, while their abundance decreased under higher HPr/HAc ratios. Therefore, this study demonstrated that higher HPr/HAc ratios would adversely impact electro-methanogenic activity in MEC-AD systems. However, further research is required to elaborate on the significance of HPr/HAc ratios under high-strength feedstocks.

# Chapter 5

# An intermittent power supply scheme to minimize electrical energy input in a microbial electrolysis cell assisted anaerobic digester

*A version of this chapter was published in Bioresource Technology, 319, 124109.*

## 5.1. Introduction

Anaerobic digestion (AD) is a well-established and cost-effective technology for simultaneous treatment of organic waste and biogas (50–60% $CH_4$ and 40–50% $CO_2$) production (Barua et al., 2018; Barua and Dhar, 2017; Chen et al., 2008). Nevertheless, conventional anaerobic digestion faces various challenges, including sensitivity to the environmental parameters (pH, temperature, alkalinity, etc.), slow hydrolysis process, and chemical inhibition (organic acids, ammonia, etc.) (Ma et al., 2013; Tomei et al., 2009). For instance, digesters' operation at higher organic loading rates causes the accumulation of volatile fatty acids (VFAs) inside the digester, creating an acidic environment and leading to digester instability (Ma et al., 2013). Consequently, the methanogenesis could be inhibited and become a rate-limiting step, which leads to poor biogas yield and quality (Ma et al., 2013). Hence, developing a stable bioreactor system with a balanced microbiome is critical in attaining higher methane yields.

Recently, various microbial electrochemical systems, such as microbial fuel cells (MFCs), microbial electrolysis cells (MECs), have been extensively researched as nascent approaches for waste/wastewater treatment with value-added applications, including bioenergy (i.e., electricity, biomethane, biohydrogen, etc.), and chemicals (i.e., nutrients, $H_2O_2$, alkali, etc.) production (Barua et al., 2019b; Choi et al., 2017; Ki et al., 2017b; Li et al., 2016; Siegert et al., 2014b; Xin et al., 2019). Notably, coupling MECs with AD holds great promise to enhance the methanogenesis process by introducing a pair of electrodes with an external supply of small voltage or applied voltage. This process is called electro-methanogenesis, and integrated systems are known as MEC-AD (Siegert et al., 2015; Zakaria and Dhar, 2019).

Previous studies reported that electroactive bacteria in MEC-AD systems could divert electrons from organic acids to the anode that can be transformed into hydrogen gas on the cathode (Cho et al., 2019; Heidrich et al., 2013). Thus, fast-growing hydrogenotrophic methanogens could be enriched on the cathode, while electroactive bacterial bacteria could outcompete slow-growing acetoclastic methanogens (Li et al., 2016; Siegert et al., 2015). Moreover, hydrogenotrophic methanogens have a higher tolerance for harsh environmental conditions (e.g., pH, temperature, high ammonia levels) than acetoclastic methanogens (Cai et al., 2018; Jiang et al., 2018). Thus, MEC-AD systems could provide superior process kinetics, stability, and methane productivity (Choi et al., 2017; Zakaria and Dhar, 2019).

Despite these benefits, the operation of MEC-AD will increase the operational cost due to the requirement of energy input in the form of applied voltage/potential (Lim et al., 2020). The laboratory-scale MEC-AD systems can be operated with low energy input (0.3-1.5 V) (Choi et al., 2017; Zakaria and Dhar, 2019). However, based on energy efficiencies, studies reported mixed results. For instance, Luo et al. (2016) reported no clear benefit in terms of energy recovery between conventional AD and MEC-AD systems. In contrast, Zhao et al. (2016) suggested that the energy income from the increased methane production from a MEC-AD system could be as high as 13.4 times as more as the electrical energy input. Nonetheless, it is expected that the operation of large-scale MEC-AD systems would substantially increase the energy input due to high system overpotentials (Ge and He, 2016; Heidrich et al., 2014, 2013). There have been numerous researches on the development of operational strategies for MEC-AD systems. However, most of these researches have been focused on the optimization of applied voltage/potential, where systems were operated with a continuous supply of external voltage or potential (Choi et al., 2017; Zakaria et al., 2019; Zhao et al., 2016). Although few studies have demonstrated that intermittent power supply could improve energy recovery and organics removal with MECs (Ailijiang et al., 2016; Cho et al., 2019; Hussain et al., 2018). Hussain et al. (2018) reported that on/off mode of operation of MEC could significantly lower the internal resistance of the system, and thereby increased the fraction of electroactive bacterial species within the anode biofilms. Cho et al. (2019) suggested that continuous applied voltage in MECs could lead to excessive energy input required for a cathodic hydrogen evolution reaction. In addition to improving energy efficiency, the on/off mode operation could increase effective cathode surface

area for hydrogen evolution reaction by alleviating the attachment of small hydrogen gas bubbles. Moreover, hydrogen partial pressure around the cathode can be reduced under on/off mode operation (Cho et al., 2019), which can potentially benefit the anaerobic digestion process. Higher hydrogen partial pressure may inhibit the consumption of volatile fatty acids (VFAs) during anaerobic digestion (Magdalena et al., 2019; Oh and Logan, 2005). Considering these aspects, it can be hypothesized that the on/off mode operation can potentially benefit the operation of MEC-AD systems. However, limited information is available on the impact of intermittent power supply in MEC-AD systems. However, limited information is available on the impact of intermittent power supply in MEC-AD systems.

Therefore, this study assessed cycling open/closed circuit operation scheme for an applied potential controlled MEC-AD reactor fed with a complex fermentable substrate, glucose. Under different on/off times for applied potential, the system's performance was compared in terms of methane production, current density, and organics removal. Moreover, the qualitative and quantitative shifts of microbial communities under the different duration of applied potential were examined with 16S rRNA approaches and qPCR. To the best of the authors' knowledge, the findings of this study are the first of the few efforts to optimize an on/off applied potential scheme, which can potentially increase the economic benefits of MEC-AD systems.

## 5.2. Material and methods

### *5.2.1. Setup and operation of MEC-AD*

A single-chamber MEC-AD was fabricated using plexiglass tubes with a working volume of 360 mL. Carbon fibers (2293-A, 24A Carbon Fiber, Fibre Glast Development Corp., Ohio, USA) integrated with a stainless-steel frame was used as the anode electrode, and a stainless-steel mesh (304, McMaster-CARR, USA) was used as the cathode electrode. Carbon fibers were pretreated according to the method previously described by Dhar et al. (2013). Ag/AgCl reference electrode (MF-2052, Bioanalytical System Inc., USA) was placed with a distance of ~1 cm to the anode electrode. A multi-channel potentiostat (Squidstat Prime, Admiral Instruments, Arizona, USA) was used to set a fixed anode potential of -0.4 V vs. Ag/AgCl. During the entire experiment, the liquid medium in the reactor was mixed at 130 ± 5 rpm using a magnetic stirrer.

In the beginning, the reactor was seeded with 15 mL of anaerobic digester sludge and 30 mL effluent from an identical mother MEC that has been operated with a 25 mM acetate medium for >12 months. An anaerobic glucose synthetic wastewater media (2061±32 mg COD/L) was supplemented as a feed with 50 mM phosphate buffer and trace minerals. The detailed composition of the trace minerals used in this study could be found in the literature (Dhar et al., 2013). This followed by monitoring the current generation until a steady-state current of ~14.33 mA was attained prior to run the experiment. Then, the reactor was evacuated and fed with a fresh glucose synthetic wastewater media (2061±32 mg COD/L) in a fed-batch mode. The MEC-AD reactor was operated under three conditions; the applied potential switched on for 24 hours (closed-circuit) as a control condition (referred to as 24 hrs ON). For the second condition, the applied potential switched on for 18 hours (closed-circuit), followed by switched off (open-circuit) for 6 hours (referred to as 18 hrs ON). For the third condition, the applied potential switched on for 12 hours, followed by switch off for 12 hours (referred to as 12 hrs ON). The reactor operated under each condition until it reached a steady-state for several consecutive cycles. Here, results from three representative cycles were presented. All experiments were performed at room temperature (21±1°C) with a mixing speed of 130 rpm.

### *5.2.2. Analytical methods*

The current generation from the reactor was recorded every 4.8 min using a potentiostat (Squidstat Prime, Admiral Instruments, USA). Chemical oxygen demand (COD) was measured with the HACH kit (HACH, Loveland, Colorado, USA). The produced biogas was collected from the reactor using 500 mL gas bags. The biogas composition determined by a Gas Chromatograph (7890B, Agilent Technologies, Santa Clara, USA). Volatile fatty acids (VFAs) concentrations were measured by the Ion chromatograph (Dionex$^{TM}$ ICS-2100, Thermos Scientific, USA) (Zakaria et al., 2019).

### *5.2.3. Characterization of microbial community*

Several portions of anode and cathode biofilm were collected by sterile pipet tips at the end of each operating condition. The samples were washed 3x times with 0.1 M PBS buffer (pH 7.4), followed by centrifugation to remove any contaminant. The DNA was extracted using the

PowerSoil® DNA Isolation Kit (MoBio Laboratories, Carlsbad, USA) according to the manufacturer's instructions. The purity and concentration of the extracted DNA were measured using NanoDrop™ 2000C spectrophotometer (Thermo Scientific, USA). Then, the DNA was stored immediately at -70 °C for further analysis. Illumina Miseq Sequencing was constructed and performed by the Research and Testing Laboratory (RTL genomics, Lubbock, TX, USA). The analysis methodology for sequencing (https://rtlgenomics.com/documents) was provided by the laboratory. 16s rRNA was targeted by using universal bacterial primers 341F: CCTACGGGNGGCWGCAG and 805R: GACTACHVGGGTATCTAATCC (Klindworth et al., 2013), and archaeal specific primers 517F: 5' GCYTAAAGSRNCCGTAGC 3' and 909R: 5' TTTCAGYCTTGCGRCCGTAC 3'. Also, qPCR was performed to quantify microbial cell number.

For microbial diversity and community analysis, raw sequencing data were provided from RTL genomics. Initially, USEARCH UCHIME was used for denoising process and chimera detection in order to remove noisy reads and chimeric sequences (Edgar et al., 2011). The reads were assigned and clustered into operational taxonomic units (OTUs) using the Greengenes database at a 97% sequence similarity level (Edgar, 2010). The alignment process was performed using PyNAST tool. The microbial taxonomy was analyzed using the Quantitative Insights Into Microbial Ecology (QIIME 2) pipeline (https://qiime.org/, Bolyen et al., 2019).

Additionally, qPCR was performed to quantify microbial cell numbers at the three operating conditions. 16S universal primers, 357Wf: CCTACGGGNGGCWGCAG and 785R: GACTACHVGGGTATCTAATCC, were used to quantify the DNA samples (Klindworth et al., 2013). qPCR mixtures were prepared in 25 µL reactions using QuantiFast SYBR® Green PCR Kit (Qiagen, CA) as the following: 2 µL of the DNA template, 12.5 µL 2x master mix, 2.5 µL forward and reverse specific primer, and 5.5 µL nuclease-free water. CFX 96 real-time PCR system with a C1000 Thermal Cycler (Bio-Rad, USA) was used with the following cycling conditions according to the QuantiFast SYBR® Green PCR Kit's protocol; PCR initial heat activation cycle at 95 ˚C for 5 min, 35 cycles at 95 ˚C for 10 sec and 60 ˚C for 30 sec, and finally, one cycle at 40 ˚C for 30 seconds. Triplicate reactions were run for all samples.

### *5.2.4. Calculation of energy income*

The net energy income under different operating conditions was determined, according to Zhao et al. (2016) and Lim et al. (2020), after some modifications. The net energy income per cycle ($W_{net}$, kJ) (Eq. 1) determined based on the difference between the total energy income from methane produced ($W_{CH4}$, kJ) and the total electric energy consumed via applied potential ($W_e$, kJ).

$$W_{net} = W_{CH4} - W_e \qquad \text{(Eq. 1)}$$

The total energy income from methane production ($W_{CH4}$, kJ) was calculated by multiplying the energy content of methane-based on the heat of combustion ($\Delta H_s = 890.31 \times 10^3$ J/mol) and total moles of methane produced. The total electric energy input ($W_e$, kJ) was calculated by multiplying the applied voltage and cumulative coulombs.

## 5.3. Results and discussion

### *5.3.1. Current generation*

Figure 5.1 shows the variations in the current generation in MEC-AD under different conditions. The current generation under 24 hrs ON and 18 hrs ON modes were comparable (12.2±0.7 vs. 11.0±0.3 mA) while it declined when the reactor switched to 12 hrs ON mode (6.8±0.7 mA). Thus, it appeared that switching off the applied potential for 6 hours did not interrupt the electrocatalytic activity of the microbiome. However, when the applied potential was switched off for 12 hours, the performance deteriorated compared to the other two conditions with a sharp decline in the current generation. Closed-circuit operation plays an important role in the enrichment of an electroactive microbiome (Huang et al., 2014). Notably, the closed-circuit operation would be critical for facilitating the metabolic function of anodic electroactive bacteria (Huang et al., 2014; Michie et al., 2020). For instance, several studies reported that certain electroactive bacteria, particularly from the *Deltaproteobacteria* class, could be enriched under closed-circuit rather than open-circuit operation (Huang et al., 2014; Shehab et al., 2013; Yu et al., 2015). Under intermittent open-circuit conditions, electroactive bacteria would oxidize the substrate and accumulate electrons in the anode biofilms (Bonanni et al., 2012; Chung et al., 2020).

After switching to the closed-circuit condition, the accumulated electrons would be quickly discharged, which would provide a temporary peak current. Such peak currents could also be observed in this study (Figure 5.1b & 5.1c). Nonetheless, the results of this study suggested that switching off the applied potential for 12 hours might disturb or affect the anode biofilms. As discussed later, intermittently applied potential caused a shift of microbial communities and allowed enrichment of non-electroactive bacteria (discussed later).

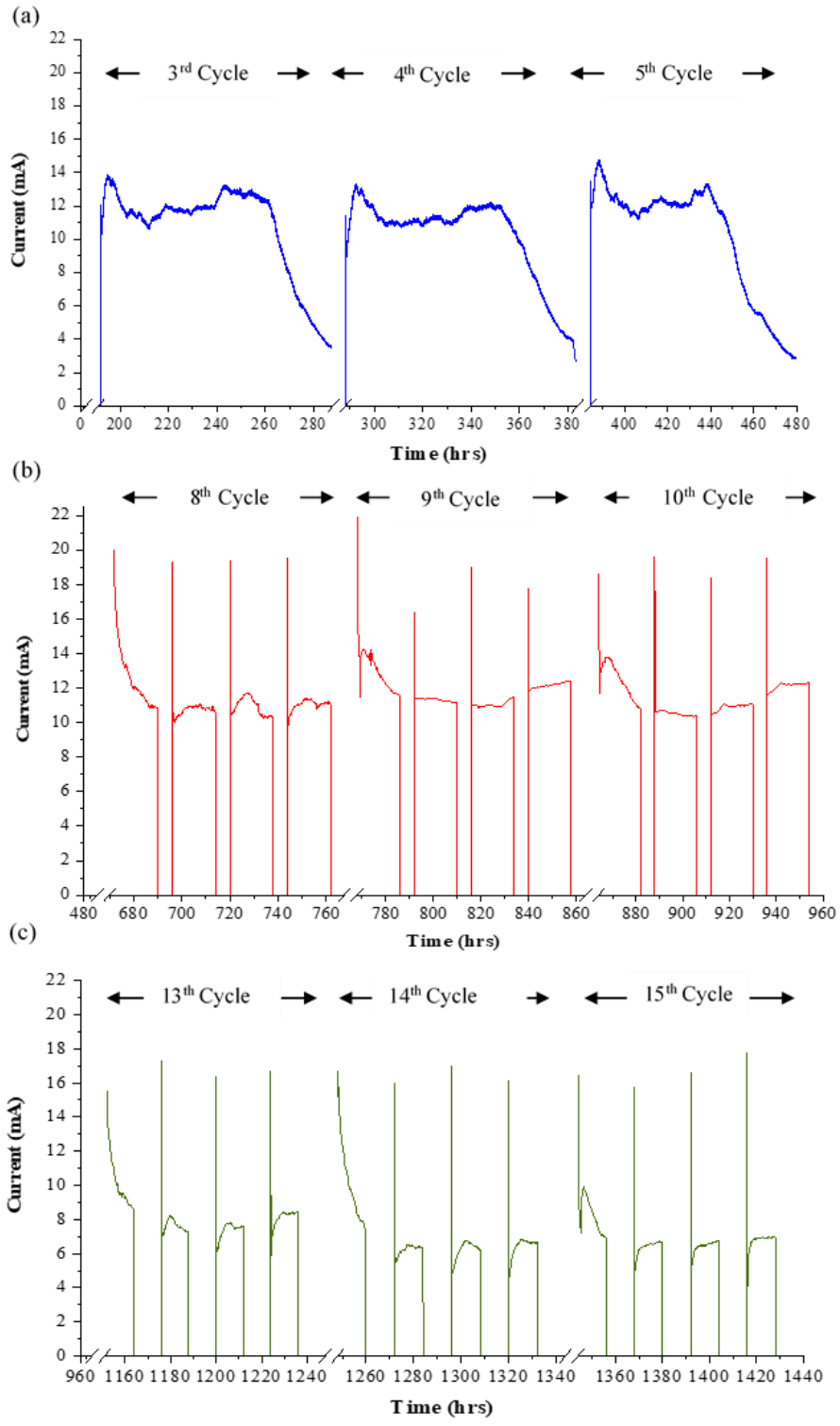


**Figure 5.1** The current generation under different operating conditions, 24 hrs ON (a), 18 hrs ON (b), and 12 hrs ON (c)

### *5.3.2. Methane generation and organics degradation*

Figure 5.2a shows volumetric methane generation profiles under different operating modes (Fig. 2a). The pattern of methane generation was almost comparable under 24 hrs ON and 18 hrs ON conditions. At the end of the batch cycle, the total cumulative methane production reached 429±13.7 $CH_4/m^3$ (24 hrs ON) and 433±7.9 L $CH_4/m^3$ (18 hrs ON), respectively. Thus, switching off the applied potential for 6 hours/day literally had no impact on methane production compared to operation under continuous applied potential. When the applied potential was switched off for 12 hours/day (i.e., 12 hrs ON), decreases in methane production was observed. The total cumulative methane production considerably decreased to 283±7.9 L $CH_4/m^3$ under this condition. As discussed later, enrichment of hydrogenotrophic methanogens and electroactive bacterial communities under 24 hrs ON and 18 hrs ON conditions benefited the methane production. The prolonged operation of MEC-AD systems under open-circuit conditions could hinder the metabolic activities of both hydrogenotrophic methanogens and electroactive bacteria. First, intermittent applied potential can affect growth and substrate (e.g., acetate) utilization by electroactive bacteria. Second, cathodic hydrogen production would be hindered, which would create substrate limiting conditions for hydrogenotrophic methanogens. Nonetheless, these results suggested that a balanced microbiome could be maintained when the power supply was switched off for 6 hours/day (18 hrs ON).

Figure 5.2b shows the degradation pattern of glucose under different conditions. Under 24 hrs ON and 18 hrs ON modes, effluent COD concentrations were 221±7.0 and 290±14.0 mg COD/L, respectively, which resulted in COD removal efficiencies of 90±2.1% and 87%±2.6%, respectively. However, for 12 hrs ON mode, effluent COD concentration was considerably higher than the other two conditions (537±4.0 mg COD/L) with a lower COD removal efficiency of 75±1.9%. These results suggested that turning off the applied potential for a prolonged period of 12 hours affected the substrate utilization by microbial communities. As discussed earlier, the open-circuit operation would affect the anodic electroactive bacterial communities that oxidize VFAs (particularly acetate) and generate electrical current (Huang et al., 2014; Michie et al., 2020). Therefore, profiles of VFAs were monitored throughout the experiment (Figure 5.3). VFA profiles were similar under all the operating conditions; Acetate>Propionate>Butyrate. However, total

VFA (TVFA) concentration under 24 hrs ON and 18 hrs ON modes reached a maximum concentration of ~700 mg COD/L, as compared to ~560 mg COD/L under 12 hrs ON mode. There was no substantial difference in concentrations propionate and butyrate under all conditions. However, acetate concentrations were as high as 521±0.4 and 489±1.8 mg COD/L under 24 hrs ON and 18 hrs ON condition, respectively. In contrast, the maximum acetate concentration of 363±4.4 mg COD/L was observed under 12 hrs ON mode. At the end of operational cycles, TVFA concentration was as low as 60±2.5 and 76±3.0 mg COD/L under 24 hrs ON and 18 hrs ON modes, as compared to 205±3.5 mg COD/L under 12 hrs ON. Notably, the effluent from 12 hrs ON condition showed considerably higher accumulation of acetate (197±3.4 mg COD/L), as compared to the other two conditions (<39±3.1 mg COD/L). The higher accumulation of acetate indicated that the electroactive bacterial community was adversely affected under 12 hrs ON mode, which are considered the main acetate-utilizing bacteria (discussed later). Moreover, these results suggested that fermentative bacterial communities could also be negatively affected under 12 hrs ON condition, as indicated by the decline in glucose degradation and TVFA production.

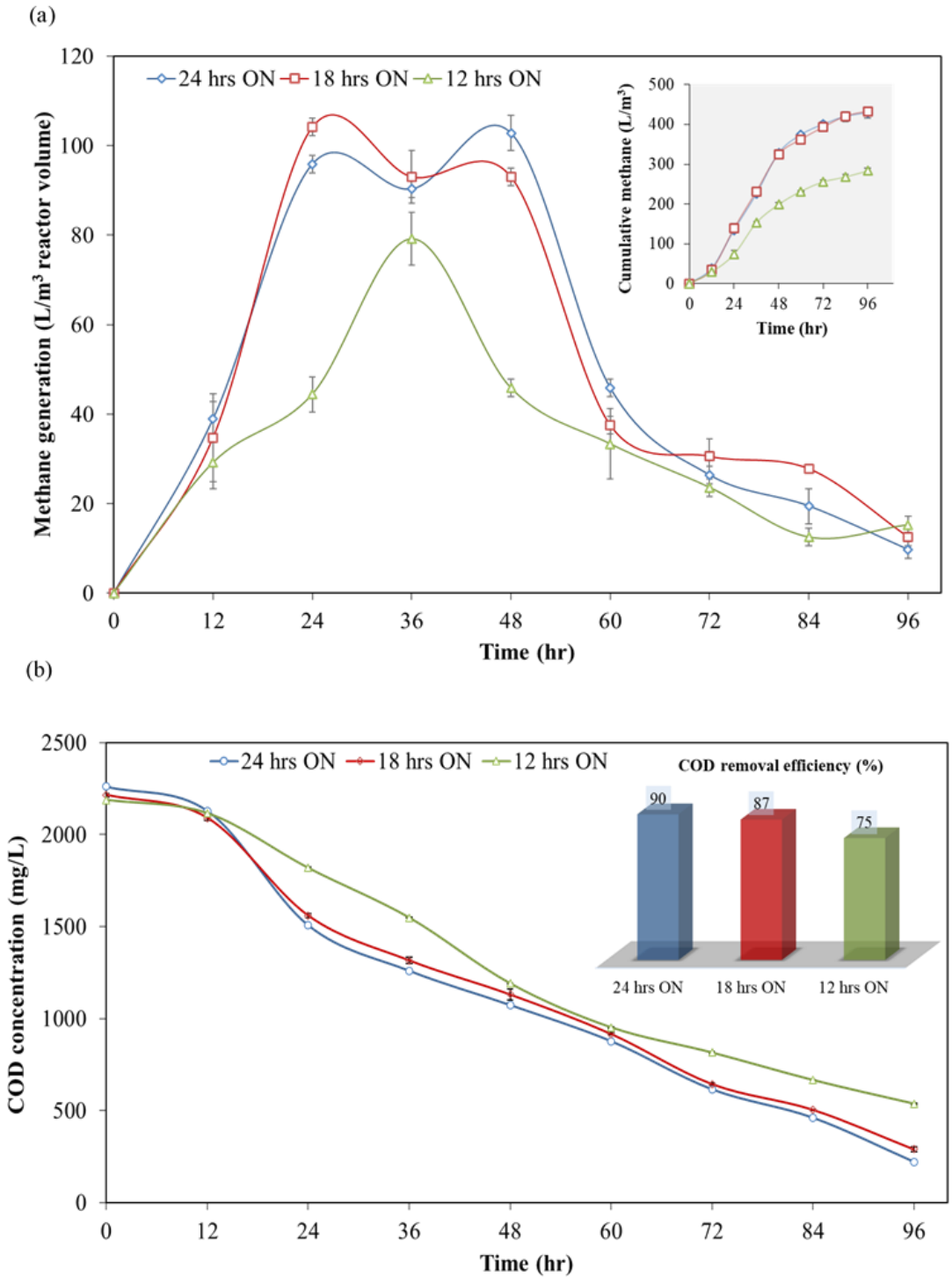


**Figure 5.2** Methane generation profile (inset shows cumulative methane generation) (a), and changes in COD concentrations (inset shows overall COD removal efficiency) (b) under different operating conditions

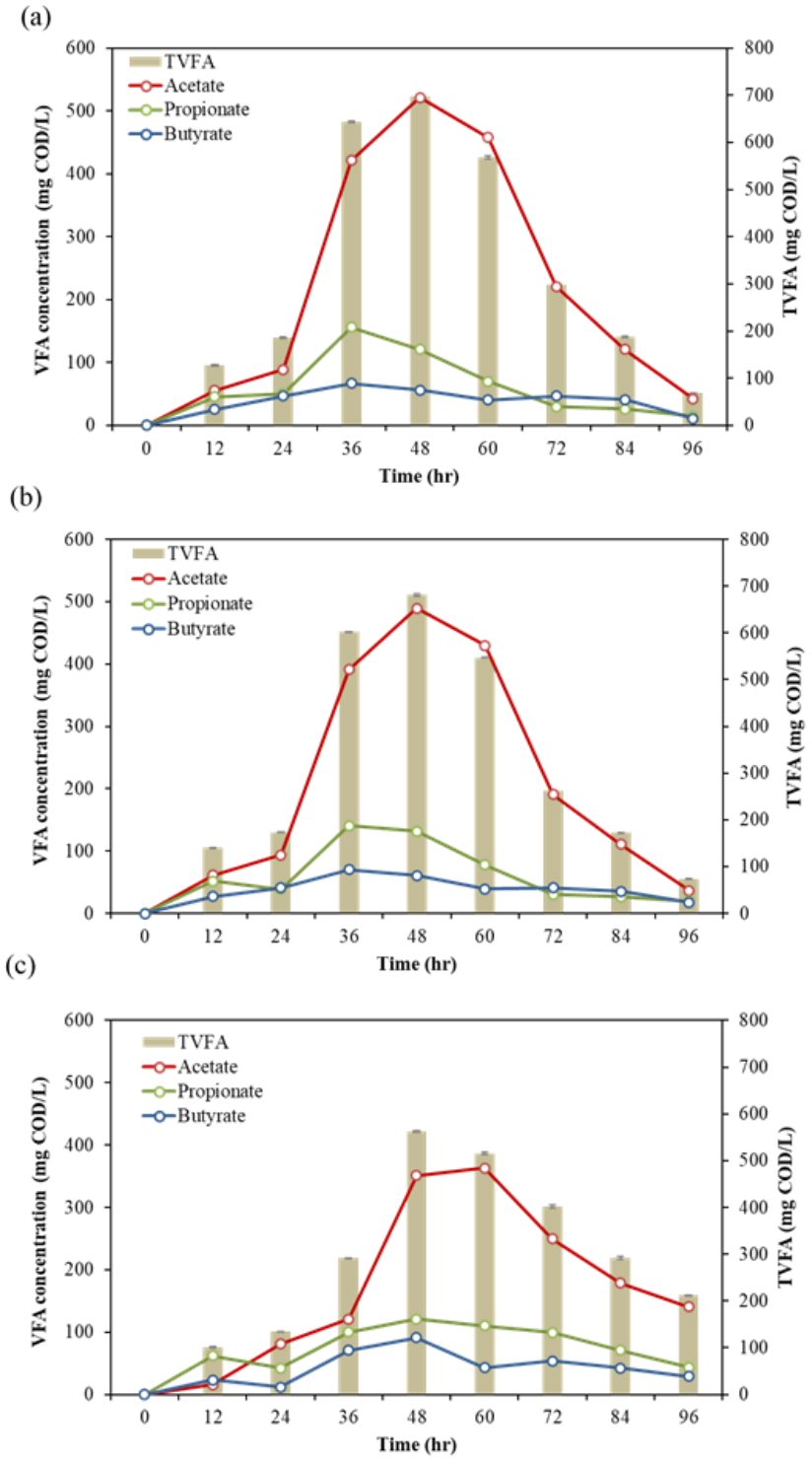


**Figure 5.3** Concentrations of VFAs under different operating conditions. 24 hrs ON (a), 18 hrs ON (b), and 12 hrs ON (c)

### *5.3.3. Changes in microbial community*

#### *3.3.1. Bacterial communities*

Figure 5.4 shows the effects of different operating conditions on the microbial community composition of anode biofilms. Under all conditions, *Proteobacteria* was the highest dominant phylum with an abundance of 70% (24 hrs ON), 66% (18 hrs ON), and 52% (12 hrs ON). *Bacteroidetes* was the second most abundant phylum recorded 23% (24 hrs ON), 19% (18 hrs ON), and 16% (12 hrs ON). The other dominant phyla were *Synergistetes* (4-11%) and *Firmicutes* (4-6%), while *Euryarchaeota* represented a minor portion (1.7-3%) of the microbial community. Thus, at the phylum level, there were no significant changes in the anodic microbial abundances under 24 hrs ON and 18 hrs ON modes (Figure 5.4a). However, when the reactor switched to 12 hrs ON mode, the relative abundance showed a marked change compared to two other conditions.

At the genus level, *Geobacter* belongs to *Proteobacteria* was the most dominant (31%) under 24 hrs ON mode. However, after switching the operation to intermittently applied potential, the relative abundance of *Geobacter* species decreased to 12% in 18 hrs ON and 2.5% in 12 hrs ON modes (Figure 5.4b). Alternatively, members of the *Enterobacteriaceae* family became the most dominant in 18 hrs ON mode (48%), as compared to 24 hrs ON (17%), and 12 hrs ON (32%) modes. *Bacteroides* were enriched equally (16-17%) under 24 hrs ON and 18 hrs ON modes; however, their abundance decreased to 12% under 12 hrs ON mode. Also, the abundance of *Synergistaceae_vadin*CA02 decreased from 9% (24 hrs ON) to 3% (18 hrs ON) and 2% (12 hrs ON). *Bosea* and *Pleomorphomonas* were accounted for 5% and 4% under 24 hrs ON mode, respectively. The abundance of these both genera decreased to ≤ 2% after switching to intermittent applied potential conditions (18 hrs ON and 12 hrs ON). Alternatively, higher enrichment of *Rhodocyclaceae*_K82, *Azovibrio*, and *Victivallis* was observed under 18 hrs ON mode (7%, 4%, and 4%, respectively) than 24 hrs ON (3%, 1%, and 1%), and 12 hrs ON (2%, 1%, and 2%) modes. Other genera, such as *Cloacibacillus*, *Desulfovibrio*, *Dysgonomonas*, etc., represented a small portion of the microbial communities with an abundance of ≤ 2%.

Thus, the duration of applied potential considerably influenced the microbial communities at both the genus and phylum levels. Notably, at the phylum level, the abundance of *Proteobacteria*

and *Bacteroidetes* decreased with decreasing the duration of applied potential. At the genus level, *Geobacter* species were found to be more affected by the decrease in the duration of applied potential. Previous studies also suggested that closed-circuit operation (i.e., applied potential) would be critical for the enrichment of *Geobacter* species (Shehab et al., 2013; Zakaria et al., 2019). The high abundance of *Enterobacteriaceae* family under intermittent applied potential conditions (18 hrs ON and 12 hrs ON), as compared to 24 hrs ON mode, might explain their ability to grow with or without applied potential. *Enterobacteriaceae* was identified as having a dual function of fermentation and anodic respiration (Feng et al., 2014; Rasmussen and Minteer, 2015; Toczyłowska-Mamińska et al., 2015). Several studies revealed that some species from genera *Enterobacter* (e.g., E. *cloacae*) belonging to family *Enterobacteriaceae* could generate electricity in various microbial electrochemical systems (Feng et al., 2014; Rasmussen and Minteer, 2015; Toczyłowska-Mamińska et al., 2015). For instance, Feng et al. (2014) found that *Enterobacter* strains, isolated from a microbial fuel cell, generate nanowires, which might contribute to extracellular electron transport for the current generation. Under 18 hrs ON mode, other known fermentative bacterial genera, such as *Rhodocyclaceae*_K82, *Azovibrio*, and *Victivallis* were identified in anode biofilms (Mei et al., 2015; Ruiz et al., 2014). Interestingly, despite the fact that microbial community shifted due to intermittently applied potential, performances of MEC-AD were comparable for both 24 hrs ON and 18 hrs ON conditions. This might be due to the increase in the abundance of the *Enterobacteriaceae* family, which can act as fermentative and electroactive bacteria (Feng et al., 2014; Rasmussen and Minteer, 2015; Toczyłowska-Mamińska et al., 2015). Based on the comparable current generation under 24 hrs ON and 18 hrs ON modes (discussed earlier), it can be argued that other electroactive bacteria like members from the *Enterobacteriaceae* family possibly compensated for the decrease in the abundance of *Geobacter* species under 18 hrs ON condition.

Similar to anode biofilm communities, there was a substantial shift in the cathodic biofilm communities (Figure 5.4). *Proteobacteria* (75% vs. 50% vs. 65%) and *Bacteroidetes* (22% vs. 32% vs. 13%) were the two most dominant phyla in the cathode biofilms. At the genus level, *Enterobacteriaceae* (61% vs. 56% vs. 36%) and *Bacteroides* (25% vs. 18% vs. 9%) were the two most dominant genera. The abundance of genera *Rhodocyclaceae*_K82 and *Azovibrio* was almost similar (5% vs. 4% vs. 3%). Interestingly, under 18 hrs ON mode, the abundance of

*Acidaminococcus* increased from 0.5% (24 hrs ON) to 4.5% (18 hrs ON). Other genera, *Desulfovibrio, Pleomorphomonas, Bosea*, etc., represented <2% of the cathode biofilm communities. Notably, genus *Acidaminococcus*, a member of class *Clostridia*, is known as homoacetogens (Chowdhury et al., 2014). As discussed later, some hydrogenotrophic methanogens were marginally affected after switching to intermittent applied potential conditions, which could provide a kinetic advantage to homoacetogens. Nonetheless, the abundance of genus *Acidaminococcus* was still low, and their abundance further decreased from 4.5% (18 hrs ON) to 1.9% (12 hrs ON). Thus, homo-acetogenesis appeared to play a minor role under different conditions.

### *3.3.2. Archaeal communities*

Figure 5.4b shows the abundance of archaeal communities sequenced using 16s rRNA primer. The abundance of *Methanobacterium* in cathode biofilms was higher than that of anode biofilms under all conditions. The members of the genus *Methanobacterium* are known as hydrogenotrophic methanogens (Zakaria and Dhar, 2019). The hydrogen produced on the cathode could stimulate the enrichment of hydrogenotrophic methanogens, which is consistent with previous studies (Choi and Sang, 2016; Saheb-Alam et al., 2019). On the other hand, acetoclastic methanogens could be either outcompeted by electroactive bacteria or washed out due to the operation of the reactor under shorter hydraulic residence time (~4 days) (Ho et al., 2014; Li et al., 2016; Zakaria et al., 2019). However, the abundance of *Methanobacterium* in cathode biofilms decreased with decreasing the duration of applied potential. Their relative abundances were 6%, 5%, and 1%, under 24 hrs ON, 18 hrs ON, and 12 hrs ON modes, respectively. Thus, the results suggested that substrate (i.e., $H_2$) limitations caused by intermittently applied potential might adversely affect the hydrogenotrophic methanogenic communities on the cathode. under 12 hrs ON mode. On the other hand, similar methane production from 24 hrs ON and 18 hrs ON modes suggested that the archaeal community was kinetically balanced to the fermentative and electroactive bacterial communities to maintain similar performance under 18 hrs ON mode.

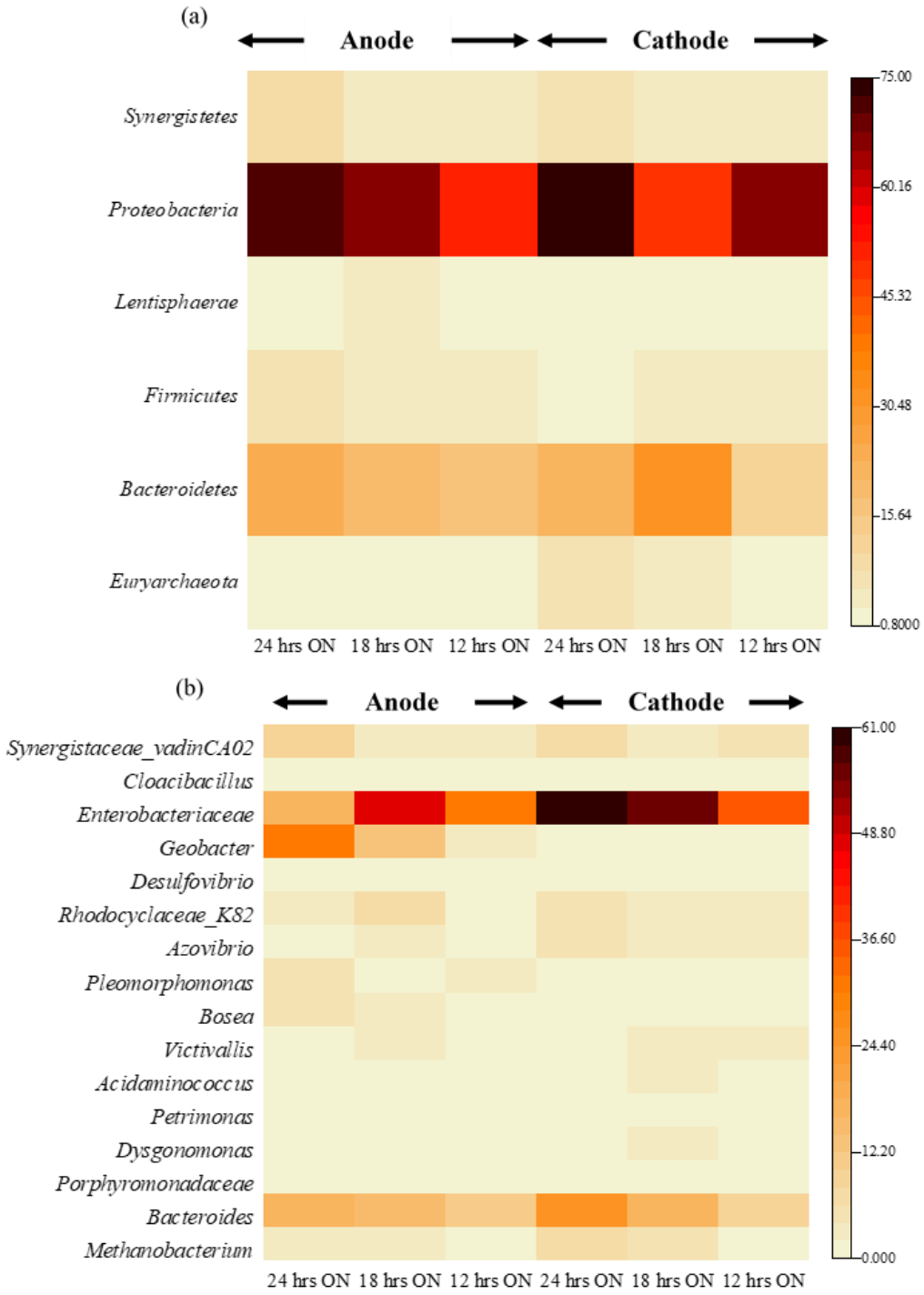


**Figure 5.4** Heatmap of the relative abundance of the microbial community using 16s rDNA primer; phylum level (a), and genus level (b)

To get more insights into the shifts in the archaeal communities, the archaeal communities on the anode and cathode biofilms under different operating modes were further analyzed using a specific archaeal primer (Figure 5.5a). As shown in Figure 5.5a, the archaeal communities in both anode and cathode biofilms were dominated by *Methanobacterium*, with a relative abundance of >90% under all conditions. Recent studies suggested that *Methanobacterium* could produce methane via directly accepting electrons from the cathode or direct interspecies electron transfer (DIET) with syntrophic partners (i.e., bacteria) (Siegert et al., 2015; Zhao et al., 2015), which could explain their abundance on the anode biofilms under different conditions. However, 16S rRNA gene sequencing does not provide precise information about the specific methanogenesis pathways. The other major archaeal genus identified in both biofilms was *Methanocorpusculum*, with a relative abundance from 6% to 7%. Also, metabolically versatile *Methanosarcina* (Luo et al., 2018) presented a minor portion of archaeal communities in cathode biofilms under 24 hrs ON (2%), and 18 hrs ON (3%) modes. However, under 12 hrs ON mode, *Methanosarcina* completely disappeared from the cathode biofilms, suggesting the significance of cathodic hydrogen production for their metabolism. However, the absence of *Methanosarcina* might also occur due to the low acetate production levels (De Vrieze et al., 2012). Nonetheless, based on the results of this study, archaeal communities were less sensitive to the intermittently applied potential.

### *3.3.3. Quantity and diversity of microbial communities*

The quantitative analysis of microbial communities was performed with qPCR analysis (Figure 5.5b). For the anode biofilms, microbial cell number under 24 hrs ON mode ($1.25\times10^{10}$ cells/cm$^2$) was higher than 18 hrs ON mode ($5.7\times10^{9}$ cells/cm$^2$). Then, it further decreased ($2.1\times10^{8}$ cells/cm$^2$) after switching to 12 hrs ON mode. Thus, microbial cell numbers were adversely affected by the intermittently applied potential. The microbial cell numbers in the cathode biofilms under 24 hrs ON, 18 hrs ON, and 12 hrs ON modes were $2.5\times10^{9}$, $7\times10^{9}$, and $1\times10^{7}$ cells/cm$^2$, respectively. These results indicated that the microbial cell numbers in anode and cathode biofilms were unaffected after switching off the applied potential for 6 hrs; however, it was negatively affected after the applied potential was switched off for 12 hrs. As a result, the performance of MEC-AD deteriorated at 12 hrs ON condition.

The diversity of anode and cathode microbial communities were assessed with QIIME2 (Table 1). For 24 hrs ON and 18 hrs ON modes, diversity analysis of anode biofilms in terms of Shannon index (4.1-4.2) indicated similarity between two conditions ($p = 0.09$). However, as evident from the increase in Shannon index to 4.7, anodic microbial communities became more diverse under 12 hrs ON mode ($p = 0.01$). Previous studies also suggested that the open-circuit operation of various microbial electrochemical systems could lead to more diverse anodic biofilm communities (Huang et al., 2014; Shehab et al., 2013). The evenness of cathode biofilms showed a similar pattern like anode biofilms, 4 vs. 3.9 vs. 4.5. Thus, switching operation to alternating open/closed circuit operation led to more diverse microbial communities. However, there were no significant changes in Chao1 and OTUS results. These indicated that the richness of the anode and cathode microbial communities was unaffected under different operating conditions.

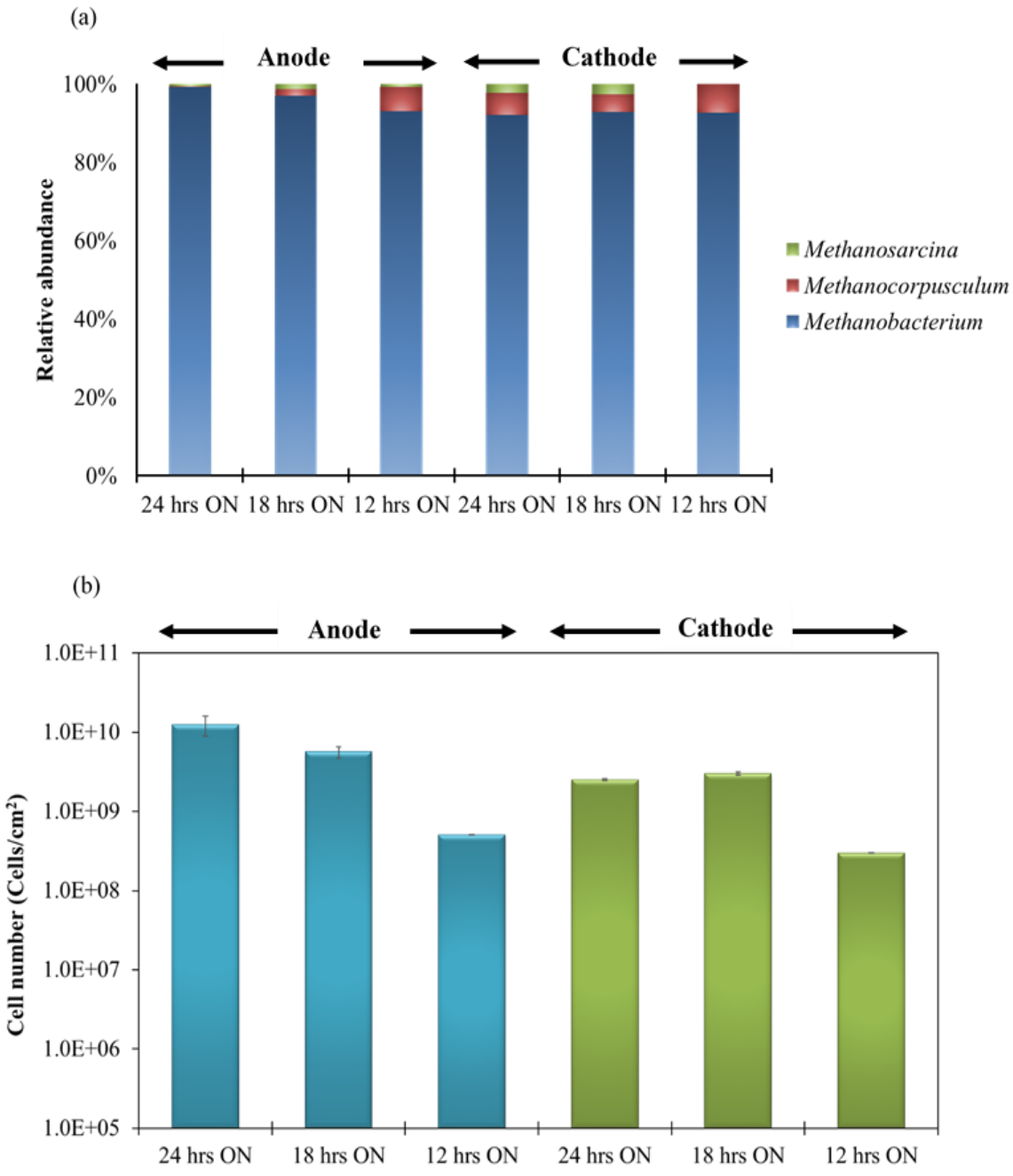


**Figure 5.5** The archaeal community analyzed with a specific archaeal primer (a), and total cell numbers (b) under different operating conditions

### *5.3.4. Energy efficiency*

As compared to 24 hrs ON condition, the electrical energy inputs under 18 hrs ON and 12 hrs ON modes were 25% and 50% lower, respectively. However, the total energy income from methane produced under 24 hrs ON and 18 hrs ON conditions were comparable (~4.8 kJ per batch cycle) (Figure 5.6). Thus, despite a 25% decrease in electrical energy input, 18 hrs ON mode provided slightly higher (6%) net energy income, as compared to 24 hrs ON condition. For 12 hrs ON mode, the total energy income from methane production was 35% lower than the other two conditions (3.1 vs. 4.8 kJ per batch cycle), which led to a marked decrease in net energy income (2.8 vs. 4-4.3 kJ per batch cycle). Thus, our results suggested power supply in MEC-AD systems can intermittently be switched off for up to 6 hours without compromising the overall energy output. For instance, the power supply in the reactors can be turned off during the pick hours of electricity, which can provide saving in operational cost.

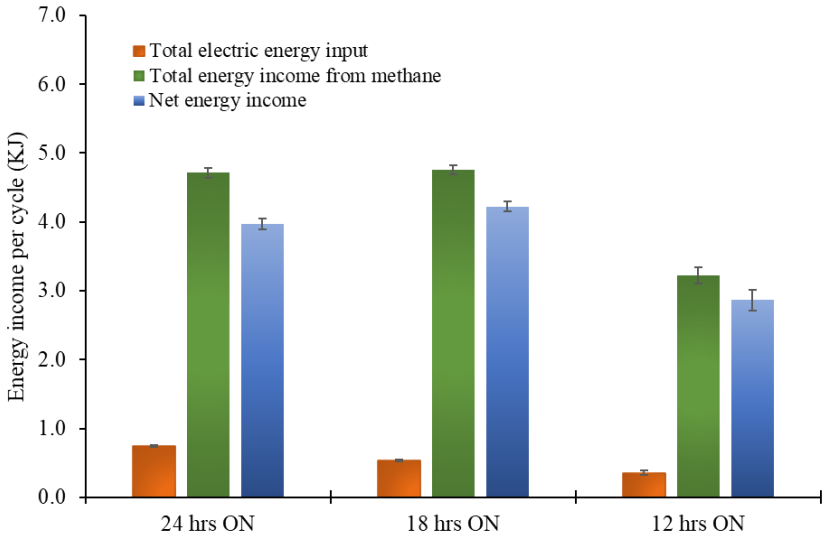


**Figure 5.6** Energy income under different operating conditions

## 5.4. Conclusion

The results of this study demonstrated that intermittent power supply could be a practical solution for minimizing electrical energy input for the operation of MEC-AD systems. According to these results, the applied potential in MEC-AD systems can intermittently be switched off for up to 6 hours/day without compromising the system performance. However, turning off the applied potential for 12 hours caused a decrease in the methane generation and overall energy efficiency. In addition to known electroactive bacteria, the archaeal community was negatively affected. However, further optimization would be needed to determine precise and more optimum on/off switching times.

# Chapter 6

# Insights into intermittent over continuous energization during biomethane recovery from sewage sludge with microbial electrolysis cell assisted anaerobic digester

*A version of this chapter will be submitted in a journal for peer-review and publication*

## 5.1. Introduction

Anaerobic digestion (AD) is a well-established and cost-effective technology for organic waste stabilization and bioenergy generation (Barua et al., 2019e; Bose et al., 2021; L. Lin et al., 2019a; Ryue et al., 2019). Anaerobic digestion consists of multi-stages; hydrolysis, acidogenesis, acetogenesis, and methanogenesis. Hydrolysis and methanogenesis are considered the two major rate-limiting steps in anaerobic digestion depending on the complexity of the substrate. Hydrolysis is considered the rate-limiting step, especially when complex particulate substrates are used (Ma et al., 2013; Zakaria and Dhar, 2019). In contrast, methanogenesis can be the rate-limiting step if simple or soluble organic substrates are used (Ma et al., 2013; Zakaria and Dhar, 2019). Particularly, at high organic loading rates, volatile fatty acids (VFAs) can be generated by acidogenic bacteria at a faster rate, which is considered more kinetically faster than acetoclastic methanogenesis (Ma et al., 2013). Due to the slow kinetic features of acetoclastic methanogens, VFAs may accumulate in digesters, leading to depletion of the buffering capacity followed by acidification (Ma et al., 2013; Shi et al., 2017; Tomei et al., 2009). Thus, methanogenesis becomes a rate-limiting step, which impedes digester performance (Ma et al., 2013). Therefore, establishing a kinetically efficient digester microbiome is essential for developing a stable system and improving methane recovery.

In addition to traditional AD, methane can also be generated by integrating microbial electrolysis cells in anaerobic digestion (MEC-AD) (Ren et al., 2018; Rousseau et al., 2020; Zakaria and Dhar, 2019). Such configurations are usually known as MEC-assisted AD (MEC-AD) systems (Ren et al., 2018; Rousseau et al., 2020; Zakaria and Dhar, 2019). In MEC-AD systems,

a unique group of bacteria, called electroactive bacteria (EAB), can be enriched on the anode electrode (D. Liu et al., 2016; Logan et al., 2019; Lu and Ren, 2016; Siegert et al., 2014b). EAB can oxidize simple organic acids, particularly acetate, outcompeting slow-growing acetoclastic methanogens due to their faster growth kinetics (D. Liu et al., 2016; Logan et al., 2019; Lu and Ren, 2016; Siegert et al., 2014b). The relatively fast-growing hydrogenotrophic methanogens (e.g., *Methanobacterium* and *Methanobrevibacter*) are enriched on the cathode biofilms, where $H_2$ is produced via cathodic electrochemical reduction of protons (Lee et al., 2009; Siegert et al., 2014b). Nonetheless, different forms of extracellular electron transfer (EET) can also contribute to methane generation in MEC-AD systems. For instance, some methanogens can directly capture electrons from the cathode (Lee et al., 2009; Siegert et al., 2014b). Moreover, a recent study showed the potentiality of the direct interspecies electron transport (DIET) between methanogens and EAB for methane generation in the anode biofilm (Baek et al., 2021). Most studies demonstrated enhanced methane recovery with MEC-AD systems compared to conventional AD (Ren et al., 2018; Rousseau et al., 2020; Zakaria and Dhar, 2019). However, the operation of MEC-AD systems requires external energy input via power supply/potentiostat to overcome the thermodynamic barriers, primarily for the cathodic hydrogen generation (Ditzig et al., 2007; Logan et al., 2008; Zakaria and Dhar, 2021b, 2019).

One of the critical challenges in deploying MEC-AD systems on a large scale is the operational cost due to the requirement of energy input in applied voltage/potential (Lim et al., 2020; Wang et al., 2020; Zakaria and Dhar, 2021a). A few reports demonstrated that intermittent power supply could achieve better methane generation and reactor performance (Ailijiang et al., 2016; Hussain et al., 2018; Wang et al., 2020; Zakaria and Dhar, 2021a). Our previous study investigated the intermittent power supply scheme on MEC-AD fed with glucose (Zakaria and Dhar, 2021a). Our results suggested that the applied potential in MEC-AD systems can intermittently be switched off for up to 6 hours/day without compromising the system performance. It was reported that the continuous energy supply might cause an intensive cathodic hydrogen evolution reaction (HER). Consequently, the over accumulation of hydrogen gas bubbles on the cathode electrode will reduce the effective surface area. The intermittent power supply will elevate the attached small gas bubbles (Cho et al., 2019). However, previous efforts to optimize power supply schemes for MEC-AD systems were limited to the synthetic substrate only (Cho et

al., 2019; Wang et al., 2020; Zakaria and Dhar, 2021a). However, conventional digesters are typically operated with more complex substrates (Ahn et al., 2017; W. Liu et al., 2016). Notably, EAB can easily oxidize simple soluble substrates like acetate; however, when dealing with complex substrate, the syntrophic interactions between hydrolytic/fermentative bacteria and EAB and their diversity are critical (Lovley, 2008; Saratale et al., 2017; Shao et al., 2019). Although methane recovery from sewage sludge with MEC-AD systems have been investigated by previous studies (Ahn et al., 2017; W. Liu et al., 2016), the impact of the intermittent power supply in MEC-AD systems fed with sewage sludge has never been reported.

Therefore, this study investigated the MEC-AD performance under cycling on/off the applied potential fed with a mixture of primary and sewage sludge. We comprehensively evaluated the current density, methane generation, sludge degradation efficiency, the expression of EET genes, and microbial cell numbers based on 16S rRNA gene copies using qPCR. To the best of the authors' knowledge, the novelty of this study is to optimize an on/off applied potential scheme in MEC-AD systems fed with a mixture of primary and sewage sludge rather than the synthetic substrate.

## 5.2. Material and methods

### *5.2.1. Setup and enrichment of MEC-AD*

A single-chamber MEC-AD was fabricated using plexiglass tubes with a working volume of 360 mL. Carbon fibers (2293-A, 24A Carbon Fiber, Fibre Glast Development Corp., Ohio, USA) integrated with a stainless-steel frame was used as the anode and cathode electrodes. Carbon fibers were pretreated according to the method previously described by Dhar et al. (2013). Ag/AgCl reference electrode (MF-2052, Bioanalytical System Inc., USA) was placed with a distance of ~1 cm to the anode electrode. A multi-channel potentiostat (Squidstat Prime, Admiral Instruments, Arizona, USA) was used to set a fixed anode potential of -0.4 V vs. Ag/AgCl. During the entire experiment, the liquid medium in the reactor was mixed at 130 ± 5 rpm using a magnetic stirrer.

In the beginning, the reactor was seeded with 15 mL of anaerobic digester sludge and 30 mL effluent from an identical mother MEC that has been operated with a 25 mM acetate medium for >12 months. An anaerobic glucose synthetic wastewater media (2120±56 mg COD/L) was supplemented as a feed with 50 mM phosphate buffer and trace minerals. The detailed composition

of the trace minerals used in this study could be found in the literature (Dhar et al., 2013). This followed by monitoring the current generation until a steady-state current of ~14.33 mA was attained prior to run the experiment. Then, the reactor was evacuated and fed with a mixture of primary and sewage sludge (1:1 on a volume basis) in a semi-continuous mode.

### *5.2.2. Experiments with sludge*

The primary sludge and sewage sludge were collected from the Gold Bar Wastewater Treatment Plant (Edmonton, Alberta, Canada) and stored at 4 °C before use. The average characteristics of mixed sludge were as follows: total chemical oxygen demand (TCOD): 7198 ± 57 mg/L, soluble chemical oxygen demand (SCOD): 935±11 mg/L, total suspended solids (TSS): 5627±105 mg/L, volatile suspended solids (VSS): 4700±88 mg/L, total volatile fatty acids: 628±21 mg COD/L, pH: 6.4 ± 0.1, alkalinity: 1065±32 mg as $CaCO_3$/L. The sludge was fed into the reactor in semi-continuous mode (45 mL/d) at a hydraulic residence time (HRT) of 8 d. This HRT was reported to be optimum for efficient solids removal in sewage sludge-fed MECs (Ki et al., 2017a; Song et al., 2016). Before feeding, the pH of the primary sludge was always adjusted to 7.2 ± 0.1 using 1 N NaOH.

The MEC-AD reactor was operated under three conditions; the applied potential switched on for 24 hours (closed-circuit) as a control condition (referred to as 24 hrs ON). For the second condition, the applied potential switched on for 18 hours (closed-circuit), followed by switched off (open-circuit) for 6 hours (referred to as 18 hrs ON). The applied potential switched on for 12 hours for the third condition, followed by a switch off for 12 hours (referred to as 12 hrs ON). . The reactor operated under each condition until it reached a steady-state. Here, results from four representative cycles were presented. All experiments were performed at room temperature (21±1°C) with a mixing speed of 130 rpm.

### *5.2.3. Quantification of cell number and EET gene expression analyses*

qPCR was performed to quantify microbial cell numbers at the three operating conditions. 16S universal bacterial primers 341F: 5' CCTACGGGNGGCWGCAG 3' and 805R: 5' GACTACHVGGGTATCTAATCC 3' (Klindworth et al., 2013; Logares et al., 2013), archaeal primers 517F: 5' GCYTAAAGSRNCCGTAGC 3' and 909R: 5' TTTCAGYCTTGCGRCCGTAC

3' and specific *mcr*A archaeal primers *mcr*Af: 5' GGTGGTGTMGGATTCACACARTAYGCWACAGC 3' and *mcr*Ar: 5' TTCATTGCRTAGTTWGGRTAGTT 3' (Morris et al., 2014). qPCR mixtures were prepared in 25 µL reactions using QuantiFast SYBR® Green PCR Kit (Qiagen, CA) as the following: 2 µL of the DNA template, 12.5 µL 2x master mix, 2.5 µL forward and reverse specific primer, and 5.5 µL nuclease-free water. CFX 96 real-time PCR system with a C1000 Thermal Cycler (Bio-Rad, USA) was used with the following cycling conditions according to the QuantiFast SYBR® Green PCR Kit's protocol; PCR initial heat activation cycle at 95 ˚C for 5 min, 35 cycles at 95 ˚C for 10 sec and 60 ˚C for 30 sec, and finally, one cycle at 40 ˚C for 30 seconds. Triplicate reactions were run for all samples.

The expressions of EET genes (i.e., *pil*A, *omc*B, *omc*C, *omc*E, *omc*Z, and *omc*S) were also quantified (for details and method, see Supplementary Information). The primer design was performed similarly to Lin et al. (Lin et al., 2019), and *rec*A housekeeping gene was used as a reference (Rivas et al., 2005). The genome sequences of the anode biofilm were collected from the National Center for Biotechnology Information (NCBI) (https://www.ncbi.nlm.nih.gov). These followed by multiple-aligned using the ClustalX alignment tool (http://www.clustal.org/clustal2/) to select most of the homologous gene regions (Thompson, 1997). Then, gene-specific primers for RT-PCR were designed with Primer3 software (http://bioinfo.ut.ee/primer3) by selecting an almost similar range of melting temperatures. The Basic Local Alignment Search Tool (BLAST) (https://blast.ncbi.nlm.nih.gov/Blast.cgi) was used to check the specificity of the primers. Also, the primers were experimentally examined using agarose gel electrophoresis. The primers were prepared by Integrated DNA Technologies (IDT, USA) and are listed in Table A.2.

Total RNA was extracted using RNeasy PowerSoil Total RNA Kit (Qiagen, CA), then the purity and concentration were examined using Nanodrop (2000C, Thermo Scientific, USA). Subsequently, cDNA synthesis was performed using QuantiTect Reverse Transcription Kit (Qiagen, CA). Then, RT-PCR mixtures were prepared in 25 uL reactions using QuantiFast SYBR® Green PCR Kit (Qiagen, CA) as the following: 1 µL of the template, 12.5 µL 2x master mix, 2.5 µL forward and reverse specific primer, and 6.5 µL nuclease-free water. CFX 96 real-time PCR system with a C1000 Thermal Cycler (Bio-Rad, USA) was used with the following cycling conditions according to the QuantiFast SYBR® Green PCR Kit's protocol; PCR initial heat

activation cycle at 95 ˚C for 5 min, 35 cycles at 95 ˚C for 10 sec and 60 ˚C for 30 sec, and finally, one cycle at 40 ˚C for 30 seconds. Triplicate reactions were run for all samples.

### *5.2.4. Calculation of energy income*

The net energy income under different operating conditions was determined according to (Zakaria and Dhar, 2021a). The net energy income per cycle ($W_{net}$, kJ) (Eq. 1) determined based on the difference between the total energy income from methane produced ($W_{CH4}$, J) and the total electric energy consumed via applied potential ($W_e$, kJ).

$$W_{net} = W_{CH4} - W_e \qquad \text{(Eq. 1)}$$

The total energy income from methane production ($W_{CH4}$, kJ) was calculated by multiplying the energy content of methane-based on the heat of combustion ($\Delta H_s = 890.31 \times 10^3$ J/mol) and total moles of methane produced. The total electric energy input ($W_e$, kJ) was calculated by multiplying the applied voltage and cumulative coulombs.

### *5.2.5. Analytical methods*

The current generation from the reactor was recorded every 4.8 min using a potentiostat (Squidstat Prime, Admiral Instruments, USA). Chemical oxygen demand (COD) was measured with the HACH kit (HACH, Loveland, Colorado, USA). Suspended solids (VSS and TSS) concentrations were measured according to the standard method (Federation and American, 2005). pH was measured with a benchtop pH meter (Accumet AR15, Fisher Scientific, Pittsburgh, PA, USA). The produced biogas was collected from the reactor using 500 mL gas bags. The biogas composition determined by a Gas Chromatograph (7890B, Agilent Technologies, Santa Clara, USA). Volatile fatty acids (VFAs) concentrations were measured by the Ion chromatograph (Dionex$^{TM}$ ICS-2100, Thermos Scientific, USA) (Zakaria et al., 2019).

## 5.3. Results and Discussion

### *5.3.1. Current density*

Figure 6.1 shows the fluctuation of volumetric current density in MEC-AD under different operational conditions. The maximum current density was observed for 12 hrs ON mode (16.1±0.2 mA, $p = 0.0001$), followed by the 18 hrs ON mode (14.5±0.2 mA, $p = 0.004$) and then the 24 hrs ON mode (10.4±0.3 mA). Initially, the maximum current density was observed immediately at the 18 hrs ON and 12 hrs ON modes once the applied potential switched on, and then maintained a steady-state, demonstrating the sudden electrocatalytic activity of the anode biofilm (Aelterman et al., 2008; Wang et al., 2020; Zakaria and Dhar, 2021a). Previous studies reported the diverse impact of intermittent power supply on MECs and MEC-AD systems. Our previous study showed a decrease in current density when the power supply in a MEC-AD system fed with glucose was switched off for 12 hours (Zakaria and Dhar, 2021a). Another recent study reported an increase in current density in a MEC fed with acetate when external energy input was provided for 12 hours per day (Wang et al., 2020). It is expected that the complexity of substrate in different studies would be an influential factor, leading to mixed results. Notably, EAB can directly oxidize simple substrates like acetate, while syntrophic interactions between EAB and hydrolytic/fermentative bacteria would be critical for complex substrates (Lovley, 2008; Saratale et al., 2017; Shao et al., 2019). In this study, the MEC-AD system was operated with a more complex feedstock (i.e., sewage sludge).

Generally, current density is directly associated with the electrocatalytic activity of EAB (Babauta et al., 2012; Michie et al., 2020; Tahernia et al., 2020), while applied potential is critical in the selection and enrichment of EAB (Baek et al., 2021; Huang et al., 2014; Michie et al., 2020; Shehab et al., 2013; Yu et al., 2015). However, during the intermittent applied potential, the cytochromes present within EAB can act as pseudocapacitor to store the energy in the forms of electrons and immediately discharge after switching to closed-circuit mode (Bonanni et al., 2012; Chung et al., 2020; Esteve-Núñez et al., 2008; Houghton et al., 2016; Schrott et al., 2011; Uría et al., 2011; Wang et al., 2020). For instance, *Geobacter sulfurreducens* showed a high capability to oxidize organic substrates in the absence of an external acceptor utilizing their cytochromes as an

electron sink (Esteve-Núñez et al., 2008; Schrott et al., 2011). Moreover, Uría et al. (2011) indicated the ability of *Shewanella oneidensis* MR-1 to store the electric charge while oxidizing organic substrates without an external acceptor. Also, this study found that the current generated after the open-circuit condition period is proportional to the period of the open-circuit mode. Similarly, a maximum current peak was observed after switching on the applied potential immediately. Therefore, the intermittent supply of the applied potential enhanced the electrocatalytic activity of the anode biofilm, demonstrating a higher current density at 12 hrs ON mode.

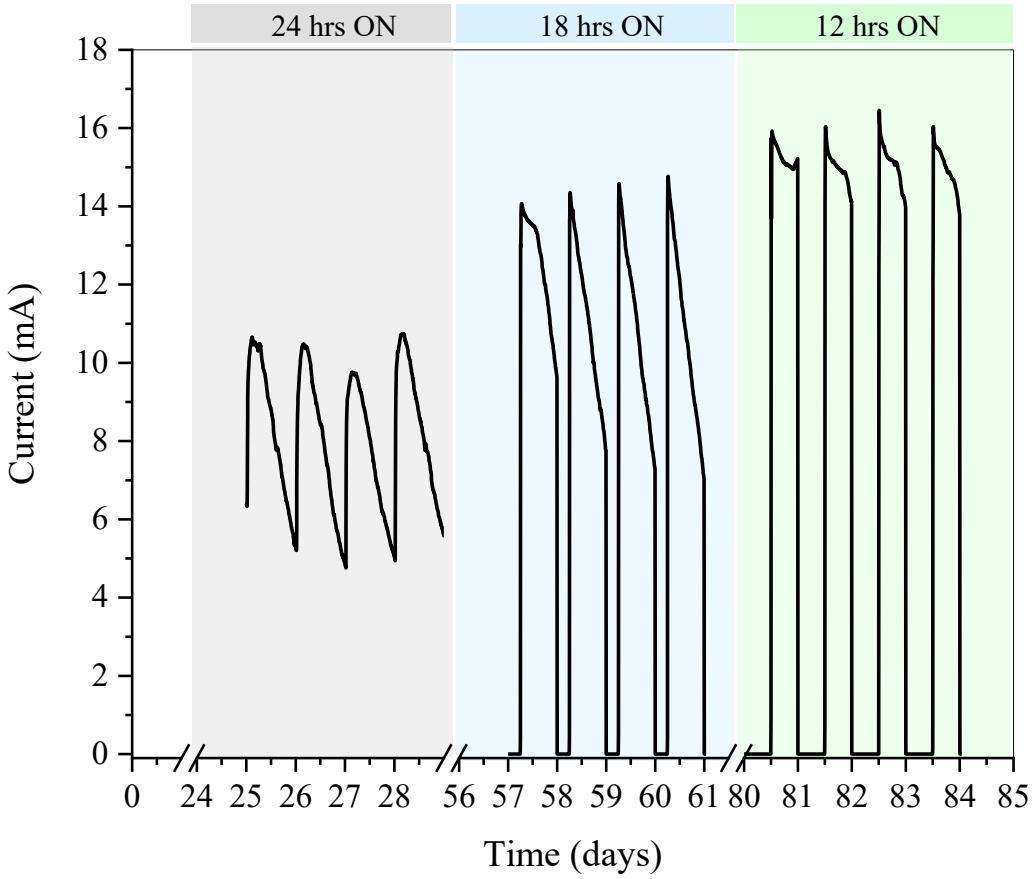


**Figure 6.1** The current generation under different operating conditions

### *5.3.2. Methane generation*

The methane generation profile was monitored under different operating conditions (Figure 6.2). The maximum methane generation of 214±1.5 L $CH_4/m^3$ ($p = 0.002$) was attained when the applied potential was switched on for 12 hours, followed by 206±1.5 L $CH_4/m^3$ ($p = 0.01$) for 18 hrs ON mode. The methane production further decreased to 199±2.9 L $CH_4/m^3$ for 24 hrs ON mode. Thus, intermittent applied potential demonstrated better methane recovery over continuous applied potential. During the continuous operation of applied potential, EAB might reached a high electrocatalytic activity and consume the organic acids, particularly acetate (Huang et al., 2014; Shehab et al., 2013; Wang et al., 2020; Yu et al., 2015). However, excess hydrogen production on the cathode might exceed the microbial utilization capacity of hydrogenotrophic methanogens, which consequently directed to other microorganisms present in the cathode biofilm for byproducts formation instead of $CH_4$ generation (Lee et al., 2009; Sangeetha et al., 2017; Wang et al., 2020). Notably, acetogenic species can utilize electrons/$H_2$ and $CO_2$ to acetate and other multicarbon compounds (Aryal et al., 2017; Izadi et al., 2020; Nevin et al., 2011, 2009; Parameswaran et al., 2012; Zaybak et al., 2013). Nonetheless, elevated $H_2$ partial pressure may also create thermodynamically unfavorable conditions for fermentation. As shown in **Error! Reference source not found.**, the highest methane yield ($COD_{methane}/COD_{removed}$) was observed at 12 hrs ON mode (70.7±0.6%, $p = 0.01$). In addition to methane, the potential sink of the COD might include biomass synthesis, sludge accumulation, and dissolved methane (Freguia et al., 2007; Hari et al., 2016b; Lee et al., 2008).

Additionally, it was found based on the intensive literature that known hydrogenotrophic methanogens, such as *Methanobacterium* and *Methanobrevibacter* were mostly enriched on the biocathode (Cheng et al., 2009; Dykstra and Pavlostathis, 2017; Siegert et al., 2015, 2014a; Zakaria and Dhar, 2021b). Interestingly, few reports also found the enrichment of known hydrogenotrophic methanogens on the anode biofilms (Hari et al., 2016b; W. Liu et al., 2018; Zakaria and Dhar, 2021b). For instance, *Methanoculleus, Methanocorpusculum, Methanococcus* and *Methanobacterium* were enriched on the anode biofilms (W. Liu et al., 2018). Therefore, EAB can act as a pseudocapacitor storing the electrons, which could stimulate DIET between the methanogens and electroactive bacteria present on the conductive anode electrode. Several

previous reports supported the potential of DIET between EAB and methanogens on anode biofilms and other conductive materials (Flores-Rodriguez and Min, 2020; C. Lin et al., 2019; Yin et al., 2016; Zheng et al., 2020). Rotaru et al. (2014b) and (2014a) demonstrated the DIET mechanism between methanogens and EAB. It has been suggested that a few methanogens have the unique capability for DIET (Gao and Lu, 2021; Lovley, 2017; Rotaru et al., 2014b, 2014a; Shi et al., 2016; Walker et al., 2019). Also, a recent study indicated that hydrogenotrophic methanogens, particularly *Methanospirillum hungatei*, have the capability for long-range electrical connections using e-pili (Walker et al., 2019). Another recent study explored the capability of *Methanobacterium* to produce methane via the DIET mechanism (Zheng et al., 2020). Therefore, longer switching off the applied potential for 12 hrs might stimulate the DIET between methanogens and EAB, allowing the efficient utilization of the electrons towards methane generation.

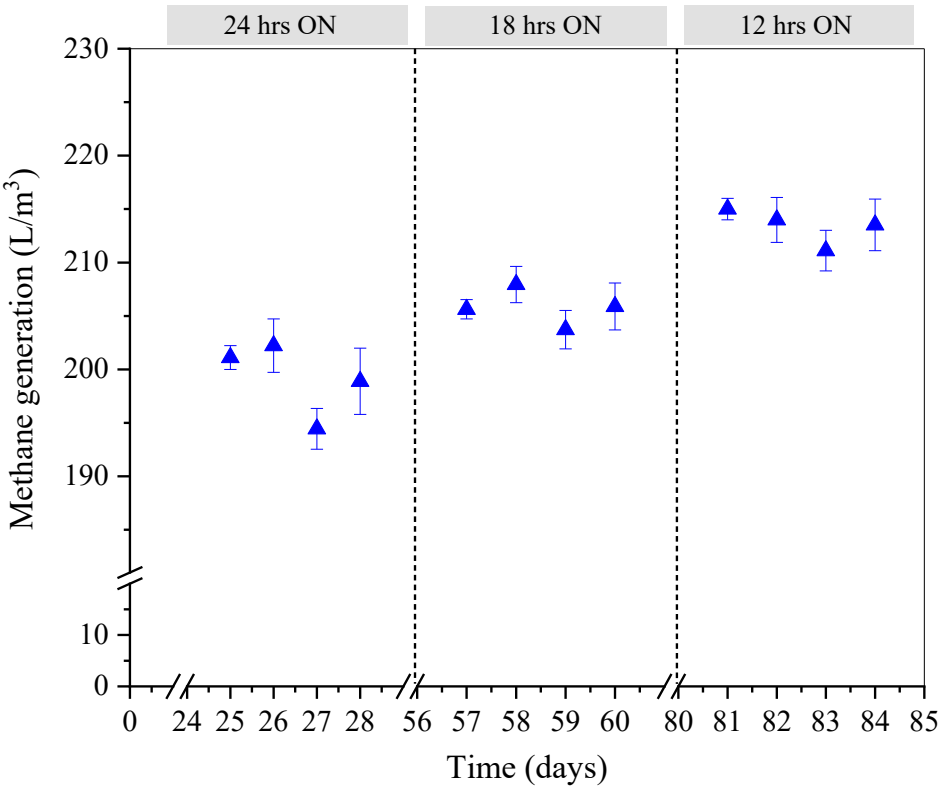


**Figure 6.2** Methane generation profile under different operating conditions. The error bars indicate the standard deviation of three replicates (n = 3)

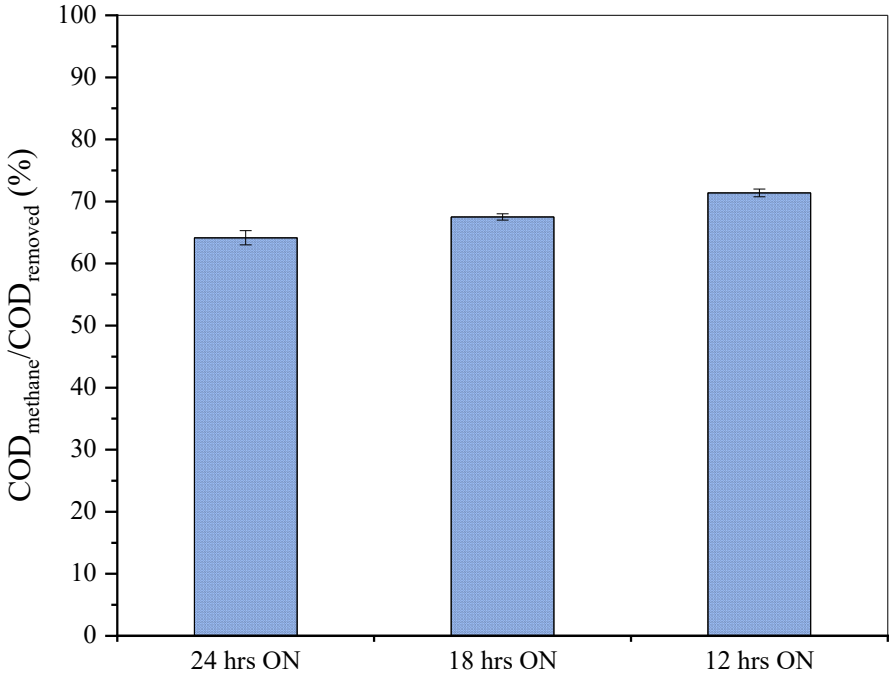


**Figure 6.3** Removed COD recovered as methane under different operating conditions. The error bars indicate the standard deviation of three replicates (n = 3)

### *5.3.3. Sludge removal*

Figure 6.4a shows the TCOD effluent concentrations and TCOD removal efficiencies at different operating modes. Under continuous applied potential, TCOD removal efficiency reached 51.5±0.8% with effluent concentration 3842.3±65.8 mg COD/L. However, the TCOD removal efficiency increased at 18 hrs ON mode to 57.7±0.7% ($p$ = 0.0001), then further increased to the highest removal efficiency of 60.5±0.7% ($p$ = 0.0001) under 12 hrs ON mode with effluent concentrations of 3354.3±57.4 and 3130.7±53.6 mg COD/L, respectively. Also, 12 hrs off mode exhibited the highest VSS removal efficiency of 67.0±0.5% ($p$ = 0.0003), compared to 63.8±0.5% and 62.7±0.5% observed for 18 hrs ON and 24 hrs ON modes, respectively (Figure 6.4b). Moreover, the SCOD/TCOD ratio of the sludge effluent slightly increased from 0.42±0.009 at the continuous operation mode to 0.51±0.008 ($p$ = 0.005) and 0.57±0.006 ($p$ = 0.002) for 6 hrs off mode and 12 hrs off mode (Figure 6.5), respectively, suggesting that the sludge hydrolysis has been improved at 12 hrs off operational mode (Liang et al., 2019). A previous study showed that the intermittent voltage gradient stimulated the sludge hydrolysis and dewaterability (Ibeid et al.,

2013). Moreover, the intermittent power supply might create a pore opening in the cell membrane followed by the release of soluble components and increase the bioavailability of organics (H. Zhang et al., 2009).

Figure 6.6a shows the average three major VFAs (acetate, butyrate, and propionate) effluent concentrations at different operating modes. Although the sludge hydrolysis improved at 12 hrs off mode, the VFAs concentration at the continuous operational mode (1192±5.2 mg COD/L) was higher ($p = 0.007$) than the other two operational modes; at 18 hrs ON mode (1085±8.5 mg COD/L) and 12 hrs ON mode (1087±10.5 mg COD/L) operational mode. These might have resulted from the extensive release of the protons within the anode biofilm at the continuous operational mode resulted in a pH drop in the anode biofilm (Dhar et al., 2017; Torres et al., 2008). This might cause a slower EAB activity, leading to the accumulation of VFAs at the continuously applied potential. Nonetheless, slight differences in the VFA concentrations did not affect the recorded pH values of 6.85 (continuous mode), 6.80 (18 hrs ON mode) and 6.90 (12 hrs ON mode). However, the bulk fluid pH measurement may not reflect the actual pH inside the biofilms (Dhar et al., 2017; Hollmann et al., 2021; Torres et al., 2008).

Figure 6.6b shows the impact of the operating conditions on the distribution of particulate COD, other soluble COD fractions, and VFAs in the MEC-AD effluents. Although 24 hrs ON mode showed higher VFAs in the effluent, particulate COD fractions were higher at 24 hrs ON than 18 hrs ON and 12 hrs ON modes. However, soluble COD (VFAs+ Other soluble COD) was higher at 18 hrs ON and 12 hrs ON mode than 24 hrs ON mode. Thus, it was evident that intermittently switching off the applied potential could enhance the sludge solubilization.

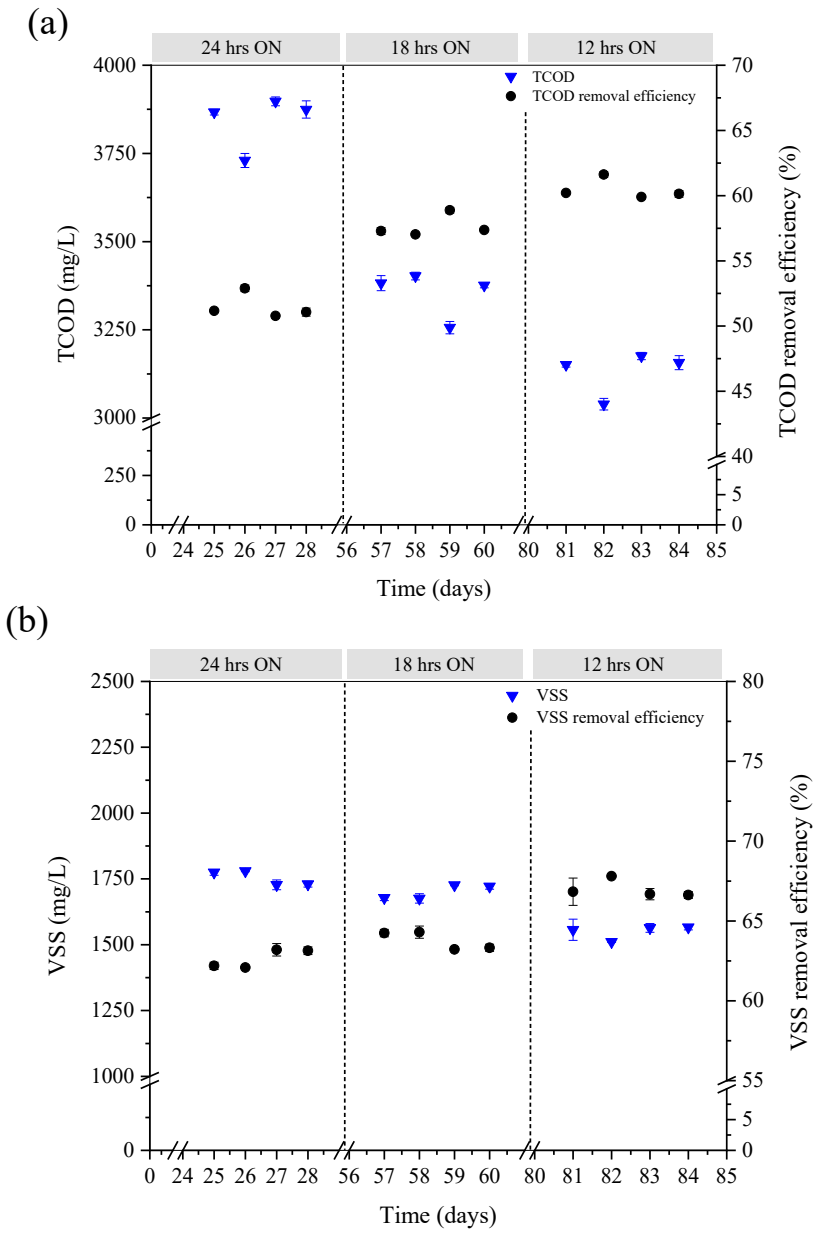


**Figure 6.4** Effluent (a) TCOD concentrations and removal efficiency, and (b) VSS concentrations and removal efficiency. The error bars indicate the standard deviation of three replicates (n = 3)

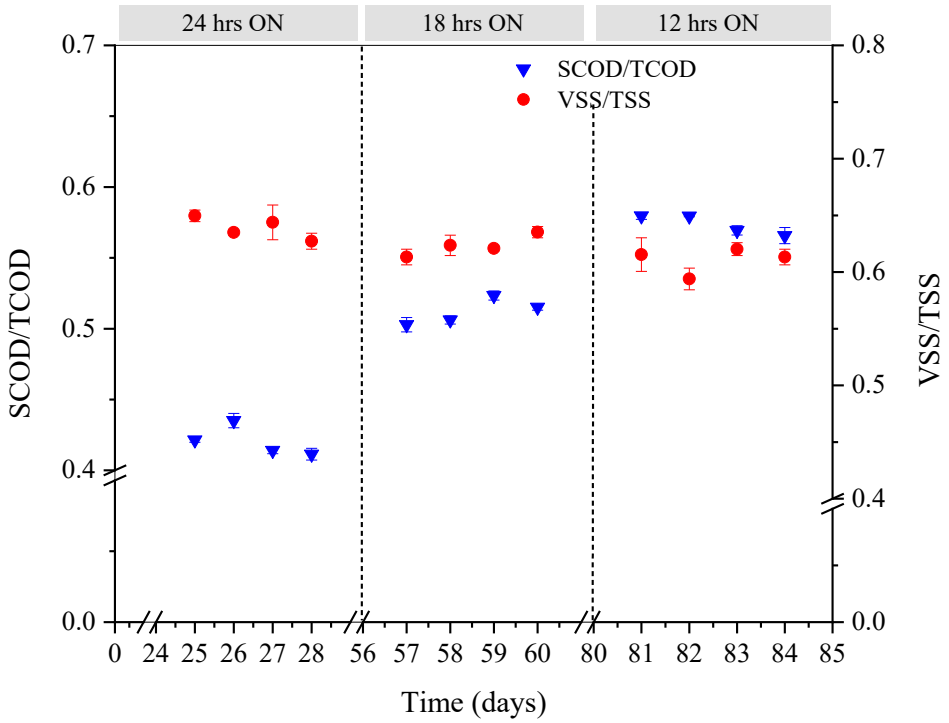


**Figure 6.5** Effluent SCOD/TCOD and VSS/TSS ratios under different operating conditions. The error bars indicate the standard deviation of three replicates (n = 3)

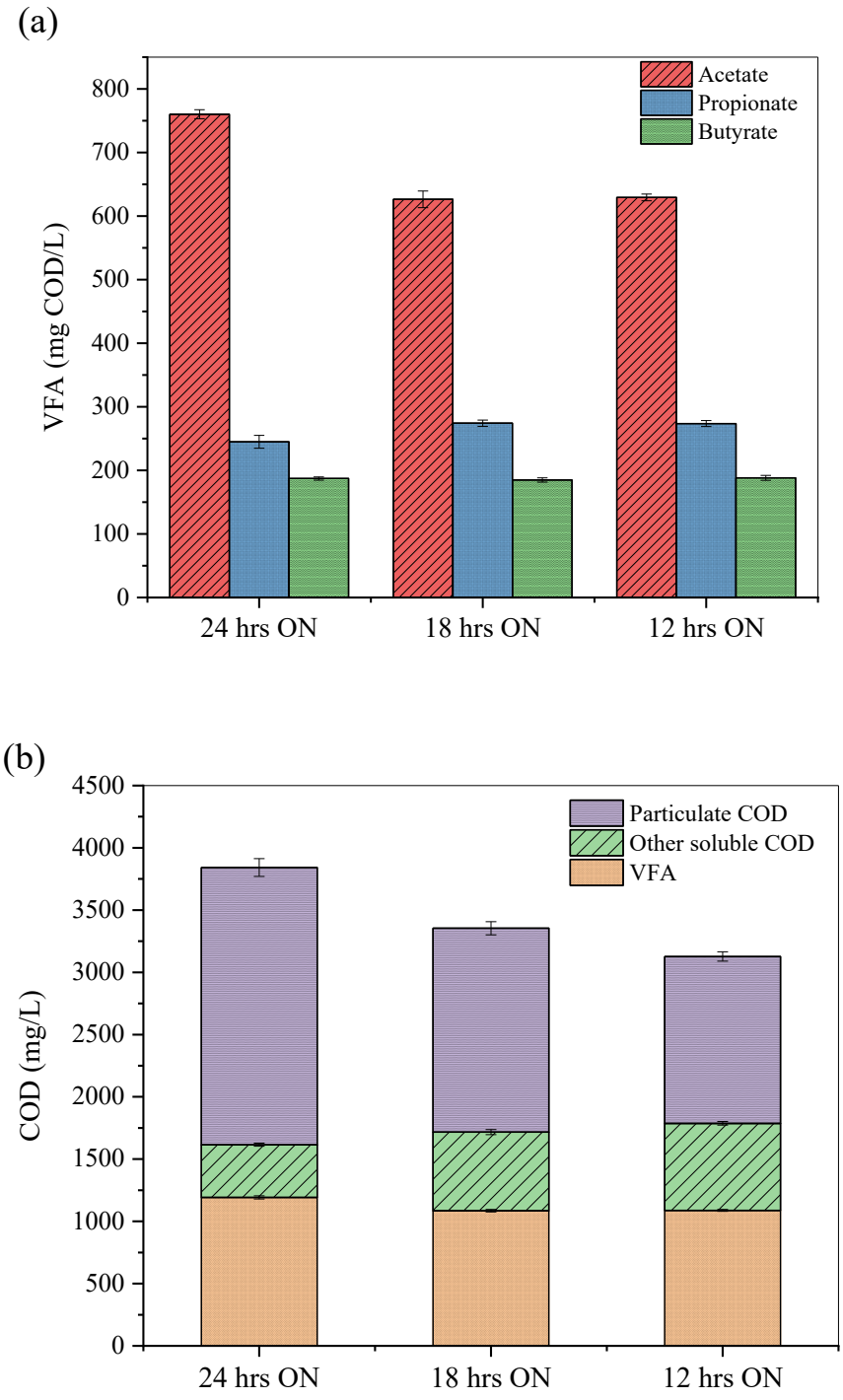


**Figure 6.6** Changes in effluent (a) VFA concentrations, and (b) various TCOD fractions. The error bars indicate the standard deviation of three replicates (n = 3)

### *5.3.4. Expression of EET genes*

Figure 6.7 shows the EET-associated genes expression levels at different operating conditions. The EET-associated genes expression, such as c-type cytochromes and *pil*A, on the anode and cathode biofilms, have been measured under different conditions. Generally, the EET-associated genes showed the highest expression at 12 hrs ON mode ($p = 0.008$), followed by 18 hrs ON mode ($p = 0.01$). Multi-heme c-type cytochromes and electrically conductive e-pili are the key components that mediate the electron exchange between the electroactive biofilms and anode electrodes (Gorby and Lovley, 1991; Heidary et al., 2020; Hernández-Eligio et al., 2020; Logan et al., 2019; Lovley and Walker, 2019; Reguera et al., 2005). For instance, Nevin et al. (2009) observed significantly low current generation and inhibited biofilm formation after deleting *pil*A and *omc*Z genes in *Geobacter sulfurreducens* biofilms. EAB can still oxidize organic compounds during open-circuit conditions in the absence of external electron acceptors (Esteve-Núñez et al., 2008; Schrott et al., 2011; Uría et al., 2011). In such conditions, cytochromes present within EAB can act as pseudo-capacitors to store electrons and liberate them when switched to closed-circuit mode (Houghton et al., 2016; Schrott et al., 2011; Uría et al., 2011; Wang et al., 2020). Thus, the pseudocapacitance of electroactive biofilms possibly explains the upregulation of the EET-associated genes observed during the closed-circuit condition in 12 hrs ON mode (see Figure 6.7). Meanwhile, some methanogens also have the capability of DIET (Gao and Lu, 2021; Lovley, 2017; Rotaru et al., 2014b, 2014a; Shi et al., 2016; Walker et al., 2019). Also, the possibility of the potential DIET mechanism between methanogens and EAB might contribute to the high EET-gene expressions during open-circuit conditions (Rotaru et al., 2014b, 2014a). In order to further clarify whether the EET-associated genes are still expressed during the off period of the applied potential for the DIET mechanism, expressions of EET genes have been measured during the switching off period at the 18 hrs ON mode and 12 hrs ON mode. The results showed that the EET-associated genes were still expressed in both anode and cathode biofilms during the off period, which supports the potentiality of the DIET mechanism between EAB and methanogens on the anode biofilm.

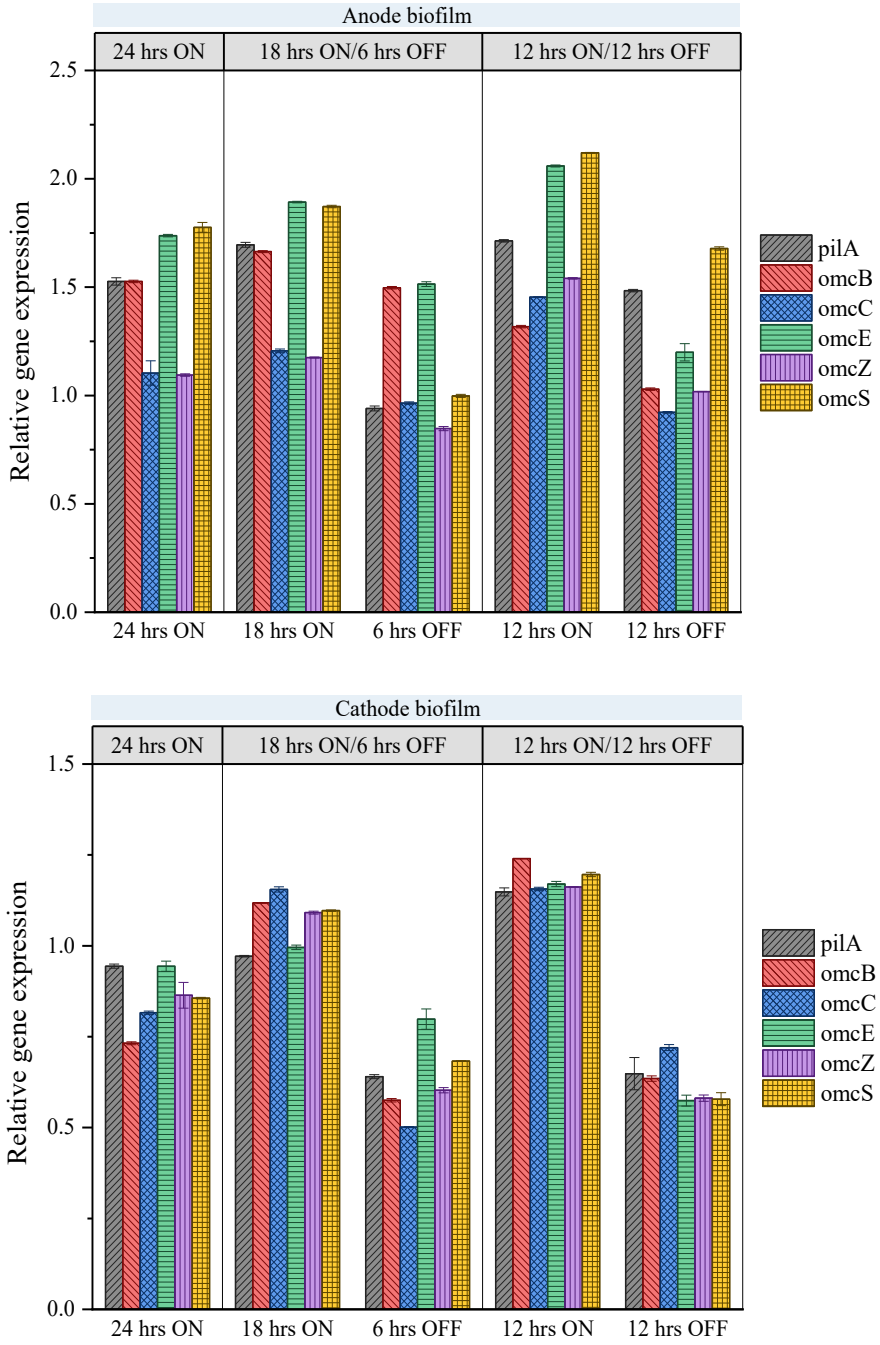


**Figure 6.7** Expression of genes known to regulate extracellular electron transfer in biofilms. The error bars indicate the standard deviation of three replicates (n = 3)

### *5.3.5. Quantitative analysis with qPCR*

Under different operating modes, bacterial cell numbers on the anode and cathode biofilms and the suspension were quantified with universal primers using qPCR (Figure 6.8). Also, the archaeal cell numbers were quantified using specific archaeal and *mcr*A primers (Figure 6.8). For the anode biofilms, the total microbial cells using 16S rRNA universal primer decreased significantly ($p = 0.0017$) after switching from 24 hrs ON mode to 18 hrs ON and 12 hrs ON modes ($4.9 \times 10^{10}$ cells/cm$^2$ vs. $3.2 \times 10^{10}$ vs. $4.2 \times 10^{10}$ cells/cm$^2$). On the contrary, the archaeal cell number increased using specific archaeal primers ($2.5 \times 10^4$ vs. $9.8 \times 10^4$ vs. $9.1 \times 10^5$ cells/cm$^2$), and *mcr*A primers ($3.3 \times 10^2$ vs. $4.3 \times 10^2$ vs. $8.1 \times 10^3$ cells/cm$^2$), respectively. The increase of the methanogens on the anode biofilm could stimulate DIET with EAB present on the anode electrode. This could also be associated with the higher methane generation observed for intermittent applied potential conditions. Several previous reports supported the potential of DIET between EAB and methanogens on anode biofilms and other conductive materials (Flores-Rodriguez and Min, 2020; C. Lin et al., 2019; W. Liu et al., 2018; Yin et al., 2016; Zheng et al., 2020).

For the cathode biofilms, there were no significant changes in the archaeal cell numbers using the archaeal primers and *mcr*A primers ($2.0 \times 10^7$ vs. $2.3 \times 10^7$ vs. $3.5 \times 10^7$ cells/cm$^2$) and ($4.2 \times 10^5$ vs. $1.3 \times 10^5$ vs. $3.9 \times 10^5$ cells/cm$^2$), respectively. Also, the bacterial cell numbers using universal primers showed minimal differences between 24 hrs ON and 18 hrs ON modes ($3.4 \times 10^9$ vs. $2.1 \times 10^9$ cells/cm$^2$). However, it further decreased ($4.4 \times 10^8$ cells/cm$^2$) after switching off the applied potential for 12 hours. As aforementioned, at 24 hrs ON mode, excess hydrogen production on the cathode might exceed the microbial utilization capacity of hydrogenotrophic methanogens, which consequently directed to other microorganisms present in the cathode biofilm for byproducts formation instead of $CH_4$ generation (Lee et al., 2009; Sangeetha et al., 2017; Wang et al., 2020). Notably, acetogenic species can outcompete hydrogenotrophic methanogens for the utilization of electrons/$H_2$ and $CO_2$ to acetate and other multicarbon compounds (Aryal et al., 2017; Izadi et al., 2020; Nevin et al., 2011, 2009; Parameswaran et al., 2012; Zaybak et al., 2013). This is also supported by the higher acetate concentrations observed at 24 hrs ON mode (Figure 6.6). However, at 12 hrs ON mode, the cathodic hydrogen production might be decreased, which

consequently decreasing the growth of acetogens. Thus, $H_2$/electrons are mostly directed to be utilized via methanogens. There were no significant changes in the microbial and archaeal cell numbers for the suspension under different operating modes, suggesting that applied potential primarily influenced the electrode-attached biofilms communities.

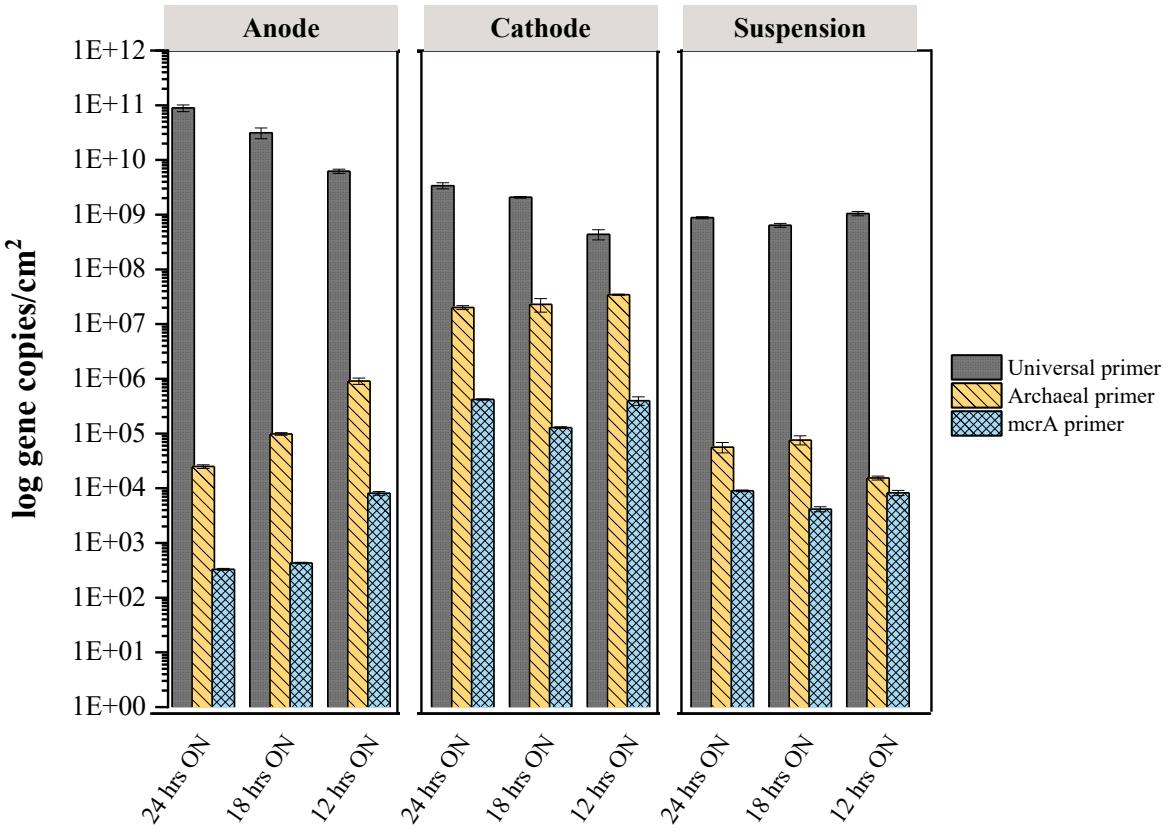


**Figure 6.8** Total cell number using 16S, archaeal primers, and mcrA gene copies. The error bars indicate the standard deviation of three replicates (n = 3)

### *5.3.6. Energy efficiency*

The intermittent applied potential for 18 and 12 hours decreased electrical energy input by 21.5±1.8% and 42.3±0.4%, compared to the continuous operation with applied potential. Nonetheless, methane recovery showed a marked increase under 18 hrs ON and 12 hrs ON conditions compared to 24 hrs ON condition by 15.6±3.2% and 31.7±5.8%, respectively. Thus, the total energy income (as methane) also showed a significant increase for switching from 24 hrs ON mode to 18 hrs ON (2.5 vs. 2.7 kJ/d; $p = 0.05$) and 12 hrs ON mode (2.5 vs. 2.8 kJ/d; $p = 0.03$) (Figure 6.9). Compared to the continuous applied potential, the reduction in electrical energy input and the increment of the total energy income led to an increased net energy income for 18 hrs ON (2.3 vs. 2.5 kJ/d, $p = 0.05$) and 12 hrs ON (2.3 vs. 2.6 kJ/d, $p = 0.03$). Thus, these results suggested that the intermittent applied potential for 12 hours per day could provide an attractive opportunity to saving electrical energy input in MEC-AD systems, thereby its economic benefits.

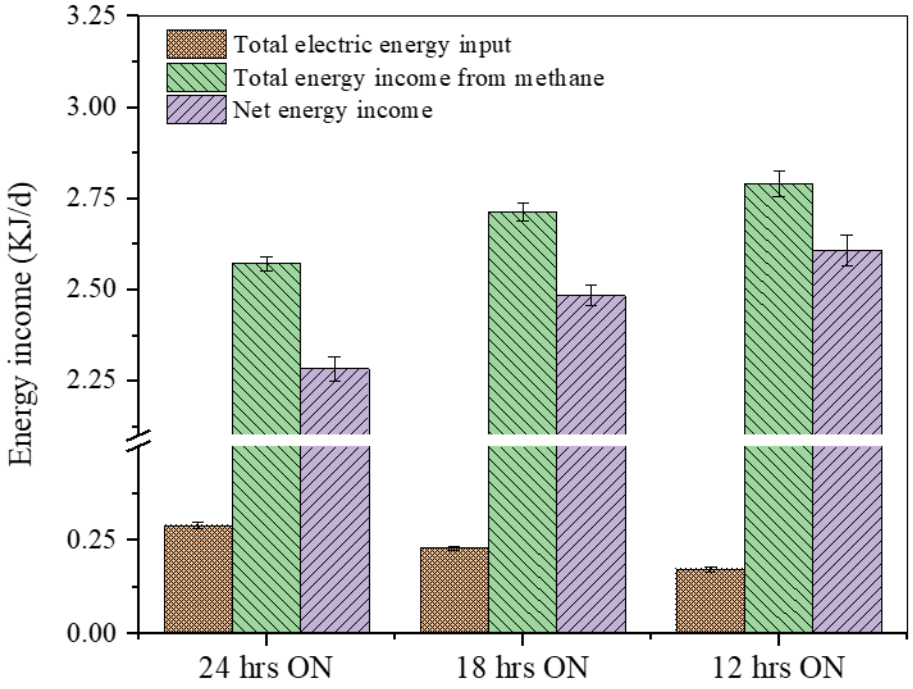


**Figure 6.9** Energy income under different operating conditions. The error bars indicate the standard deviation of three replicates (n = 3)

## 5.4. Conclusions

In the present study, we investigated the MEC-AD performance under cycling on/off the applied potential fed with a mixture of primary and sewage sludge. Intermittent power supply at switching off the applied potential for 12 hrs/day to MEC-AD enhance the methane generation from 199 L $CH_4/m^3$ to 214 L $CH_4/m^3$. Also, sludge degradation efficiency and expression of EET-genes improved. However, continuous operation of applied potential or switching off for 6 hrs/day showed less performance of MEC-AD. Accordingly, the intermittent applied potential for 12 hours per day could provide an attractive opportunity to saving electrical energy input in MEC-AD systems, thereby its economic benefits.

# Chapter 7

# Conclusions and Recommendations

## 7.1. Conclusions

This doctoral thesis focused on exploring fundamental and applied aspects of the developments of microbial electrolysis assisted anaerobic digestion (MEC-AD) for effective methane recovery from organic waste. Particularly, the results provide insights into the significance of functional microbiome, extracellular polymeric substances, and power supply schemes on electro-methanogenesis.

This thesis presents a comparative study on the effectiveness of the carbonaceous (carbon fiber) and metallic (stainless-steel mesh) cathode electrodes for MEC-AD. The stainless-steel electrode improved electro-methanogenic efficiency by promoting a higher abundance of hydrogenotrophic archaea and homoacetogenic bacteria, owing to the faster catalysis of hydrogen evolution reaction. The concentrations of major EPS components in the stainless-steel cathode biofilm were higher than that of carbon fiber cathode biofilm, which might facilitate the electron transfer mechanism. Also, EET gene expression patterns and redox activity of biocathode-derived EPS provided evidence that cathodic EET was also involved in methanogenesis in both biocathodes. The results of this study are also significant for selecting efficient biocathode material to realize improved performance from MEC-AD systems.

To determine the detrimental ratio of HPr/HAc towards the electro-methanogenesis process in MEC-AD, different propionate/acetate ratios of 0.5, 1.5, 2.5, 5 with varying concentrations were tested. Our results showed that the performance of the reactor was comparable at HPr/HAc ratios 0.5 and 1.5, which showed the highest performance in terms of current density and methane generation. *Geobacter* and *Methanobacterium* species were abundant under lower HPr/HAc ratios of 0.5 and 1.5. However, the performance of MEC-AD has been adversely affected at HPr/HAc ratios higher than 1.5. Overall, this study demonstrated that higher HPr/HAc ratios would adversely impact methanogenesis rates in MEC-AD systems.

From the perspective of energy saving in the operation of MEC-AD, this thesis investigated a cycling on-off power supply scheme for the operation of MEC-AD fed with glucose and sewage sludge. The overall performance of MEC-AD fed with glucose showed no differences in biomethane generation and net energy income when the applied potential turned off for 6 hrs/day. However, performance substantially deteriorated when the applied potential turned off for 12 hrs/day. On the other hand, when MEC-AD was fed with sewage sludge, the maximum methane generation was attained when the applied potential was switched off for 12 hrs/day. Also, the extracellular electron transfer-associated genes showed the highest expression at 12 hrs ON mode. Thus, the complexity of the substrate influenced the intermittent power supply scheme, indicating that substrate-specific optimization of the power supply scheme would be critical for MEC-AD systems.

## 7.2. Recommendations

- The results of this study indicated the significance of EPS on electro-methanogenic activity, while further investigation is needed to get more insights into the quantitative electrochemical features of EPS and establish their relationship with electro-methanogenesis kinetics.

- Given that most of the single-chamber MEC-AD studies used carbon-based biocathode, the results of this study are significant for selecting efficient cathode materials to realize improved performance. However, it should be noted that the results presented here are from specific operating conditions with two selected electrode materials. Hence, further research is warranted with more carbon and metal electrodes with similar textures and surface areas with more complex substrates.

- For the determination of the detrimental ratio of HPr/HAc towards the electro-methanogenesis, this study demonstrated the different HPr/HAc ratios at COD concentrations of~ 2000 mg/L. However, conventional digesters are usually operated with high-strength complex substrates. Therefore, further investigation is required to elaborate on the significance of HPr/HAc ratios for MEC-AD systems operated with high-strength feedstock. Also, the different inoculum strategies are essential to be examined towards different propionate/acetate ratios.

- For the intermittent power supply scheme of MEC-AD, further optimization would be needed to determine precise and more optimum on/off switching times.

## References


Aelterman, P., Freguia, S., Keller, J., Verstraete, W., Rabaey, K., 2008. The anode potential regulates bacterial activity in microbial fuel cells. Appl. Microbiol. Biotechnol. 78, 409–418. https://doi.org/10.1007/s00253-007-1327-8

Ahn, Y., Im, S., Chung, J.-W., 2017. Optimizing the operating temperature for microbial electrolysis cell treating sewage sludge. Int. J. Hydrogen Energy 42, 27784–27791. https://doi.org/10.1016/J.IJHYDENE.2017.05.139

Ailijiang, N., Chang, J., Liang, P., Li, P., Wu, Q., Zhang, X., Huang, X., 2016. Electrical stimulation on biodegradation of phenol and responses of microbial communities in conductive carriers supported biofilms of the bioelectrochemical reactor. Bioresour. Technol. 201, 1–7. https://doi.org/10.1016/j.biortech.2015.11.026

Alonso, R.M., Escapa, A., Sotres, A., Morán, A., 2020. Integrating microbial electrochemical technologies with anaerobic digestion to accelerate propionate degradation. Fuel 267, 117158. https://doi.org/10.1016/j.fuel.2020.117158

Anderson, K., Sallis, P., Uyanik, S., 2003. Anaerobic treatment processes. Handb. Water Wastewater Microbiol. 391–426. https://doi.org/10.1016/B978-012470100-7/50025-X

Angelaalincy, M.J., Navanietha Krishnaraj, R., Shakambari, G., Ashokkumar, B., Kathiresan, S., Varalakshmi, P., 2018. Biofilm Engineering Approaches for Improving the Performance of Microbial Fuel Cells and Bioelectrochemical Systems. Front. Energy Res. 6, 1–12. https://doi.org/10.3389/fenrg.2018.00063

Aryal, N., Tremblay, P.L., Lizak, D.M., Zhang, T., 2017. Performance of different Sporomusa species for the microbial electrosynthesis of acetate from carbon dioxide. Bioresour. Technol. 233, 184–190. https://doi.org/10.1016/j.biortech.2017.02.128

Asztalos, J.R., Kim, Y., 2015. Enhanced digestion of waste activated sludge using microbial electrolysis cells at ambient temperature. Water Res. 87, 503–512.

Babapoor, A., Azizi, M., Karimi, G., 2015. Thermal management of a Li-ion battery using carbon

fiber-PCM composites. Appl. Therm. Eng. 82, 281–290. https://doi.org/10.1016/j.applthermaleng.2015.02.068

Babauta, J., Renslow, R., Lewandowski, Z., Beyenal, H., 2012. Electrochemically active biofilms: Facts and fiction. A review. Biofouling 28, 789–812. https://doi.org/10.1080/08927014.2012.710324

Baek, G., Kim, J., Lee, S., Lee, C., 2017. Development of biocathode during repeated cycles of bioelectrochemical conversion of carbon dioxide to methane. Bioresour. Technol. 241, 1201–1207. https://doi.org/10.1016/J.BIORTECH.2017.06.125

Baek, G., Saikaly, P.E., Logan, B.E., 2021. Addition of a carbon fiber brush improves anaerobic digestion compared to external voltage application. Water Res. 188, 116575. https://doi.org/10.1016/j.watres.2020.116575

Barua, S., Dhar, B.R., 2017. Advances towards understanding and engineering direct interspecies electron transfer in anaerobic digestion. Bioresour. Technol. https://doi.org/10.1016/j.biortech.2017.08.023

Barua, S., Zakaria, B.S., Al-Mamun, A., Dhar, B.R., 2019a. Anodic performance of microbial electrolysis cells in response to ammonia nitrogen. J. Environ. Eng. Sci. 14, 37–43. https://doi.org/10.1680/jenes.18.00010

Barua, S., Zakaria, B.S., Chung, T., Hai, F.I., Haile, T., Al-Mamun, A., Dhar, B.R., 2019b. Microbial electrolysis followed by chemical precipitation for effective nutrients recovery from digested sludge centrate in WWTPs. Chem. Eng. J. 361, 256–265.

Barua, S., Zakaria, B.S., Dhar, B.R., 2018. Enhanced methanogenic co-degradation of propionate and butyrate by anaerobic microbiome enriched on conductive carbon fibers. Bioresour. Technol. 266, 259–266. https://doi.org/10.1016/j.biortech.2018.06.053

Barua, S., Zakaria, B.S., Lin, L., Dhar, B.R., 2019c. Magnetite doped granular activated carbon as an additive for high-performance anaerobic digestion. Mater. Sci. Energy Technol. 2, 377–384. https://doi.org/10.1016/J.MSET.2019.04.002

Barua, S., Zakaria, B.S., Lin, L., Dhar, B.R., 2019d. Shaping microbial communities with

conductive carbon fibers to enhance methane productivity and kinetics. Bioresour. Technol. Reports 5, 20–27. https://doi.org/10.1016/J.BITEB.2018.11.008

Barua, S., Zakaria, B.S., Lin, L., Dhar, B.R., 2019e. Shaping microbial communities with conductive carbon fibers to enhance methane productivity and kinetics. Bioresour. Technol. Reports 5, 20–27. https://doi.org/10.1016/j.biteb.2018.11.008

Beegle, J.R., Borole, A.P., 2017. An integrated microbial electrolysis-anaerobic digestion process combined with pretreatment of wastewater solids to improve hydrogen production. Environ. Sci. Water Res. Technol. 3, 1073–1085. https://doi.org/10.1039/C7EW00189D

Bian, B., Shi, D., Cai, X., Hu, M., Guo, Q., Zhang, C., Wang, Q., Sun, A.X., Yang, J., 2018. 3D printed porous carbon anode for enhanced power generation in microbial fuel cell. Nano Energy 44, 174–180. https://doi.org/10.1016/j.nanoen.2017.11.070

Blumenkrantz, N., Asboe-Hansen, G., 1973. New method for quantitative determination of uronic acids. Anal. Biochem. 54, 484–489. https://doi.org/10.1016/0003-2697(73)90377-1

Bolyen, E., Rideout, J.R., Dillon, M.R., Bokulich, N.A., Abnet, C.C., Al-Ghalith, G.A., Alexander, H., Alm, E.J., Arumugam, M., Asnicar, F., Bai, Y., Bisanz, J.E., Bittinger, K., Brejnrod, A., Brislawn, C.J., Brown, C.T., Callahan, B.J., Caraballo-Rodríguez, A.M., Chase, J., Cope, E.K., Da Silva, R., Diener, C., Dorrestein, P.C., Douglas, G.M., Durall, D.M., Duvallet, C., Edwardson, C.F., Ernst, M., Estaki, M., Fouquier, J., Gauglitz, J.M., Gibbons, S.M., Gibson, D.L., Gonzalez, A., Gorlick, K., Guo, J., Hillmann, B., Holmes, S., Holste, H., Huttenhower, C., Huttley, G.A., Janssen, S., Jarmusch, A.K., Jiang, L., Kaehler, B.D., Kang, K. Bin, Keefe, C.R., Keim, P., Kelley, S.T., Knights, D., Koester, I., Kosciolek, T., Kreps, J., Langille, M.G.I., Lee, J., Ley, R., Liu, Y.X., Loftfield, E., Lozupone, C., Maher, M., Marotz, C., Martin, B.D., McDonald, D., McIver, L.J., Melnik, A. V., Metcalf, J.L., Morgan, S.C., Morton, J.T., Naimey, A.T., Navas-Molina, J.A., Nothias, L.F., Orchanian, S.B., Pearson, T., Peoples, S.L., Petras, D., Preuss, M.L., Pruesse, E., Rasmussen, L.B., Rivers, A., Robeson, M.S., Rosenthal, P., Segata, N., Shaffer, M., Shiffer, A., Sinha, R., Song, S.J., Spear, J.R., Swafford, A.D., Thompson, L.R., Torres, P.J., Trinh, P., Tripathi, A., Turnbaugh, P.J., Ul-Hasan, S., van der Hooft, J.J.J., Vargas, F., Vázquez-Baeza, Y., Vogtmann, E., von Hippel,

M., Walters, W., Wan, Y., Wang, M., Warren, J., Weber, K.C., Williamson, C.H.D., Willis, A.D., Xu, Z.Z., Zaneveld, J.R., Zhang, Y., Zhu, Q., Knight, R., Caporaso, J.G., 2019. Reproducible, interactive, scalable and extensible microbiome data science using QIIME 2. Nat. Biotechnol. https://doi.org/10.1038/s41587-019-0209-9

Bonanni, P.S., Schrott, G.D., Robuschi, L., Busalmen, J.P., 2012. Charge accumulation and electron transfer kinetics in Geobacter sulfurreducens biofilms. Energy Environ. Sci. 5, 6188–6195. https://doi.org/10.1039/c2ee02672d

Bose, R.S., Zakaria, B.S., Kumar Tiwari, M., Ranjan Dhar, B., 2021. High-rate blackwater anaerobic digestion under septic tank conditions with the amendment of biosolids-derived biochar synthesized at different temperatures. Bioresour. Technol. 331, 125052. https://doi.org/10.1016/j.biortech.2021.125052

Brunk, C.F., Jones, K.C., James, T.W., 1979. Assay for nanogram quantities of DNA in cellular homogenates. Anal. Biochem. 92, 497–500. https://doi.org/10.1016/0003-2697(79)90690-0

Brunschweiger, S., Ojong, E.T., Weisser, J., Schwaferts, C., Elsner, M., Ivleva, N.P., Haseneder, R., Hofmann, T., Glas, K., 2020. The effect of clogging on the long-term stability of different carbon fiber brushes in microbial fuel cells for brewery wastewater treatment. Bioresour. Technol. Reports 11, 100420. https://doi.org/10.1016/j.biteb.2020.100420

Cai, W., Liu, W., Yang, C., Wang, L., Liang, B., Thangavel, S., Guo, Z., Wang, A., 2016. Biocathodic Methanogenic Community in an Integrated Anaerobic Digestion and Microbial Electrolysis System for Enhancement of Methane Production from Waste Sludge. ACS Sustain. Chem. Eng. 4, 4913–4921. https://doi.org/10.1021/acssuschemeng.6b01221

Cai, W., Liu, W., Zhang, Z., Feng, K., Ren, G., Pu, C., Sun, H., Li, J., Deng, Y., Wang, A., 2018. mcrA sequencing reveals the role of basophilic methanogens in a cathodic methanogenic community. Water Res. 136, 192–199.

Call, D.F., Merrill, M.D., Logan, B.E., 2009. High surface area stainless steel brushes as cathodes in microbial electrolysis cells. Environ. Sci. Technol. 43, 2179–2183. https://doi.org/10.1021/es803074x

Caporaso, J.G., Kuczynski, J., Stombaugh, J., Bittinger, K., Bushman, F.D., Costello, E.K., Fierer, N., Peña, A.G., Goodrich, J.K., Gordon, J.I., Huttley, G.A., Kelley, S.T., Knights, D., Koenig, J.E., Ley, R.E., Lozupone, C.A., McDonald, D., Muegge, B.D., Pirrung, M., Reeder, J., Sevinsky, J.R., Turnbaugh, P.J., Walters, W.A., Widmann, J., Yatsunenko, T., Zaneveld, J., Knight, R., 2010. QIIME allows analysis of high-throughput community sequencing data. Nat. Methods 7, 335–6. https://doi.org/10.1038/nmeth.f.303

Cerrillo, M., Viñas, M., Bonmatí, A., 2018. Anaerobic digestion and electromethanogenic microbial electrolysis cell integrated system: Increased stability and recovery of ammonia and methane. Renew. Energy 120, 178–189. https://doi.org/10.1016/j.renene.2017.12.062

Cerrillo, M., Viñas, M., Bonmatí, A., 2017. Startup of Electromethanogenic Microbial Electrolysis Cells with Two Different Biomass Inocula for Biogas Upgrading. ACS Sustain. Chem. Eng. 5, 8852–8859. https://doi.org/10.1021/acssuschemeng.7b01636

Cerrillo, M., Viñas, M., Bonmatí, A., 2016. Overcoming organic and nitrogen overload in thermophilic anaerobic digestion of pig slurry by coupling a microbial electrolysis cell. Bioresour. Technol. 216, 362–372.

Champigneux, P., Delia, M.L., Bergel, A., 2018. Impact of electrode micro- and nano-scale topography on the formation and performance of microbial electrodes. Biosens. Bioelectron. https://doi.org/10.1016/j.bios.2018.06.059

Chen, H., Wang, W., Xue, L., Chen, C., Liu, G., Zhang, R., 2016. Effects of Ammonia on Anaerobic Digestion of Food Waste: Process Performance and Microbial Community. Energy & Fuels 30, 5749–5757. https://doi.org/10.1021/acs.energyfuels.6b00715

Chen, Y., Cheng, J.J., Creamer, K.S., 2008. Inhibition of anaerobic digestion process: A review. Bioresour. Technol. 99, 4044–4064.

Chen, Y., Yu, B., Yin, C., Zhang, C., Dai, X., Yuan, H., Zhu, N., 2016. Biostimulation by direct voltage to enhance anaerobic digestion of waste activated sludge. RSC Adv. 6, 1581–1588. https://doi.org/10.1039/C5RA24134K

Cheng, C.-Y., Cheng, K.-L., Wan, T.-J., Kuo, W.-N., Chu, F.-J., Shu, C.-M., 2015. Effects of

applied voltage on hydrogen production rate of a single reactor BML with Clostridium sp. Process Saf. Environ. Prot. 98, 383–389. https://doi.org/10.1016/J.PSEP.2015.09.009

Cheng, S., Logan, B.E., 2007. Sustainable and efficient biohydrogen production via electrohydrogenesis. Proc. Natl. Acad. Sci. U. S. A. 104, 18871–3. https://doi.org/10.1073/pnas.0706379104

Cheng, S., Xing, D., Call, D.F., Logan, B.E., 2009. Direct Biological Conversion of Electrical Current into Methane by Electromethanogenesis. Environ. Sci. Technol. 43, 3953–3958. https://doi.org/10.1021/es803531g

Cho, J., Hermanowicz, S.W., Hur, J., 2012. Effects of experimental conditions on extraction yield of extracellular polymeric substances by cation exchange resin. Sci. World J. 2012. https://doi.org/10.1100/2012/751965

Cho, S.K., Lee, M.E., Lee, W., Ahn, Y., 2019. Improved hydrogen recovery in microbial electrolysis cells using intermittent energy input. Int. J. Hydrogen Energy 44, 2253–2257. https://doi.org/10.1016/j.ijhydene.2018.07.025

Choi, K.S., Kondaveeti, S., Min, B., 2017. Bioelectrochemical methane (CH4) production in anaerobic digestion at different supplemental voltages. Bioresour. Technol. 245, 826–832. https://doi.org/10.1016/J.BIORTECH.2017.09.057

Choi, O., Sang, B.-I., 2016. Extracellular electron transfer from cathode to microbes: application for biofuel production. Biotechnol. Biofuels 9, 11. https://doi.org/10.1186/s13068-016-0426-0

Chowdhury, N.P., Mowafy, A.M., Demmer, J.K., Upadhyay, V., Koelzer, S., Jayamani, E., Kahnt, J., Hornung, M., Demmer, U., Ermler, U., Buckel, W., 2014. Studies on the mechanism of electron bifurcation catalyzed by electron transferring flavoprotein (Etf) and butyryl-CoA dehydrogenase (Bcd) of acidaminococcus fermentans. J. Biol. Chem. 289, 5145–5157. https://doi.org/10.1074/jbc.M113.521013

Chung, T.H., Meshref, M.N.A., Dhar, B.R., 2020. Microbial electrochemical biosensor for rapid detection of naphthenic acid in aqueous solution. J. Electroanal. Chem. 873, 114405.

https://doi.org/10.1016/j.jelechem.2020.114405

Comstat 2 [WWW Document], n.d. URL http://www.comstat.dk/ (accessed 3.23.21).

Dai, Y.F., Xiao, Y., Zhang, E.H., Liu, L.D., Qiu, L., You, L.X., Mahadevan, G.D., Chen, B.L., Zhao, F., 2016. Effective methods for extracting extracellular polymeric substances from Shewanella oneidensis MR-1. Water Sci. Technol. 74, 2987–2996. https://doi.org/10.2166/wst.2016.473

De Vrieze, J., Gildemyn, S., Arends, J.B.A., Vanwonterghem, I., Verbeken, K., Boon, N., Verstraete, W., Tyson, G.W., Hennebel, T., Rabaey, K., 2014. Biomass retention on electrodes rather than electrical current enhances stability in anaerobic digestion. Water Res. 54, 211–221.

De Vrieze, J., Hennebel, T., Boon, N., Verstraete, W., 2012. Methanosarcina: The rediscovered methanogen for heavy duty biomethanation. Bioresour. Technol. https://doi.org/10.1016/j.biortech.2012.02.079

Dhar, B.R., Elbeshbishy, E., Hafez, H., Lee, H.S., 2015. Hydrogen production from sugar beet juice using an integrated biohydrogen process of dark fermentation and microbial electrolysis cell. Bioresour. Technol. 198, 223–230. https://doi.org/10.1016/j.biortech.2015.08.048

Dhar, B.R., Gao, Y., Yeo, H., Lee, H.S., 2013. Separation of competitive microorganisms using anaerobic membrane bioreactors as pretreatment to microbial electrochemical cells. Bioresour. Technol. 148, 208–214. https://doi.org/10.1016/j.biortech.2013.08.138

Dhar, B.R., Nakhla, G., Ray, M.B., 2012. Techno-economic evaluation of ultrasound and thermal pretreatments for enhanced anaerobic digestion of municipal waste activated sludge. Waste Manag. 32, 542–549. https://doi.org/10.1016/J.WASMAN.2011.10.007

Dhar, B.R., Park, J.H., Park, H.D., Lee, H.S., 2019. Hydrogen-based syntrophy in an electrically conductive biofilm anode. Chem. Eng. J. 359, 208–216. https://doi.org/10.1016/j.cej.2018.11.138

Dhar, B.R., Ryu, H., Ren, H., Domingo, J.W.S., Chae, J., Lee, H.-S., 2016a. High biofilm

conductivity maintained despite anode potential changes in a Geobacter-enriched biofilm. ChemSusChem 9, 3485–3491. https://doi.org/10.1002/cssc.201601007

Dhar, B.R., Ryu, H., Santo Domingo, J.W., Lee, H.-S., 2016b. Ohmic resistance affects microbial community and electrochemical kinetics in a multi-anode microbial electrochemical cell. J. Power Sources 331, 315–321. https://doi.org/10.1016/J.JPOWSOUR.2016.09.055

Dhar, B.R., Sim, J., Ryu, H., Ren, H., Santo Domingo, J.W., Chae, J., Lee, H.-S.S., 2017. Microbial activity influences electrical conductivity of biofilm anode. Water Res. 127, 230–238. https://doi.org/10.1016/j.watres.2017.10.028

Dhar, B.R., Youssef, E., Nakhla, G., Ray, M.B., 2011. Pretreatment of municipal waste activated sludge for volatile sulfur compounds control in anaerobic digestion. Bioresour. Technol. 102, 3776–3782.

Ditzig, J., Liu, H., Logan, B.E., 2007. Production of hydrogen from domestic wastewater using a bioelectrochemically assisted microbial reactor (BEAMR). Int. J. Hydrogen Energy 32, 2296–2304. https://doi.org/10.1016/j.ijhydene.2007.02.035

DuBois, M., Gilles, K.A., Hamilton, J.K., Rebers, P.A., Smith, F., 1956. Colorimetric method for determination of sugars and related substances. Anal. Chem. 28, 350–356. https://doi.org/10.1021/ac60111a017

Dyksma, S., Gallert, C., 2019. Candidatus Syntrophosphaera thermopropionivorans: a novel player in syntrophic propionate oxidation during anaerobic digestion. Environ. Microbiol. Rep. 11, 558–570. https://doi.org/10.1111/1758-2229.12759

Dykstra, C.M., Pavlostathis, S.G., 2017. Methanogenic Biocathode Microbial Community Development and the Role of Bacteria. Environ. Sci. Technol. 51, 5306–5316. https://doi.org/10.1021/acs.est.6b04112

Edgar, R.C., 2010. Search and clustering orders of magnitude faster than BLAST. Bioinformatics 26, 2460–2461.

Edgar, R.C., Brian, H.J., Jose, C.C., Christopher, Q., Knight, R., 2011. UCHIME improves

sensitivity and speed of chimera detection. Bioinformatics 27, 2194–2200.

Escapa, A., San-Martín, M.I., Mateos, R., Morán, A., 2015. Scaling-up of membraneless microbial electrolysis cells (MECs) for domestic wastewater treatment: Bottlenecks and limitations. Bioresour. Technol. 180, 72–78. https://doi.org/10.1016/J.BIORTECH.2014.12.096

Esteve-Núñez, A., Sosnik, J., Visconti, P., Lovley, D.R., 2008. Fluorescent properties of c-type cytochromes reveal their potential role as an extracytoplasmic electron sink in Geobacter sulfurreducens. Environ. Microbiol. 10, 497–505. https://doi.org/10.1111/j.1462-2920.2007.01470.x

Federation, W., American, A., 2005. Standard methods for the examination of water and wastewater. Am. Public Heal. Assoc. (APHA), Washington, D.C.

Feng, C., Li, J., Qin, D., Chen, L., Zhao, F., Chen, S., Hu, H., Yu, C.-P., 2014. Characterization of Exoelectrogenic Bacteria Enterobacter Strains Isolated from a Microbial Fuel Cell Exposed to Copper Shock Load. PLoS One 9, e113379. https://doi.org/10.1371/journal.pone.0113379

Feng, Q., Song, Y.-C., 2016. Surface Modification of a Graphite Fiber Fabric Anode for Enhanced Bioelectrochemical Methane Production. Energy & Fuels 30, 6467–6474. https://doi.org/10.1021/acs.energyfuels.6b00959

Feng, Q., Song, Y.-C., Bae, B.-U., 2016. Influence of applied voltage on the performance of bioelectrochemical anaerobic digestion of sewage sludge and planktonic microbial communities at ambient temperature. Bioresour. Technol. 220, 500–508. https://doi.org/10.1016/J.BIORTECH.2016.08.085

Feng, Y., Zhang, Y., Chen, S., Quan, X., 2015. Enhanced production of methane from waste activated sludge by the combination of high-solid anaerobic digestion and microbial electrolysis cell with iron–graphite electrode. Chem. Eng. J. 259, 787–794. https://doi.org/10.1016/J.CEJ.2014.08.048

Flores-Rodriguez, C., Min, B., 2020. Enrichment of specific microbial communities by optimum

applied voltages for enhanced methane production by microbial electrosynthesis in anaerobic digestion. Bioresour. Technol. 300, 122624. https://doi.org/10.1016/j.biortech.2019.122624

Franke-Whittle, I.H., Walter, A., Ebner, C., Insam, H., 2014. Investigation into the effect of high concentrations of volatile fatty acids in anaerobic digestion on methanogenic communities. Waste Manag. 34, 2080–2089. https://doi.org/10.1016/j.wasman.2014.07.020

Freguia, S., Rabaey, K., Yuan, Z., Keller, J., 2007. Electron and carbon balances in microbial fuel cells reveal temporary bacterial storage behavior during electricity generation. Environ. Sci. Technol. 41, 2915–2921. https://doi.org/10.1021/ES062611I/SUPPL_FILE/ES062611ISI20070208_110248.PDF

Frølund, B., Palmgren, R., Keiding, K., Nielsen, P.H., 1996. Extraction of extracellular polymers from activated sludge using a cation exchange resin. Water Res. 30, 1749–1758. https://doi.org/10.1016/0043-1354(95)00323-1

Fu, Q., Kuramochi, Y., Fukushima, N., Maeda, H., Sato, K., Kobayashi, H., 2015. Bioelectrochemical Analyses of the Development of a Thermophilic Biocathode Catalyzing Electromethanogenesis. Environ. Sci. Technol. 49, 1225–1232. https://doi.org/10.1021/es5052233

Gaby, J.C., Zamanzadeh, M., Horn, S.J., 2017. The effect of temperature and retention time on methane production and microbial community composition in staged anaerobic digesters fed with food waste. Biotechnol. Biofuels 10, 302. https://doi.org/10.1186/s13068-017-0989-4

Gajaraj, S., Huang, Y., Zheng, P., Hu, Z., 2017. Methane production improvement and associated methanogenic assemblages in bioelectrochemically assisted anaerobic digestion. Biochem. Eng. J. 117, 105–112.

Gallert, C., Winter, J., 2008. Propionic acid accumulation and degradation during restart of a full-scale anaerobic biowaste digester. Bioresour. Technol. 99, 170–178. https://doi.org/10.1016/j.biortech.2006.11.014

Gao, K., Lu, Y., 2021. Putative Extracellular Electron Transfer in Methanogenic Archaea. Front. Microbiol. 12. https://doi.org/10.3389/fmicb.2021.611739

Gardy, J.L., Spencer, C., Wang, K., Ester, M., Tusnády, G.E., Simon, I., Hua, S., deFays, K., Lambert, C., Nakai, K., Brinkman, F.S.L., 2003. PSORT-B: Improving protein subcellular localization prediction for Gram-negative bacteria. Nucleic Acids Res. 31, 3613–3617. https://doi.org/10.1093/nar/gkg602

Ge, Z., He, Z., 2016. Long-term performance of a 200 liter modularized microbial fuel cell system treating municipal wastewater: Treatment, energy, and cost. Environ. Sci. Water Res. Technol. 2, 274–281. https://doi.org/10.1039/c6ew00020g

Georg, S., de Eguren Cordoba, I., Sleutels, T., Kuntke, P., Heijne, A. ter, Buisman, C.J.N., 2020. Competition of electrogens with methanogens for hydrogen in bioanodes. Water Res. 170, 115292. https://doi.org/10.1016/j.watres.2019.115292

Geppert, F., Liu, D., van Eerten-Jansen, M., Weidner, E., Buisman, C., Ter Heijne, A., 2016. Bioelectrochemical Power-to-Gas: State of the Art and Future Perspectives. Trends Biotechnol. 34, 879–894. https://doi.org/10.1016/j.tibtech.2016.08.010

Ghods, S., Sims, I.M., Moradali, M.F., Rehma, B.H.A., 2015. Bactericidal compounds controlling growth of the plant pathogen pseudomonas syringae pv. actinidiae, which forms biofilms composed of a novel exopolysaccharide. Appl. Environ. Microbiol. 81, 4026–4036. https://doi.org/10.1128/AEM.00194-15

Gorby, Y.A., Lovley, D.R., 1991. Electron transport in the dissimilatory iron reducer, GS-15. Appl. Environ. Microbiol. 57, 867–870. https://doi.org/10.1128/aem.57.3.867-870.1991

Guo, J., Peng, Y., Ni, B.-J., Han, X., Fan, L., Yuan, Z., 2015. Dissecting microbial community structure and methane-producing pathways of a full-scale anaerobic reactor digesting activated sludge from wastewater treatment by metagenomic sequencing. Microb. Cell Fact. 14, 33. https://doi.org/10.1186/s12934-015-0218-4

Guo, K., Prévoteau, A., Patil, S.A., Rabaey, K., 2015. Engineering electrodes for microbial electrocatalysis, Current Opinion in Biotechnology.

Guo, Z., Thangavel, S., Wang, L., He, Z., Cai, W., Wang, A., Liu, W., 2017a. Efficient Methane Production from Beer Wastewater in a Membraneless Microbial Electrolysis Cell with a Stacked Cathode: The Effect of the Cathode/Anode Ratio on Bioenergy Recovery. Energy & Fuels 31, 615–620. https://doi.org/10.1021/acs.energyfuels.6b02375

Guo, Z., Thangavel, S., Wang, L., He, Z., Cai, W., Wang, A., Liu, W., 2017b. Efficient methane production from beer wastewater in a membraneless microbial electrolysis cell with a stacked cathode: The effect of the cathode/anode ratio on bioenergy recovery. Energy and Fuels 31, 615–620. https://doi.org/10.1021/acs.energyfuels.6b02375

Hari, A.R., Katuri, K.P., Gorron, E., Logan, B.E., Saikaly, P.E., 2016a. Multiple paths of electron flow to current in microbial electrolysis cells fed with low and high concentrations of propionate. Appl. Microbiol. Biotechnol. 100, 5999–6011. https://doi.org/10.1007/s00253-016-7402-2

Hari, A.R., Katuri, K.P., Logan, B.E., Saikaly, P.E., 2016b. Set anode potentials affect the electron fluxes and microbial community structure in propionate-fed microbial electrolysis cells. Sci. Rep. 6, 38690. https://doi.org/10.1038/srep38690

Hari, A.R., Venkidusamy, K., Katuri, K.P., Bagchi, S., Saikaly, P.E., 2017. Temporal Microbial Community Dynamics in Microbial Electrolysis Cells – Influence of Acetate and Propionate Concentration. Front. Microbiol. 8, 1371. https://doi.org/10.3389/fmicb.2017.01371

He, G., Gu, Y., He, S., Schröder, U., Chen, S., Hou, H., 2011. Effect of fiber diameter on the behavior of biofilm and anodic performance of fiber electrodes in microbial fuel cells. Bioresour. Technol. 102, 10763–10766. https://doi.org/10.1016/j.biortech.2011.09.006

He, J., Wang, X., Yin, X.-B., Li, Q., Li, X., Zhang, Y.-F., Deng, Y., 2018. Insights into biomethane production and microbial community succession during semi-continuous anaerobic digestion of waste cooking oil under different organic loading rates. AMB Express 8, 92. https://doi.org/10.1186/s13568-018-0623-2

Heidary, N., Kornienko, N., Kalathil, S., Fang, X., Ly, K.H., Greer, H.F., Reisner, E., 2020. Disparity of Cytochrome Utilization in Anodic and Cathodic Extracellular Electron Transfer

Pathways of Geobacter sulfurreducens Biofilms. J. Am. Chem. Soc. 142, 5194–5203. https://doi.org/10.1021/jacs.9b13077

Heidrich, E.S., Dolfing, J., Scott, K., Edwards, S.R., Jones, C., Curtis, T.P., 2013. Production of hydrogen from domestic wastewater in a pilot-scale microbial electrolysis cell. Appl. Microbiol. Biotechnol. 97, 6979–6989. https://doi.org/10.1007/s00253-012-4456-7

Heidrich, E.S., Edwards, S.R., Dolfing, J., Cotterill, S.E., Curtis, T.P., 2014. Performance of a pilot scale microbial electrolysis cell fed on domestic wastewater at ambient temperatures for a 12month period. Bioresour. Technol. 173, 87–95. https://doi.org/10.1016/j.biortech.2014.09.083

Hernández-Eligio, A., Pat-Espadas, A.M., Vega-Alvarado, L., Huerta-Amparán, M., Cervantes, F.J., Juárez, K., 2020. Global transcriptional analysis of Geobacter sulfurreducens under palladium reducing conditions reveals new key cytochromes involved. Appl. Microbiol. Biotechnol. 104, 4059–4069. https://doi.org/10.1007/s00253-020-10502-5

Heydorn, A., Nielsen, A.T., Hentzer, M., Sternberg, C., Givskov, M., Ersboll, B.K., Molin, S., 2000. Quantification of biofilm structures by the novel computer program COMSTAT. Microbiology 146, 2395–2407. https://doi.org/10.1099/00221287-146-10-2395

Hidalgo, D., Sacco, A., Hernández, S., Tommasi, T., 2015. Electrochemical and impedance characterization of Microbial Fuel Cells based on 2D and 3D anodic electrodes working with seawater microorganisms under continuous operation. Bioresour. Technol. 195, 139–146. https://doi.org/10.1016/j.biortech.2015.06.127

Hill, D.T., Cobb, S.A., Bolte, J.P., 1987. Using Volatile Fatty Acid Relationships to Predict Anaerobic Digester Failure. Trans. ASAE 30, 0496–0501. https://doi.org/10.13031/2013.31977

Hirano, S., Matsumoto, N., 2018. Analysis of a bio-electrochemical reactor containing carbon fiber textiles for the anaerobic digestion of tomato plant residues. Bioresour. Technol. 249, 809–817. https://doi.org/10.1016/J.BIORTECH.2017.09.206

Ho, D., Jensen, P., Batstone, D., 2014. Effects of temperature and hydraulic retention time on

acetotrophic pathways and performance in high-rate sludge digestion. Environ. Sci. Technol. 48, 6468–6476. https://doi.org/10.1021/es500074j

Hollmann, B., Perkins, M., Chauhan, V.M., Aylott, J.W., Hardie, K.R., 2021. Fluorescent nanosensors reveal dynamic pH gradients during biofilm formation. npj Biofilms Microbiomes 7, 1–13. https://doi.org/10.1038/s41522-021-00221-8

Hou, Y., Zhang, B., Wen, Z., Cui, S., Guo, X., He, Z., Chen, J., 2014. A 3D hybrid of layered MoS2/nitrogen-doped graphene nanosheet aerogels: An effective catalyst for hydrogen evolution in microbial electrolysis cells. J. Mater. Chem. A 2, 13795–13800. https://doi.org/10.1039/c4ta02254h

Houghton, J., Santoro, C., Soavi, F., Serov, A., Ieropoulos, I., Arbizzani, C., Atanassov, P., 2016. Supercapacitive microbial fuel cell: Characterization and analysis for improved charge storage/delivery performance. Bioresour. Technol. 218, 552–560. https://doi.org/10.1016/j.biortech.2016.06.105

Huang, J., Wang, Z., Zhu, C., Ma, J., Zhang, X., Wu, Z., 2014. Identification of Microbial Communities in Open and Closed Circuit Bioelectrochemical MBRs by High-Throughput 454 Pyrosequencing. PLoS One 9, e93842. https://doi.org/10.1371/journal.pone.0093842

Huang, Q., Liu, Y., Dhar, B.R., 2020. A critical review of microbial electrolysis cells coupled with anaerobic digester for enhanced biomethane recovery from high-strength feedstocks. Crit. Rev. Environ. Sci. Technol. https://doi.org/10.1080/10643389.2020.1813065

Hussain, S.A., Perrier, M., Tartakovsky, B., 2018. Long-term performance of a microbial electrolysis cell operated with periodic disconnection of power supply. RSC Adv. 8, 16842–16849. https://doi.org/10.1039/c8ra01863d

Ibeid, S., Elektorowicz, M., Oleszkiewicz, J.A., 2013. Modification of activated sludge properties caused by application of continuous and intermittent current. Water Res. 47, 903–910. https://doi.org/10.1016/j.watres.2012.11.020

Im, S., Ahn, Y., Chung, J.-W., 2015. Influence of Electrode Spacing on Methane Production in Microbial Electrolysis Cell Fed with Sewage Sludge. J. Korean Soc. Environ. Eng. 37, 682–

688. https://doi.org/10.4491/KSEE.2015.37.12.682

Izadi, P., Fontmorin, J.M., Godain, A., Yu, E.H., Head, I.M., 2020. Parameters influencing the development of highly conductive and efficient biofilm during microbial electrosynthesis: the importance of applied potential and inorganic carbon source. npj Biofilms Microbiomes 6, 1–15. https://doi.org/10.1038/s41522-020-00151-x

Jachlewski, S., Jachlewski, W.D., Linne, U., Bräsen, C., Wingender, J., Siebers, B., 2015. Isolation of Extracellular Polymeric Substances from Biofilms of the Thermoacidophilic Archaeon Sulfolobus acidocaldarius. Front. Bioeng. Biotechnol. 3, 123. https://doi.org/10.3389/fbioe.2015.00123

Jangir, Y., French, S., Momper, L.M., Moser, D.P., Amend, J.P., El-Naggar, M.Y., 2016. Isolation and Characterization of Electrochemically Active Subsurface Delftia and Azonexus Species. Front. Microbiol. 7, 756. https://doi.org/10.3389/fmicb.2016.00756

Jiang, Y., Banks, C., Zhang, Y., Heaven, S., Longhurst, P., 2018. Quantifying the percentage of methane formation via acetoclastic and syntrophic acetate oxidation pathways in anaerobic digesters. Waste Manag. 71, 749–756.

Jiang, Y., Zeng, R.J., 2018. Expanding the product spectrum of value added chemicals in microbial electrosynthesis through integrated process design—A review. Bioresour. Technol. 269, 503–512. https://doi.org/10.1016/J.BIORTECH.2018.08.101

Junicke, H., van Loosdrecht, M.C.M., Kleerebezem, R., 2016. Kinetic and thermodynamic control of butyrate conversion in non-defined methanogenic communities. Appl. Microbiol. Biotechnol. 100, 915–925. https://doi.org/10.1007/s00253-015-6971-9

Kariyama, I.D., Zhai, X., Wu, B., 2018. Influence of mixing on anaerobic digestion efficiency in stirred tank digesters: A review. Water Res. 143, 503–517. https://doi.org/10.1016/J.WATRES.2018.06.065

Khafipour, A., Jordaan, E.M., Flores-Orozco, D., Khafipour, E., Levin, D.B., Sparling, R., Cicek, N., 2020. Response of Microbial Community to Induced Failure of Anaerobic Digesters Through Overloading With Propionic Acid Followed by Process Recovery. Front.

Bioeng. Biotechnol. 8, 1434. https://doi.org/10.3389/FBIOE.2020.604838/BIBTEX

Ki, D., Parameswaran, P., Popat, S.C., Rittmann, B.E., Torres, C.I., 2017a. Maximizing Coulombic recovery and solids reduction from primary sludge by controlling retention time and pH in a flat-plate microbial electrolysis cell. Environ. Sci. Water Res. Technol. 3, 333–339. https://doi.org/10.1039/c6ew00305b

Ki, D., Popat, S.C., Rittmann, B.E., Torres, C.I., 2017b. H2O2 Production in Microbial Electrochemical Cells Fed with Primary Sludge. Environ. Sci. Technol. 51, 6139–6145. https://doi.org/10.1021/acs.est.7b00174

Kim, K.R., Kang, J., Chae, K.J., 2017. Improvement in methanogenesis by incorporating transition metal nanoparticles and granular activated carbon composites in microbial electrolysis cells. Int. J. Hydrogen Energy 42, 27623–27629. https://doi.org/10.1016/j.ijhydene.2017.06.142

Klindworth, A., Pruesse, E., Schweer, T., Peplies, J., Quast, C., Horn, M., Glöckner, F.O., 2013. Evaluation of general 16S ribosomal RNA gene PCR primers for classical and next-generation sequencing-based diversity studies. Nucleic Acids Res. 41, e1–e1. https://doi.org/10.1093/nar/gks808

Kokko, M., Epple, S., Gescher, J., Kerzenmacher, S., 2018. Effects of wastewater constituents and operational conditions on the composition and dynamics of anodic microbial communities in bioelectrochemical systems. Bioresour. Technol. 258, 376–389. https://doi.org/10.1016/J.BIORTECH.2018.01.090

Kokkoli, A., Zhang, Y., Angelidaki, I., 2018. Microbial electrochemical separation of CO2 for biogas upgrading. Bioresour. Technol. 247, 380–386. https://doi.org/10.1016/J.BIORTECH.2017.09.097

Kor-Bicakci, G., Ubay-Cokgor, E., Eskicioglu, C., 2020. Comparative analysis of bacterial and archaeal community structure in microwave pretreated thermophilic and mesophilic anaerobic digesters utilizing mixed sludge under organic overloading. Water (Switzerland) 12, 887. https://doi.org/10.3390/w12030887

Kracke, F., Vassilev, I., Krömer, J.O., 2015. Microbial electron transport and energy conservation - the foundation for optimizing bioelectrochemical systems. Front. Microbiol. 6, 575. https://doi.org/10.3389/fmicb.2015.00575

Krylova, N.I., Conrad, R., 1998. Thermodynamics of propionate degradation in methanogenic paddy soil. FEMS Microbiol. Ecol. 26, 281–288.

Kumar, N., Das, D., 2000. Enhancement of hydrogen production by Enterobacter cloacae IIT-BT 08. Process Biochem. 35, 589–593. https://doi.org/10.1016/S0032-9592(99)00109-0

Lanas, V., Logan, B.E., 2013. Evaluation of multi-brush anode systems in microbial fuel cells. Bioresour. Technol. 148, 379–385. https://doi.org/10.1016/j.biortech.2013.08.154

Lee, B., Park, J., Shin, W.-B., Tian, D.-J., Jun, H.-B., 2017. Microbial communities change in an anaerobic digestion after application of microbial electrolysis cells. Bioresour. Technol. 234, 273–280. https://doi.org/10.1016/J.BIORTECH.2017.02.022

Lee, D.-J., Lee, S.-Y., Bae, J.-S., Kang, J.-G., Kim, K.H., Rhee, S.-S., Park, J.-H., Cho, J.-S., Chung, J., Seo, D.-C., 2015. Effect of Volatile Fatty Acid Concentration on Anaerobic Degradation Rate from Field Anaerobic Digestion Facilities Treating Food Waste Leachate in South Korea. J. Chem. 2015. https://doi.org/10.1155/2015/640717

Lee, H.S., Parameswaran, P., Kato-Marcus, A., Torres, C.I., Rittmann, B.E., 2008. Evaluation of energy-conversion efficiencies in microbial fuel cells (MFCs) utilizing fermentable and non-fermentable substrates. Water Res. 42, 1501–1510. https://doi.org/10.1016/J.WATRES.2007.10.036

Lee, H.S., Torres, C.I., Parameswaran, P., Rittmann, B.E., 2009. Fate of H2 in an upflow single-chamber microbial electrolysis cell using a metal-catalyst-free cathode. Environ. Sci. Technol. 43, 7971–7976. https://doi.org/10.1021/es900204j

Li, S., Cheng, C., Thomas, A., 2017. Carbon-Based Microbial-Fuel-Cell Electrodes: From Conductive Supports to Active Catalysts. Adv. Mater. https://doi.org/10.1002/adma.201602547

Li, X., Zeng, C., Lu, Y., Liu, G., Luo, H., Zhang, R., 2019. Development of methanogens within

cathodic biofilm in the single-chamber microbial electrolysis cell. Bioresour. Technol. 274, 403–409.

Li, Y., Zhang, Y., Liu, Y., Zhao, Zhiqiang, Zhao, Zisheng, Liu, S., Zhao, H., Quan, X., 2016. Enhancement of anaerobic methanogenesis at a short hydraulic retention time via bioelectrochemical enrichment of hydrogenotrophic methanogens. Bioresour. Technol. 218, 505–511. https://doi.org/https://doi.org/10.1016/j.biortech.2016.06.112

Liang, D.-W., Peng, S.-K., Lu, S.-F., Liu, Y.-Y., Lan, F., Xiang, Y., 2011. Enhancement of hydrogen production in a single chamber microbial electrolysis cell through anode arrangement optimization. Bioresour. Technol. 102, 10881–5. https://doi.org/10.1016/j.biortech.2011.09.028

Liang, J., Chen, C., Yoza, B.A., Liang, Y., Li, J., Ke, M., Wang, Q., 2019. Hydrolysis and acidification of activated sludge from a petroleum refinery. Pet. Sci. 16, 428–438. https://doi.org/10.1007/s12182-019-0301-2

Lim, S.S., Fontmorin, J.M., Izadi, P., Wan Daud, W.R., Scott, K., Yu, E.H., 2020. Impact of applied cell voltage on the performance of a microbial electrolysis cell fully catalysed by microorganisms. Int. J. Hydrogen Energy 45, 2557–2568. https://doi.org/10.1016/j.ijhydene.2019.11.142

Lin, C., Wu, P., Liu, Y., Wong, J.W.C., Yong, X., Wu, X., Xie, X., Jia, H., Zhou, J., 2019. Enhanced biogas production and biodegradation of phenanthrene in wastewater sludge treated anaerobic digestion reactors fitted with a bioelectrode system. Chem. Eng. J. 365, 1–9. https://doi.org/10.1016/j.cej.2019.02.027

Lin, L., Chowdhury, B., Zakaria, B.S., Dhar, B.R., 2019a. Temperature-dependent (20–55 °C) electrocatalytic characteristics during ethanol/propionate degradation by methanogenic communities grown on conductive carbon fibers. Chem. Eng. J. 123566. https://doi.org/10.1016/j.cej.2019.123566

Lin, L., Zakaria, B.S., Hosseini Koupaie, E., Bazyar Lakeh, A.A., Hafez, H., Elbeshbishy, E., Dhar, B.R., 2019b. Evaluation of sludge liquors from acidogenic fermentation and thermal hydrolysis process as feedstock for microbial electrolysis cells. Int. J. Hydrogen Energy 44,

30031–30038. https://doi.org/10.1016/j.ijhydene.2019.09.162

Liu, D., Roca-Puigros, M., Geppert, F., Caizán-Juanarena, L., Na Ayudthaya, S.P., Buisman, C., ter Heijne, A., 2018. Granular Carbon-Based Electrodes as Cathodes in Methane-Producing Bioelectrochemical Systems. Front. Bioeng. Biotechnol. 6, 78. https://doi.org/10.3389/fbioe.2018.00078

Liu, D., Zhang, L., Chen, S., Buisman, C., ter Heijne, A., 2016. Bioelectrochemical enhancement of methane production in low temperature anaerobic digestion at 10 °C. Water Res. 99, 281–287. https://doi.org/10.1016/J.WATRES.2016.04.020

Liu, D., Zheng, T., Buisman, C., Ter Heijne, A., 2017. Heat-Treated Stainless Steel Felt as a New Cathode Material in a Methane-Producing Bioelectrochemical System. ACS Sustain. Chem. Eng. 5, 11346–11353. https://doi.org/10.1021/acssuschemeng.7b02367

Liu, S., Deng, Z., Li, H., Feng, K., 2019. Contribution of electrodes and electric current to process stability and methane production during the electro-fermentation of food waste. Bioresour. Technol. 121536. https://doi.org/10.1016/J.BIORTECH.2019.121536

Liu, S.Y., Charles, W., Ho, G., Cord-Ruwisch, R., Cheng, K.Y., 2017. Bioelectrochemical enhancement of anaerobic digestion: Comparing single- and two-chamber reactor configurations at thermophilic conditions. Bioresour. Technol. 245, 1168–1175. https://doi.org/10.1016/j.biortech.2017.08.095

Liu, W., Cai, W., Guo, Z., Wang, L., Yang, C., Varrone, C., Wang, A., 2016. Microbial electrolysis contribution to anaerobic digestion of waste activated sludge, leading to accelerated methane production. Renew. Energy 91, 334–339. https://doi.org/10.1016/j.renene.2016.01.082

Liu, W., Piao, Y., Zhang, F., Liu, L., Meng, D., Nan, J., Deng, Y., Wang, A., 2018. Hydrogen consumption and methanogenic community evolution in anodophilic biofilms in single chamber microbial electrolysis cells under different startup modes. Environ. Sci. Water Res. Technol. 4, 1839–1850. https://doi.org/10.1039/c8ew00357b

Logan, B.E., Call, D., Cheng, S., Hamelers, H.V.M., Sleutels, T.H.J.A., Jeremiasse, A.W.,

Rozendal, R.A., 2008. Microbial Electrolysis Cells for High Yield Hydrogen Gas Production from Organic Matter. Environ. Sci. Technol. 42, 8630–8640. https://doi.org/10.1021/es801553z

Logan, B.E., Rossi, R., Ragab, A., Saikaly, P.E., 2019. Electroactive microorganisms in bioelectrochemical systems. Nat. Rev. Microbiol. 17, 307. https://doi.org/10.1038/s41579-019-0173-x

Logares, R., Lindström, E.S., Langenheder, S., Logue, J.B., Paterson, H., Laybourn-Parry, J., Rengefors, K., Tranvik, L., Bertilsson, S., 2013. Biogeography of bacterial communities exposed to progressive long-term environmental change. ISME J. 7, 937–948. https://doi.org/10.1038/ismej.2012.168

Lovley, D.R., 2017. Syntrophy Goes Electric: Direct Interspecies Electron Transfer. Annu. Rev. Microbiol. 71, 643–664. https://doi.org/10.1146/annurev-micro-030117-020420

Lovley, D.R., 2008. The microbe electric: conversion of organic matter to electricity. Curr. Opin. Biotechnol. https://doi.org/10.1016/j.copbio.2008.10.005

Lovley, D.R., Walker, D.J.F., 2019. Geobacter Protein Nanowires. Front. Microbiol. https://doi.org/10.3389/fmicb.2019.02078

Lu, L., Ren, Z.J., 2016. Microbial electrolysis cells for waste biorefinery: A state of the art review. Bioresour. Technol. 215, 254–264. https://doi.org/10.1016/J.BIORTECH.2016.03.034

Luo, L., Xu, S., Jin, Y., Han, R., Liu, H., Lü, F., 2018. Evaluation of methanogenic microbial electrolysis cells under closed/open circuit operations. Environ. Technol. 39, 739–748. https://doi.org/10.1080/09593330.2017.1310934

Luo, L., Xu, S., Selvam, A., Wong, J.W.C., 2016. Assistant role of bioelectrode on methanogenic reactor under ammonia stress. Bioresour. Technol. 217, 72–81. https://doi.org/10.1016/j.biortech.2016.02.092

Lusk, B.G., Khan, Q.F., Parameswaran, P., Hameed, A., Ali, N., Rittmann, B.E., Torres, C.I., 2015. Characterization of Electrical Current-Generation Capabilities from Thermophilic

Bacterium *Thermoanaerobacter pseudethanolicus* Using Xylose, Glucose, Cellobiose, or Acetate with Fixed Anode Potentials. Environ. Sci. Technol. 49, 14725–14731. https://doi.org/10.1021/acs.est.5b04036

Ma, J., Frear, C., Wang, Z.W., Yu, L., Zhao, Q., Li, X., Chen, S., 2013. A simple methodology for rate-limiting step determination for anaerobic digestion of complex substrates and effect of microbial community ratio. Bioresour. Technol. 134, 391–395.

Ma, X., Li, Z., Zhou, A., Yue, X., 2017. Energy recovery from tubular microbial electrolysis cell with stainless steel mesh as cathode. R. Soc. Open Sci. 4, 170967. https://doi.org/10.1098/rsos.170967

Magdalena, J.A., Greses, S., González-Fernández, C., 2019. Impact of Organic Loading Rate in Volatile Fatty Acids Production and Population Dynamics Using Microalgae Biomass as Substrate. Sci. Rep. 9, 1–11. https://doi.org/10.1038/s41598-019-54914-4

Malvankar, N.S., Lau, J., Nevin, K.P., Franks, A.E., Tuominen, M.T., Lovley, D.R., 2012. Electrical conductivity in a mixed-species biofilm. Appl. Environ. Microbiol. 78, 5967–71. https://doi.org/10.1128/AEM.01803-12

May, H.D., Evans, P.J., LaBelle, E. V., 2016. The bioelectrosynthesis of acetate. Curr. Opin. Biotechnol. 42, 225–233. https://doi.org/10.1016/j.copbio.2016.09.004

Mei, X., Guo, C., Liu, B., Tang, Y., Xing, D., 2015. Shaping of bacterial community structure in microbial fuel cells by different inocula. RSC Adv. 5, 78136–78141. https://doi.org/10.1039/c5ra16382j

Michie, I.S., Dinsdale, R.M., Guwy, A.J., Premier, G.C., 2020. Electrogenic Biofilm Development Determines Charge Accumulation and Resistance to pH Perturbation. Energies 13, 3521. https://doi.org/10.3390/en13143521

Morris, R., Schauer-Gimenez, A., Bhattad, U., Kearney, C., Struble, C.A., Zitomer, D., Maki, J.S., 2014. Methyl coenzyme M reductase (mcrA) gene abundance correlates with activity measurements of methanogenic H2/CO2-enriched anaerobic biomass. Microb. Biotechnol. 7, 77. https://doi.org/10.1111/1751-7915.12094

Mostafa, A., Im, S., Lee, M.K., Song, Y.C., Kim, D.H., 2020. Enhanced anaerobic digestion of phenol via electrical energy input. Chem. Eng. J. 389, 124501. https://doi.org/10.1016/j.cej.2020.124501

Nevin, K.P., Hensley, S.A., Franks, A.E., Summers, Z.M., Ou, J., Woodard, T.L., Snoeyenbos-West, O.L., Lovley, D.R., 2011. Electrosynthesis of organic compounds from carbon dioxide is catalyzed by a diversity of acetogenic microorganisms. Appl. Environ. Microbiol. 77, 2882–2886. https://doi.org/10.1128/AEM.02642-10

Nevin, K.P., Kim, B.C., Glaven, R.H., Johnson, J.P., Woodward, T.L., Methé, B.A., Didonato, R.J., Covalla, S.F., Franks, A.E., Liu, A., Lovley, D.R., 2009. Anode biofilm transcriptomics reveals outer surface components essential for high density current production in Geobacter sulfurreducens fuel cells. PLoS One 4. https://doi.org/10.1371/journal.pone.0005628

Noori, M.T., Vu, M.T., Ali, R.B., Min, B., 2020. Recent advances in cathode materials and configurations for upgrading methane in bioelectrochemical systems integrated with anaerobic digestion. Chem. Eng. J. https://doi.org/10.1016/j.cej.2019.123689

Oh, S., Logan, B.E., 2005. Hydrogen and electricity production from a food processing wastewater using fermentation and microbial fuel cell technologies. Water Res. 39, 4673–4682. https://doi.org/10.1016/j.watres.2005.09.019

Parameswaran, P., Torres, C.I., Kang, D.W., Rittmann, B.E., Krajmalnik-Brown, R., 2012. The role of homoacetogenic bacteria as efficient hydrogen scavengers in microbial electrochemical cells (MXCs). Water Sci. Technol. 65, 1–6. https://doi.org/10.2166/wst.2011.519

Park, J., Lee, B., Jo, S.-Y., Lee, J.-S., Jun, H.-B., 2018a. Control of accumulated volatile fatty acids by recycling nitrified effluent. J. Environ. Heal. Sci. Eng. 16, 19–25. https://doi.org/10.1007/s40201-018-0291-9

Park, J., Lee, B., Park, H.-R.R., Jun, H.-B.B., 2019. Long-term evaluation of methane production in a bio-electrochemical anaerobic digestion reactor according to the organic loading rate. Bioresour. Technol. 273, 478–486.

Park, J., Lee, B., Shi, P., Kim, Y., Jun, H.-B., 2017. Effects of electrode distance and mixing velocity on current density and methane production in an anaerobic digester equipped with a microbial methanogenesis cell. Int. J. Hydrogen Energy 42, 27732–27740. https://doi.org/10.1016/J.IJHYDENE.2017.07.025

Park, J., Lee, B., Shin, W., Jo, S., Jun, H., 2018b. Application of a rotating impeller anode in a bioelectrochemical anaerobic digestion reactor for methane production from high-strength food waste. Bioresour. Technol. 259, 423–432.

Park, J., Lee, B., Tian, D., Jun, H., 2018c. Bioelectrochemical enhancement of methane production from highly concentrated food waste in a combined anaerobic digester and microbial electrolysis cell. Bioresour. Technol. 247, 226–233. https://doi.org/10.1016/j.biortech.2017.09.021

Park, J.H., Kang, H.-J., Park, K.-H., Park, H.-D., 2018. Direct interspecies electron transfer via conductive materials: A perspective for anaerobic digestion applications. Bioresour. Technol. 254, 300–311. https://doi.org/10.1016/J.BIORTECH.2018.01.095

Park, J.-H., Park, Jong-Hun, Seong, H.J., Sul, W.J., Jin, K.-H., Park, H.-D., 2018. Metagenomic insight into methanogenic reactors promoting direct interspecies electron transfer via granular activated carbon. Bioresour. Technol. 259, 414–422. https://doi.org/10.1016/j.biortech.2018.03.050

Peters, V., Janssen, P.., Conrad, R., 1998. Efficiency of hydrogen utilization during unitrophic and mixotrophic growth of Acetobacterium woodii on hydrogen and lactate in the chemostat. FEMS Microbiol. Ecol. 26, 317–324. https://doi.org/10.1111/j.1574-6941.1998.tb00516.x

Pinto, R.P., Srinivasan, B., Escapa, A., Tartakovsky, B., 2011. Multi-Population Model of a Microbial Electrolysis Cell. Environ. Sci. Technol. 45, 5039–5046. https://doi.org/10.1021/es104268g

Pullammanappallil, P.C., Chynoweth, D.P., Lyberatos, G., Svoronos, S.A., 2001. Stable performance of anaerobic digestion in the presence of a high concentration of propionic acid. Bioresour. Technol. 78, 165–169. https://doi.org/10.1016/S0960-8524(00)00187-5

Rader, G.K., Logan, B.E., 2010. Multi-electrode continuous flow microbial electrolysis cell for biogas production from acetate. Int. J. Hydrogen Energy 35, 8848–8854. https://doi.org/10.1016/j.ijhydene.2010.06.033

Rasmussen, M., Minteer, S.D., 2015. Long-term arsenic monitoring with an Enterobacter cloacae microbial fuel cell. Bioelectrochemistry 106, 207–212. https://doi.org/10.1016/j.bioelechem.2015.03.009

Reguera, G., McCarthy, K.D., Mehta, T., Nicoll, J.S., Tuominen, M.T., Lovley, D.R., 2005. Extracellular electron transfer via microbial nanowires. Nature 435, 1098–1101. https://doi.org/10.1038/nature03661

Ren, G., Hu, A., Huang, S., Ye, J., Tang, J., Zhou, S., 2018. Graphite-assisted electro-fermentation methanogenesis: Spectroelectrochemical and microbial community analyses of cathode biofilms. Bioresour. Technol. 269, 74–80. https://doi.org/https://doi.org/10.1016/j.biortech.2018.08.078

Ren, H., Jiang, C., Chae, J., 2017. Effect of temperature on a miniaturized microbial fuel cell (MFC). Micro Nano Syst. Lett. 5, 13. https://doi.org/10.1186/s40486-017-0048-8

Rivas, M., Seeger, M., Holmes, D.S., Jedlicki, E., 2005. A Lux-like quorum sensing system in the extreme acidophile Acidithiobacillus ferrooxidans. Biol. Res. 38, 283–297. https://doi.org/10.4067/S0716-97602005000200018

Rollefson, J.B., Stephen, C.S., Tien, M., Bond, D.R., 2011. Identification of an extracellular polysaccharide network essential for cytochrome anchoring and biofilm formation in Geobacter sulfurreducens. J. Bacteriol. 193, 1023–1033. https://doi.org/10.1128/JB.01092-10

Rotaru, A.-E., Shrestha, P.M., Liu, F., Markovaite, B., Chen, S., Nevin, K.P., Lovley, D.R., 2014a. Direct interspecies electron transfer between Geobacter metallireducens and Methanosarcina barkeri. Appl. Environ. Microbiol. 80, 4599–4605. https://doi.org/10.1128/AEM.00895-14

Rotaru, A.-E., Shrestha, P.M., Liu, F., Shrestha, M., Shrestha, D., Embree, M., Zengler, K.,

Wardman, C., Nevin, K.P., Lovley, D.R., 2014b. A new model for electron flow during anaerobic digestion: Direct interspecies electron transfer to Methanosaeta for the reduction of carbon dioxide to methane. Energy Environ. Sci. 7, 408–415. https://doi.org/10.1039/c3ee42189a

Rousseau, R., Etcheverry, L., Roubaud, E., Basséguy, R., Délia, M.L., Bergel, A., 2020. Microbial electrolysis cell (MEC): Strengths, weaknesses and research needs from electrochemical engineering standpoint. Appl. Energy. https://doi.org/10.1016/j.apenergy.2019.113938

Ruiz, V., Ilhan, Z.E., Kang, D.W., Krajmalnik-Brown, R., Buitrón, G., 2014. The source of inoculum plays a defining role in the development of MEC microbial consortia fed with acetic and propionic acid mixtures. J. Biotechnol. 182–183, 11–18. https://doi.org/10.1016/j.jbiotec.2014.04.016

Ruslan, A.R., Vadivelu, V.M., 2019. Nitrite pre-treatment of dewatered sludge for microbial fuel cell application. J. Environ. Sci. (China) 77, 148–155. https://doi.org/10.1016/j.jes.2018.06.023

Ryue, J., Lin, L., Liu, Y., Lu, W., McCartney, D., Dhar, B.R., 2019. Comparative effects of GAC addition on methane productivity and microbial community in mesophilic and thermophilic anaerobic digestion of food waste. Biochem. Eng. J. 146, 79–87. https://doi.org/10.1016/J.BEJ.2019.03.010

Saheb-Alam, S., Persson, F., Wilén, B.M., Hermansson, M., Modin, O., 2019. A variety of hydrogenotrophic enrichment cultures catalyse cathodic reactions. Sci. Rep. 9, 1–13. https://doi.org/10.1038/s41598-018-38006-3

Saheb-Alam, S., Singh, A., Hermansson, M., Persson, F., Schnürer, A., Wilén, B.-M., Modin, O., 2018. Effect of Start-Up Strategies and Electrode Materials on Carbon Dioxide Reduction on Biocathodes. Appl. Environ. Microbiol. 84, e02242-17. https://doi.org/10.1128/AEM.02242-17

Sangeetha, T., Guo, Z., Liu, W., Gao, L., Wang, L., Cui, M., Chen, C., Wang, A., 2017. Energy recovery evaluation in an up flow microbial electrolysis coupled anaerobic digestion (ME-

AD) reactor: Role of electrode positions and hydraulic retention times. Appl. Energy 206, 1214–1224. https://doi.org/10.1016/j.apenergy.2017.10.026

Saratale, R.G., Saratale, G.D., Pugazhendhi, A., Zhen, G., Kumar, G., Kadier, A., Sivagurunathan, P., 2017. Microbiome involved in microbial electrochemical systems (MESs): A review. Chemosphere 177, 176–188. https://doi.org/10.1016/J.CHEMOSPHERE.2017.02.143

Schrott, G.D., Bonanni, P.S., Robuschi, L., Esteve-Nuñez, A., Busalmen, J.P., 2011. Electrochemical insight into the mechanism of electron transport in biofilms of Geobacter sulfurreducens. Electrochim. Acta 56, 10791–10795. https://doi.org/10.1016/j.electacta.2011.07.001

Selembo, P.A., Merrill, M.D., Logan, B.E., 2010. Hydrogen production with nickel powder cathode catalysts in microbial electrolysis cells. Int. J. Hydrogen Energy 35, 428–437. https://doi.org/10.1016/j.ijhydene.2009.11.014

Shao, Q., Li, J., Yang, S., Sun, H., 2019. Effects of different substrates on microbial electrolysis cell (MEC) anodic membrane: Biodiversity and hydrogen production performance. Water Sci. Technol. 79, 1123–1133. https://doi.org/10.2166/wst.2019.107

Shaw, G.T.-W., Liu, A.-C., Weng, C.-Y., Chou, C.-Y., Wang, D., 2017. Inferring microbial interactions in thermophilic and mesophilic anaerobic digestion of hog waste. PLoS One 12, e0181395. https://doi.org/10.1371/journal.pone.0181395

Shehab, N., Li, D., Amy, G.L., Logan, B.E., Saikaly, P.E., 2013. Characterization of bacterial and archaeal communities in air-cathode microbial fuel cells, open circuit and sealed-off reactors. Appl. Microbiol. Biotechnol. 97, 9885–9895. https://doi.org/10.1007/s00253-013-5025-4

Shi, L., Dong, H., Reguera, G., Beyenal, H., Lu, A., Liu, J., Yu, H.Q., Fredrickson, J.K., 2016. Extracellular electron transfer mechanisms between microorganisms and minerals. Nat. Rev. Microbiol. 14, 651–662. https://doi.org/10.1038/nrmicro.2016.93

Shi, X., Lin, J., Zuo, J., Li, P., Li, X., Guo, X., 2017. Effects of free ammonia on volatile fatty

acid accumulation and process performance in the anaerobic digestion of two typical bio-wastes. J. Environ. Sci. (China) 55, 49–57. https://doi.org/10.1016/j.jes.2016.07.006

Shin, S.G., Han, G., Lim, J., Lee, C., Hwang, S., 2010. A comprehensive microbial insight into two-stage anaerobic digestion of food waste-recycling wastewater. Water Res. 44, 4838–4849. https://doi.org/10.1016/J.WATRES.2010.07.019

Siegert, M., Li, X.-F., Yates, M.D., Logan, B.E., 2014a. The presence of hydrogenotrophic methanogens in the inoculum improves methane gas production in microbial electrolysis cells. Front. Microbiol. 5, 778. https://doi.org/10.3389/fmicb.2014.00778

Siegert, M., Yates, M.D., Call, D.F., Zhu, X., Spormann, A., Logan, B.E., 2014b. Comparison of Nonprecious Metal Cathode Materials for Methane Production by Electromethanogenesis. ACS Sustain. Chem. Eng. 2, 910–917. https://doi.org/10.1021/sc400520x

Siegert, M., Yates, M.D., Spormann, A.M., Logan, B.E., 2015. Methanobacterium Dominates Biocathodic Archaeal Communities in Methanogenic Microbial Electrolysis Cells. ACS Sustain. Chem. Eng. 3, 1668–1676. https://doi.org/10.1021/acssuschemeng.5b00367

Singh, S., Bairagi, P.K., Verma, N., 2018. Candle soot-derived carbon nanoparticles: An inexpensive and efficient electrode for microbial fuel cells. Electrochim. Acta 264, 119–127. https://doi.org/10.1016/j.electacta.2018.01.110

Singh, S., Pophali, A., Omar, R.A., Kumar, R., Kumar, P., Mondal, D.P., Pant, D., Verma, N., 2021. A nickel oxide-decoratedin situgrown 3-D graphitic forest engrained carbon foam electrode for microbial fuel cells. Chem. Commun. 57, 879–882. https://doi.org/10.1039/d0cc07303b

Song, M., Shin, S.G., Hwang, S., 2010. Methanogenic population dynamics assessed by real-time quantitative PCR in sludge granule in upflow anaerobic sludge blanket treating swine wastewater. Bioresour. Technol. 101, S23–S28. https://doi.org/10.1016/J.BIORTECH.2009.03.054

Song, Y.C., Feng, Q., Ahn, Y., 2016. Performance of the Bio-electrochemical Anaerobic Digestion of Sewage Sludge at Different Hydraulic Retention Times. Energy and Fuels 30,

352–359. https://doi.org/10.1021/acs.energyfuels.5b02003

Speers, A.M., Reguera, G., 2012. Electron donors supporting growth and electroactivity of geobacter sulfurreducens anode biofilms. Appl. Environ. Microbiol. 78, 437–444. https://doi.org/10.1128/AEM.06782-11

Stöckl, M., Teubner, N.C., Holtmann, D., Mangold, K.M., Sand, W., 2019. Extracellular Polymeric Substances from Geobacter sulfurreducens Biofilms in Microbial Fuel Cells. ACS Appl. Mater. Interfaces 11, 8961–8968. https://doi.org/10.1021/acsami.8b14340

Summers, Z.M., Fogarty, H.E., Leang, C., Franks, A.E., Malvankar, N.S., Lovley, D.R., 2010. Direct exchange of electrons within aggregates of an evolved syntrophic coculture of anaerobic bacteria. Science 330, 1413–5. https://doi.org/10.1126/science.1196526

Sun, D., Call, D.F., Kiely, P.D., Wang, A., Logan, B.E., 2012. Syntrophic interactions improve power production in formic acid fed MFCs operated with set anode potentials or fixed resistances. Biotechnol. Bioeng. 109, 405–414. https://doi.org/10.1002/bit.23348

Tahernia, M., Mohammadifar, M., Liu, L., Choi, S., 2020. A Disposable, Papertronic Three-Electrode Potentiostat for Monitoring Bacterial Electrochemical Activity. ACS Omega 5, 24717–24723. https://doi.org/10.1021/acsomega.0c03299

Tan, B., Zhou, S., Wang, Y., Zhang, B.P., Zhou, L.H., Yuan, Y., 2019. Molecular insight into electron transfer properties of extracellular polymeric substances of electroactive bacteria by surface-enhanced Raman spectroscopy. Sci. China Technol. Sci. 62, 1679–1687. https://doi.org/10.1007/s11431-018-9437-0

Tang, J., Yuan, Y., Liu, T., Zhou, S., 2015. High-capacity carbon-coated titanium dioxide core–shell nanoparticles modified three dimensional anodes for improved energy output in microbial fuel cells. J. Power Sources 274, 170–176. https://doi.org/10.1016/J.JPOWSOUR.2014.10.035

Thompson, J., 1997. The CLUSTAL_X windows interface: flexible strategies for multiple sequence alignment aided by quality analysis tools. Nucleic Acids Res. 25, 4876–4882. https://doi.org/10.1093/nar/25.24.4876

Tian, T., Qiao, S., Yu, C., Zhou, J., 2019. Effects of nano-sized MnO2 on methanogenic propionate and butyrate degradation in anaerobic digestion. J. Hazard. Mater. 364, 11–18. https://doi.org/10.1016/j.jhazmat.2018.09.081

Toczyłowska-Mamińska, R., Szymona, K., Madej, H., Wong, W.Z., Bala, A., Brutkowski, W., Krajewski, K., H'ng, P.S., Mamiński, M., 2015. Cellulolytic and electrogenic activity of Enterobacter cloacae in mediatorless microbial fuel cell. Appl. Energy 160, 88–93. https://doi.org/10.1016/j.apenergy.2015.09.067

Toh, H., Sharma, V.K., Oshima, K., Kondo, S., Hattori, M., Ward, F.B., Free, A., Taylor, T.D., 2011. Complete genome sequences of Arcobacter butzleri ED-1 and Arcobacter sp. strain L, both isolated from a microbial fuel cell. J. Bacteriol. 193, 6411–2. https://doi.org/10.1128/JB.06084-11

Tomei, M.C., Braguglia, C.M., Cento, G., Mininni, G., 2009. Modeling of Anaerobic Digestion of Sludge. Crit. Rev. Environ. Sci. Technol. 39, 1003–1051. https://doi.org/10.1080/10643380801977818

Torres, C.I., Kato Marcus, A., Rittmann, B.E., 2007. Kinetics of consumption of fermentation products by anode-respiring bacteria. Appl. Microbiol. Biotechnol. 77, 689–697. https://doi.org/10.1007/s00253-007-1198-z

Torres, C.I., Marcus, A.K., Lee, H.-S., Parameswaran, P., Krajmalnik-Brown, R., Rittmann, B.E., 2010. A kinetic perspective on extracellular electron transfer by anode-respiring bacteria. FEMS Microbiol. Rev. 34, 3–17. https://doi.org/10.1111/j.1574-6976.2009.00191.x

Torres, C.I., Marcus, A.K., Rittmann, B.E., 2008. Proton transport inside the biofilm limits electrical current generation by anode-respiring bacteria. Biotechnol. Bioeng. 100, 872–881. https://doi.org/10.1002/bit.21821

Torres, C.I.C.I., Krajmalnik-Brown, R., Parameswaran, P., Marcus, A.K., Wanger, G., Gorby, Y.A., Rittmann, B.E., 2009. Selecting Anode-Respiring Bacteria Based on Anode Potential: Phylogenetic, Electrochemical, and Microscopic Characterization. Environ. Sci. Technol. 43, 9519–9524. https://doi.org/10.1021/es902165y

Tremblay, P.L., Angenent, L.T., Zhang, T., 2017. Extracellular Electron Uptake: Among Autotrophs and Mediated by Surfaces. Trends Biotechnol. 35, 360–371. https://doi.org/10.1016/j.tibtech.2016.10.004

Uría, N., Muñoz Berbel, X., Sánchez, O., Muñoz, F.X., Mas, J., 2011. Transient storage of electrical charge in biofilms of Shewanella oneidensis MR-1 growing in a microbial fuel cell. Environ. Sci. Technol. 45, 10250–10256. https://doi.org/10.1021/es2025214

Van Eerten-Jansen, M.C.A.A., Veldhoen, A.B., Plugge, C.M., Stams, A.J.M., Buisman, C.J.N., Ter Heijne, A., 2013. Microbial community analysis of a methane-producing biocathode in a bioelectrochemical system. Archaea 2013, 481784. https://doi.org/10.1155/2013/481784

van Wolferen, M., Orell, A., Albers, S.V., 2018. Archaeal biofilm formation. Nat. Rev. Microbiol. https://doi.org/10.1038/s41579-018-0058-4

Villano, M., Aulenta, F., Ciucci, C., Ferri, T., Giuliano, A., Majone, M., 2010. Bioelectrochemical reduction of CO2 to CH4 via direct and indirect extracellular electron transfer by a hydrogenophilic methanogenic culture. Bioresour. Technol. 101, 3085–3090. https://doi.org/10.1016/j.biortech.2009.12.077

Villano, M., Ralo, C., Zeppilli, M., Aulenta, F., Majone, M., 2016. Influence of the set anode potential on the performance and internal energy losses of a methane-producing microbial electrolysis cell. Bioelectrochemistry 107, 1–6. https://doi.org/10.1016/j.bioelechem.2015.07.008

Vorregaard, M., 2008. Comstat2 - a modern 3D image analysis environment for biofilms. undefined.

Walker, D.J.F., Martz, E., Holmes, D.E., Zhou, Z., Nonnenmann, S.S., Lovley, D.R., 2019. The archaellum of methanospirillum hungatei is electrically conductive. MBio 10, 1–6. https://doi.org/10.1128/mBio.00579-19

Wang, B., Liu, W., Zhang, Y., Wang, A., 2020. Bioenergy recovery from wastewater accelerated by solar power: Intermittent electro-driving regulation and capacitive storage in biomass. Water Res. 175, 115696. https://doi.org/10.1016/j.watres.2020.115696

Wang, H., Qu, Y., Li, D., Zhou, X., Feng, Y., 2015. Evaluation of an integrated continuous stirred microbial electrochemical reactor: Wastewater treatment, energy recovery and microbial community. Bioresour. Technol. 195, 89–95. https://doi.org/10.1016/J.BIORTECH.2015.06.039

Wang, J., Li, M., Liu, F., Chen, S., 2016. Stainless Steel Mesh Supported Carbon Nanofibers for Electrode in Bioelectrochemical System. J. Nanomater. 2016. https://doi.org/10.1155/2016/4246568

Wang, Y., Zhang, Y., Wang, J., Meng, L., 2009. Effects of volatile fatty acid concentrations on methane yield and methanogenic bacteria. Biomass and Bioenergy 33, 848–853. https://doi.org/10.1016/j.biombioe.2009.01.007

Wilkins, D., Lu, X.Y., Shen, Z., Chen, J., Lee, P.K.H., 2015. Pyrosequencing of mcrA and archaeal 16s rRNA genes reveals diversity and substrate preferences of methanogen communities in anaerobic digesters. Appl. Environ. Microbiol. 81, 604–613. https://doi.org/10.1128/AEM.02566-14

Wormald, R., Humphreys, P., 2019. Hydrogenotrophic methanogenesis dominates at high pH. Access Microbiol. 1, 169. https://doi.org/10.1099/acmi.ac2019.po0051

Xiao, Y., Zhang, E., Zhang, J., Dai, Y., Yang, Z., Christensen, H.E.M., Ulstrup, J., Zhao, F., 2017. Extracellular polymeric substances are transient media for microbial extracellular electron transfer. Sci. Adv. 3, e1700623. https://doi.org/10.1126/sciadv.1700623

Xin, X., Hong, J., He, J., Qiu, W., 2019. An integrated approach for waste activated sludge management towards electric energy production/resource reuse. Bioresour. Technol. 274, 225–231. https://doi.org/10.1016/j.biortech.2018.11.092

Xochitl, D.B., Sevda, S., Vanbroekhoven, K., Pant, D., 2012. The accurate use of impedance analysis for the study of microbial electrochemical systems. Chem. Soc. Rev. 41, 7228–7246. https://doi.org/10.1039/c2cs35026b

Xu, H., Wang, K., Holmes, D.E., 2014. Bioelectrochemical removal of carbon dioxide (CO2): An innovative method for biogas upgrading. Bioresour. Technol. 173, 392–398.

Xu, J., Sheng, G.P., Ma, Y., Wang, L.F., Yu, H.Q., 2013. Roles of extracellular polymeric substances (EPS) in the migration and removal of sulfamethazine in activated sludge system. Water Res. 47, 5298–5306. https://doi.org/10.1016/j.watres.2013.06.009

Xu, R., Xu, S., Florentino, A.P., Zhang, L., Yang, Z., Liu, Y., 2019. Enhancing blackwater methane production by enriching hydrogenotrophic methanogens through hydrogen supplementation. Bioresour. Technol. 278, 481–485. https://doi.org/10.1016/J.BIORTECH.2019.01.014

Xu, S., Zhang, Y., Luo, L., Liu, H., 2019. Startup performance of microbial electrolysis cell assisted anaerobic digester (MEC-AD) with pre-acclimated activated carbon. Bioresour. Technol. Reports 5, 91–98. https://doi.org/10.1016/J.BITEB.2018.12.007

Yang, G., Huang, L., Yu, Z., Liu, X., Chen, S., Zeng, J., Zhou, S., Zhuang, L., 2019a. Anode potentials regulate Geobacter biofilms: New insights from the composition and spatial structure of extracellular polymeric substances. Water Res. 159, 294–301. https://doi.org/10.1016/j.watres.2019.05.027

Yang, G., Lin, J., Zeng, E.Y., Zhuang, L., 2019b. Extraction and characterization of stratified extracellular polymeric substances in Geobacter biofilms. Bioresour. Technol. 276, 119–126. https://doi.org/10.1016/j.biortech.2018.12.100

Yang, N., Hafez, H., Nakhla, G., 2015. Impact of volatile fatty acids on microbial electrolysis cell performance. Bioresour. Technol. 193, 449–455. https://doi.org/10.1016/j.biortech.2015.06.124

Yao, S., He, Y.-L., Li, Y.-S., Xi, H., 2014. Effect of the Membrane Electrode Assemble Design on the Performance of Single Chamber Microbial Fuel Cells. Energy Procedia 61, 1947–1951. https://doi.org/10.1016/J.EGYPRO.2014.12.249

Yasri, N., Roberts, E.P.L., Gunasekaran, S., 2019. The electrochemical perspective of bioelectrocatalytic activities in microbial electrolysis and microbial fuel cells. Energy Reports. https://doi.org/10.1016/j.egyr.2019.08.007

Ye, J., Hu, A., Ren, G., Chen, M., Tang, J., Zhang, P., Zhou, S., He, Z., 2018. Enhancing sludge

methanogenesis with improved redox activity of extracellular polymeric substances by hematite in red mud. Water Res. 134, 54–62. https://doi.org/10.1016/j.watres.2018.01.062

Yin, C., Shen, Y., Yuan, R., Zhu, N., Yuan, H., Lou, Z., 2019. Sludge-based biochar-assisted thermophilic anaerobic digestion of waste-activated sludge in microbial electrolysis cell for methane production. Bioresour. Technol. 284, 315–324. https://doi.org/10.1016/J.BIORTECH.2019.03.146

Yin, Q., Zhu, X., Zhan, G., Bo, T., Yang, Y., Tao, Y., He, X., Li, D., Yan, Z., 2016. Enhanced methane production in an anaerobic digestion and microbial electrolysis cell coupled system with co-cultivation of Geobacter and Methanosarcina. J. Environ. Sci. 42, 210–214. https://doi.org/10.1016/j.jes.2015.07.006

Yu, H.Q., 2020. Molecular Insights into Extracellular Polymeric Substances in Activated Sludge. Environ. Sci. Technol. 54, 7742–7750. https://doi.org/10.1021/acs.est.0c00850

Yu, J., Kim, S., Kwon, O.-S., 2019. Effect of applied voltage and temperature on methane production and microbial community in microbial electrochemical anaerobic digestion systems treating swine manure. J. Ind. Microbiol. Biotechnol. 1–13. https://doi.org/10.1007/s10295-019-02182-6

Yu, J., Park, Y., Lee, T., 2015. Electron flux and microbial community in microbial fuel cells (open-circuit and closed-circuit modes) and fermentation. J. Ind. Microbiol. Biotechnol. 42, 979–983. https://doi.org/10.1007/s10295-015-1629-2

Yu, Z., Leng, X., Zhao, S., Ji, J., Zhou, T., Khan, A., Kakde, A., Liu, P., Li, X., 2018. A review on the applications of microbial electrolysis cells in anaerobic digestion, Bioresource Technology.

Yuan, H., He, Z., 2017. Platinum Group Metal-free Catalysts for Hydrogen Evolution Reaction in Microbial Electrolysis Cells. Chem. Rec. 17, 641–652. https://doi.org/10.1002/tcr.201700007

Zakaria, B.S., Dhar, B.R., 2021a. An intermittent power supply scheme to minimize electrical energy input in a microbial electrolysis cell assisted anaerobic digester. Bioresour. Technol.

319, 124109. https://doi.org/10.1016/j.biortech.2020.124109

Zakaria, B.S., Dhar, B.R., 2021b. Characterization and significance of extracellular polymeric substances, reactive oxygen species, and extracellular electron transfer in methanogenic biocathode. Sci. Rep. 11, 7933. https://doi.org/10.1038/s41598-021-87118-w

Zakaria, B.S., Dhar, B.R., 2020. Changes in syntrophic microbial communities, EPS matrix, and gene-expression patterns in biofilm anode in response to silver nanoparticles exposure. Sci. Total Environ. 734, 139395. https://doi.org/10.1016/j.scitotenv.2020.139395

Zakaria, B.S., Dhar, B.R., 2019. Progress towards catalyzing electro-methanogenesis in anaerobic digestion process: Fundamentals, process optimization, design and scale-up considerations. Bioresour. Technol. https://doi.org/10.1016/j.biortech.2019.121738

Zakaria, B.S., Lin, L., Chung, T., Dhar, B.R., 2020. An overview of complementary microbial electrochemical technologies for advancing anaerobic digestion. Elsevier, pp. 129–167. https://doi.org/10.1016/bs.aibe.2020.04.004

Zakaria, B.S., Lin, L., Dhar, B.R., 2019. Shift of biofilm and suspended bacterial communities with changes in anode potential in a microbial electrolysis cell treating primary sludge. Sci. Total Environ. 689, 691–699. https://doi.org/10.1016/j.scitotenv.2019.06.519

Zamalloa, C., Arends, J.B.A., Boon, N., Verstraete, W., 2013. Performance of a lab-scale bio-electrochemical assisted septic tank for the anaerobic treatment of black water. N. Biotechnol. 30, 573–580. https://doi.org/10.1016/J.NBT.2013.01.009

Zaybak, Z., Pisciotta, J.M., Tokash, J.C., Logan, B.E., 2013. Enhanced start-up of anaerobic facultatively autotrophic biocathodes in bioelectrochemical systems. J. Biotechnol. 168, 478–485. https://doi.org/10.1016/j.jbiotec.2013.10.001

Zhang, H., Banaszak, J.E., Parameswaran, P., Alder, J., Krajmalnik-Brown, R., Rittmann, B.E., 2009. Focused-Pulsed sludge pre-treatment increases the bacterial diversity and relative abundance of acetoclastic methanogens in a full-scale anaerobic digester. Water Res. 43, 4517–4526. https://doi.org/10.1016/j.watres.2009.07.034

Zhang, L., Zhu, X., Li, J., Liao, Q., Ye, D., 2011. Biofilm formation and electricity generation of

a microbial fuel cell started up under different external resistances. J. Power Sources 196, 6029–6035. https://doi.org/10.1016/j.jpowsour.2011.04.013

Zhang, R., Neu, T.R., Li, Q., Blanchard, V., Zhang, Y., Schippers, A., Sand, W., 2019. Insight into interactions of thermoacidophilic archaea with elemental sulfur: Biofilm dynamics and EPS analysis. Front. Microbiol. 10. https://doi.org/10.3389/fmicb.2019.00896

Zhang, T., Nie, H., Bain, T.S., Lu, H., Cui, M., Snoeyenbos-West, O.L., Franks, A.E., Nevin, K.P., Russell, T.P., Lovley, D.R., 2013. Improved cathode materials for microbial electrosynthesis. Energy Environ. Sci. 6, 217–224. https://doi.org/10.1039/C2EE23350A

Zhang, X., Cheng, S., Wang, X., Huang, X., Logan, B.E., 2009. Separator Characteristics for Increasing Performance of Microbial Fuel Cells. Environ. Sci. Technol. 43, 8456–8461. https://doi.org/10.1021/es901631p

Zhang, Y., Merrill, M.D., Logan, B.E., 2010. The use and optimization of stainless steel mesh cathodes in microbial electrolysis cells. Int. J. Hydrogen Energy 35, 12020–12028. https://doi.org/10.1016/j.ijhydene.2010.08.064

Zhao, Z., Zhang, Y., Chen, S., Quan, X., Yu, Q., 2014. Bioelectrochemical enhancement of anaerobic methanogenesis for high organic load rate wastewater treatment in a up-flow anaerobic sludge blanket (UASB) reactor. Sci. Rep. 4, 6658. https://doi.org/10.1038/srep06658

Zhao, Zhiqiang, Zhang, Y., Ma, W., Sun, J., Sun, S., Quan, X., 2016a. Enriching functional microbes with electrode to accelerate the decomposition of complex substrates during anaerobic digestion of municipal sludge. Biochem. Eng. J. 111, 1–9.

Zhao, Zisheng, Zhang, Y., Quan, X., Zhao, H., 2016. Evaluation on direct interspecies electron transfer in anaerobic sludge digestion of microbial electrolysis cell. Bioresour. Technol. 200, 235–244. https://doi.org/10.1016/j.biortech.2015.10.021

Zhao, Z., Zhang, Y., Wang, L., Quan, X., 2015. Potential for direct interspecies electron transfer in an electric-anaerobic system to increase methane production from sludge digestion. Sci. Rep. 5, 1–12. https://doi.org/10.1038/srep11094

Zhao, Zhiqiang, Zhang, Y., Yu, Q., Ma, W., Sun, J., Quan, X., 2016b. Enhanced decomposition of waste activated sludge via anodic oxidation for methane production and bioenergy recovery. Int. Biodeterior. Biodegradation 106, 161–169. https://doi.org/10.1016/J.IBIOD.2015.10.020

Zhen, G., Kobayashi, T., Lu, X., Kumar, G., Xu, K., 2016a. Biomethane recovery from Egeria densa in a microbial electrolysis cell-assisted anaerobic system: Performance and stability assessment. Chemosphere 149, 121–129. https://doi.org/10.1016/J.CHEMOSPHERE.2016.01.101

Zhen, G., Kobayashi, T., Lu, X., Xu, K., 2015. Understanding methane bioelectrosynthesis from carbon dioxide in a two-chamber microbial electrolysis cells (MECs) containing a carbon biocathode. Bioresour. Technol. 186, 141–148.

Zhen, G., Lu, X., Kobayashi, T., Kumar, G., Xu, K., 2016b. Promoted electromethanosynthesis in a two-chamber microbial electrolysis cells (MECs) containing a hybrid biocathode covered with graphite felt (GF). Chem. Eng. J. 284, 1146–1155. https://doi.org/10.1016/j.cej.2015.09.071

Zhen, G., Zheng, S., Lu, X., Zhu, X., Mei, J., Kobayashi, T., Xu, K., Li, Y.-Y., Zhao, Y., 2018. A comprehensive comparison of five different carbon-based cathode materials in CO2 electromethanogenesis: Long-term performance, cell-electrode contact behaviors and extracellular electron transfer pathways. Bioresour. Technol. 266, 382–388. https://doi.org/10.1016/J.BIORTECH.2018.06.101

Zheng, L., Zhang, Z., Tian, L., Zhang, L., Cheng, S., Li, Z., Cang, D., 2019. Mechanistic investigation of toxicological change in ZnO and TiO2 multi-nanomaterial systems during anaerobic digestion and the microorganism response. Biochem. Eng. J. 147, 62–71. https://doi.org/10.1016/j.bej.2019.03.017

Zheng, S., Liu, F., Wang, B., Zhang, Y., Lovley, D.R., 2020. Methanobacterium Capable of Direct Interspecies Electron Transfer. Environ. Sci. Technol. 54, 15347–15354. https://doi.org/10.1021/acs.est.0c05525

Zhu, X., Yates, M.D., Hatzell, M.C., Ananda Rao, H., Saikaly, P.E., Logan, B.E., 2014.

Microbial Community Composition Is Unaffected by Anode Potential. Environ. Sci. Technol. 48, 1352–1358. https://doi.org/10.1021/es404690q

# Appendix A

## *Supplementary Information for Chapter 3*

### Text A.1 Estimation of specific surface area of electrodes

#### 1. Stainless-steel mesh electrode

The surface area was calculated according to Zhang et al. (Zhang et al., 2010) with minor modification.

$$S = 2\pi bdn(n+1) + \frac{3}{2}\pi d^2(n+1)^2$$

Where, (b) is the pore size, and (d) is the wire diameter, (n) is 70 mesh

b= 0.02 cm, d = 0.016 cm

The specific surface area based on reactor volume = 0.0016/0.00038 $m^2/m^3$ = 4.23 $m^2/m^3$

#### 2. Carbon fiber electrode

The surface area of carbon fiber was calculated using two approaches previously reported in the literature (Brunschweiger et al., 2020; Lanas and Logan, 2013):

1. Considering every single filament in the carbon fiber bundle (filament bundle consists of 24000 single filaments, each with diameter 7 μm, and the length = 130 cm)

S.A. = 2πrh x n = 2 x 3.14 x 0.0007 cm x 130 cm x 24000 = 13715.5 $cm^2$

The specific surface area based on reactor volume = 1.372 $m^2$ / 0.00038 $m^3$ = 3609 $m^2/m^3$

2. Considering all filaments in a bundle act together as a single fiber (width = 0.5 cm, length = 130 cm, height = 0.1 cm).

S.A.= 2 (wh +Lw + Lh) = 156.4 $cm^2$

The specific surface area based on reactor volume = 0.0156 $m^2$ / 0.00038 $m^3$ = 41 $m^2/m^3$

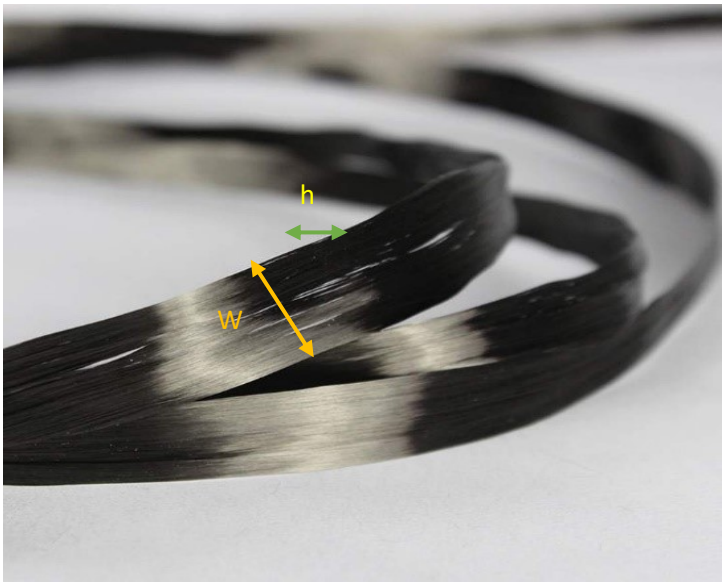


**Figure A.1** Photograph of carbon fiber bundle

**Text A.2 EPS extraction protocol and analytical methods for EPS measurement**

**EPS Extraction:** CER method for EPS extraction was performed according to Frølund et al. (Frølund et al., 1996) with some minor modification, 52 $cm^2$ of carbon fiber and 0.054 $cm^2$ of stainless-steel were resuspended in 0.1 M PBS buffer, pH 7.4. Then, 2 g CER (Dowex Marathon C sodium form, Sigma-Aldrich, USA), washed with 0.1 M PBS for 15 min (10 mL $g^{-1}$ Dowex), was added to each sample. The samples were agitated at a high capacity for 20 min on the shaker (Vortex Mixer, Fisher Scientific, USA). The heating method was conducted according to Xu et al. (Xu et al., 2013), the electrodes were washed twice with 0.9% NaCl (w/v), then resuspended in 0.9% NaCl (w/v). The samples were heated at 60ºC in a water bath for 30 minutes. For both methods, the EPS were harvested by centrifugation three times at 20,000 × g for 20 minutes at 4ºC. The supernatant was collected and filtered using a 0.2 µm filter and the EPS stored at -20ºC for further analysis. Also, the pellets were collected to examine the cell lysis using Glucose-6-Phosphate Dehydrogenase kit (Sigma-Aldrich, USA). EPS levels were presented as the mass of EPS per unit surface area of the electrode ($mg/cm^2$) for comparing EPS levels in two reactors.

**Analytical methods for EPS measurement:** The total carbohydrate content was measured using a phenol-sulfuric acid method using glucose standards according to DuBois et al. (DuBois et al., 1956) with some minor modification. 2 mL of EPS was mixed with 5 mL of concentrated sulfuric acid followed by the addition of 0.05 mL of 80% wt. phenol. Then, the samples were incubated at room temperature for 10 minutes, then shake followed by incubation for 20 minutes at 30ºC. The samples were measured at 490 nm using UV-spectrophotometer (Model DR 3900, HACH, Germany). The protein contents of the EPS were measured using Pierce Modified Lowry Protein Assay Kit (Thermo Fisher, USA) according to the manufacturer's instructions. Uronic acid was measured according to Blumenkrantz and Asboe-Hansen (Blumenkrantz and Asboe-Hansen, 1973) and Ghods et al. (Ghods et al., 2015) with glucuronic acid (Sigma-Aldrich, USA) as a standard. Heme contents were measured using the Heme Assay Kit (Heme Assay Kit, Sigma-Aldrich, USA) according to the manufacturer's instructions. The extracellular DNA (eDNA) was quantified using the diphenylamine colorimetric method with calf thymus DNA as the standard (Brunk et al., 1979). 100 µL EPS was pipetted in a cuvette and 2.5 mL of the reagent (0.2 ppm

DAPI (4, 6-diaminodino-2-phenylindole) in 100 mM NaC1, l0 mM EDTA, 10 mM PBS, pH 7.2) was added. All the above measurements were conducted in triplicate.

**Table A.1** EPS composition using CER and heating methods

| | **Carbohydrate ($mg/cm^2$)** | **Proteins ($mg/cm^2$)** | **Heme ($mg/cm^2$)** | **Uronic Acid ($mg/cm^2$)** | **eDNA ($mg/cm^2$)** |
|---|---|---|---|---|---|
| **CER Method** | | | | | |
| **Anode (CF-CF)** | 28.225 | 133.545 | 40.58 | 10.6 | 0.55 |
| **Cathode (CF-CF)** | 25.775 | 170.025 | 16.52 | 6.2 | 0.39 |
| **Anode (CF-SS)** | 34.775 | 146.405 | 37.94 | 11.665 | 0.685 |
| **Cathode (CF-SS)** | 52.14 | 212.79 | 34.22 | 15 | 1.525 |
| **Heating Method** | | | | | |
| **Anode (CF-CF)** | 35.575 | 109.29 | 50.45 | 13.065 | 0.69 |
| **Cathode (CF-CF)** | 27.78 | 163.29 | 18.62 | 8.27 | 0.365 |
| **Anode (CF-SS)** | 24.1 | 172.855 | 41.13 | 11.32 | 0.46 |
| **Cathode (CF-SS)** | 52.61 | 223.885 | 37.57 | 15.2 | 1.715 |

**Text A.3 Method for CLSM imaging**

Confocal laser scanning microscopy (CLSM) was used to visualize and examine the EPS structure on the electrodes. Portions of carbon fibers and stainless-steel mesh were cut with an aseptic scissor from different locations and washed with 0.1 M PBS buffer (pH 7.4) to remove any debris. The electrodes were fluorescently stained with TOTO-1 (Thermo Fisher, USA) and Concanavalin A (ConA) Alexa Fluor 633 Conjugate (Thermo Fisher, USA) for one hour in the dark for eDNA and EPS visualization, respectively. Then, the samples were washed again with PBS buffer to remove any non-specific binding stains. The stained electrodes were placed on MatTek dishes with a 1.5 coverslip (MatTek co., USA) to ensure that the biofilm was not compressed. The visualization of the electrodes was performed using a Leica inverted DMI 6000 B microscope (Leica Microsystems, USA). CLSM was equipped with an argon laser and helium-neon lasers. The images were acquired using x63/1.3 water immersion lens using LAS AF software (Leica Microsystems, USA, https://www.leica-microsystems.com/) at a resolution of 1024 x 1024 with 120 nm pixel size. Images z-stack were acquired with several steps 29 with z-step size 0.29 µm with smart grain 687. The quantitative analysis of EPS structure was carried out using biofilm image processing COMSTAT software (COMSTAT2, Version 2.1, Dk, http://www.comstat.dk/) ("Comstat 2," n.d.; Heydorn et al., 2000; Vorregaard, 2008). The EPS intensities were reported as intensity/$um^3$ of the electrode.

**Text A.4 Methods for measurement of EET gene expression levels.**

The concept is to design primers to detect most of the *omc*B, *omc*C, *omc*E, *omc*Z, *omc*S, and *pil*A gene sequences as possible. The primer design was performed similarly to Lin et al. (L. Lin et al., 2019a), and *rec*A housekeeping gene was used as a reference (Rivas et al., 2005). The genome sequences of the anode biofilm were collected from the National Center for Biotechnology Information (NCBI) (https://www.ncbi.nlm.nih.gov). These followed by multiple-aligned using the ClustalX alignment tool (ClustalX, Version 2.1, http://www.clustal.org/clustal2/) to select most of the homologous gene regions (Thompson, 1997). Then, gene-specific primers for RT-PCR were designed with Primer3 software (Primer3, Version 4.1.0, http://bioinfo.ut.ee/primer3) by selecting an almost similar range of melting temperatures. The Basic Local Alignment Search Tool (BLAST) (https://blast.ncbi.nlm.nih.gov/Blast.cgi) was used to check the specificity of the primers. Also, the primers were experimentally examined using agarose gel electrophoresis. The primers were prepared by Integrated DNA Technologies (IDT, USA) and are listed in Table S1.

Total RNA was extracted using RNeasy PowerSoil Total RNA Kit (Qiagen, CA), then the purity and concentration were examined using Nanodrop (2000C, Thermo Scientific, USA). Subsequently, cDNA synthesis was performed using QuantiTect Reverse Transcription Kit (Qiagen, CA). Then, RT-PCR mixtures were prepared in 25 uL reactions using QuantiFast SYBR Green PCR Kit (Qiagen, CA) as the following: 1 µL of the template, 12.5 µL 2x master mix, 2.5 µL forward and reverse specific primer, and 6.5 µL nuclease-free water. CFX 96 real-time PCR system with a C1000 Thermal Cycler (Bio-Rad, USA) was used with the following cycling conditions according to the QuantiFast SYBR Green PCR Kit's protocol; PCR initial heat activation cycle at 95 ˚C for 5 min, 35 cycles at 95 ˚C for 10 sec and 60 ˚C for 30 sec, and finally, one cycle at 40 ˚C for 30 seconds. Triplicate reactions were run for all samples.

**Table A.2** Primers used for studying gene expression levels

| | Forward (5'-3') | Reverse (5'-3') |
|---|---|---|
| *rec*A | CACCGGCATAATCTCCAAGT | ATCTTGCGGATATCGAGACG |
| *pil*A | TTATGATCGTGGTTGCCATT | CCGCAGTTAAACCTTCTGCT |
| | GAGCGATGTTCTTTCCGTTT | AATCCTGATAGGCGGGAATC |
| *omc*B | CCGAAAATTACGCAGGTGTT | GGAGTTCACGAAACCAAGGA |
| | GAGGGACGATGTCAACCTGT | TTCGCAAGGTAGCTGTTGTG |
| *omc*C | CTGGTACTCTGGGTGGCATT | GCTGTGGTTAGCAGCATTGA |
| | ACGAGTTCCAGACCAACACC | GGCAGTATCGTCCCAGTTGT |
| *omc*E | ATGTCCTACGGCGATGCTAT | GTAACCTGCAGGAAGGTGGA |
| | CTCGTCCAGCAGCATGAATA | GGGGTGATCATTGCTCAGAT |
| *omc*Z | GGACGTATTGTGGCAGAGGT | GGCCACTACATTCCGACCTA |
| | GGCCACTACATTCCGACCTA | GGACGTATTGTGGCAGAGGT |
| *omc*S | GCTGACTACACCGTGCTCAA | TGAACTCGTATGCCAGGTTG |
| | GGCAAGTACCGTCGTTTTGT | GTAGCTTCCGTCCGGTTGTA |

**Text A.5 Microbial quantification using RT-PCR**

qPCR was performed to quantify bacterial cell numbers before and after AgNPs injection. 16S universal primers, 357Wf: CCTACGGGNGGCWGCAG and 785R: GACTACHVGGGTATCTAATCC, were used to quantify the DNA samples. qPCR mixtures were prepared in 25 uL reactions using QuantiFast SYBR Green PCR Kit (Qiagen, CA) as the following: 2 µL of the DNA template, 12.5 µL 2x master mix, 2.5 µL forward and reverse specific primer, and 5.5 µL nuclease-free water. CFX 96 real-time PCR system with a C1000 Thermal Cycler (Bio-Rad, USA) was used with the following cycling conditions according to the QuantiFast SYBR Green PCR Kit's protocol; PCR initial heat activation cycle at 95 ˚C for 5 min, 35 cycles at 95 ˚C for 10 sec and 60 ˚C for 30 sec, and finally, one cycle at 40 ˚C for 30 seconds. Triplicate reactions were run for all samples.

**Text A.6 Electrochemical impedance spectroscopy (EIS)**

EIS was performed with a multi-channel VSP potentiostat (VSP, Bio-Logic Science Instruments, France), and the data was recorded using EC-Lab software (EC-Lab, Version 10.38, BioLogic Science Instruments, France, https://www.biologic.net/). EIS measurements performed using two reactor configurations; two-electrode configuration for the whole cell (anode as working electrode and cathode and reference electrodes as counter electrodes), and three-electrode configuration to test anode and cathode electrodes separately, where anode/cathode as working electrode and the other as counter electrode, and Ag/AgCl was used as a reference electrode (Hidalgo et al., 2015; Wang et al., 2020; Xochitl et al., 2012). The potentials set depending on the potential of anode and cathode electrodes. The sinusoidal amplitude was fixed at 1 mV with a frequency range of 100 kHz to 0.01 Hz. Then, the data were fitted using Z-fit with an equivalent circuit model (ECM), as previously described in the literature (Wang et al., 2020). Equivalent circuit model provided as following; [Rs (ohmic resistance)] [Rct (activation resistance) Q1 (phase element)] [Rd (concentration resistance) Q2 (phase element)], was used for the whole cell, and [Rs (ohmic resistance)] [(Rct (activation resistance) Q1 (phase element)] Rs (ohmic resistance) [Rd (concentration resistance) Q2 (phase element)] ECM was used for testing the individual electrodes.

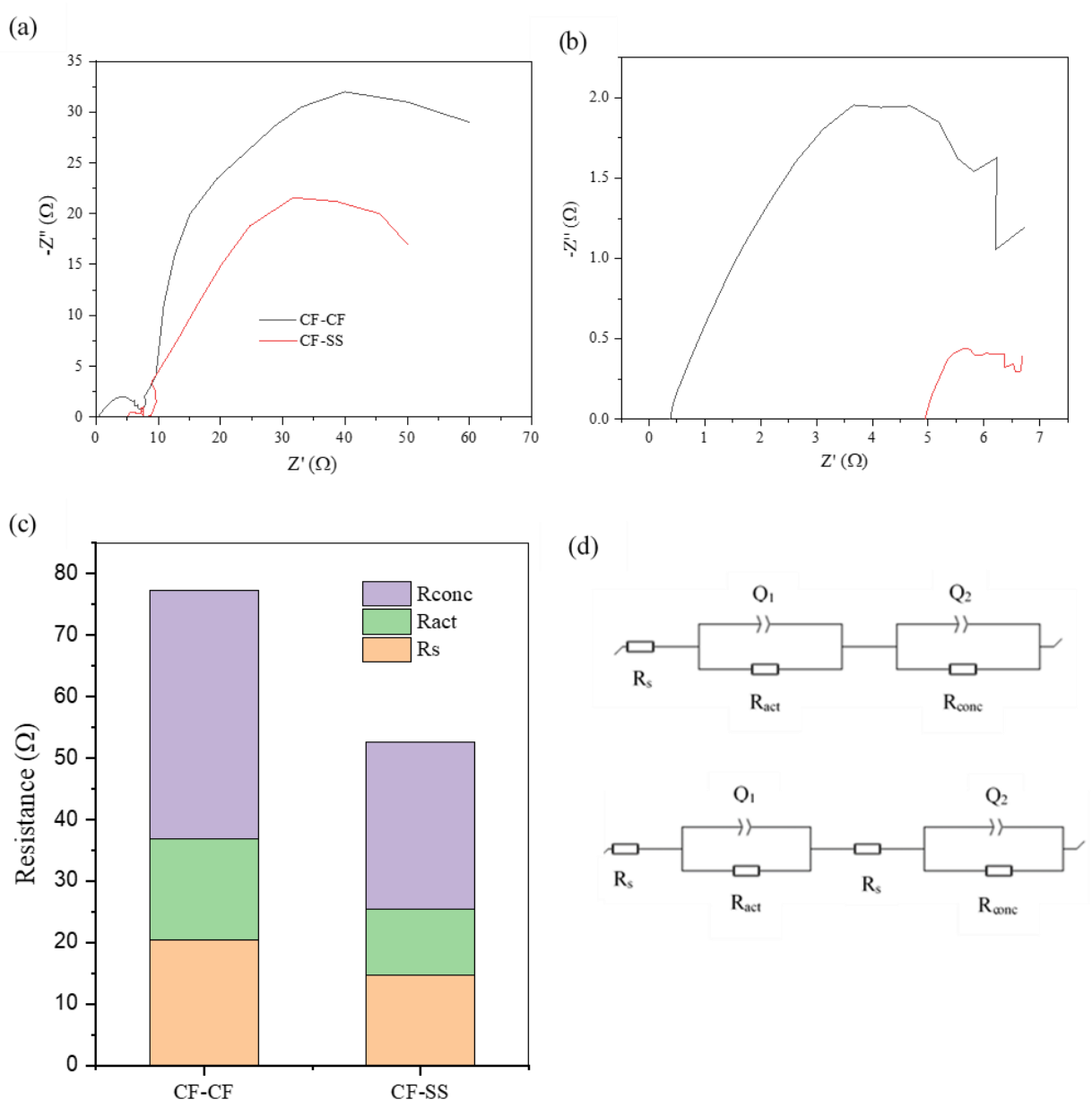


**Figure A.2** Nyquist plot for whole cell (a), the enlarged Nyquist plot for the highest frequency region (b), internal resistances (c), equivalent circuit models (d) of CF-CF and CF-SS reactors

**Table A.3** The diversity and richness of the biofilms of both systems

| Reactor/electrode | | Chao 1 | Phylogenetic distance | OTUs | Pielou's evenness | Shannon | Coverage |
|---|---|---|---|---|---|---|---|
| **CF-CF** | **Anode** | 137 | 11.68 | 132 | 0.45 | 3.14 | 1.0 |
| | **Cathode** | 76 | 7.19 | 76 | 0.63 | 3.95 | 1.0 |
| **CF-SS** | **Anode** | 146 | 13.57 | 146 | 0.72 | 5.18 | 1.0 |
| | **Cathode** | 155 | 12.32 | 150 | 0.71 | 5.10 | 1.0 |

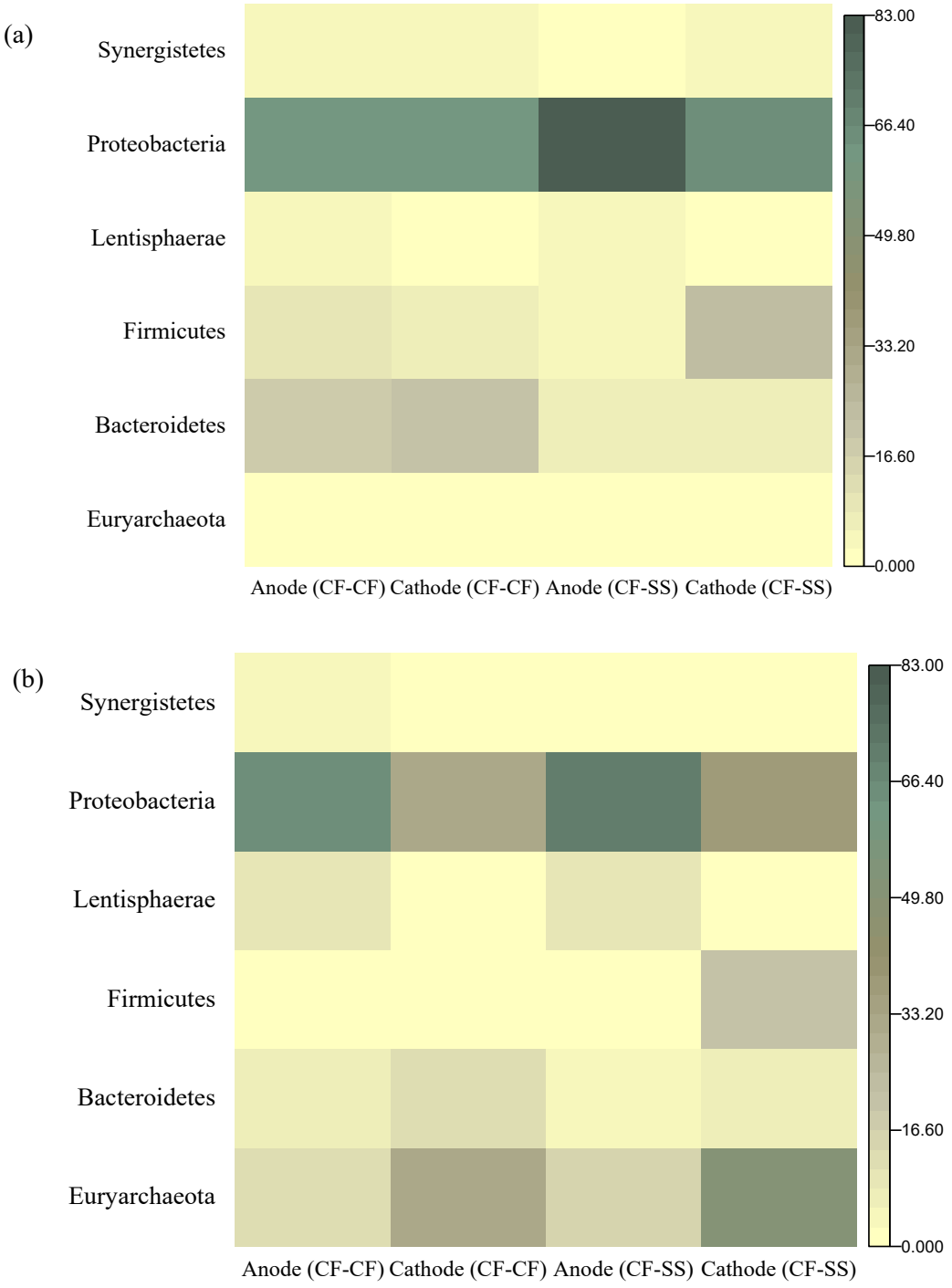


**Figure A.4** Relative abundance of microbial community. Bacterial primer phylum level (a), and archaeal primer phylum level (b)

# Appendix B

## *Supplementary Information for Chapter 4*

**Table B.1** EPS composition using CER and heating methods

| | | Carbohydrate ($mg/cm^2$) | Proteins ($mg/cm^2$) | Heme ($mg/cm^2$) | Uronic Acid ($mg/cm^2$) | eDNA ($mg/cm^2$) |
|---|---|---|---|---|---|---|
| **CER method** | | | | | | |
| **Anode** | **HPr/HAc 0.5** | 26.55 | 136.47 | 45.12 | 11.22 | 0.62 |
| | **HPr/HAc 1.5** | 34.66 | 133.28 | 46.59 | 12.33 | 0.71 |
| | **HPr/HAc 2.5** | 50.41 | 100.43 | 26.37 | 10.36 | 0.49 |
| | **HPr/HAc 5** | 57.77 | 75.44 | 29.12 | 10.9 | 0.4 |
| **Cathode** | **HPr/HAc 0.5** | 30.71 | 131.4 | 28.35 | 7.2 | 0.29 |
| | **HPr/HAc 1.5** | 33.55 | 135.41 | 27.77 | 6.4 | 0.28 |
| | **HPr/HAc 2.5** | 60.21 | 87.94 | 16.31 | 6.9 | 0.18 |
| | **HPr/HAc 5** | 59.44 | 80.32 | 18.55 | 5.9 | 0.21 |
| **Heating method** | | | | | | |
| **Anode** | **HPr/HAc 0.5** | 28.21 | 140.55 | 47.32 | 12.1 | 0.71 |
| | **HPr/HAc 1.5** | 32.11 | 133.49 | 45.11 | 12.34 | 0.67 |
| | **HPr/HAc 2.5** | 51.94 | 94.85 | 24.28 | 9.99 | 0.51 |
| | **HPr/HAc 5** | 55.51 | 79.13 | 31.55 | 9.47 | 0.42 |
| **Cathode** | **HPr/HAc 0.5** | 34.61 | 133.48 | 29.31 | 6.94 | 0.31 |
| | **HPr/HAc 1.5** | 34.59 | 139.29 | 24.39 | 7.1 | 0.3 |
| | **HPr/HAc 2.5** | 66.58 | 87.2 | 20.39 | 7.08 | 0.14 |
| | **HPr/HAc 5** | 66.31 | 84.13 | 18.21 | 6.1 | 0.19 |

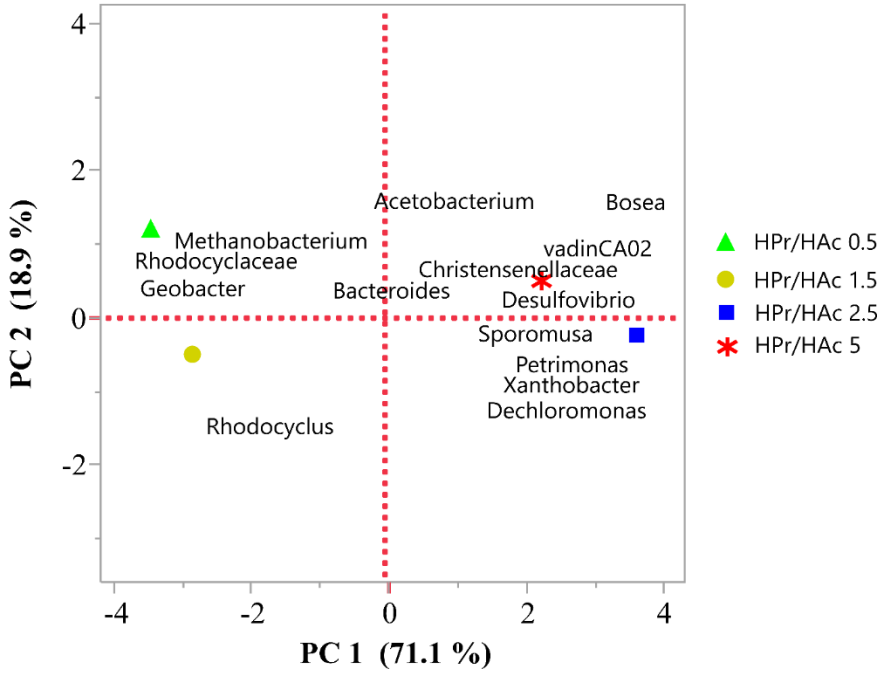


**Figure B.2** Principal Component Analysis of the microbial communities at different HPr/HAc ratios

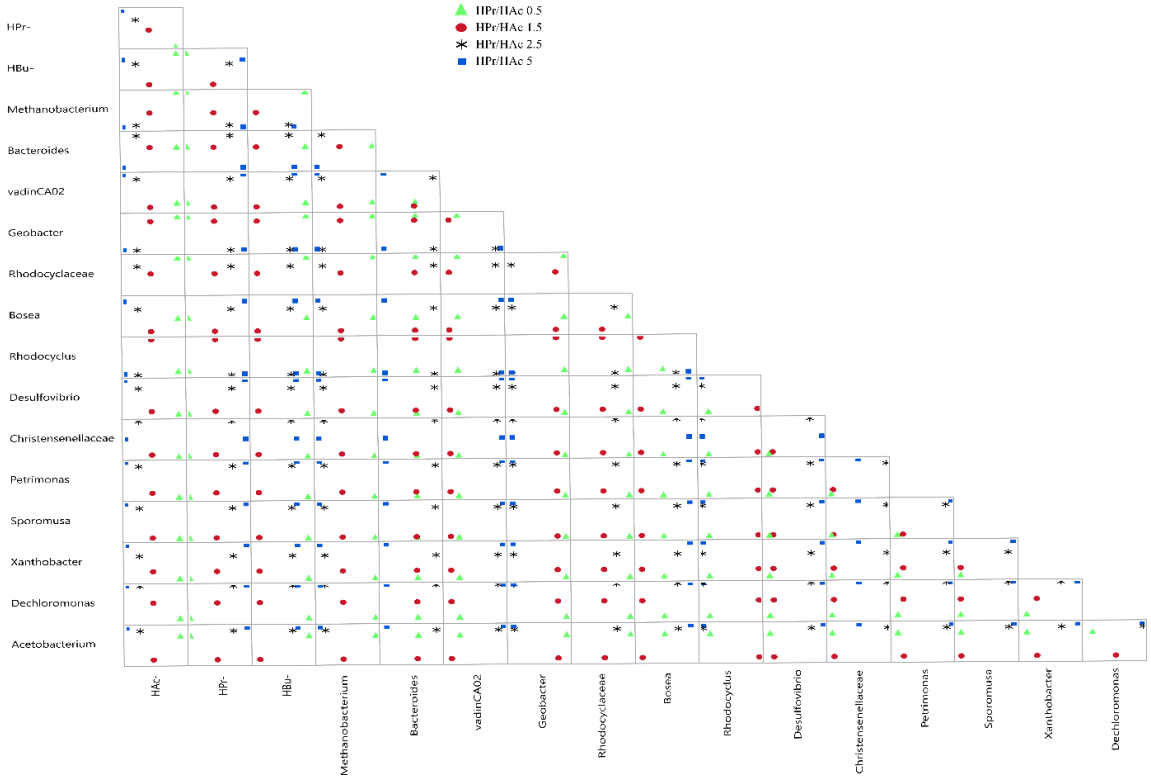


**Figure B.2** Scatterplot matrix of the microbial communities at different HPr/HAc ratios

**Table B.2** Correlation analysis of the microbial communities at different HPr/HAc ratios

| | | | | | | | | | | | | | | | | | |
|---|---|---|---|---|---|---|---|---|---|---|---|---|---|---|---|---|---|
| HAc- | 1.0 | | | | | | | | | | | | | | | | |
| IIPr- | -1.0 | 1.0 | | | | | | | | | | | | | | | |
| HBu- | 0.2 | -0.1 | 1.0 | | | | | | | | | | | | | | |
| *Methanobacterium* | 1.0 | -1.0 | 0.2 | 1.0 | | | | | | | | | | | | | |
| *Bacteroides* | 0.4 | -0.4 | -0.1 | 0.2 | 1.0 | | | | | | | | | | | | |
| *vadinCA02* | -0.8 | 0.8 | 0.4 | -0.8 | -0.3 | 1.0 | | | | | | | | | | | |
| *Geobacter* | 0.9 | -0.9 | -0.2 | 0.9 | 0.2 | -1.0 | 1.0 | | | | | | | | | | |
| *Rhodocyclaceae* | 0.8 | -0.8 | 0.2 | 0.7 | 0.8 | -0.6 | 0.6 | 1.0 | | | | | | | | | |
| *Bosea* | -0.6 | 0.6 | 0.7 | -0.5 | -0.4 | 0.9 | -0.8 | -0.5 | 1.0 | | | | | | | | |
| *Rhodocyclus* | 0.2 | -0.2 | -0.9 | 0.2 | 0.1 | -0.7 | 0.6 | 0.0 | -0.9 | 1.0 | | | | | | | |
| *Desulfovibrio* | -0.9 | 0.9 | 0.3 | -0.9 | -0.4 | 1.0 | -1.0 | -0.7 | 0.9 | -0.6 | 1.0 | | | | | | |
| *Christensenellaceae* | -0.7 | 0.7 | 0.2 | -0.7 | 0.3 | 0.8 | -0.9 | -0.2 | 0.6 | -0.6 | 0.8 | 1.0 | | | | | |
| *Petrimonas* | -0.9 | 0.9 | 0.2 | -0.9 | -0.3 | 1.0 | -1.0 | -0.6 | 0.8 | -0.6 | 1.0 | 0.9 | 1.0 | | | | |
| *Sporomusa* | -0.9 | 0.9 | 0.3 | -0.9 | -0.3 | 1.0 | -1.0 | -0.6 | 0.9 | -0.7 | 1.0 | 0.9 | 1.0 | 1.0 | | | |
| *Xanthobacter* | -1.0 | 1.0 | 0.1 | -0.9 | -0.5 | 0.9 | -1.0 | -0.8 | 0.8 | -0.5 | 1.0 | 0.7 | 1.0 | 1.0 | 1.0 | | |
| *Dechloromonas* | -1.0 | 1.0 | -0.1 | -1.0 | -0.2 | 0.9 | -1.0 | -0.7 | 0.6 | -0.3 | 0.9 | 0.8 | 0.9 | 0.9 | 0.9 | 1.0 | |
| *Acetobacterium* | -0.3 | 0.4 | 0.9 | -0.3 | -0.2 | 0.8 | -0.7 | -0.2 | 1.0 | -1.0 | 0.7 | 0.6 | 0.7 | 0.8 | 0.6 | 0.4 | 1.0 |

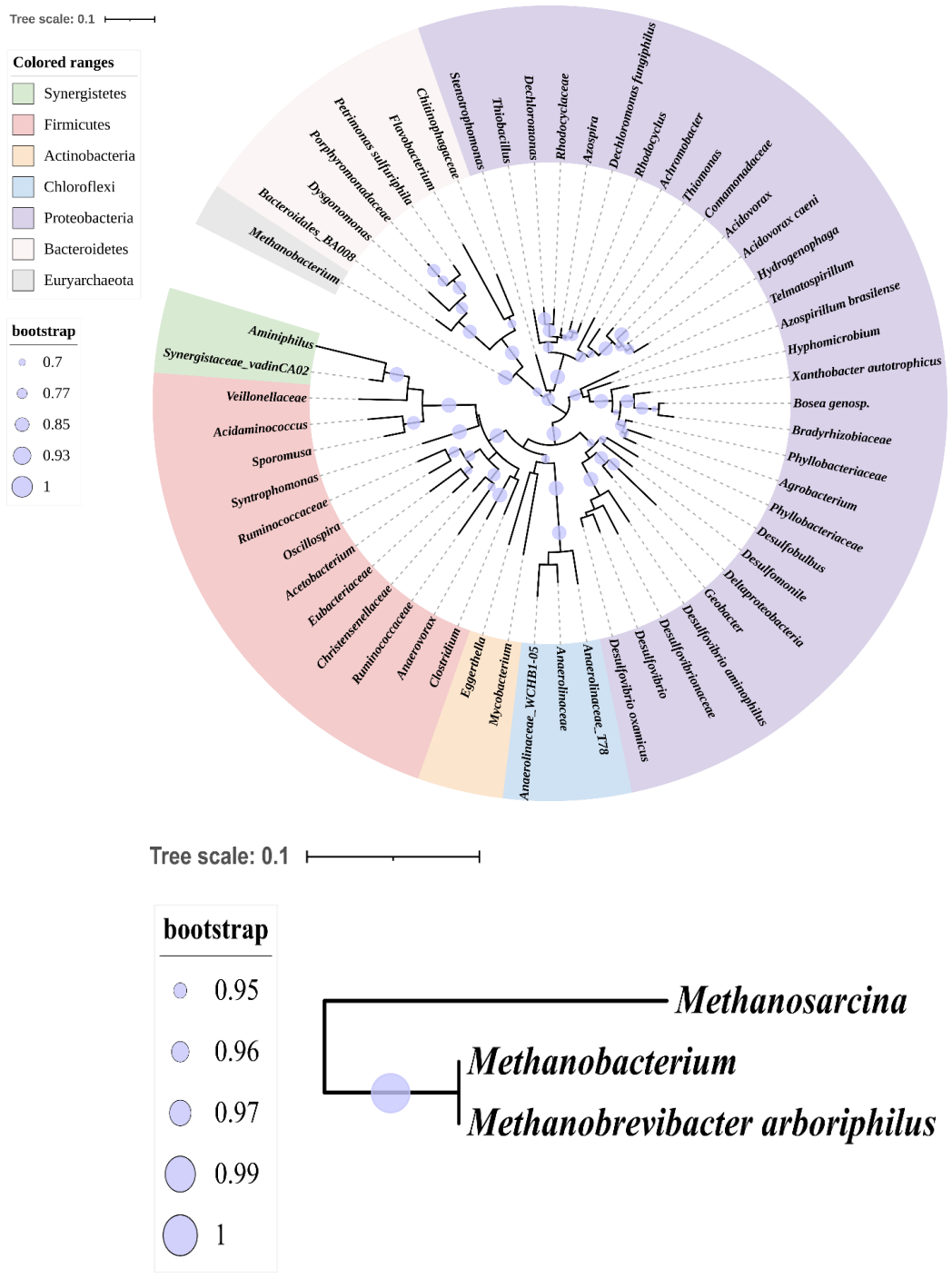


**Figure B.4** Phylogenetic tree using bacterial and archaeal primer at HPr/HAc ratio of 0.5

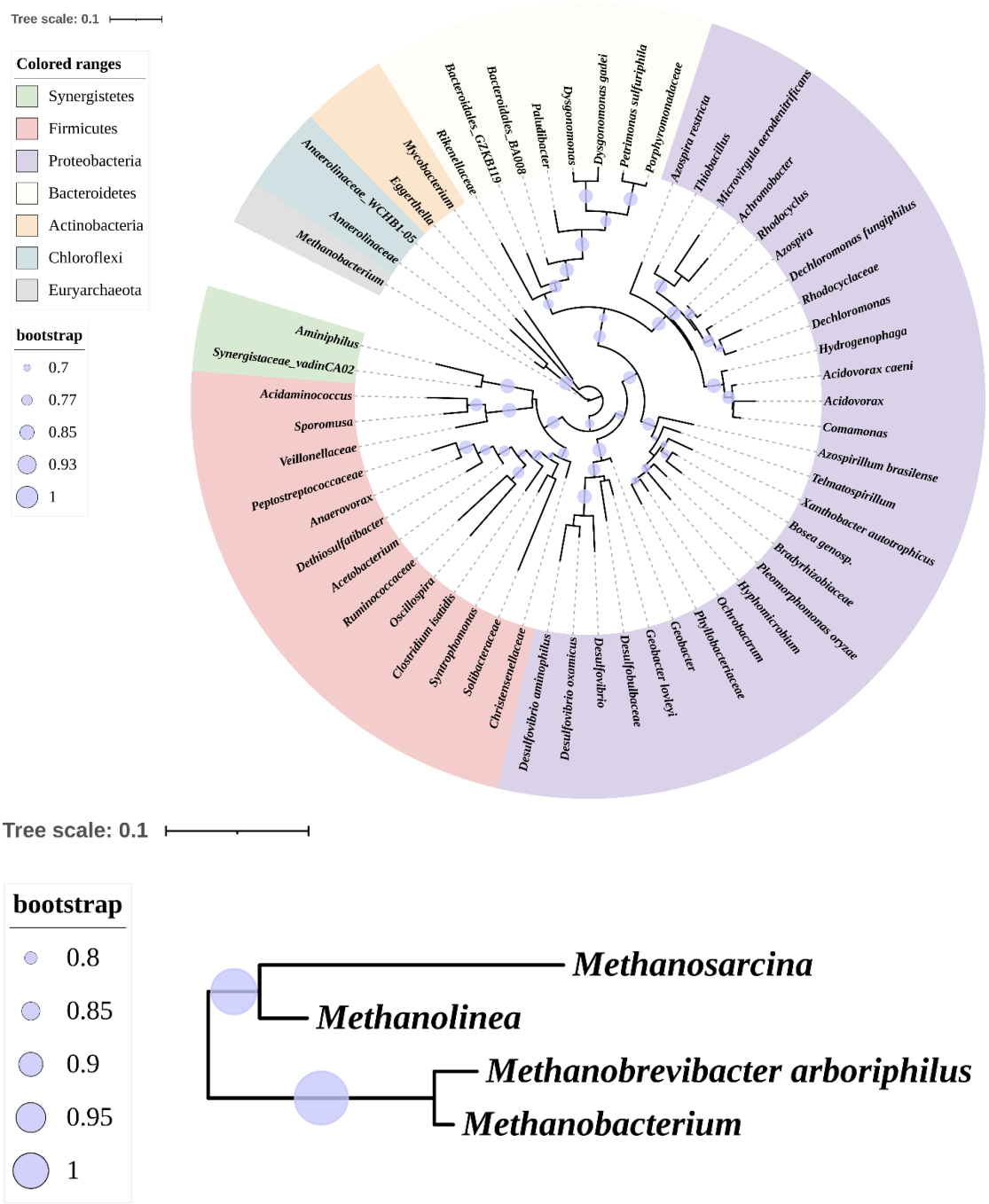


**Figure B.5** Phylogenetic tree using bacterial and archaeal primer at HPr/HAc ratio of 1.5

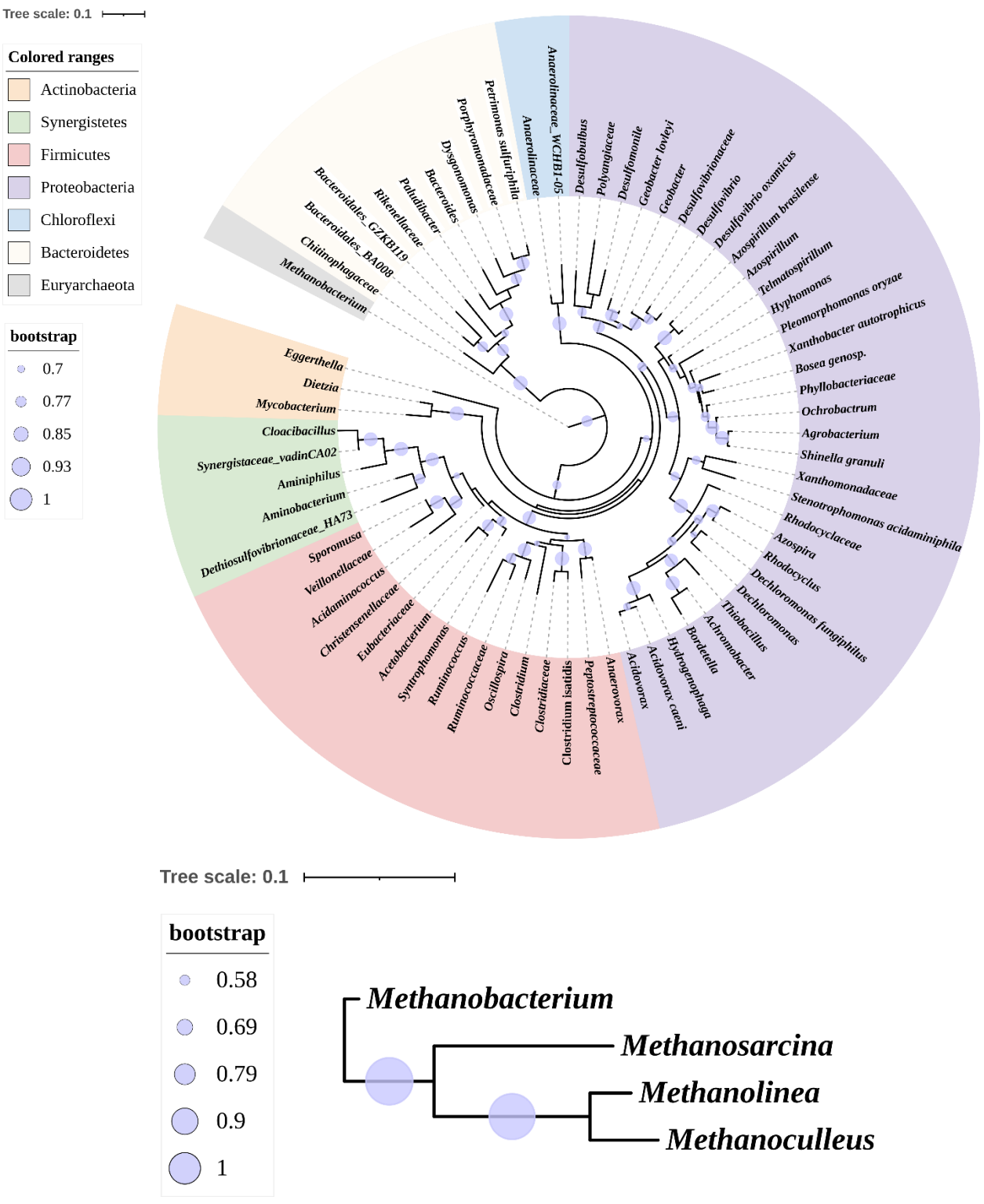


**Figure B.6** Phylogenetic tree using bacterial and archaeal primer at HPr/HAc ratio of 2.5

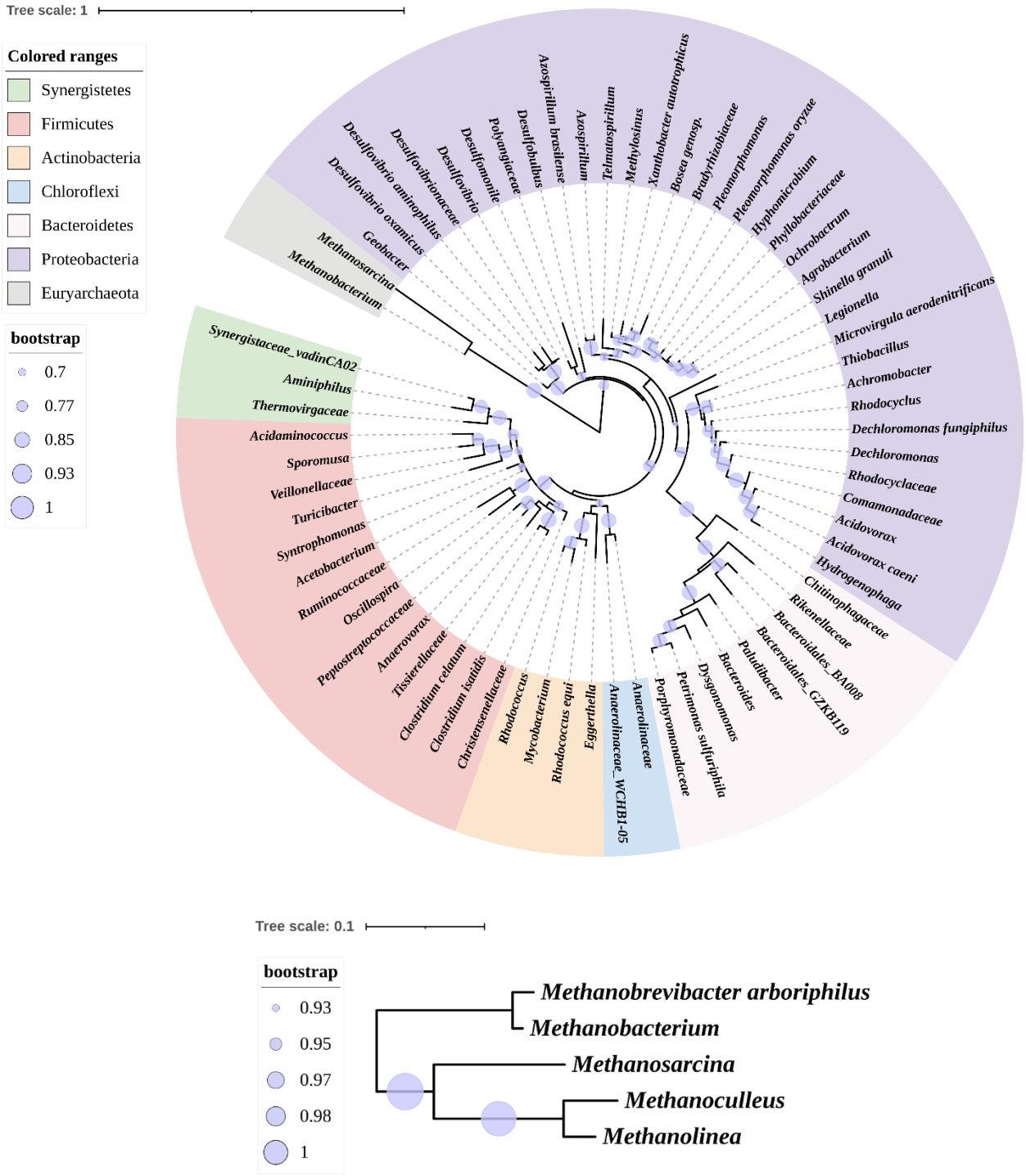


**Figure B.7** Phylogenetic tree using bacterial and archaeal primer at HPr/HAc ratio of 5